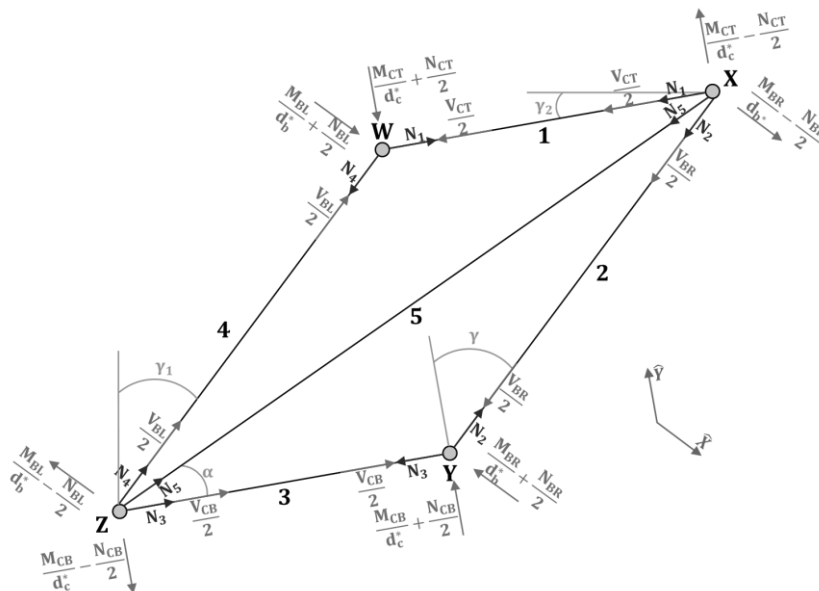


Characterization of the Full Non-Linear Behaviour up to Failure of the Sheared Panel Zone under Monotonic Loading Conditions

by

Adrien CORMAN



APPENDICES

Characterization of the Full Non-Linear Behaviour up to Failure of the Sheared Panel Zone under Monotonic Loading Conditions

APPENDICES

by

Adrien CORMAN

Supervisor : Jean-Pierre JASPART

Co-supervisor : Jean-Fançois DEMONCEAU

TABLE OF CONTENT

TABLE OF CONTENT	5
A. EXPERIMENTAL RESULTS	7
A.1 Welded joints.....	9
A.2 Bolted joints.....	21
B. CHARACTERIZATION OF THE JOINT BEHAVIOUR FROM THE FE RESULTS.....	37
B.1 Extraction of the $V - \gamma_{num}$ deformation curves of the PZ, CWP and SE	39
B.2 Extraction of the $MB - \Phi_{num}$ deformation curve of the joint	56
C. NUMERICAL RESULTS	59
C.1 Model NR4	61
C.2 Model NR16	69
C.3 Model A.....	77
C.4 Model B	85
D. PLASTIC HINGE CHARACTERIZATION	95
D.1 Geometric properties	97
D.2 Mechanical properties.....	99
E. GEOMETRIC 2 nd ORDER EFFECTS.....	103
E.1 Exterior joints.....	105
E.2 Interior joints.....	110
F. prEN 1993-1-8: PROPOSALS FOR IMPROVEMENT OF THE PZ CONSTITUTIVE MODEL	117
F.1 Stiffness coefficient $k_{ini, EU * PZ}$	119
F.2 Design resistance $V_y, Rd, EU * PZ$	120
F.3 Ultimate deformation capacity $\gamma_u, EU * PZ$	123
BIBLIOGRAPHY	125

A. EXPERIMENTAL RESULTS

A.1 Welded joints

A.1.1 Test B1

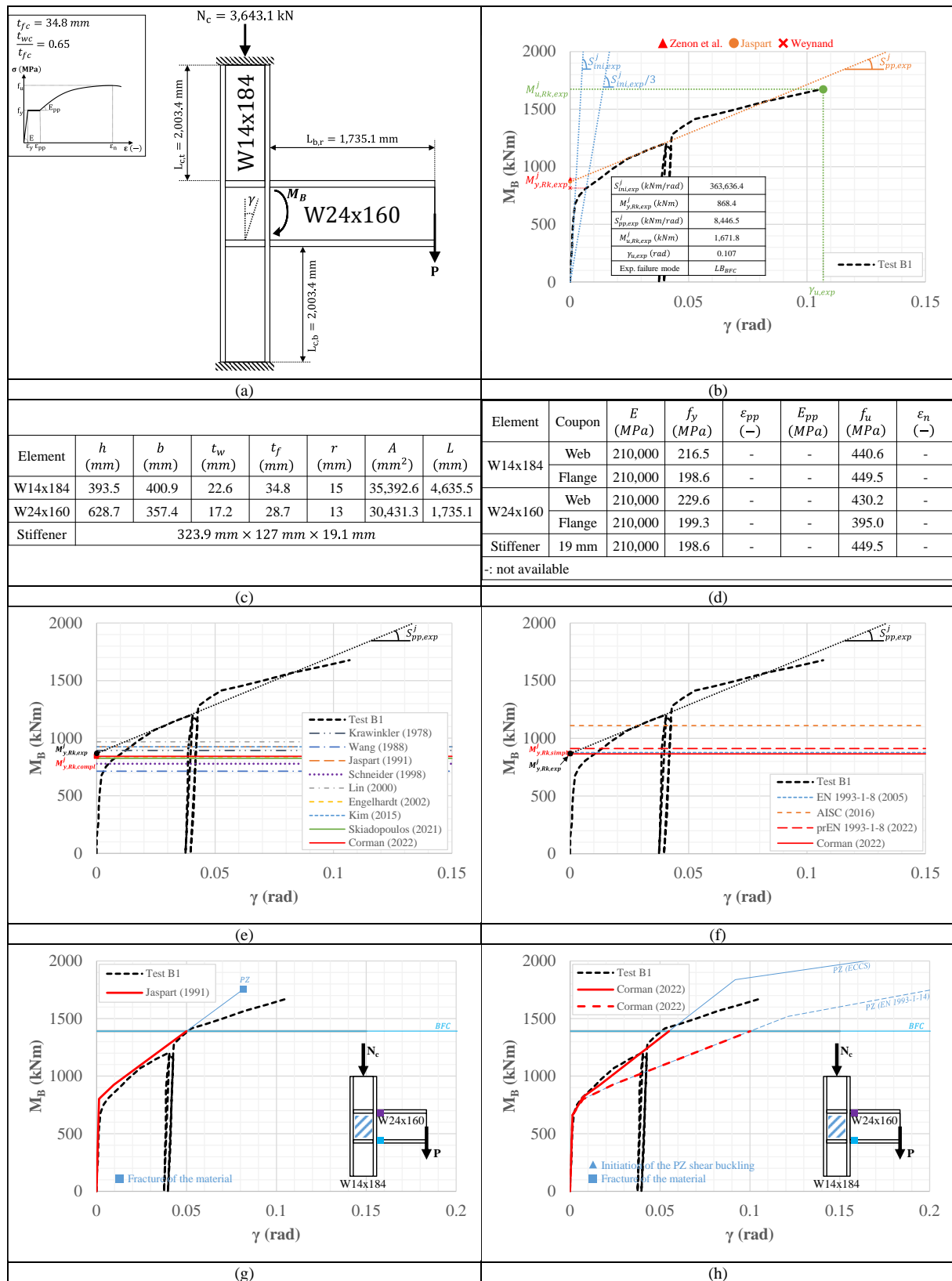


Fig. A-1. Experimental results for the welded test B1: (a) experimental setup, (b) performance parameters, (c) geometric properties, (d) mechanical properties, (e) complex rigid plastic models, (f) simplified rigid plastic models, (g) full-range Jaspert model, (h) full-range Corman model.

A.1.2 Test NR2

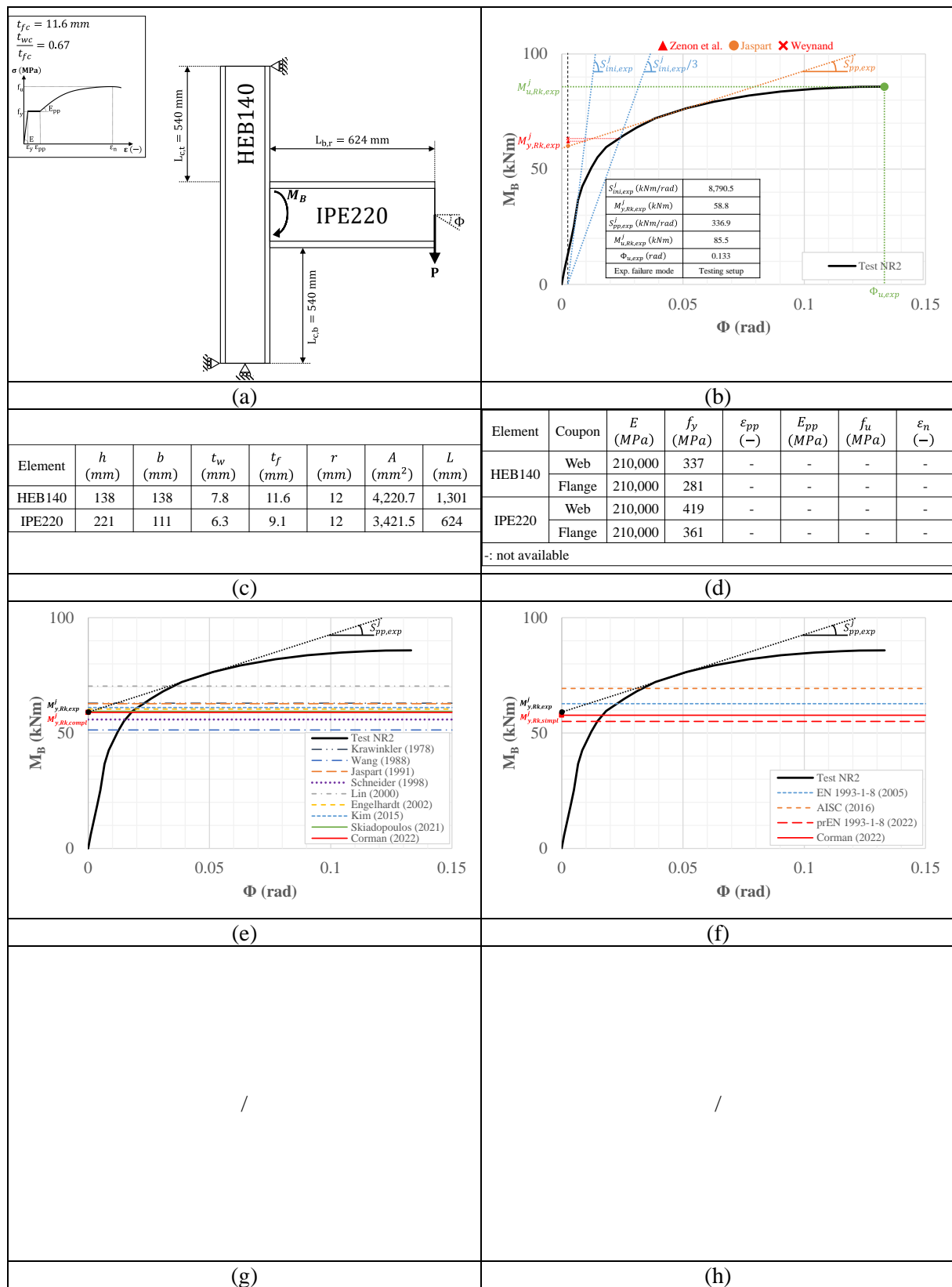


Fig. A-2. Experimental results for the welded test NR2: (a) experimental setup, (b) performance parameters, (c) geometric properties, (d) mechanical properties, (e) complex rigid plastic models, (f) simplified rigid plastic models, (g) full-range Jaspert model, (h) full-range Corman model.

A.1.3 Test NR3

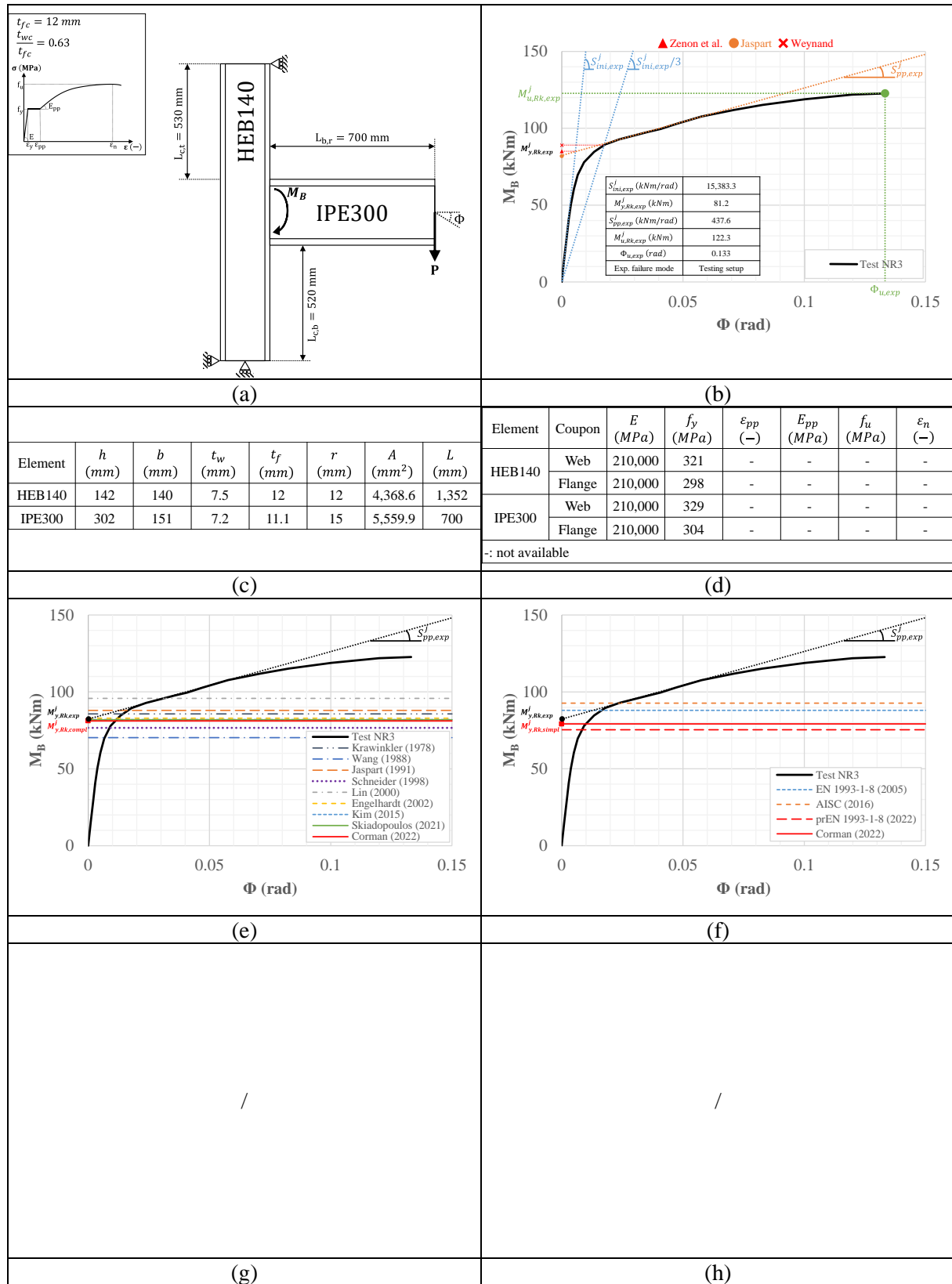


Fig. A-3. Experimental results for the welded test NR3: (a) experimental setup, (b) performance parameters, (c) geometric properties, (d) mechanical properties, (e) complex rigid plastic models, (f) simplified rigid plastic models, (g) full-range Jaspert model, (h) full-range Corman model.

A.1.4 Test NR4

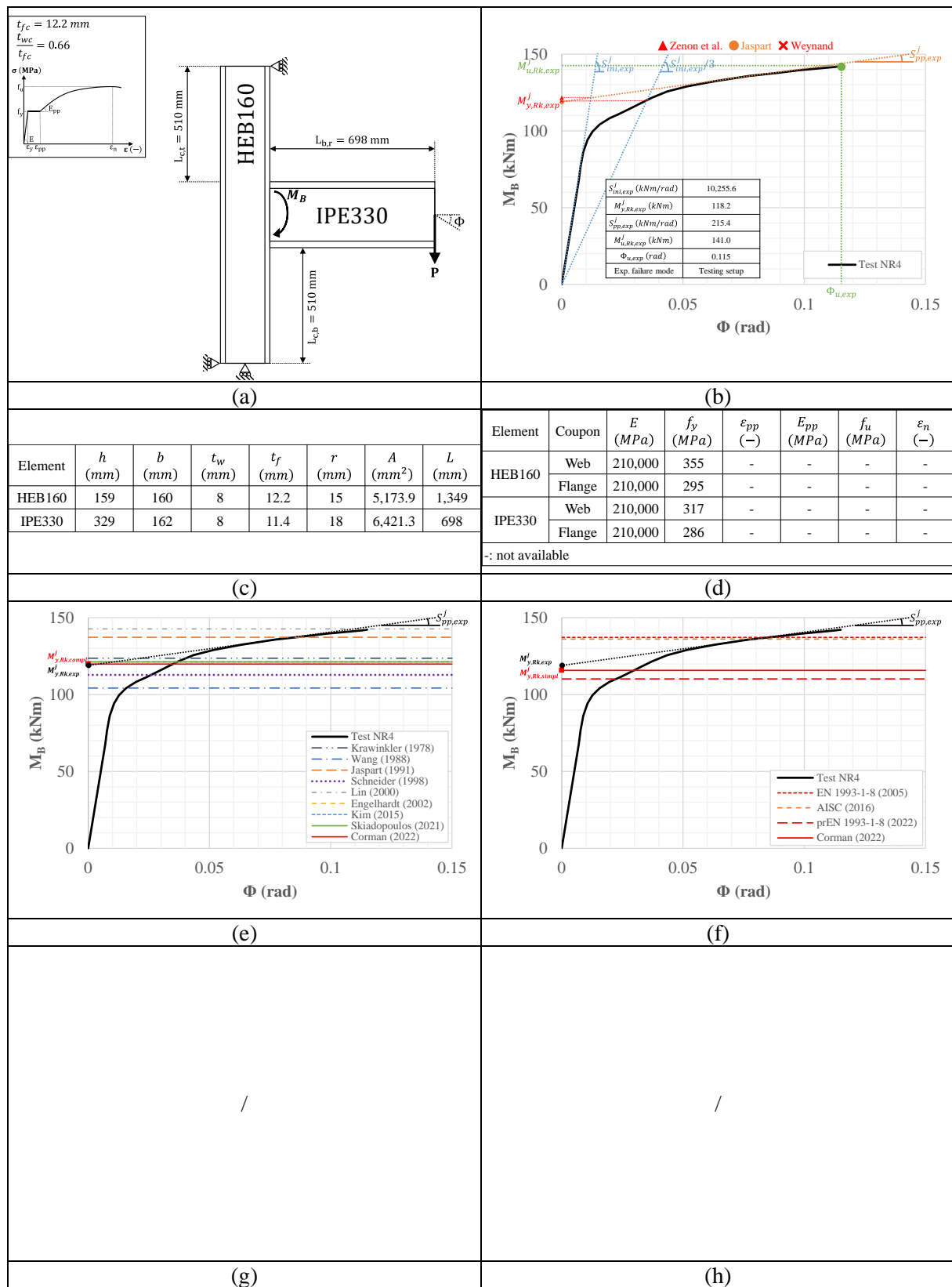


Fig. A-4. Experimental results for the welded test NR4: (a) experimental setup, (b) performance parameters, (c) geometric properties, (d) mechanical properties, (e) complex rigid plastic models, (f) simplified rigid plastic models, (g) full-range Jaspert model, (h) full-range Corman model.

A.1.5 Test NR7

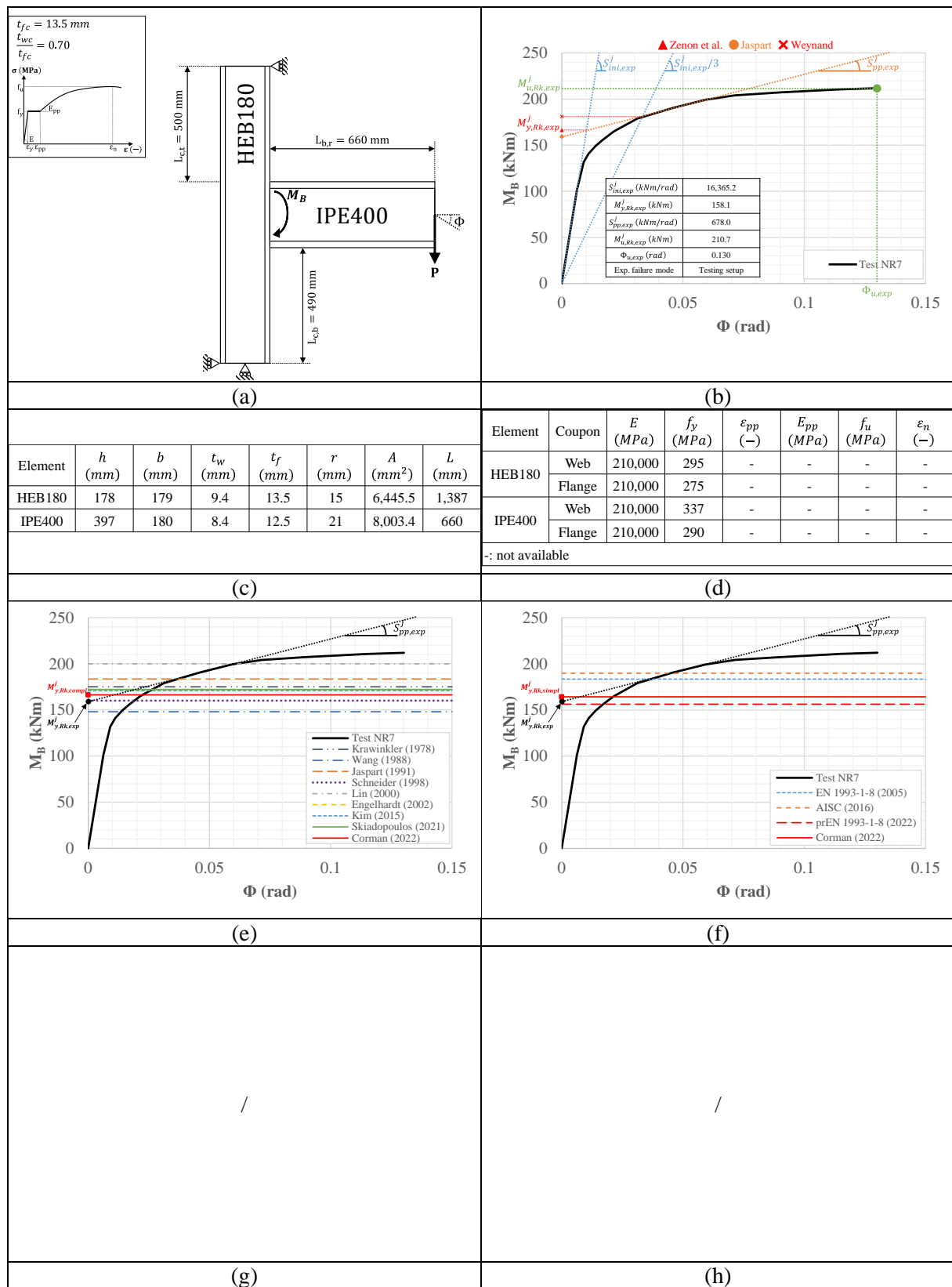


Fig. A-5. Experimental results for the welded test NR7: (a) experimental setup, (b) performance parameters, (c) geometric properties, (d) mechanical properties, (e) complex rigid plastic models, (f) simplified rigid plastic models, (g) full-range Jaspert model, (h) full-range Corman model.

A.1.6 Test BCC5-E

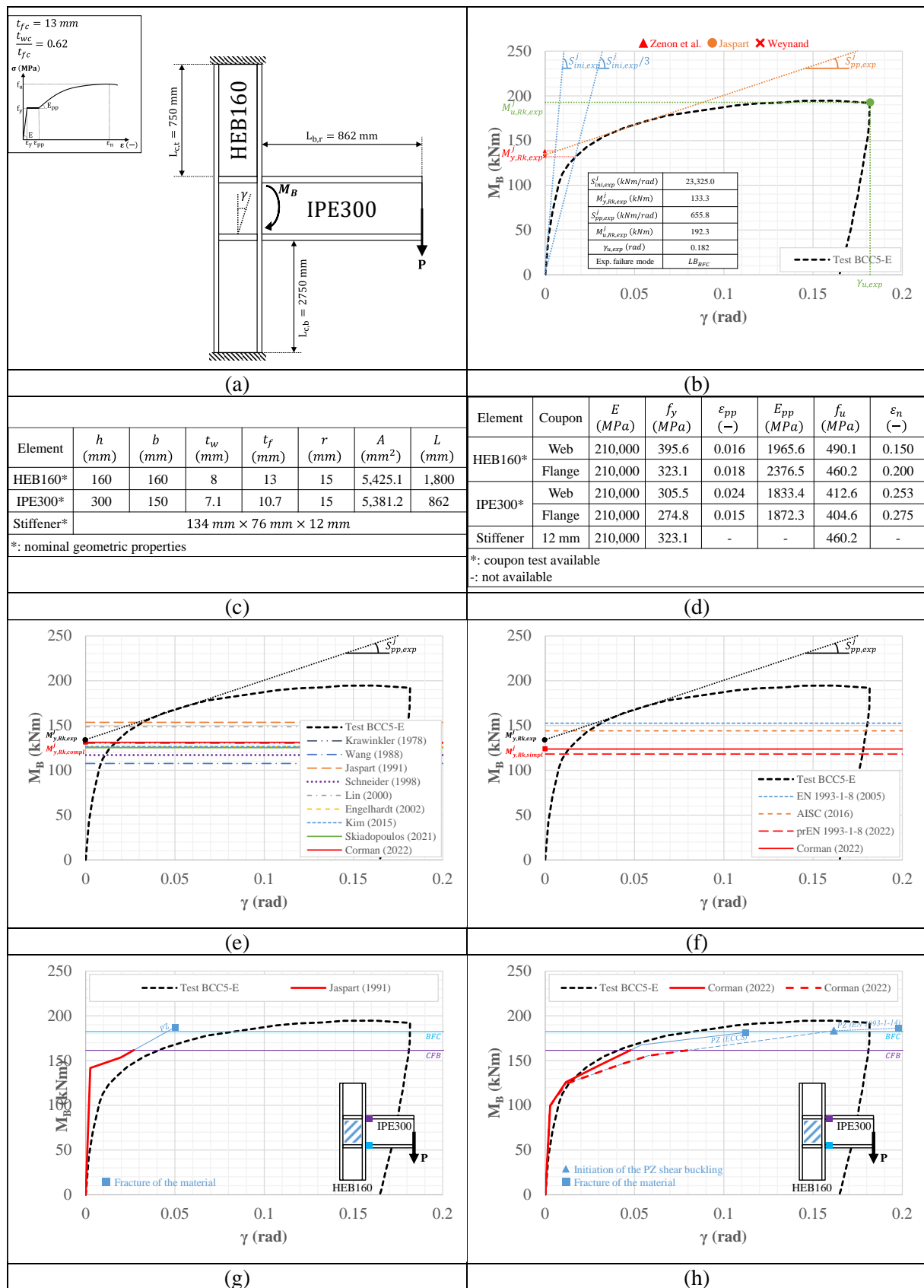


Fig. A-6. Experimental results for the welded test BCC5-E: (a) experimental setup, (b) performance parameters, (c) geometric properties, (d) mechanical properties, (e) complex rigid plastic models, (f) simplified rigid plastic models, (g) full-range Jaspert model, (h) full-range Corman model.

A.1.7 Test XU-W1

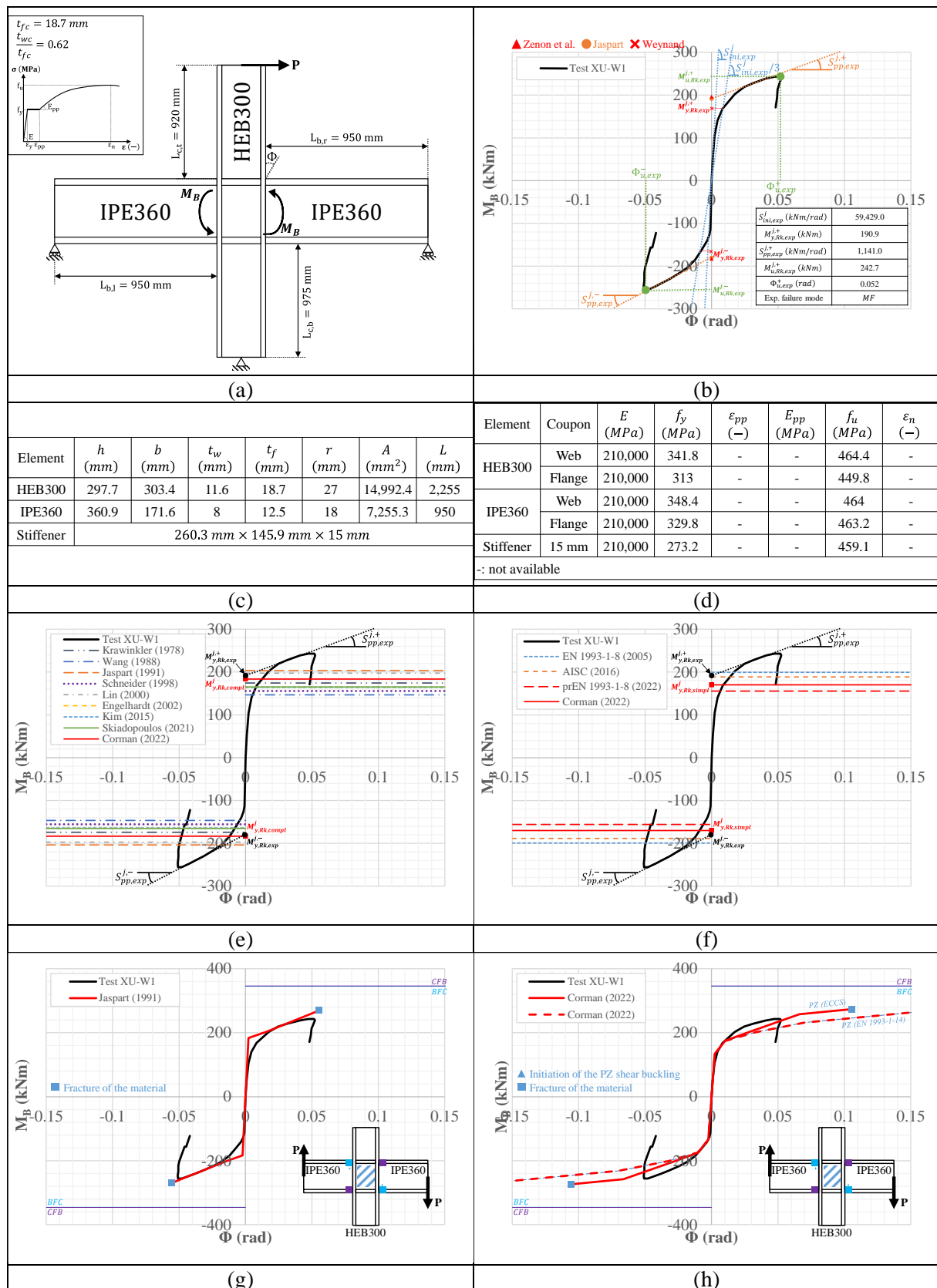


Fig. A-7. Experimental results for the welded test XU-W1: (a) experimental setup, (b) performance parameters, (c) geometric properties, (d) mechanical properties, (e) complex rigid plastic models, (f) simplified rigid plastic models, (g) full-range Jaspert model, (h) full-range Corman model.

A.1.8 Test XU-CWP1

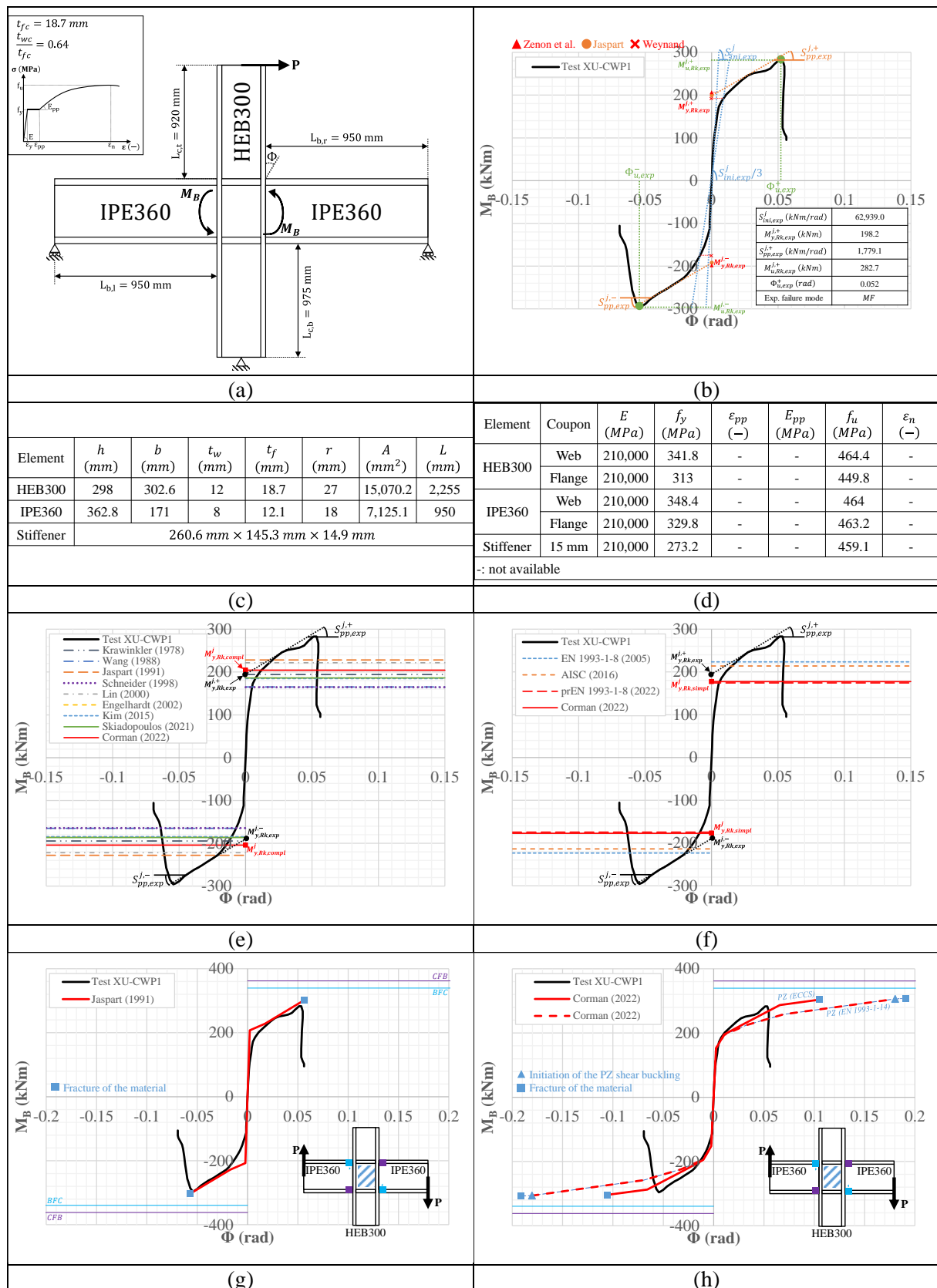


Fig. A-8. Experimental results for the welded test XU-CWP1: (a) experimental setup, (b) performance parameters, (c) geometric properties, (d) mechanical properties, (e) complex rigid plastic models, (f) simplified rigid plastic models, (g) full-range Jaspert model, (h) full-range Corman model.

A.1.9 Test E1.1

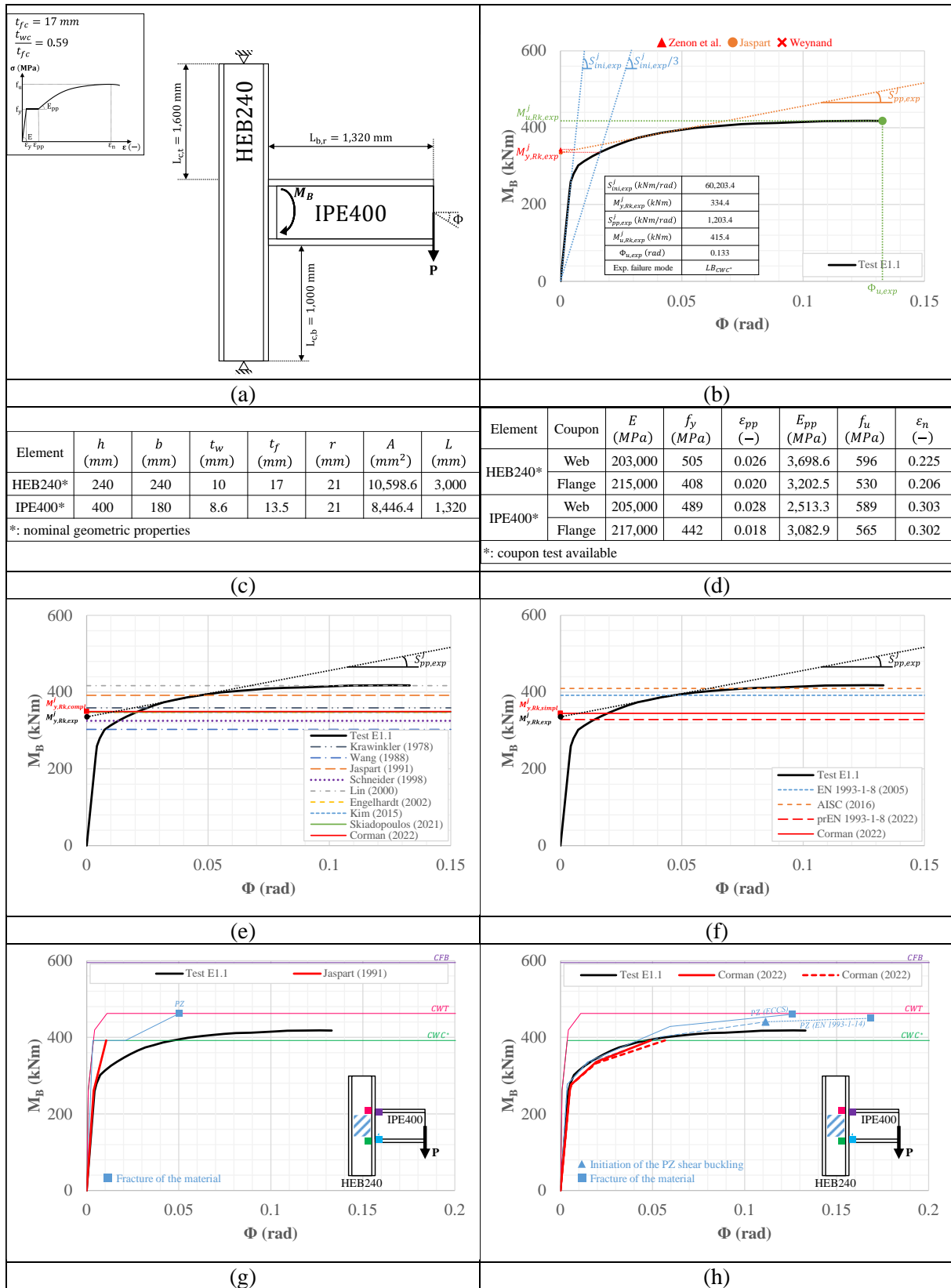


Fig. A-9. Experimental results for the welded test E1.1: (a) experimental setup, (b) performance parameters, (c) geometric properties, (d) mechanical properties, (e) complex rigid plastic models, (f) simplified rigid plastic models, (g) full-range Jaspert model, (h) full-range Corman model.

A.1.10 Test E1.2

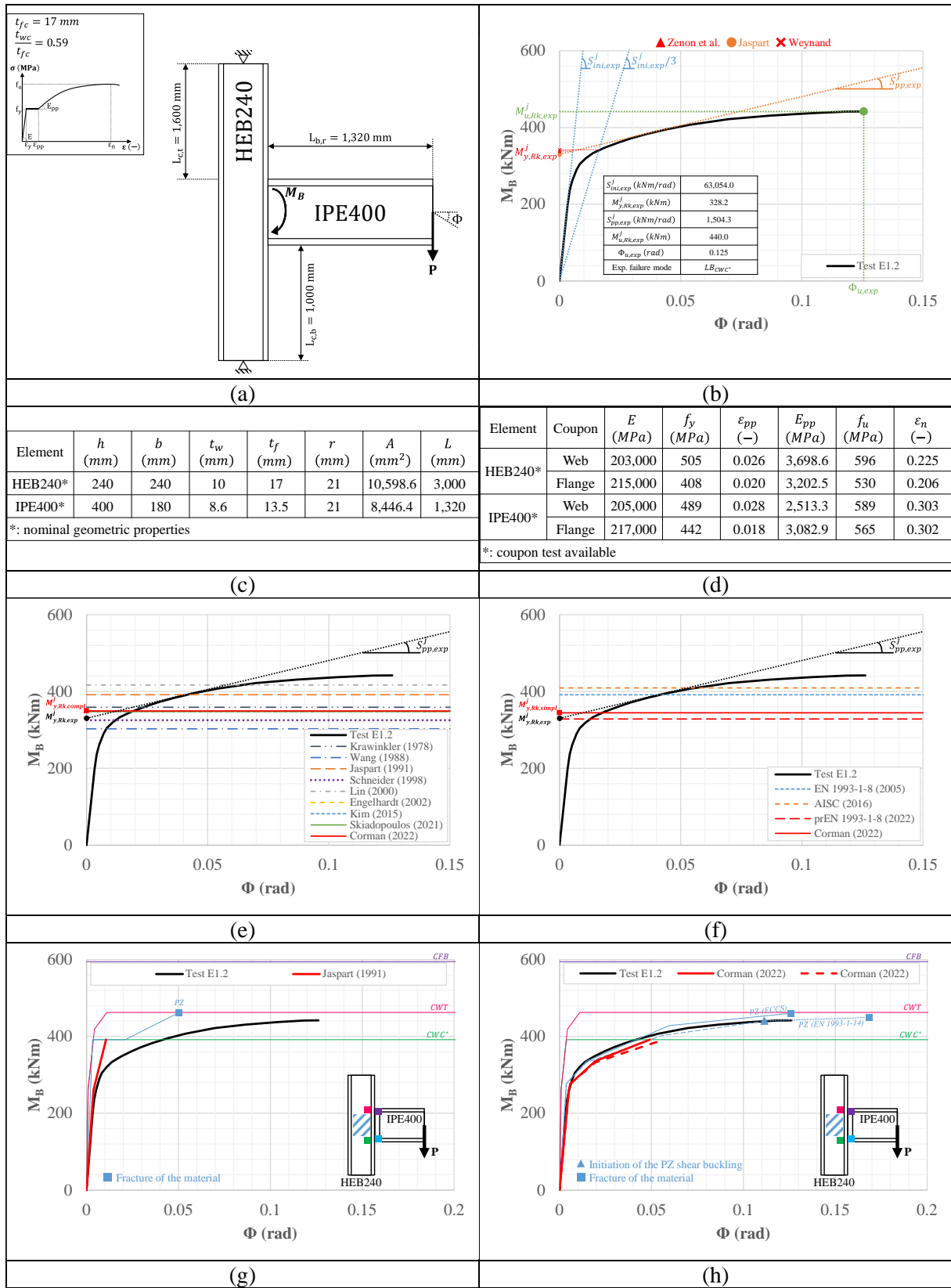


Fig. A-10. Experimental results for the welded test E1.2: (a) experimental setup, (b) performance parameters, (c) geometric properties, (d) mechanical properties, (e) complex rigid plastic models, (f) simplified rigid plastic models, (g) full-range Jaspert model, (h) full-range Corman model.

A.1.11 Test CP-R-M

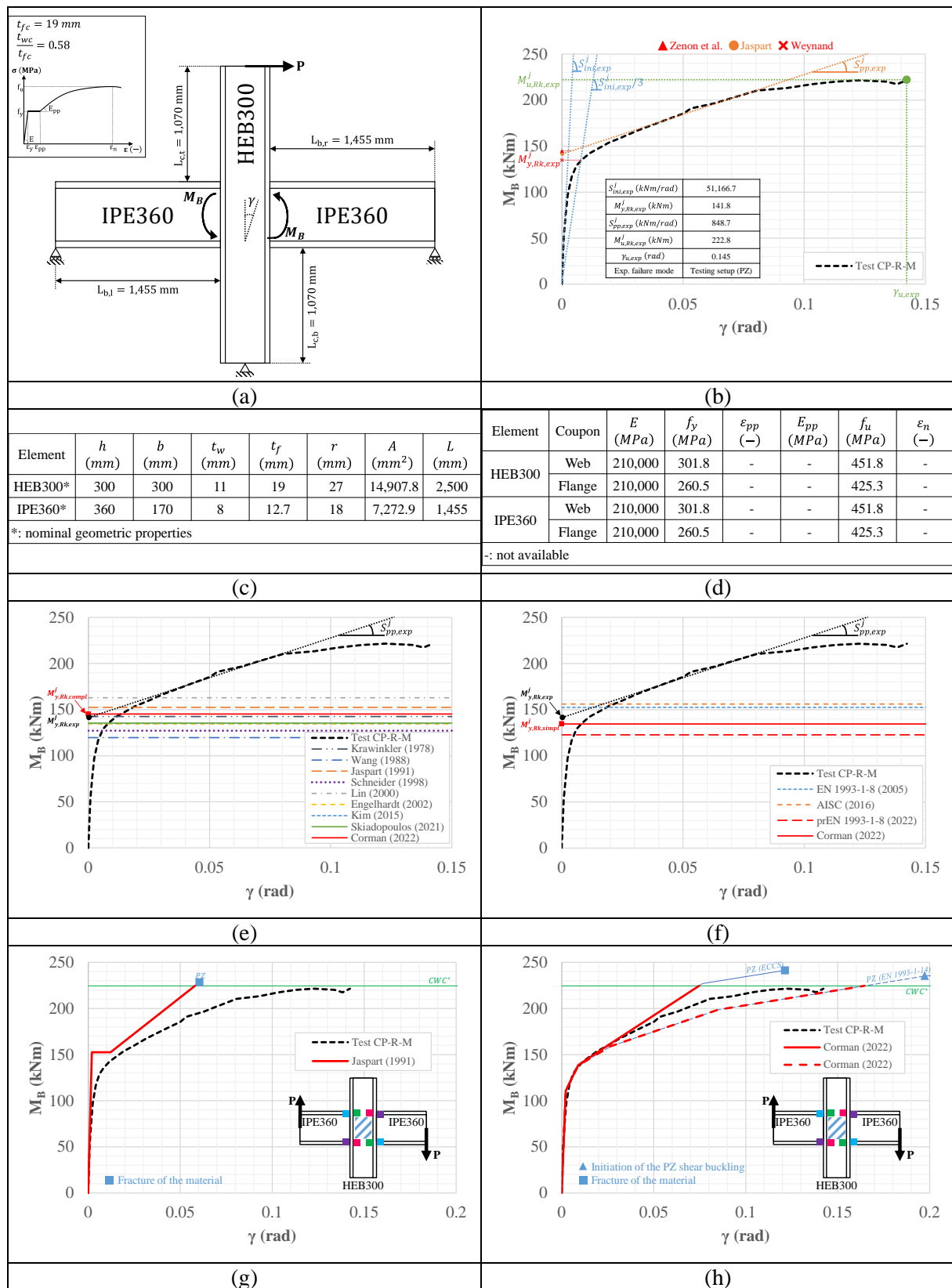


Fig. A-11. Experimental results for the welded test CP-R-M: (a) experimental setup, (b) performance parameters, (c) geometric properties, (d) mechanical properties, (e) complex rigid plastic models, (f) simplified rigid plastic models, (g) full-range Jaspert model, (h) full-range Corman model.

A.1.12 Test No. 3

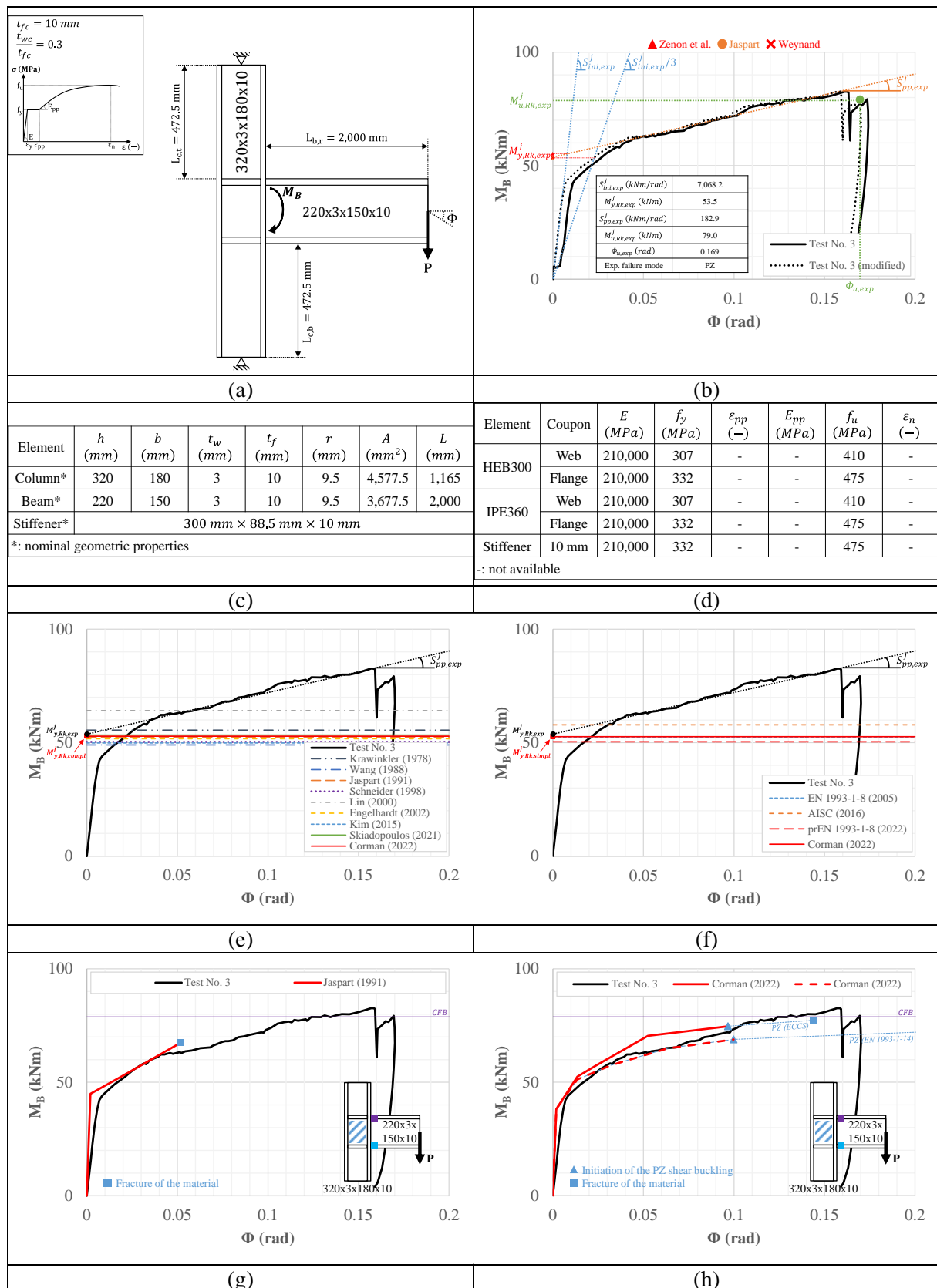


Fig. A-12. Experimental results for the welded test No. 3: (a) experimental setup, (b) performance parameters, (c) geometric properties, (d) mechanical properties, (e) complex rigid plastic models, (f) simplified rigid plastic models, (g) full-range Jaspert model, (h) full-range Corman model.

A.2 Bolted joints

A.2.1 Test 01

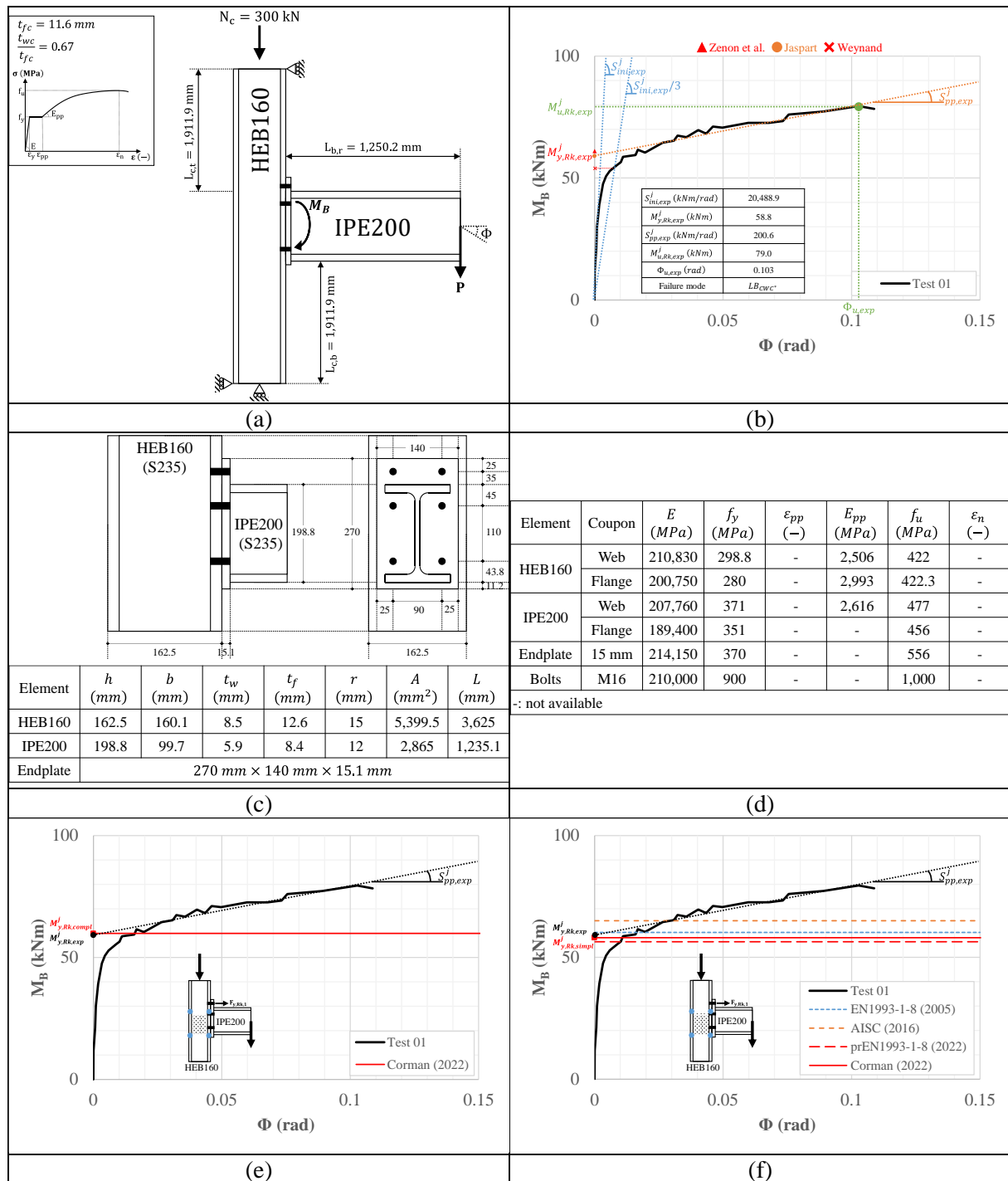


Fig. A-13. Experimental results for the bolted test 01: (a) experimental setup, (b) performance parameters, (c) geometric properties, (d) mechanical properties, (e) complex rigid plastic Corman model, (f) simplified rigid plastic models.

A.2.2 Test 04

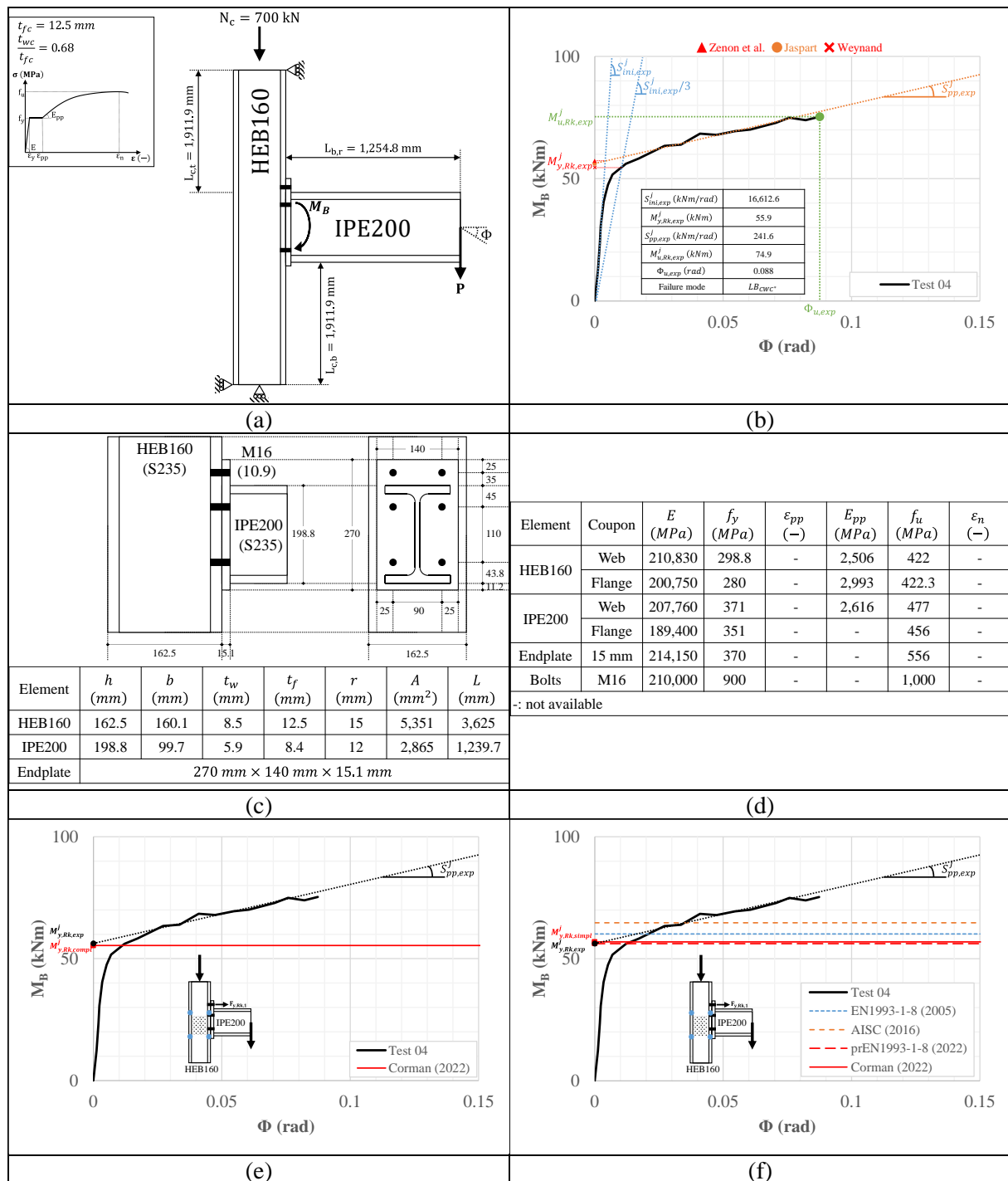


Fig. A-14. Experimental results for the bolted test 04: (a) experimental setup, (b) performance parameters, (c) geometric properties, (d) mechanical properties, (e) complex rigid plastic Corman model, (f) simplified rigid plastic models.

A.2.3 Test 07

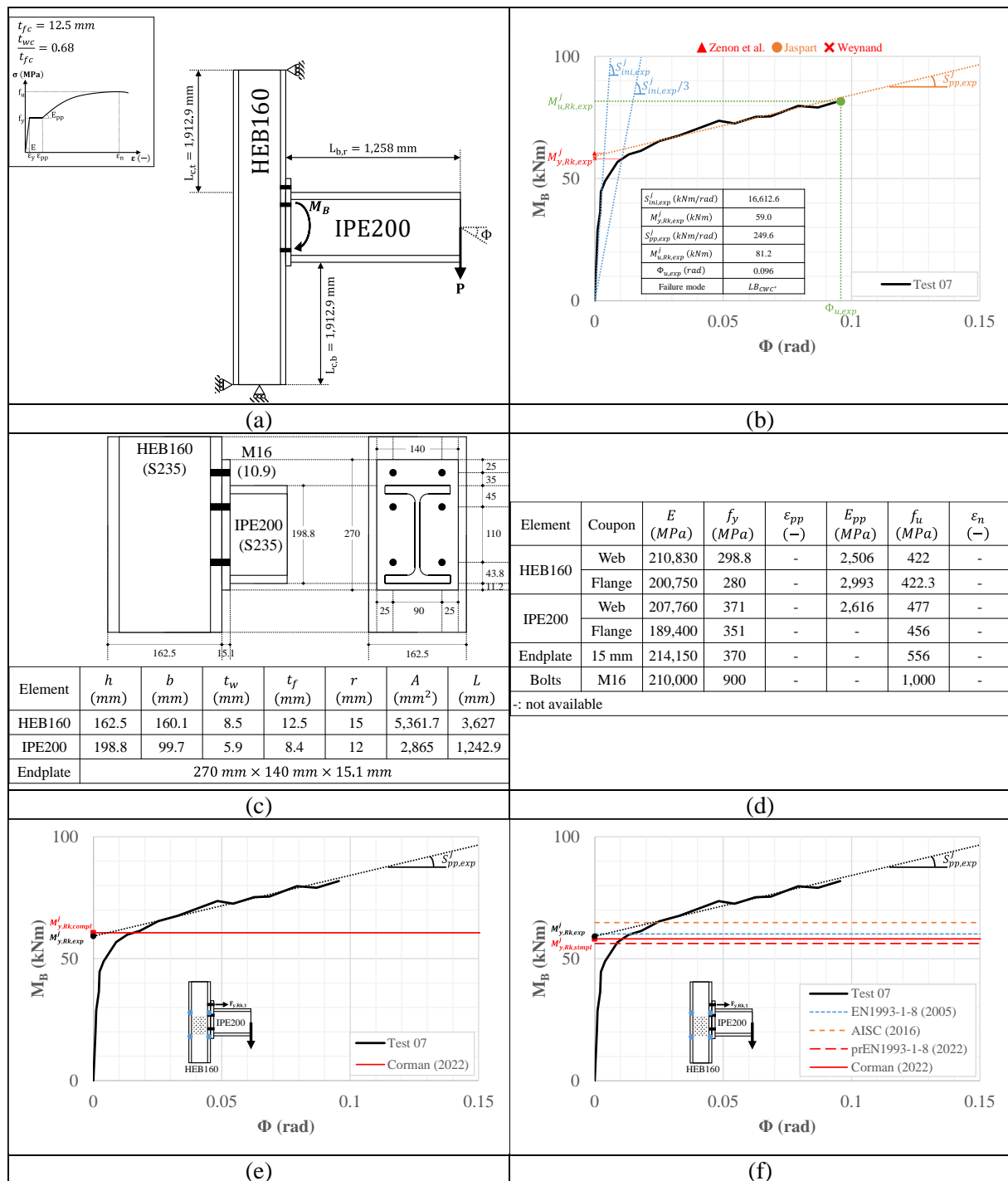


Fig. A-15. Experimental results for the bolted test 07: (a) experimental setup, (b) performance parameters, (c) geometric properties, (d) mechanical properties, (e) complex rigid plastic Corman model, (f) simplified rigid plastic models.

A.2.4 Test 010

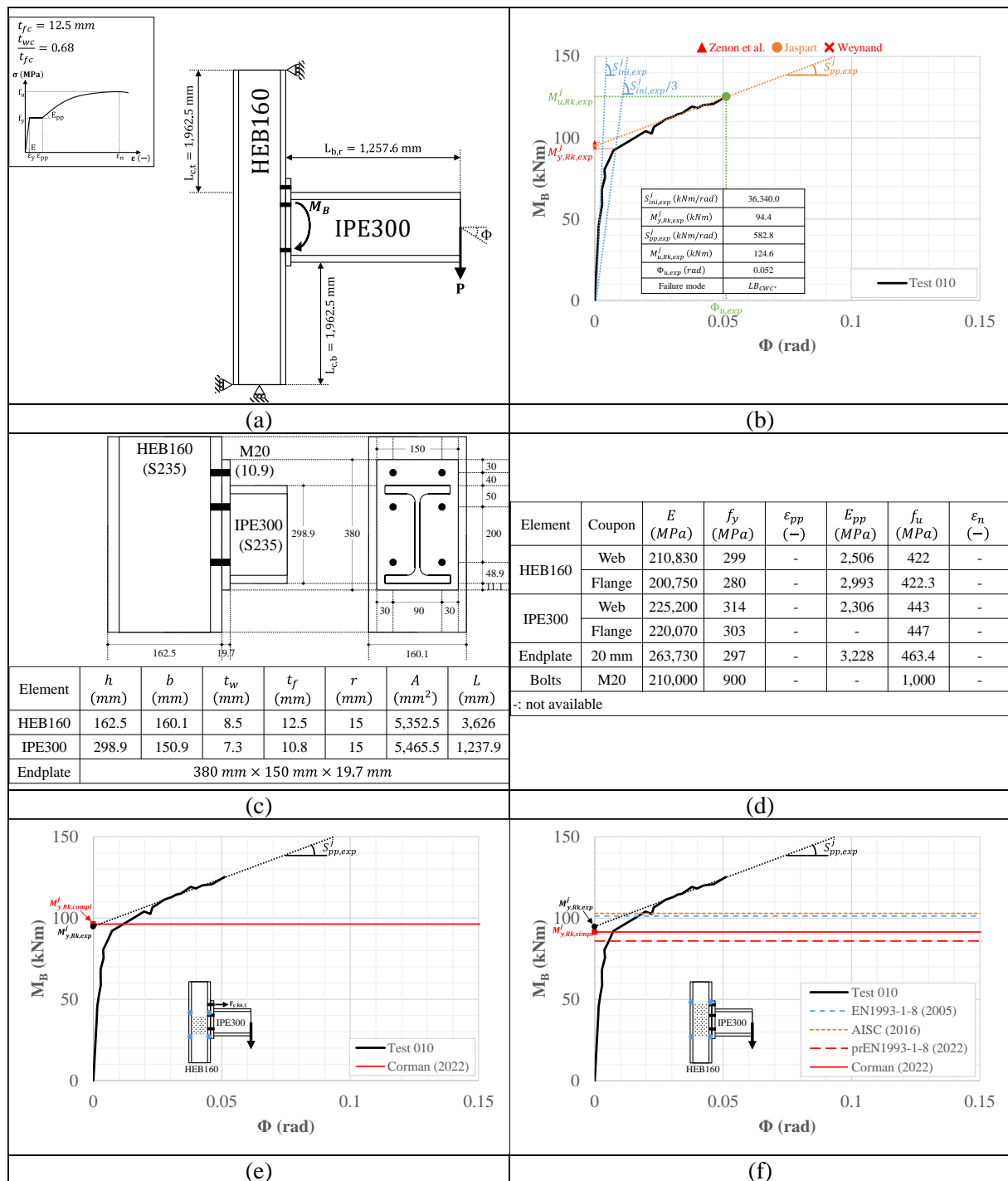


Fig. A-16. Experimental results for the bolted test 010: (a) experimental setup, (b) performance parameters, (c) geometric properties, (d) mechanical properties, (e) complex rigid plastic Corman model, (f) simplified rigid plastic models.

A.2.5 Test J1.1

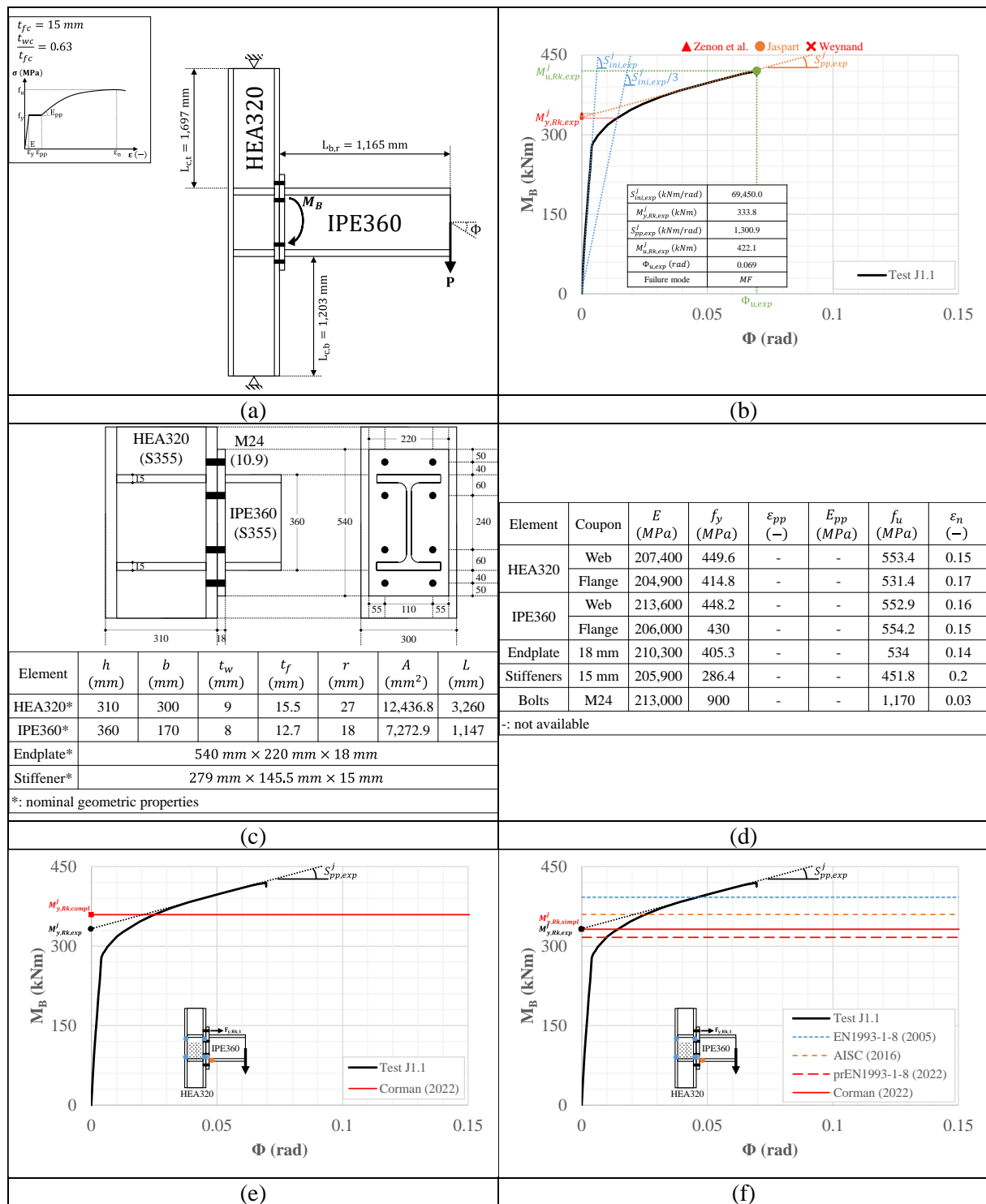


Fig. A-17. Experimental results for the bolted test J1.1: (a) experimental setup, (b) performance parameters, (c) geometric properties, (d) mechanical properties, (e) complex rigid plastic Corman model, (f) simplified rigid plastic models.

A.2.6 Test J2.1

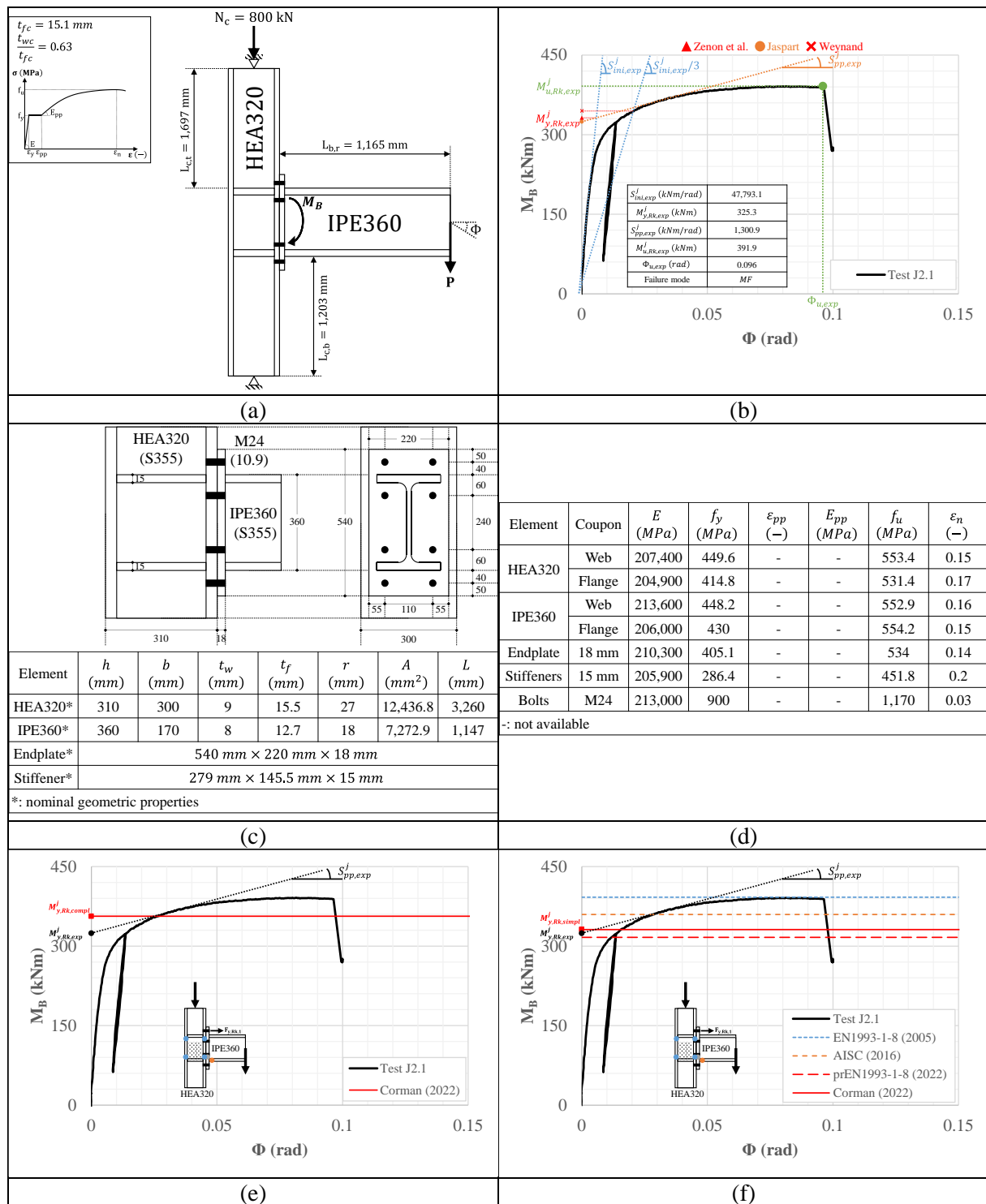


Fig. A-18. Experimental results for the bolted test J2.1: (a) experimental setup, (b) performance parameters, (c) geometric properties, (d) mechanical properties, (e) complex rigid plastic Corman model, (f) simplified rigid plastic models.

A.2.7 Test J3.1

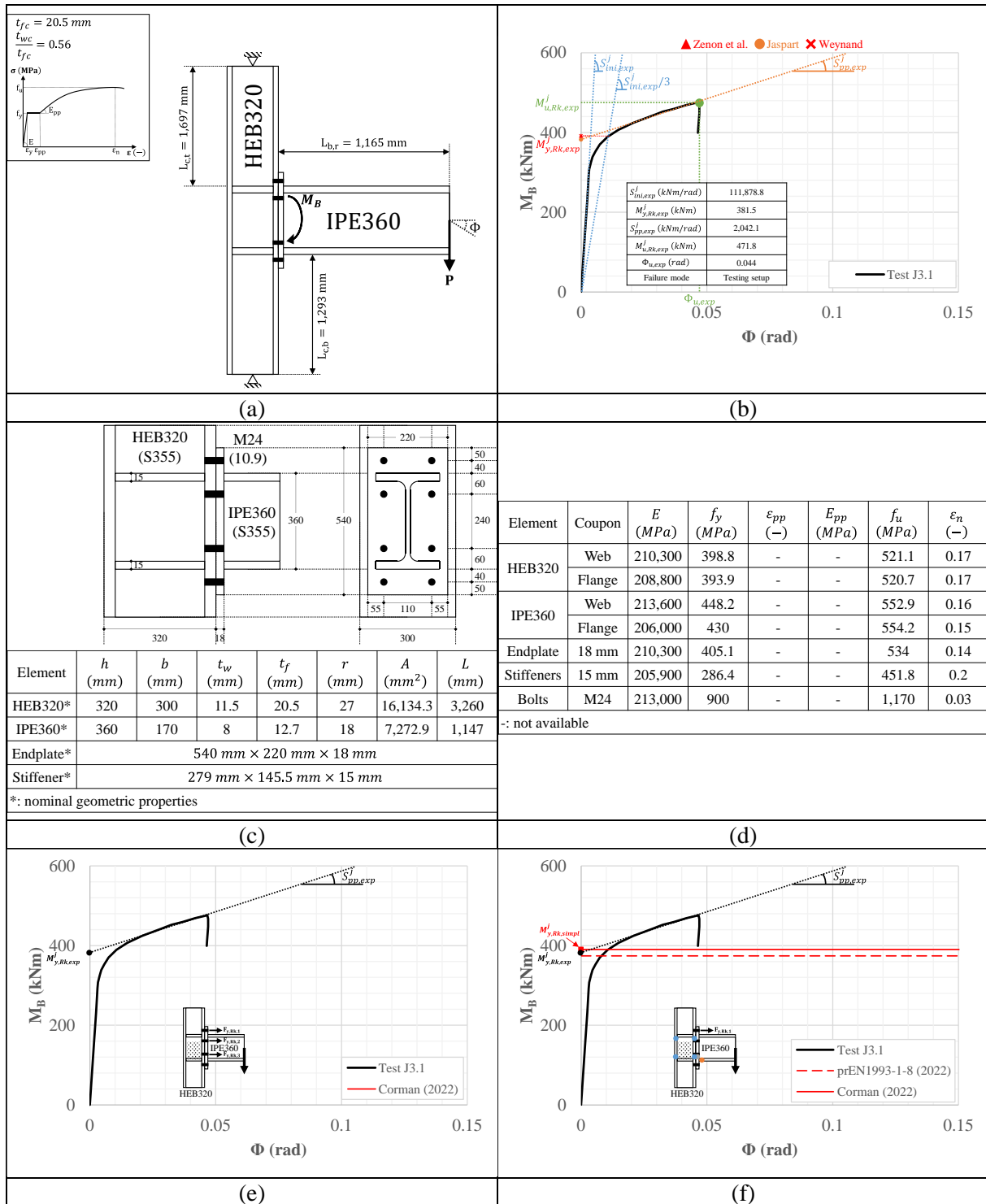


Fig. A-19. Experimental results for the bolted test J3.1: (a) experimental setup, (b) performance parameters, (c) geometric properties, (d) mechanical properties, (e) complex rigid plastic Corman model, (f) simplified rigid plastic models.

A.2.8 Test J4.1

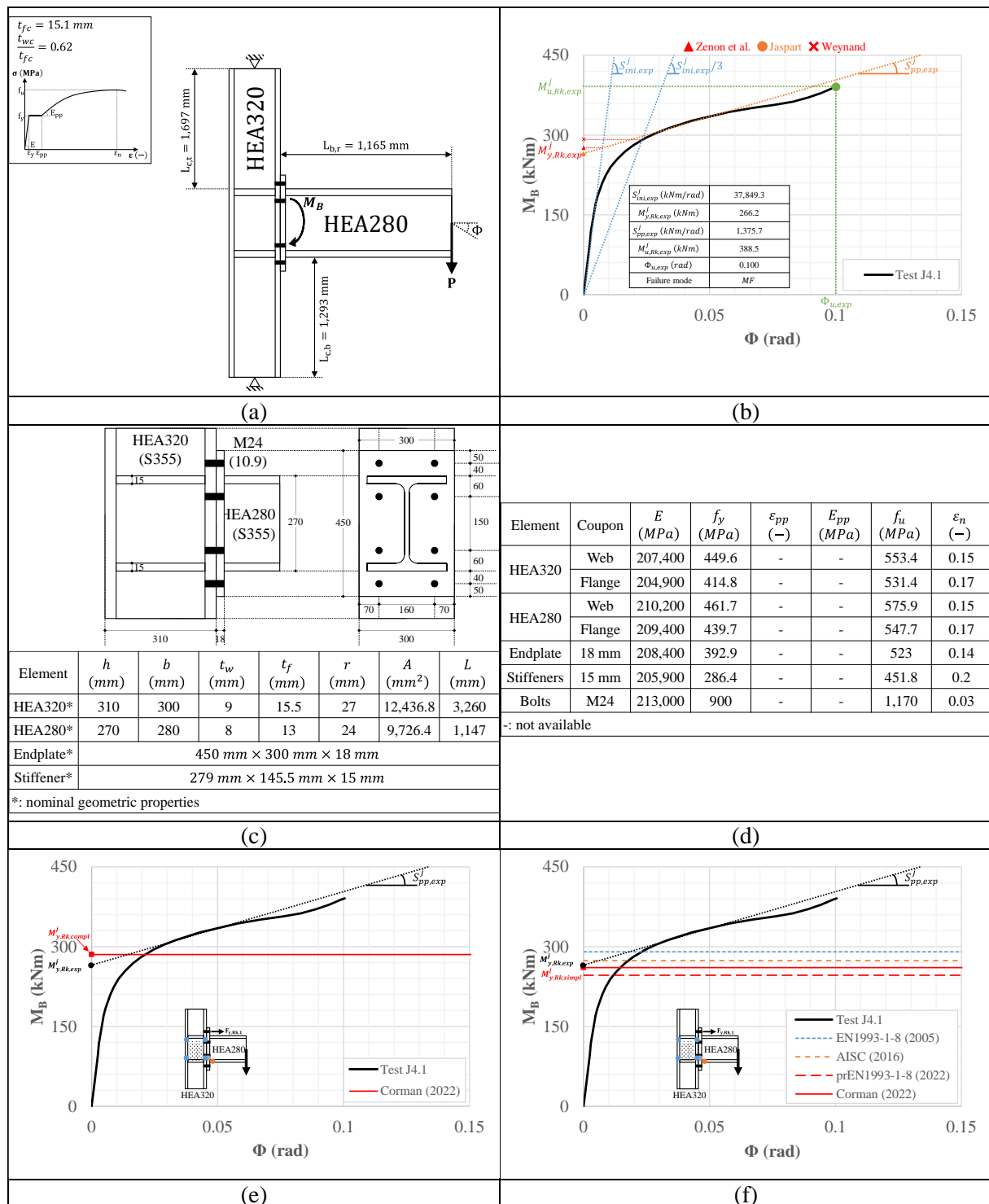


Fig. A-20. Experimental results for the bolted test J4.1: (a) experimental setup, (b) performance parameters, (c) geometric properties, (d) mechanical properties, (e) complex rigid plastic Corman model, (f) simplified rigid plastic models.

A.2.9 Test E1-TB-E-M

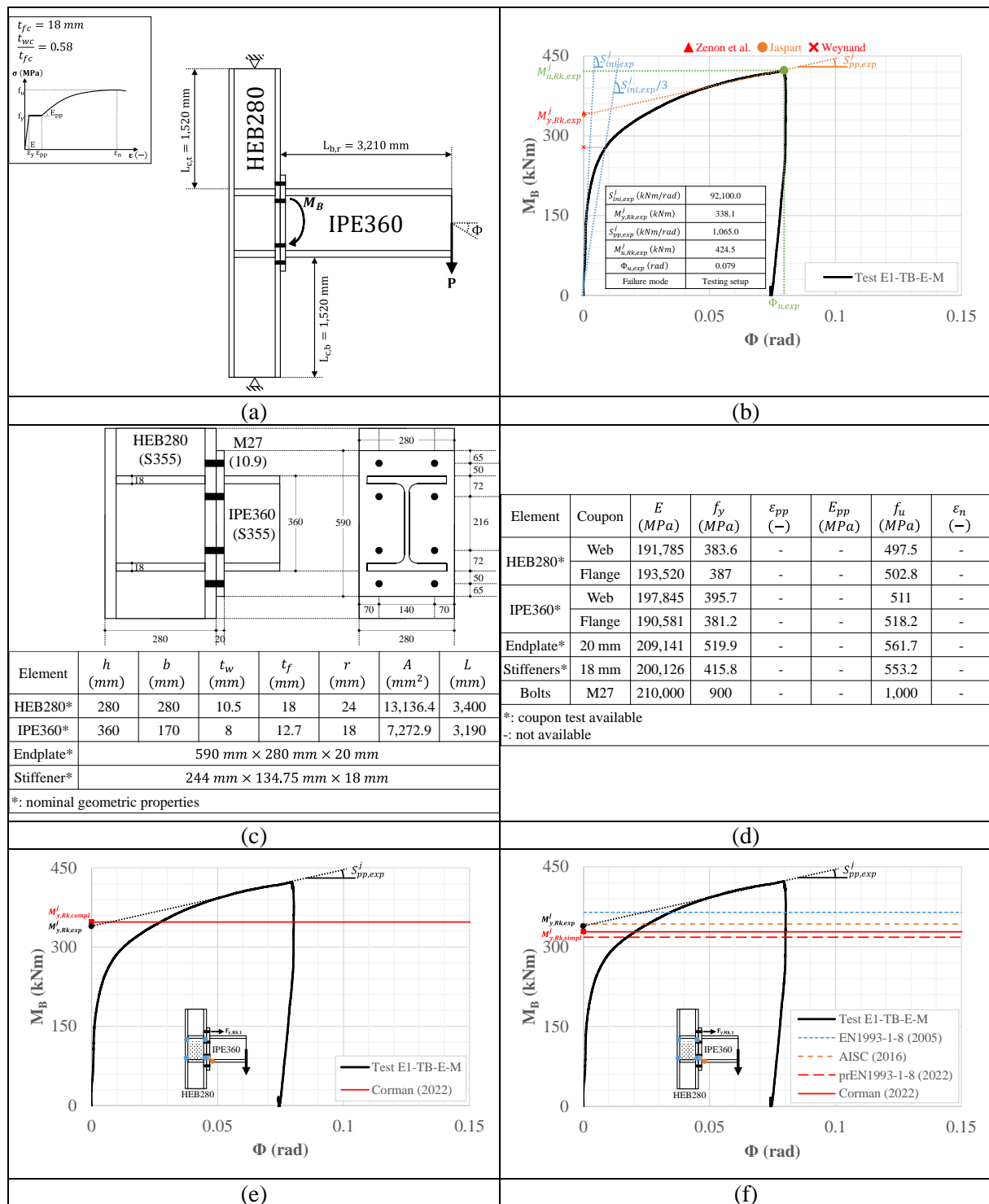


Fig. A-21. Experimental results for the bolted test E1-TB-E-M: (a) experimental setup, (b) performance parameters, (c) geometric properties, (d) mechanical properties, (e) complex rigid plastic Corman model, (f) simplified rigid plastic models.

A.2.10 Test E1-XW-P-C1

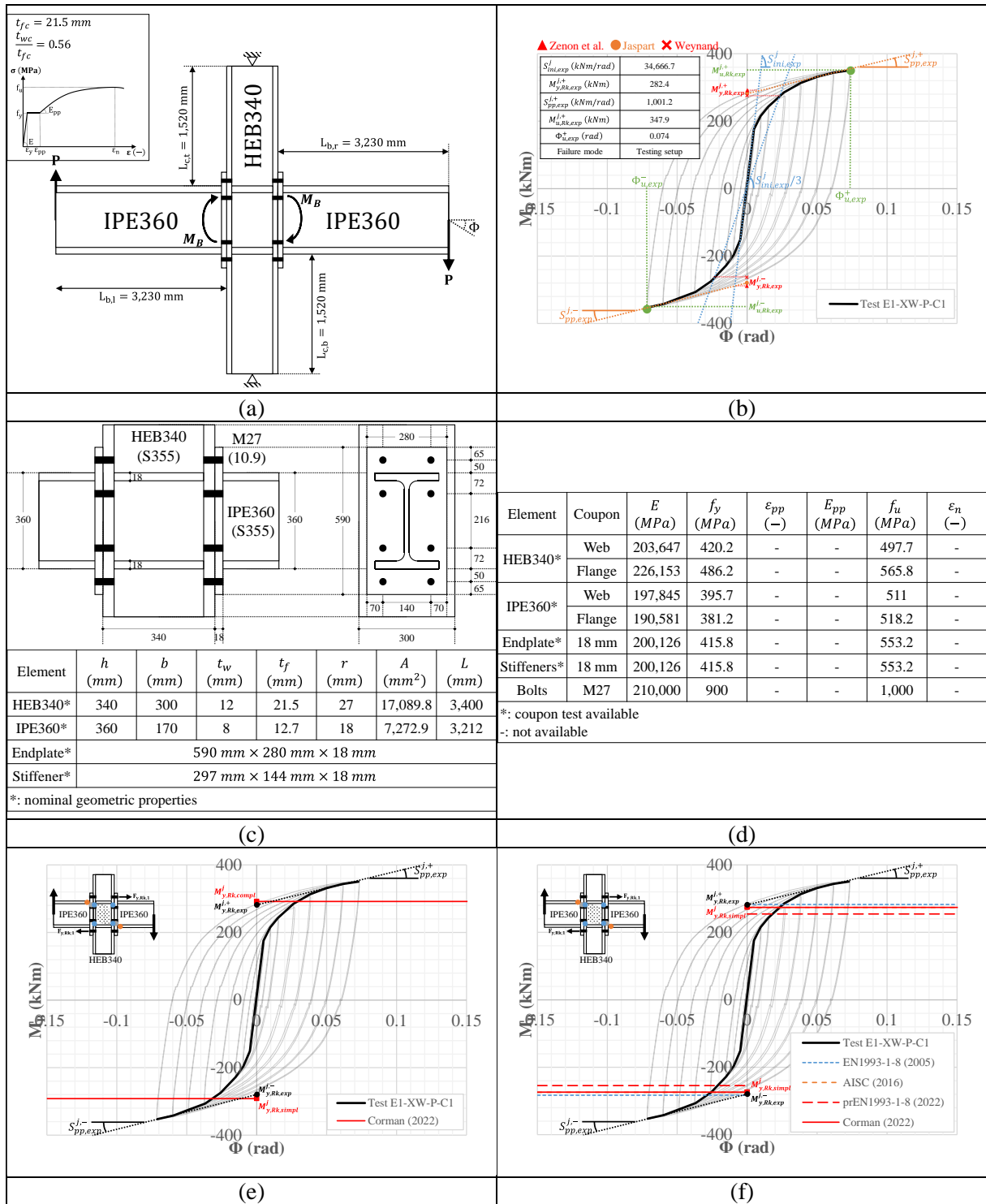


Fig. A-22. Experimental results for the bolted test E1-XW-P-C1: (a) experimental setup, (b) performance parameters, (c) geometric properties, (d) mechanical properties, (e) complex rigid plastic Corman model, (f) simplified rigid plastic models.

A.2.11 Test E2-TB-E-M

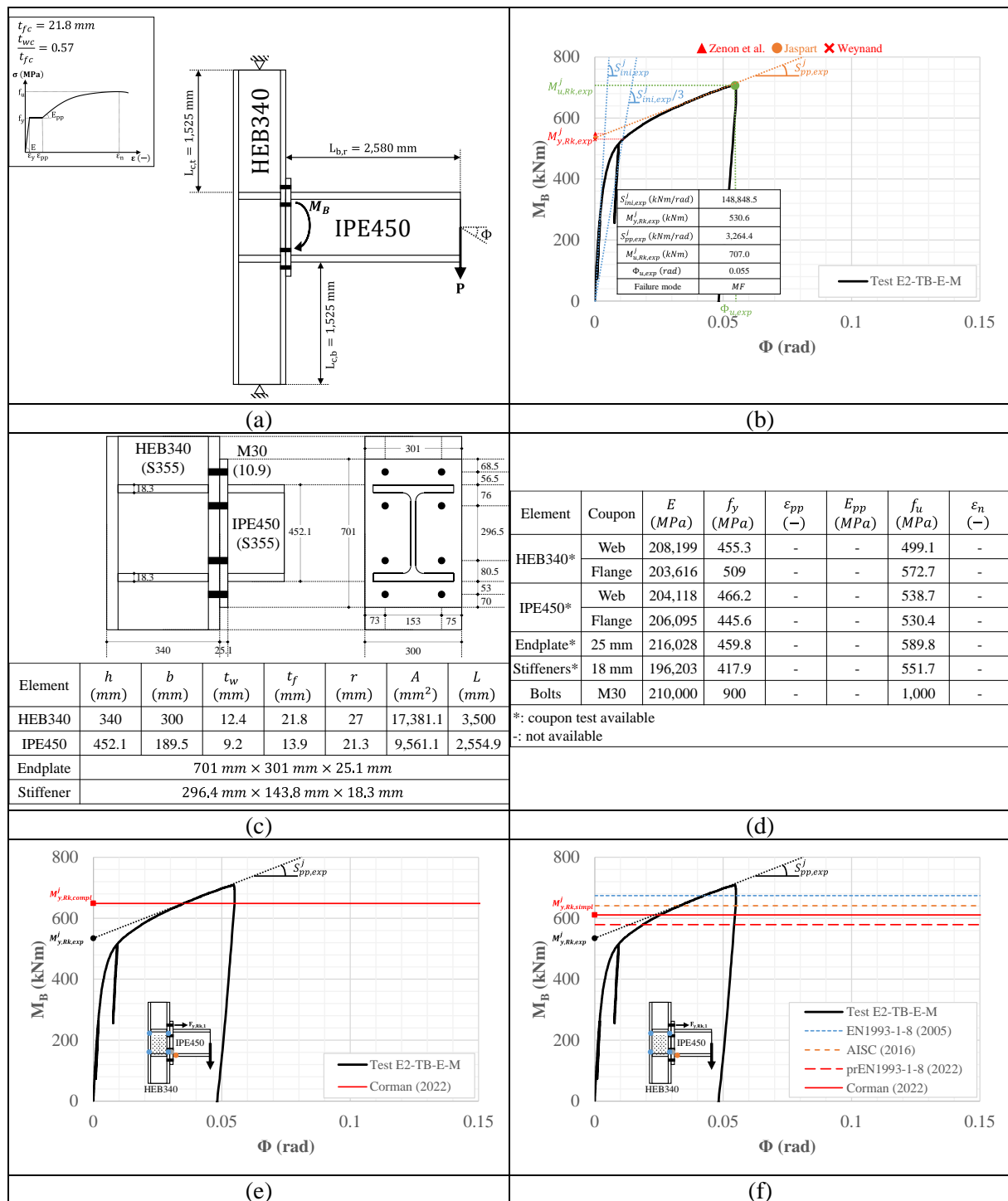


Fig. A-23. Experimental results for the bolted test E2-TB-E-M: (a) experimental setup, (b) performance parameters, (c) geometric properties, (d) mechanical properties, (e) complex rigid plastic Corman model, (f) simplified rigid plastic models.

A.2.12 Test E2-XW-P-C2

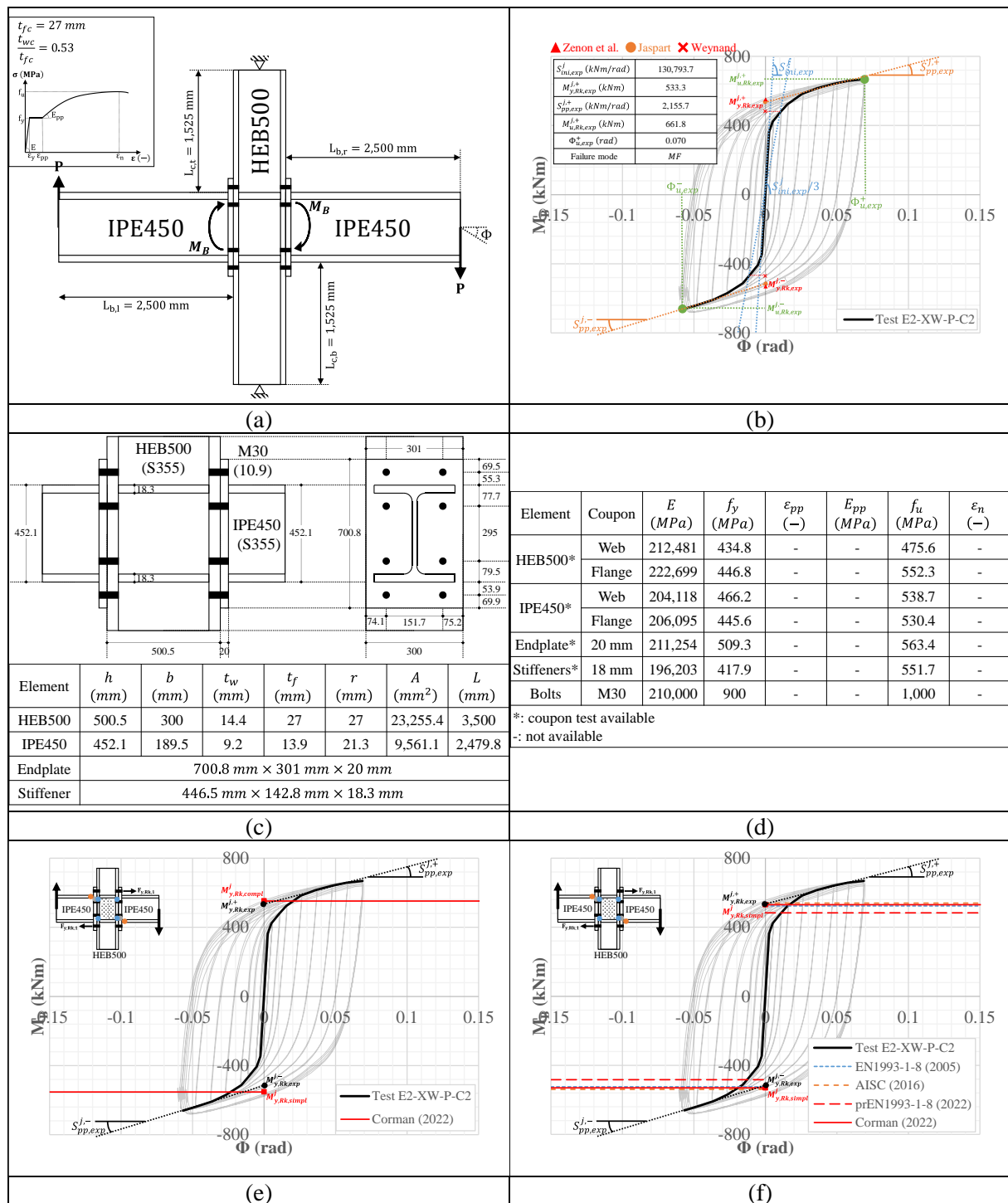


Fig. A-24. Experimental results for the bolted test E2-XW-P-C2: (a) experimental setup, (b) performance parameters, (c) geometric properties, (d) mechanical properties, (e) complex rigid plastic Corman model, (f) simplified rigid plastic models.

A.2.13 Test E3-TB-E-C2

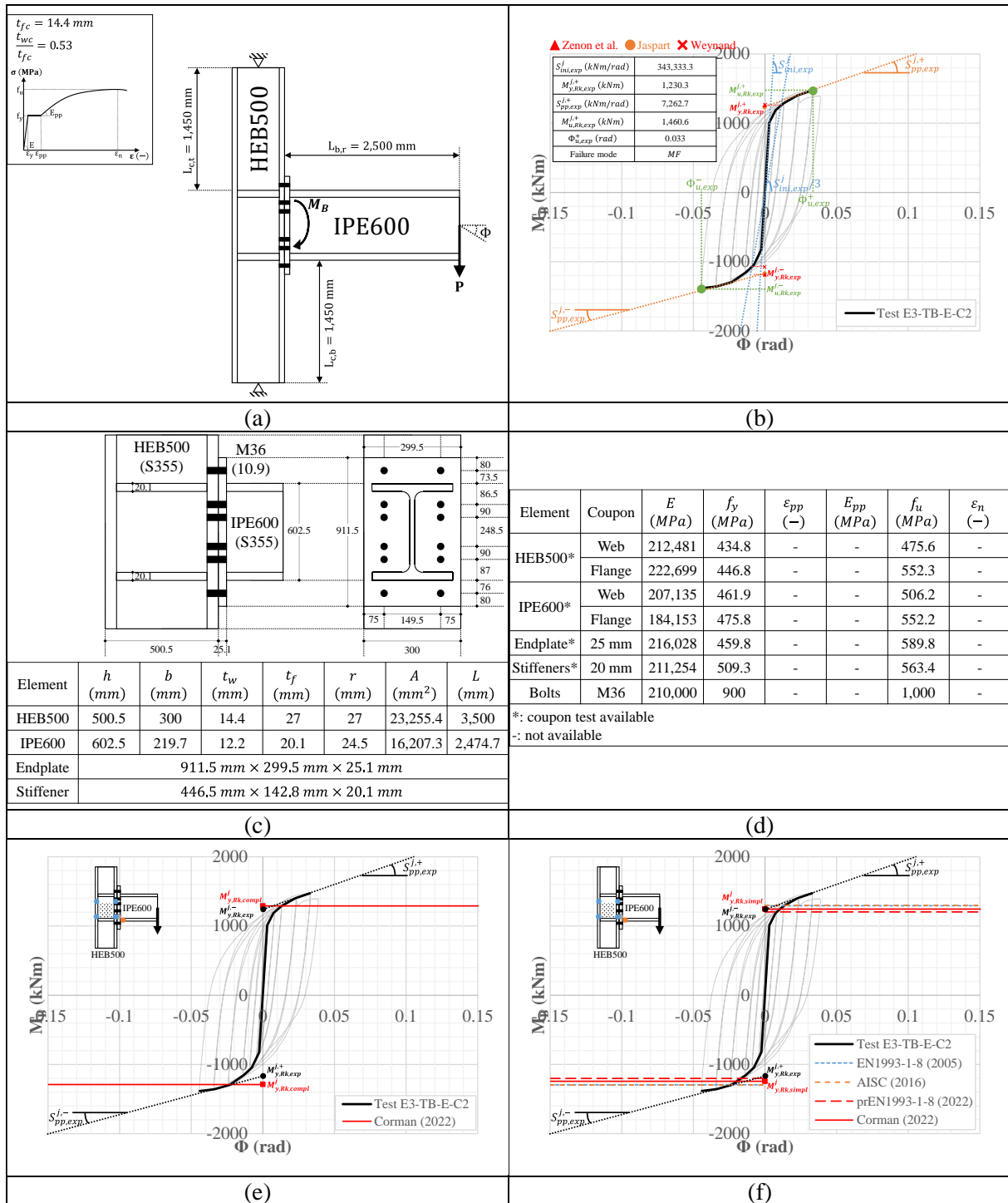


Fig. A-25. Experimental results for the bolted test E3-TB-E-C2: (a) experimental setup, (b) performance parameters, (c) geometric properties, (d) mechanical properties, (e) complex rigid plastic Corman model, (f) simplified rigid plastic models.

A.2.14 Test E3-XW-P-C2

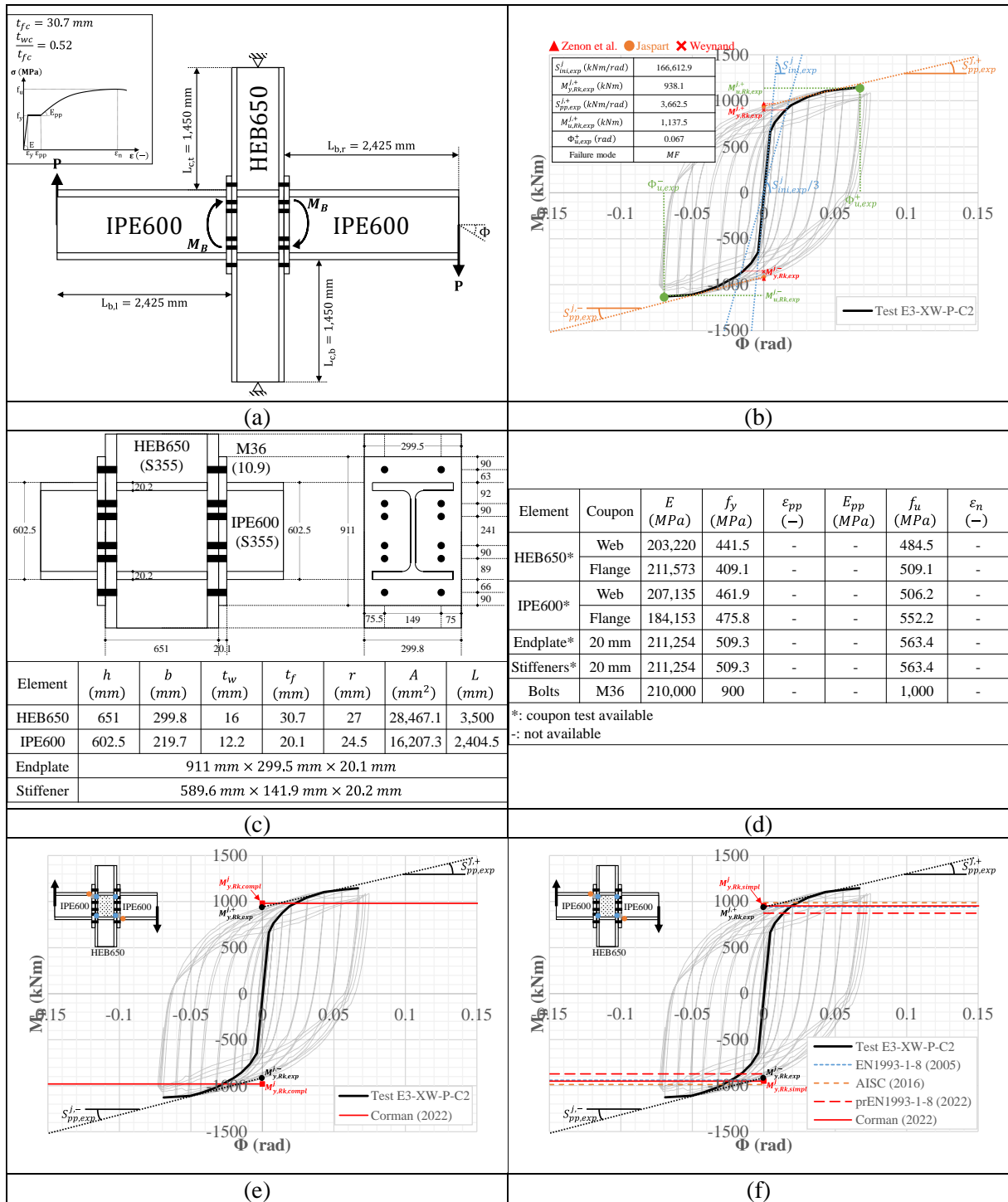


Fig. A-26. Experimental results for the bolted test E3-XW-P-C2: (a) experimental setup, (b) performance parameters, (c) geometric properties, (d) mechanical properties, (e) complex rigid plastic Corman model, (f) simplified rigid plastic models.

B. CHARACTERIZATION OF THE JOINT BEHAVIOUR FROM THE FE RESULTS

B.1 Extraction of the $(V - \gamma)_{num}$ deformation curves of the PZ, CWP and SE

B.1.1 Shear deformation γ of the PZ

The shear deformation γ^t of the PZ at each time step t of the numerical simulations can be expressed through Eq. (B-1) as the sum of two contributions, namely a rotation γ_1^t of the beam(s) axis with the horizontal and a rotation γ_2^t of the column axis with the vertical (see Fig. B-1(b)). These latter can be computed through Eq. (B-2) and Eq. (B-3), respectively, where d_b^* and d_c^* are the PZ depth and width (see Fig. B-1(a)) and where u_i^t , v_i^t and w_i^t are the displacement fields at time step t of the i^{th} predefined node (among the four nodes defined in Fig. B-1(a) and (b)). These displacement fields u_i^t , v_i^t and w_i^t can be extracted from Abaqus© using Eq. (B-4).

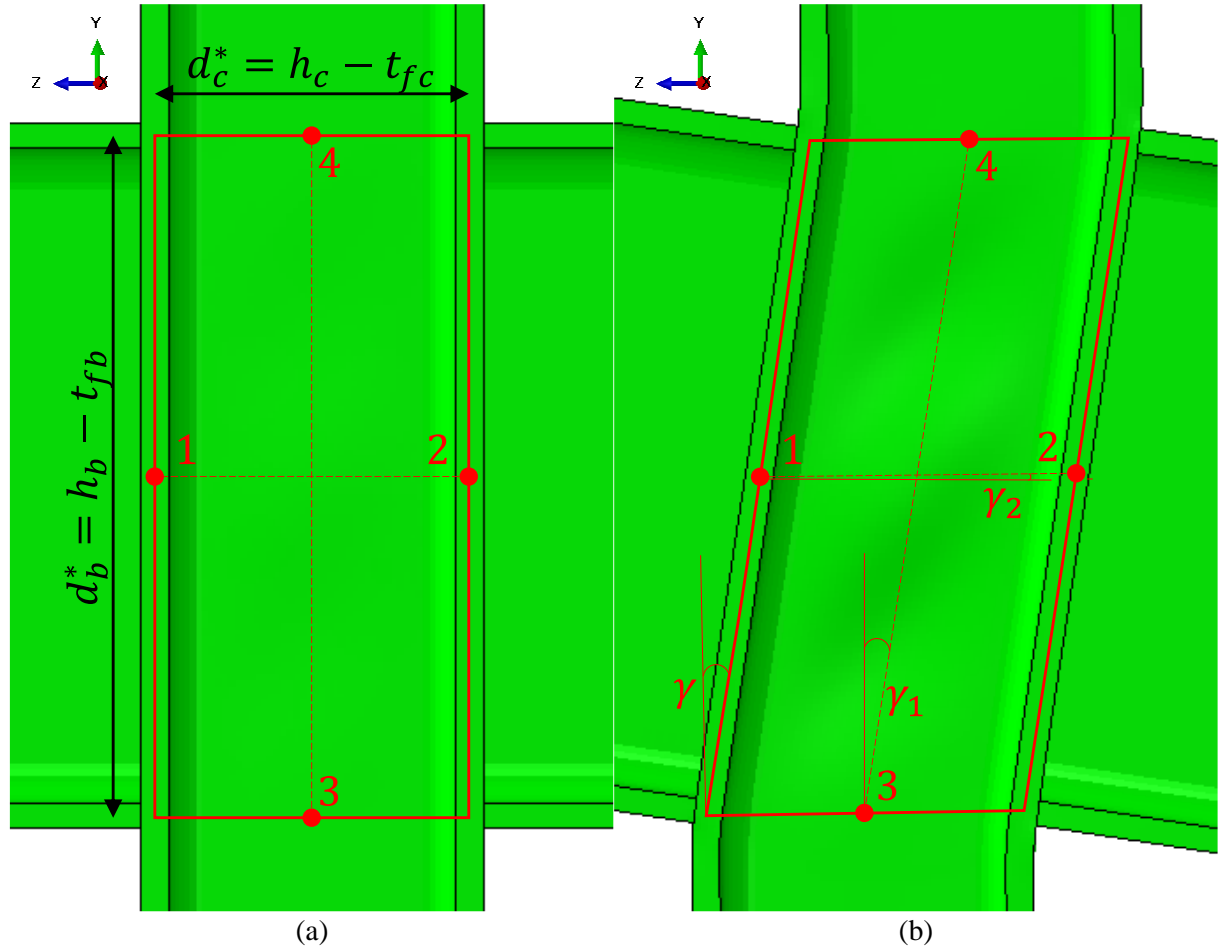


Fig. B-1. Description of the procedure for the extraction of the shear deformation γ : (a) numerical model in undeformed shape and (b) numerical model in deformed shape at time step t .

$$\gamma^t = \gamma_1^t + \gamma_2^t \quad (\text{B-1})$$

$$\gamma_1^t = \text{atan} \left(\frac{w_3^t - w_4^t}{d_b^* + v_4^t - v_3^t} \right) \quad (\text{B-2})$$

$$\gamma_2^t = \text{atan} \left(\frac{v_2^t - v_1^t}{d_c^* + w_1^t - w_2^t} \right) \quad (\text{B-3})$$

$$\begin{cases} u_i^t = x_i^t - x_i^0 \\ v_i^t = y_i^t - y_i^0 \\ w_i^t = z_i^t - z_i^0 \end{cases} \quad i = 1 \rightarrow 4 \quad (\text{B-4})$$

B.1.2 Equivalent shear force $V_{Ek,num}^{PZ}$ acting on the PZ

A. Introduction

The procedure of extraction of the equivalent shear force $V_{Ek,num}^{PZ}$ acting on the PZ from the FE results is relatively tedious in terms of mathematical developments. These latter are presented in the following Sections B and C for exterior and interior joints, respectively.

In these Sections, the exterior and interior welded joints considered in Chapter 4 and Chapter 5 are presented in undeformed (see Fig. B-2 and Fig. B-8, respectively) and deformed shapes (see Fig. B-3 and Fig. B-9, respectively). The system of internal forces acting on the PZ (see the blue arrows in Fig. B-2, Fig. B-3, Fig. B-8 and Fig. B-9) causes significant shear in the PZ, which leads to the shear deformation of the PZ. In Fig. B-3 and Fig. B-9, the shear angle γ between the beam(s) and column axes is the sum of two contributions, namely a rotation γ_1 of the beam(s) axis with the horizontal and a rotation γ_2 of the column axis with the vertical, as described in Section B.1.1. The angle between the diagonal and the lower side of the PZ is called α . Analytical expressions of the horizontal support reactions R are given in Table B-1 and Table B-4 as a function of the external load P , for exterior and interior joints, respectively. They are obtained by considering the moment equilibrium about the bottom support for the exterior joint and about the centre of the PZ for the interior joint. Similarly, analytical expressions of the internal forces acting on the PZ are reported in Table B-1 and Table B-4. They are obtained by considering that all the members surrounding the PZ (i.e. the lower and upper parts of the column, the right beam and the left beam, if any) are in a state of rotational and translational equilibrium.

To evaluate the equivalent shear force $V_{Ek,num}^{PZ}$ acting on the PZ (see the red arrows in Fig. B-2, Fig. B-3, Fig. B-8 and Fig. B-9), a simplified truss model has been used. This model is given in Fig. B-4 and Fig. B-5 for exterior joints and in Fig. B-10 and Fig. B-11 for interior joints, respectively. It consists of four hinges located at the corners “W”, “X”, “Y” and “Z” of the PZ. These nodes are connected together by means of four rigid links, which are named link No. 1 to link No. 4, and which model the contours “WX”, “XY”, “YZ” and “ZX” of the PZ. An additional diagonal link, named link No. 5, is used as bracing and carries internal shear force in the model.

This truss model is loaded through point loads at the nodes. Therefore, each M_B and M_C bending moment acting on the PZ is replaced by an equivalent couple of normal compressive and tensile forces. Shear and axial forces acting on a particular side of the PZ are divided by two, one half being assigned to each node surrounding the so-considered side of the PZ.

The whole truss model is in a state of rotational and translational equilibrium under the point loads applied to the nodes. Therefore, values of all N_1 to N_5 internal forces in the rigid links may be obtained by solving horizontal and vertical equilibrium equations at each node. Analytical expressions for these internal forces are given in Table B-2 for exterior joints and in Table B-5 for interior joints, as a function of the main parameters of the model, namely angles (α , γ , γ_1 and γ_2), geometrical dimensions (L_b , L_c , d_b^* and d_c^*) and external loads (N_c and P).

The equivalent shear force $V_{Ek,num}^{PZ,\parallel}$ (resp. $V_{Ek,num}^{PZ,\perp}$), acting on the horizontal (resp. vertical) edge of the PZ, is then simply obtained by projecting the internal axial force N_5 in the diagonal link No. 5 along the link No. 1 (resp. No. 4). This is shown in Fig. B-6 and Fig. B-7 for exterior joints and in Fig. B-12 and Fig. B-13 for interior joints. The 1st and 2nd order expressions of the equivalent shear force $V_{Ek,num}^{PZ,\parallel}$ (resp. $V_{Ek,num}^{PZ,\perp}$) acting on the horizontal (resp. vertical) edge of the PZ are provided in Table B-3 for exterior joints and in Table B-6 for interior joints, where they are expressed as a function of the main parameters of the model, namely angles (α , γ , γ_1 and γ_2), geometrical dimensions (L_b , L_c , d_b^* and d_c^*) and external loads (N_c and P).

Based on these expressions, it was possible to derive the shear force $V_{Ek,num}^{PZ,t}$ applied to the PZ at each time step t of the numerical simulations. Knowing the shear deformation γ^t at each time step t (see Eq. (B-1)) allowed to derive the PZ deformation curve $(V^{PZ} - \gamma)_{num}$ for each of the 32 numerical simulations. The results obtained with the fictitious elastic, perfectly-plastic material law are presented in APPENDIX A for each numerical simulation (see the blue solid curves in Fig. C-1(c) to Fig. C-32(c)). The results obtained with the full-range material law are presented in APPENDIX A for each numerical simulation (see the blue solid curves in Fig. C-1(d) to Fig. C-32(d)).

B. Exterior joints

Table B-1. Determination of the internal forces acting on the PZ of an exterior joint.

		Internal forces acting on the PZ	
		Undeformed configuration (1 st order)	Deformed configuration (2 nd order)
		<p>Fig. B-2. Exterior joint in undeformed shape.</p>	<p>Fig. B-3. Exterior joint in deformed shape.</p>
		Horizontal support reactions	
R		$\frac{P}{2} \cdot \frac{2 \cdot L_b + d_c^*}{L_c}$	$\frac{P}{2} \cdot \frac{2 \cdot L_b \cdot \cos \gamma_1 + d_c^* \cdot \cos \gamma_2 + d_b^* \cdot \sin \gamma_1 - (L_c - d_b^*) \cdot \sin \gamma_2}{(L_c - d_b^*) \cdot \cos \gamma_2 + d_b^* \cdot \cos \gamma_1} - N_c \cdot \frac{(L_c - d_b^*) \cdot \sin \gamma_2 - d_b^* \cdot \sin \gamma_1}{(L_c - d_b^*) \cdot \cos \gamma_2 + d_b^* \cdot \cos \gamma_1}$
		Internal forces	
N_{BL}/N_{BR}	/	0	$-P \cdot \sin \gamma_1$
V_{BL}/V_{BR}	/	P	$P \cdot \cos \gamma_1$
M_{BL}/M_{BR}	/	$P \cdot L_b$	$P \cdot L_b \cdot \cos \gamma_1$
N_{CT}/N_{CB}	N_c	$P + N_c$	$N_c \cdot \cos \gamma_2 - R \cdot \sin \gamma_2$ $(P + N_c) \cdot \cos \gamma_2 - R \cdot \sin \gamma_2$
V_{CT}/V_{CB}	R	R	$R \cdot \cos \gamma_2 + N_c \cdot \sin \gamma_2$ $R \cdot \cos \gamma_2 + (P + N_c) \cdot \sin \gamma_2$
M_{CT}/M_{CB}	$R \cdot \frac{L_c - d_b^*}{2}$	$R \cdot \frac{L_c - d_b^*}{2}$	$R \cdot \frac{L_c - d_b^*}{2} \cdot \cos \gamma_2 + N_c \cdot \frac{L_c - d_b^*}{2} \cdot \sin \gamma_2$ $[R \cdot \cos \gamma_2 + (P + N_c) \cdot \sin \gamma_2] \cdot \frac{L_c - d_b^*}{2}$

Table B-2. Determination of the axial forces acting in the equivalent truss model of the PZ in an exterior joint.

Equivalent truss model		
	Undeformed configuration (1 st order)	Deformed configuration (2 nd order)
	Fig. B-4. Equivalent truss model of the PZ for the exterior joint in undeformed shape.	Fig. B-5. Equivalent truss model of the PZ for the exterior joint in deformed shape.
Axial forces in the truss model: computation		
Node W		
\hat{X} :	$N_1 - \frac{V_{CT}}{2} = 0$ $\Leftrightarrow N_1 = \frac{V_{CT}}{2}$ $\Leftrightarrow N_1 = \frac{R}{2}$	$N_1 \cdot \cos \gamma - \frac{V_{CT}}{2} \cdot \cos \gamma + \left(\frac{M_{CT}}{d_c^*} + \frac{N_{CT}}{2} \right) \cdot \sin \gamma = 0$ $\Leftrightarrow N_1 = \frac{V_{CT}}{2} - \left(\frac{M_{CT}}{d_c^*} + \frac{N_{CT}}{2} \right) \cdot \tan \gamma$ $\Leftrightarrow N_1 = \frac{R}{2} \cdot \cos \gamma_2 \cdot \left[1 - \frac{L_c - d_b^*}{d_c^*} \cdot \tan \gamma + \tan \gamma_2 \cdot \tan \gamma \right] + \frac{N_c}{2} \cdot \sin \gamma_2 \cdot \left[1 - \frac{L_c - d_b^*}{d_c^*} \cdot \tan \gamma - \cot \gamma_2 \cdot \tan \gamma \right]$
\hat{Y} :	$-N_4 - \left(\frac{M_{CT}}{d_c^*} + \frac{N_{CT}}{2} \right) = 0$ $\Leftrightarrow N_4 = - \left(\frac{M_{CT}}{d_c^*} + \frac{N_{CT}}{2} \right)$	$-N_4 \cdot \cos \gamma - \left(\frac{M_{CT}}{d_c^*} + \frac{N_{CT}}{2} \right) = 0$ $\Leftrightarrow N_4 = - \left(\frac{M_{CT}}{d_c^*} + \frac{N_{CT}}{2} \right) \cdot \sec \gamma$

	$\Leftrightarrow N_4 = -\frac{R}{2} \cdot \frac{L_c - d_b^*}{d_c^*} - \frac{N_c}{2}$	$\Leftrightarrow N_4 = \frac{R}{2} \cdot \sin \gamma_2 \cdot \sec \gamma \cdot \left[1 - \frac{L_c - d_b^*}{d_c^*} \cdot \cot \gamma_2 \right] - \frac{N_c}{2} \cdot \cos \gamma_2 \cdot \sec \gamma \cdot \left[1 + \frac{L_c - d_b^*}{d_c^*} \cdot \tan \gamma_2 \right]$
Node Y		
\hat{X} :	$-N_3 + \frac{V_{CB}}{2} - \left(\frac{M_{BR}}{d_b^*} + \frac{N_{BR}}{2} \right) = 0$ $\Leftrightarrow N_3 = \frac{V_{CB}}{2} - \left(\frac{M_{BR}}{d_b^*} + \frac{N_{BR}}{2} \right)$ $\Leftrightarrow N_3 = -P \cdot \frac{L_b}{d_b^*} + \frac{R}{2}$	$-N_3 \cdot \cos \gamma + \frac{V_{CB}}{2} \cdot \cos \gamma - \left(\frac{M_{CB}}{d_c^*} + \frac{N_{CB}}{2} \right) \cdot \sin \gamma - \left(\frac{M_{BR}}{d_b^*} + \frac{N_{BR}}{2} \right) = 0$ $\Leftrightarrow N_3 = \frac{V_{CB}}{2} - \left(\frac{M_{CB}}{d_c^*} + \frac{N_{CB}}{2} \right) \cdot \tan \gamma - \left(\frac{M_{BR}}{d_b^*} + \frac{N_{BR}}{2} \right) \cdot \sec \gamma$ $\Leftrightarrow N_3 = \frac{P}{2} \cdot \sin \gamma_2 \cdot \left[1 - \frac{L_c - d_b^*}{d_c^*} \cdot \tan \gamma - \cot \gamma_2 \cdot \tan \gamma \right] + \frac{P}{2} \cdot \sin \gamma_1 \cdot \sec \gamma \cdot \left[1 - 2 \cdot \frac{L_b}{d_b^*} \cdot \cot \gamma_1 \right] + \frac{R}{2} \cdot \cos \gamma_2 \cdot \left[1 - \frac{L_c - d_b^*}{d_c^*} \cdot \tan \gamma + \tan \gamma_2 \cdot \tan \gamma \right] + \frac{N_c}{2} \cdot \sin \gamma_2 \cdot \left[1 - \frac{L_c - d_b^*}{d_c^*} \cdot \tan \gamma - \cot \gamma_2 \cdot \tan \gamma \right]$
\hat{Y} :	$N_2 - \frac{V_{BR}}{2} + \left(\frac{M_{CB}}{d_c^*} + \frac{N_{CB}}{2} \right) = 0$ $\Leftrightarrow N_2 = \frac{V_{BR}}{2} - \left(\frac{M_{CB}}{d_c^*} + \frac{N_{CB}}{2} \right)$ $\Leftrightarrow N_2 = -\frac{R}{2} \cdot \frac{L_c - d_b^*}{d_c^*} - \frac{N_c}{2}$	$N_2 \cdot \cos \gamma - \frac{V_{BR}}{2} \cdot \cos \gamma + \left(\frac{M_{BR}}{d_b^*} + \frac{N_{BR}}{2} \right) \cdot \sin \gamma + \left(\frac{M_{CB}}{d_c^*} + \frac{N_{CB}}{2} \right) = 0$ $\Leftrightarrow N_2 = \frac{V_{BR}}{2} - \left(\frac{M_{BR}}{d_b^*} + \frac{N_{BR}}{2} \right) \cdot \tan \gamma - \left(\frac{M_{CB}}{d_c^*} + \frac{N_{CB}}{2} \right) \cdot \sec \gamma$ $\Leftrightarrow N_2 = \frac{P}{2} \cdot \cos \gamma_1 \cdot \left[1 - 2 \cdot \frac{L_b}{d_b^*} \cdot \tan \gamma + \tan \gamma_1 \cdot \tan \gamma \right] - \frac{P}{2} \cdot \cos \gamma_2 \cdot \sec \gamma \cdot \left[1 + \frac{L_c - d_b^*}{d_c^*} \cdot \tan \gamma_2 \right] + \frac{R}{2} \cdot \sin \gamma_2 \cdot \sec \gamma \cdot \left[1 - \frac{L_c - d_b^*}{d_c^*} \cdot \cot \gamma_2 \right] - \frac{N_c}{2} \cdot \cos \gamma_2 \cdot \sec \gamma \cdot \left[1 + \frac{L_c - d_b^*}{d_c^*} \cdot \tan \gamma_2 \right]$
Node Z		
\hat{X} :	$N_3 + \frac{V_{CB}}{2} + N_{5,x} \cdot \cos \alpha = 0$ $\Leftrightarrow N_{5,x} = \sec \alpha \cdot \left[-V_{CB} + \left(\frac{M_{BR}}{d_b^*} + \frac{N_{BR}}{2} \right) \right]$ $\Leftrightarrow N_{5,x} = \sec \alpha \cdot \left[P \cdot \frac{L_b}{d_b^*} - R \right]$	$N_3 \cdot \cos \gamma + \frac{V_{CB}}{2} \cdot \cos \gamma + N_{5,x} \cdot \cos(\alpha + \gamma) + \left(\frac{M_{CB}}{d_c^*} - \frac{N_{CB}}{2} \right) \cdot \sin \gamma = 0$ $\Leftrightarrow N_{5,x} = \sec(\alpha + \gamma) \cdot \left[-V_{CB} \cdot \cos \gamma + N_{CB} \cdot \sin \gamma + \left(\frac{M_{BR}}{d_b^*} + \frac{N_{BR}}{2} \right) \right]$ $\Leftrightarrow N_{5,x} = \sec(\alpha + \gamma) \cdot \left[\frac{P}{2} \cdot \sin \gamma_1 + P \cdot \frac{L_b}{d_b^*} \cdot \cos \gamma_1 - R \cdot \cos \gamma_1 + N_c \cdot \sin \gamma_1 \right]$

\hat{Y} :	$N_4 + N_{5,y} \cdot \sin \alpha - \left(\frac{M_{CB}}{d_b^*} - \frac{N_{CB}}{2} \right) = 0$ $\Leftrightarrow N_{5,y} = \csc \alpha \cdot \left[\left(\frac{M_{CB}}{d_c^*} - \frac{N_{CB}}{2} \right) + \left(\frac{M_{CT}}{d_c^*} + \frac{N_{CT}}{2} \right) \right]$ $\Leftrightarrow N_{5,y} = \csc \alpha \cdot \left[-\frac{P}{2} + R \cdot \frac{L_c - d_b^*}{d_c^*} \right]$	$N_4 \cdot \cos \gamma + N_{5,y} \cdot \sin \alpha - \left(\frac{M_{CB}}{d_c^*} - \frac{N_{CB}}{2} \right) = 0$ $\Leftrightarrow N_{5,y} = \csc \alpha \cdot \left[\left(\frac{M_{CB}}{d_c^*} - \frac{N_{CB}}{2} \right) + \left(\frac{M_{CT}}{d_c^*} + \frac{N_{CT}}{2} \right) \right]$ $\Leftrightarrow N_{5,y} = \csc \alpha \cdot \left[-\frac{P}{2} \cdot \cos \gamma_2 \cdot \left(1 - \frac{L_c - d_b^*}{d_c^*} \cdot \tan \gamma_2 \right) + R \cdot \frac{L_c - d_b^*}{d_c^*} \cdot \cos \gamma_2 + N_c \cdot \frac{L_c - d_b^*}{d_c^*} \cdot \sin \gamma_2 \right]$
Check:	$N_{5,x} = N_{5,y}$ $\Leftrightarrow \sec \alpha \cdot \left[P \cdot \frac{L_b}{d_b^*} - R \right] = \csc \alpha \cdot \left[-\frac{P}{2} + R \cdot \frac{L_c - d_b^*}{d_c^*} \right]$ $\Leftrightarrow P \cdot \frac{L_b}{d_b^*} - R = \frac{\csc \alpha}{\sec \alpha} \cdot \left[-\frac{P}{2} + R \cdot \frac{L_c - d_b^*}{d_c^*} \right]$ $\frac{\csc \alpha \cdot d_c^*}{\sec \alpha \cdot d_b^*}$ $\Leftrightarrow P \cdot \frac{L_b}{d_b^*} - R = -\frac{P}{2} \cdot \frac{d_c^*}{d_b^*} + R \cdot \frac{L_c - d_b^*}{d_b^*}$ $\Leftrightarrow \frac{P}{2} \cdot [2 \cdot L_b + d_c^*] - R \cdot L_c = 0$ $\frac{\text{inject } R}{\Leftrightarrow} \frac{P}{2} \cdot [2 \cdot L_b + d_c^*] - \frac{P}{2} \cdot [2 \cdot L_b + d_c^*] = 0$ $\frac{\text{OK!}}{\Leftrightarrow} 0 \stackrel{\text{OK!}}{=} 0$	$N_{5,x} = N_{5,y}$ $\Leftrightarrow \sec(\alpha + \gamma) \cdot \left[\frac{P}{2} \cdot \sin \gamma_1 + P \cdot \frac{L_b}{d_b^*} \cdot \cos \gamma_1 - R \cdot \cos \gamma_1 + N_c \cdot \sin \gamma_1 \right] = \csc \alpha \cdot \left[-\frac{P}{2} \cdot \cos \gamma_2 \cdot \left(1 - \frac{L_c - d_b^*}{d_c^*} \cdot \tan \gamma_2 \right) + R \cdot \frac{L_c - d_b^*}{d_c^*} \cdot \cos \gamma_2 + N_c \cdot \frac{L_c - d_b^*}{d_c^*} \cdot \sin \gamma_2 \right]$ $\Leftrightarrow \frac{P}{2} \cdot \sin \gamma_1 + P \cdot \frac{L_b}{d_b^*} \cdot \cos \gamma_1 - R \cdot \cos \gamma_1 + N_c \cdot \sin \gamma_1 = \frac{\csc \alpha}{\sec(\alpha + \gamma)} \cdot \left[-\frac{P}{2} \cdot \cos \gamma_2 \cdot \left(1 - \frac{L_c - d_b^*}{d_c^*} \cdot \tan \gamma_2 \right) + R \cdot \frac{L_c - d_b^*}{d_c^*} \cdot \cos \gamma_2 + N_c \cdot \frac{L_c - d_b^*}{d_c^*} \cdot \sin \gamma_2 \right]$ $\frac{\csc \alpha}{\sec(\alpha + \gamma)} \cdot \frac{d_c^*}{d_b^*}$ $\Leftrightarrow \frac{P}{2} \cdot \sin \gamma_1 + P \cdot \frac{L_b}{d_b^*} \cdot \cos \gamma_1 - R \cdot \cos \gamma_1 + N_c \cdot \sin \gamma_1 = -\frac{P}{2} \cdot \frac{d_c^*}{d_b^*} \cdot \cos \gamma_2 \cdot \left(1 - \frac{L_c - d_b^*}{d_c^*} \cdot \tan \gamma_2 \right) + R \cdot \frac{L_c - d_b^*}{d_b^*} \cdot \cos \gamma_2 + N_c \cdot \frac{L_c - d_b^*}{d_b^*} \cdot \sin \gamma_2$ $\Leftrightarrow \frac{P}{2} \cdot [d_b^* \cdot \sin \gamma_1 + 2 \cdot L_b \cdot \cos \gamma_1 + d_c^* \cdot \cos \gamma_2 - (L_c - d_b^*) \cdot \sin \gamma_2] - R \cdot [d_b^* \cdot \cos \gamma_1 + (L_c - d_b^*) \cdot \cos \gamma_2] - N_c \cdot [(L_c - d_b^*) \cdot \sin \gamma_2 - d_b^* \cdot \sin \gamma_1] = 0$ $\frac{\text{inject } R}{\Leftrightarrow} \frac{P}{2} \cdot [d_b^* \cdot \sin \gamma_1 + 2 \cdot L_b \cdot \cos \gamma_1 + d_c^* \cdot \cos \gamma_2 - (L_c - d_b^*) \cdot \sin \gamma_2] - \frac{P}{2} \cdot [d_b^* \cdot \sin \gamma_1 + 2 \cdot L_b \cdot \cos \gamma_1 + d_c^* \cdot \cos \gamma_2 - (L_c - d_b^*) \cdot \sin \gamma_2] + N_c \cdot [(L_c - d_b^*) \cdot \sin \gamma_2 - d_b^* \cdot \sin \gamma_1] - N_c \cdot [(L_c - d_b^*) \cdot \sin \gamma_2 - d_b^* \cdot \sin \gamma_1] = 0$ $\frac{\text{OK!}}{\Leftrightarrow} 0 \stackrel{\text{OK!}}{=} 0$
Node X		
\hat{X} :	$-N_1 - \frac{V_{CT}}{2} - N_{5,x} \cdot \cos \alpha + \left(\frac{M_{BR}}{d_b^*} - \frac{N_{BR}}{2} \right) = 0$ $\Leftrightarrow N_{5,x} = \sec \alpha \cdot \left[-V_{CT} + \left(\frac{M_{BR}}{d_b^*} - \frac{N_{BR}}{2} \right) \right]$ $\Leftrightarrow N_{5,x} = \sec \alpha \cdot \left[P \cdot \frac{L_b}{d_b^*} - R \right]$	$-N_1 \cdot \cos \gamma - \frac{V_{CT}}{2} \cdot \cos \gamma - N_{5,x} \cdot \cos(\alpha + \gamma) - \left(\frac{M_{CT}}{d_c^*} - \frac{N_{CT}}{2} \right) \cdot \sin \gamma + \left(\frac{M_{BR}}{d_b^*} - \frac{N_{BR}}{2} \right) = 0$ $\Leftrightarrow N_{5,x} = \sec(\alpha + \gamma) \cdot \left[-V_{CT} \cdot \cos \gamma + N_{CT} \cdot \sin \gamma + \left(\frac{M_{BR}}{d_b^*} - \frac{N_{BR}}{2} \right) \right]$ $\Leftrightarrow N_{5,x} = \sec(\alpha + \gamma) \cdot \left[\frac{P}{2} \cdot \sin \gamma_1 + P \cdot \frac{L_b}{d_b^*} \cdot \cos \gamma_1 - R \cdot \cos \gamma_1 + N_c \cdot \sin \gamma_1 \right]$

\hat{Y} :	$-N_2 - \frac{V_{BR}}{2} - N_{5,y} \cdot \sin \alpha + \left(\frac{M_{CT}}{d_c^*} - \frac{N_{CT}}{2} \right) = 0$ $\Leftrightarrow N_{5,y} = \csc \alpha \cdot \left[-V_{BR} + \left(\frac{M_{CB}}{d_c^*} + \frac{N_{CB}}{2} \right) + \left(\frac{M_{CT}}{d_c^*} - \frac{N_{CT}}{2} \right) \right]$ $\Leftrightarrow N_{5,y} = \csc \alpha \cdot \left[-\frac{P}{2} + R \cdot \frac{L_c - d_b^*}{d_c^*} \right]$	$-N_2 \cdot \cos \gamma - \frac{V_{BR}}{2} \cdot \cos \gamma - N_{5,y} \cdot \sin \alpha - \left(\frac{M_{BR}}{d_b^*} - \frac{N_{BR}}{2} \right) \cdot \sin \gamma + \left(\frac{M_{CT}}{d_c^*} - \frac{N_{CT}}{2} \right) = 0$ $\Leftrightarrow N_{5,y} = \csc \alpha \cdot \left[-V_{BR} \cdot \cos \gamma + N_{BR} \cdot \sin \gamma + \left(\frac{M_{CB}}{d_c^*} + \frac{N_{CB}}{2} \right) + \left(\frac{M_{CT}}{d_c^*} - \frac{N_{CT}}{2} \right) \right]$ $\Leftrightarrow N_{5,y} = \csc \alpha \cdot \left[-\frac{P}{2} \cdot \cos \gamma_2 \cdot \left(1 - \frac{L_c - d_b^*}{d_c^*} \cdot \tan \gamma_2 \right) + R \cdot \frac{L_c - d_b^*}{d_c^*} \cdot \cos \gamma_2 + N_c \cdot \frac{L_c - d_b^*}{d_c^*} \cdot \sin \gamma_2 \right]$
Check:	<i>Similar to node Z</i>	<i>Similar to node Z</i>
Axial forces in the truss model: summary		
N_1	$\frac{R}{2}$	$\frac{R}{2} \cdot \cos \gamma_2 \cdot \left[1 - \frac{L_c - d_b^*}{d_c^*} \cdot \tan \gamma + \tan \gamma_2 \cdot \tan \gamma \right]$ $+ \frac{N_c}{2} \cdot \sin \gamma_2 \cdot \left[1 - \frac{L_c - d_b^*}{d_c^*} \cdot \tan \gamma - \cot \gamma_2 \cdot \tan \gamma \right]$
N_2	$-\frac{R}{2} \cdot \frac{L_c - d_b^*}{d_c^*} - \frac{N_c}{2}$	$\frac{P}{2} \cdot \cos \gamma_1 \cdot \left[1 - 2 \cdot \frac{L_b}{d_b^*} \cdot \tan \gamma + \tan \gamma_1 \cdot \tan \gamma \right]$ $- \frac{P}{2} \cdot \cos \gamma_2 \cdot \sec \gamma \cdot \left[1 + \frac{L_c - d_b^*}{d_c^*} \cdot \tan \gamma_2 \right]$ $+ \frac{R}{2} \cdot \sin \gamma_2 \cdot \sec \gamma \cdot \left[1 - \frac{L_c - d_b^*}{d_c^*} \cdot \cot \gamma_2 \right]$ $- \frac{N_c}{2} \cdot \cos \gamma_2 \cdot \sec \gamma \cdot \left[1 + \frac{L_c - d_b^*}{d_c^*} \cdot \tan \gamma_2 \right]$
N_3	$-P \cdot \frac{L_b}{d_b^*} + \frac{R}{2}$	$\frac{P}{2} \cdot \sin \gamma_2 \cdot \left[1 - \frac{L_c - d_b^*}{d_c^*} \cdot \tan \gamma - \cot \gamma_2 \cdot \tan \gamma \right]$ $+ \frac{P}{2} \cdot \sin \gamma_1 \cdot \sec \gamma \cdot \left[1 - 2 \cdot \frac{L_b}{d_b^*} \cdot \cot \gamma_1 \right]$ $\frac{R}{2} \cdot \cos \gamma_2 \cdot \left[1 - \frac{L_c - d_b^*}{d_c^*} \cdot \tan \gamma + \tan \gamma_2 \cdot \tan \gamma \right]$ $+ \frac{N_c}{2} \cdot \sin \gamma_2 \cdot \left[1 - \frac{L_c - d_b^*}{d_c^*} \cdot \tan \gamma - \cot \gamma_2 \cdot \tan \gamma \right]$
N_4	$-\frac{R}{2} \cdot \frac{L_c - d_b^*}{d_c^*} - \frac{N_c}{2}$	$\frac{R}{2} \cdot \sin \gamma_2 \cdot \sec \gamma \cdot \left[1 - \frac{L_c - d_b^*}{d_c^*} \cdot \cot \gamma_2 \right]$ $- \frac{N_c}{2} \cdot \cos \gamma_2 \cdot \sec \gamma \cdot \left[1 + \frac{L_c - d_b^*}{d_c^*} \cdot \tan \gamma_2 \right]$
N_5	$\begin{cases} \sec \alpha \cdot \left[P \cdot \frac{L_b}{d_b^*} - R \right] \\ \csc \alpha \cdot \left[-\frac{P}{2} + R \cdot \frac{L_c - d_b^*}{d_c^*} \right] \end{cases}$	$\begin{cases} \sec(\alpha + \gamma) \cdot \left[\frac{P}{2} \cdot \sin \gamma_1 + P \cdot \frac{L_b}{d_b^*} \cdot \cos \gamma_1 - R \cdot \cos \gamma_1 + N_c \cdot \sin \gamma_1 \right] \\ \csc \alpha \cdot \left[-\frac{P}{2} \cdot \cos \gamma_2 \cdot \left(1 - \frac{L_c - d_b^*}{d_c^*} \cdot \tan \gamma_2 \right) + R \cdot \frac{L_c - d_b^*}{d_c^*} \cdot \cos \gamma_2 + N_c \cdot \frac{L_c - d_b^*}{d_c^*} \cdot \sin \gamma_2 \right] \end{cases}$

Table B-3. Determination of the equivalent shear force $V_{Ek,num}^{PZ}$ acting on the PZ of an exterior joint.

Determination of the equivalent shear force $V_{Ek,num}^{PZ}$ acting on the PZ		
	Undeformed configuration (1 st order)	Deformed configuration (2 nd order)
	<p>Fig. B-6. Geometric relationship between N_5 and $V_{Ek,num}^{PZ, }$ (resp. $V_{Ek,num}^{PZ,\perp}$) for the exterior joint in undeformed shape.</p>	<p>Fig. B-7. Geometric relationship between N_5 and $V_{Ek,num}^{PZ, }$ (resp. $V_{Ek,num}^{PZ,\perp}$) for the exterior joint in deformed shape.</p>
$V_{Ek,num}^{PZ, }$	$= \cos \alpha \cdot N_5$ $= \left[P \cdot \frac{L_b}{d_b^*} - R \right]$ $= \frac{P}{2} \cdot \frac{1}{d_b^*} \cdot \frac{2 \cdot L_b \cdot L_c - 2 \cdot L_b \cdot d_b^* - d_c^* \cdot d_b^*}{L_c} \quad (\text{B-5})$	$= \frac{\cos(\alpha+\gamma)}{\cos \gamma} \cdot N_5$ $= \frac{1}{\cos \gamma} \cdot \left[\frac{P}{2} \cdot \sin \gamma_1 + P \cdot \frac{L_b}{d_b^*} \cdot \cos \gamma_1 - R \cdot \cos \gamma_1 + N_c \cdot \sin \gamma_1 \right]$ $= \frac{P}{2} \cdot \frac{\cos \gamma_1 \cdot \cos \gamma_2}{\cos \gamma} \cdot \frac{1}{d_b^*} \cdot \frac{2 \cdot L_b \cdot L_c - 2 \cdot L_b \cdot d_b^* - d_c^* \cdot d_b^* + d_b^* \cdot (L_c - d_b^*) \cdot (\tan \gamma_2 + \tan \gamma_1)}{(L_c - d_b^*) \cdot \cos \gamma_2 + d_b^* \cdot \cos \gamma_1}$ $+ N_c \cdot \tan \gamma \cdot \frac{L_c - d_b^*}{(L_c - d_b^*) \cdot \cos \gamma_2 + d_b^* \cdot \cos \gamma_1} \quad (\text{B-6})$
$V_{Ek,num}^{PZ,\perp}$	$= \sin \alpha \cdot N_5$ $= \left[-\frac{P}{2} + R \cdot \frac{L_c - d_b^*}{d_c^*} \right]$ $= \frac{P}{2} \cdot \frac{1}{d_c^*} \cdot \frac{2 \cdot L_b \cdot L_c - 2 \cdot L_b \cdot d_b^* - d_c^* \cdot d_b^*}{L_c}$ $= V_{Ek,num}^{PZ, } \cdot \frac{d_b^*}{d_c^*} \quad (\text{B-7})$	$= \frac{\sin \alpha}{\cos \gamma} \cdot N_5$ $= \frac{1}{\cos \gamma} \cdot \left[-\frac{P}{2} \cdot \cos \gamma_2 \cdot \left(1 - \frac{L_c - d_b^*}{d_c^*} \cdot \tan \gamma_2 \right) + R \cdot \frac{L_c - d_b^*}{d_c^*} \cdot \cos \gamma_2 + N_c \cdot \frac{L_c - d_b^*}{d_c^*} \cdot \sin \gamma_2 \right]$ $= \frac{P}{2} \cdot \frac{\cos \gamma_1 \cdot \cos \gamma_2}{\cos \gamma} \cdot \frac{1}{d_c^*} \cdot \frac{2 \cdot L_b \cdot L_c - 2 \cdot L_b \cdot d_b^* - d_c^* \cdot d_b^* + d_b^* \cdot (L_c - d_b^*) \cdot (\tan \gamma_2 + \tan \gamma_1)}{(L_c - d_b^*) \cdot \cos \gamma_2 + d_b^* \cdot \cos \gamma_1}$ $+ N_c \cdot \frac{d_b^*}{d_c^*} \cdot \tan \gamma \cdot \frac{L_c - d_b^*}{(L_c - d_b^*) \cdot \cos \gamma_2 + d_b^* \cdot \cos \gamma_1} \quad (\text{B-8})$ $= V_{Ek,num}^{PZ, } \cdot \frac{d_b^*}{d_c^*}$

C. Interior joints

Table B-4. Determination of the internal forces acting on the PZ of an interior joint.

Internal forces acting on the PZ				
	Undeformed configuration (1 st order)		Deformed configuration (2 nd order)	
	Fig. B-8. Interior joint in undeformed shape.		Fig. B-9. Interior joint in deformed shape.	
Horizontal support reactions				
R	$P \cdot \frac{2 \cdot L_b + d_c}{L_c}$		$P \cdot \frac{2 \cdot L_b \cdot \cos \gamma_1 + d_c \cdot \cos \gamma_2}{(L_c - d_h^+) \cdot \cos \gamma_2 + d_h^+ \cdot \cos \gamma_1} - N_c \cdot \frac{(L_c - d_h^+) \cdot \sin \gamma_2 - d_h^+ \cdot \sin \gamma_1}{(L_c - d_h^+) \cdot \cos \gamma_2 + d_h^+ \cdot \cos \gamma_1}$	
Internal forces				
N_{BL}/N_{BR}	0	0	$-P \cdot \sin \gamma_1$	$-P \cdot \sin \gamma_1$
V_{BL}/V_{BR}	P	P	$P \cdot \cos \gamma_1$	$P \cdot \cos \gamma_1$
M_{BL}/M_{BR}	$P \cdot L_b$	$P \cdot L_b$	$P \cdot L_b \cdot \cos \gamma_1$	$P \cdot L_b \cdot \cos \gamma_1$
N_{CT}/N_{CB}	N_c	N_c	$N_c \cdot \cos \gamma_2 - R \cdot \sin \gamma_2$	$N_c \cdot \cos \gamma_2 - R \cdot \sin \gamma_2$
V_{CT}/V_{CB}	R	R	$R \cdot \cos \gamma_2 + N_c \cdot \sin \gamma_2$	$R \cdot \cos \gamma_2 + N_c \cdot \sin \gamma_2$
M_{CT}/M_{CB}	$R \cdot \frac{L_c - d_b^+}{2}$	$R \cdot \frac{L_c - d_b^+}{2}$	$R \cdot \frac{L_c - d_b^+}{2} \cdot \cos \gamma_2 + N_c \cdot \frac{L_c - d_b^+}{2} \cdot \sin \gamma_2$	$R \cdot \frac{L_c - d_b^+}{2} \cdot \cos \gamma_2 + N_c \cdot \frac{L_c - d_b^+}{2} \cdot \sin \gamma_2$

Table B-5. Determination of the axial forces acting in the equivalent truss model of the PZ in an interior joint.

Equivalent truss model	
Undeformed configuration (1 st order)	Deformed configuration (2 nd order)
Fig. B-10. Equivalent truss model of the PZ for the interior joint in undeformed shape.	Fig. B-11. Equivalent truss model of the PZ for the interior joint in deformed shape.
Axial forces in the truss model: computation	
Node W	
$N_1 - \frac{V_{CT}}{2} + \left(\frac{M_{BL}}{d_b^*} + \frac{N_{BL}}{2} \right) = 0$ $\Leftrightarrow N_1 = \frac{V_{CT}}{2} - \left(\frac{M_{BL}}{d_b^*} + \frac{N_{BL}}{2} \right)$ $\Leftrightarrow N_1 = -P \cdot \frac{L_b}{d_b^*} + \frac{R}{2} = N_3$	$N_1 \cdot \cos \gamma - \frac{V_{CT}}{2} \cdot \cos \gamma + \left(\frac{M_{BL}}{d_b^*} + \frac{N_{BL}}{2} \right) + \left(\frac{M_{CT}}{d_c^*} + \frac{N_{CT}}{2} \right) \cdot \sin \gamma = 0$ $\Leftrightarrow N_1 = \frac{V_{CT}}{2} - \left(\frac{M_{BL}}{d_b^*} + \frac{N_{BL}}{2} \right) \cdot \sec \gamma - \left(\frac{M_{CT}}{d_c^*} + \frac{N_{CT}}{2} \right) \cdot \tan \gamma$ $\Leftrightarrow N_1 = \frac{P}{2} \cdot \sin \gamma_1 \cdot \sec \gamma \cdot \left[1 - 2 \cdot \frac{L_b}{d_b^*} \cdot \cot \gamma_1 \right] + \frac{R}{2} \cdot \cos \gamma_2$ $\cdot \left[1 - \frac{L_c - d_b^*}{d_c^*} \cdot \tan \gamma + \tan \gamma_2 \cdot \tan \gamma \right] + \frac{N_c}{2} \cdot \sin \gamma_2$ $\cdot \left[1 - \frac{L_c - d_b^*}{d_c^*} \cdot \tan \gamma - \cot \gamma_2 \cdot \tan \gamma \right] = N_3$
$\hat{X}: \quad -N_4 + \frac{V_{BL}}{2} - \left(\frac{M_{CT}}{d_c^*} + \frac{N_{CT}}{2} \right) = 0$	$-N_4 \cdot \cos \gamma + \frac{V_{BL}}{2} \cdot \cos \gamma - \left(\frac{M_{CT}}{d_c^*} + \frac{N_{CT}}{2} \right) - \left(\frac{M_{BL}}{d_b^*} + \frac{N_{BL}}{2} \right) \cdot \sin \gamma = 0$
$\hat{Y}: \quad -N_4 + \frac{V_{BL}}{2} - \left(\frac{M_{CT}}{d_c^*} + \frac{N_{CT}}{2} \right) = 0$	$-N_4 \cdot \cos \gamma + \frac{V_{BL}}{2} \cdot \cos \gamma - \left(\frac{M_{CT}}{d_c^*} + \frac{N_{CT}}{2} \right) - \left(\frac{M_{BL}}{d_b^*} + \frac{N_{BL}}{2} \right) \cdot \sin \gamma = 0$

	$\Leftrightarrow N_4 = \frac{V_{BL}}{2} - \left(\frac{M_{CT}}{d_c^*} + \frac{N_{CT}}{2} \right)$ $\Leftrightarrow N_4 = \frac{P}{2} - \frac{R}{2} \cdot \frac{L_c - d_b^*}{d_c^*} - \frac{N_c}{2} = N_2$	$\Leftrightarrow N_4 = \frac{V_{BL}}{2} - \left(\frac{M_{BL}}{d_b^*} + \frac{N_{BL}}{2} \right) \cdot \tan \gamma - \left(\frac{M_{CT}}{d_c^*} + \frac{N_{CT}}{2} \right) \cdot \sec \gamma$ $\Leftrightarrow N_4 = \frac{P}{2} \cdot \cos \gamma_1 \cdot \left[1 - 2 \cdot \frac{L_b}{d_b^*} \cdot \tan \gamma + \tan \gamma_1 \cdot \tan \gamma \right] + \frac{R}{2} \cdot \sin \gamma_2 \cdot \sec \gamma$ $\cdot \left[1 - \frac{L_c - d_b^*}{d_c^*} \cdot \cot \gamma_2 \right] - \frac{N_c}{2} \cdot \cos \gamma_2 \cdot \sec \gamma$ $\cdot \left[1 + \frac{L_c - d_b^*}{d_c^*} \cdot \tan \gamma_2 \right] = N_2$
Node Y		
\hat{X} :	$-N_3 + \frac{V_{CB}}{2} - \left(\frac{M_{BR}}{d_b^*} + \frac{N_{BR}}{2} \right) = 0$ $\Leftrightarrow N_3 = \frac{V_{CB}}{2} - \left(\frac{M_{BR}}{d_b^*} + \frac{N_{BR}}{2} \right) \cdot \sec \gamma$ $\Leftrightarrow N_3 = -P \cdot \frac{L_b}{d_b^*} + \frac{R}{2} = N_1$	$-N_3 \cdot \cos \gamma + \frac{V_{CB}}{2} \cdot \cos \gamma - \left(\frac{M_{CB}}{d_c^*} + \frac{N_{CB}}{2} \right) \cdot \sin \gamma - \left(\frac{M_{BR}}{d_b^*} + \frac{N_{BR}}{2} \right) = 0$ $\Leftrightarrow N_3 = \frac{V_{CB}}{2} - \left(\frac{M_{CB}}{d_c^*} + \frac{N_{CB}}{2} \right) \cdot \tan \gamma - \left(\frac{M_{BR}}{d_b^*} + \frac{N_{BR}}{2} \right) \cdot \sec \gamma$ $\Leftrightarrow N_3 = \frac{P}{2} \cdot \sin \gamma_1 \cdot \sec \gamma \cdot \left[1 - 2 \cdot \frac{L_b}{d_b^*} \cdot \cot \gamma_1 \right] + \frac{R}{2} \cdot \cos \gamma_2 \cdot \left[1 - \frac{L_c - d_b^*}{d_c^*} \cdot \tan \gamma + \tan \gamma_2 \cdot \tan \gamma \right] + \frac{N_c}{2} \cdot \sin \gamma_2 \cdot \left[1 - \frac{L_c - d_b^*}{d_c^*} \cdot \tan \gamma - \cot \gamma_2 \cdot \tan \gamma \right] = N_1$
\hat{Y} :	$N_2 - \frac{V_{BR}}{2} + \left(\frac{M_{CB}}{d_c^*} + \frac{N_{CB}}{2} \right) = 0$ $\Leftrightarrow N_2 = \frac{V_{BR}}{2} - \left(\frac{M_{CB}}{d_c^*} + \frac{N_{CB}}{2} \right) \cdot \sec \gamma$ $\Leftrightarrow N_2 = \frac{P}{2} - \frac{R}{2} \cdot \frac{L_c - d_b^*}{d_c^*} - \frac{N_c}{2} = N_4$	$N_2 \cdot \cos \gamma - \frac{V_{BR}}{2} \cdot \cos \gamma + \left(\frac{M_{BR}}{d_b^*} + \frac{N_{BR}}{2} \right) \cdot \sin \gamma + \left(\frac{M_{CB}}{d_c^*} + \frac{N_{CB}}{2} \right) = 0$ $\Leftrightarrow N_2 = \frac{V_{BR}}{2} - \left(\frac{M_{BR}}{d_b^*} + \frac{N_{BR}}{2} \right) \cdot \tan \gamma - \left(\frac{M_{CB}}{d_c^*} + \frac{N_{CB}}{2} \right) \cdot \sec \gamma$ $\Leftrightarrow N_2 = \frac{P}{2} \cdot \cos \gamma_1 \cdot \left[1 - 2 \cdot \frac{L_b}{d_b^*} \cdot \tan \gamma + \tan \gamma_1 \cdot \tan \gamma \right] + \frac{R}{2} \cdot \sin \gamma_2 \cdot \sec \gamma \cdot \left[1 - \frac{L_c - d_b^*}{d_c^*} \cdot \cot \gamma_2 \right] - \frac{N_c}{2} \cdot \cos \gamma_2 \cdot \sec \gamma \cdot \left[1 + \frac{L_c - d_b^*}{d_c^*} \cdot \tan \gamma_2 \right] = N_4$
Node Z		
\hat{X} :	$N_3 + \frac{V_{CB}}{2} + N_{5,x} \cdot \cos \alpha - \left(\frac{M_{BL}}{d_b^*} - \frac{N_{BL}}{2} \right) = 0$ $\Leftrightarrow N_{5,x} = \sec \alpha \cdot \left[-V_{CB} + \left(\frac{M_{BL}}{d_b^*} - \frac{N_{BL}}{2} \right) + \left(\frac{M_{BR}}{d_b^*} + \frac{N_{BR}}{2} \right) \right]$ $\Leftrightarrow N_{5,x} = \sec \alpha \cdot \left[2 \cdot P \cdot \frac{L_b}{d_b^*} - R \right]$	$N_3 \cdot \cos \gamma + \frac{V_{CB}}{2} \cdot \cos \gamma + N_{5,x} \cdot \cos(\alpha + \gamma) - \left(\frac{M_{BL}}{d_b^*} - \frac{N_{BL}}{2} \right) + \left(\frac{M_{CB}}{d_c^*} - \frac{N_{CB}}{2} \right) \cdot \sin \gamma = 0$ $\Leftrightarrow N_{5,x} = \sec(\alpha + \gamma) \cdot \left[-V_{CB} \cdot \cos \gamma + N_{CB} \cdot \sin \gamma + \left(\frac{M_{BL}}{d_b^*} - \frac{N_{BL}}{2} \right) + \left(\frac{M_{BR}}{d_b^*} + \frac{N_{BR}}{2} \right) \right]$ $\Leftrightarrow N_{5,x} = \sec(\alpha + \gamma) \cdot \left[2 \cdot P \cdot \frac{L_b}{d_b^*} \cdot \cos \gamma_1 - R \cdot \cos \gamma_1 + N_c \cdot \sin \gamma_1 \right]$

\hat{Y} :	$N_4 + \frac{V_{BL}}{2} - \left(\frac{M_{CB}}{d_b^*} - \frac{N_{CB}}{2} \right) = 0$ $\Leftrightarrow N_{5,y} = \csc \alpha \cdot \left[-V_{BL} + \left(\frac{M_{CB}}{d_c^*} - \frac{N_{CB}}{2} \right) + \left(\frac{M_{CT}}{d_c^*} + \frac{N_{CT}}{2} \right) \right]$ $\Leftrightarrow N_{5,y} = \csc \alpha \cdot \left[-P + R \cdot \frac{L_c - d_b^*}{d_c^*} \right]$	$N_4 \cdot \cos \gamma + \frac{V_{BL}}{2} \cdot \cos \gamma + N_{5,y} \cdot \sin \alpha + \left(\frac{M_{BL}}{d_b^*} - \frac{N_{BL}}{2} \right) \cdot \sin \gamma - \left(\frac{M_{CB}}{d_b^*} - \frac{N_{CB}}{2} \right) = 0$ $\Leftrightarrow N_{5,y} = \csc \alpha \cdot \left[-V_{BL} \cdot \cos \gamma + N_{BL} \cdot \sin \gamma + \left(\frac{M_{CB}}{d_c^*} - \frac{N_{CB}}{2} \right) + \left(\frac{M_{CT}}{d_c^*} + \frac{N_{CT}}{2} \right) \right]$ $\Leftrightarrow N_{5,y} = \csc \alpha \cdot \left[-P \cdot \cos \gamma_2 + R \cdot \frac{L_c - d_b^*}{d_c^*} \cdot \cos \gamma_2 + N_c \cdot \frac{L_c - d_b^*}{d_c^*} \cdot \sin \gamma_2 \right]$
Check:	$N_{5,x} = N_{5,y}$ $\Leftrightarrow \sec \alpha \cdot \left[2 \cdot P \cdot \frac{L_b}{d_b^*} - R \right] = \csc \alpha \cdot \left[-P + R \cdot \frac{L_c - d_b^*}{d_c^*} \right]$ $\Leftrightarrow 2 \cdot P \cdot \frac{L_b}{d_b^*} - R = \frac{\csc \alpha}{\sec \alpha} \cdot \left[-P + R \cdot \frac{L_c - d_b^*}{d_c^*} \right]$ $\frac{\csc \alpha}{\sec \alpha} = \frac{d_c^*}{d_b^*}$ $\Leftrightarrow 2 \cdot P \cdot \frac{L_b}{d_b^*} - R = -P \cdot \frac{d_c^*}{d_b^*} + R \cdot \frac{L_c - d_b^*}{d_b^*}$ $\Leftrightarrow P \cdot [2 \cdot L_b + d_c^*] - R \cdot L_c = 0$ $\text{inject } R$ $\Leftrightarrow P \cdot [2 \cdot L_b + d_c^*] - P \cdot [2 \cdot L_b + d_c^*] = 0$ OK! $\Leftrightarrow 0 \hat{=} 0$	$N_{5,x} = N_{5,y}$ $\Leftrightarrow \sec(\alpha + \gamma) \cdot \left[2 \cdot P \cdot \frac{L_b}{d_b^*} \cdot \cos \gamma_1 - R \cdot \cos \gamma_1 + N_c \cdot \sin \gamma_1 \right] = \csc \alpha \cdot \left[-P \cdot \cos \gamma_2 + R \cdot \frac{L_c - d_b^*}{d_c^*} \cdot \cos \gamma_2 + N_c \cdot \frac{L_c - d_b^*}{d_c^*} \cdot \sin \gamma_2 \right]$ $\Leftrightarrow 2 \cdot P \cdot \frac{L_b}{d_b^*} \cdot \cos \gamma_1 - R \cdot \cos \gamma_1 + N_c \cdot \sin \gamma_1 = \frac{\csc \alpha}{\sec(\alpha + \gamma)} \cdot \left[-P \cdot \cos \gamma_2 + R \cdot \frac{L_c - d_b^*}{d_c^*} \cdot \cos \gamma_2 + N_c \cdot \frac{L_c - d_b^*}{d_c^*} \cdot \sin \gamma_2 \right]$ $\frac{\csc \alpha}{\sec(\alpha + \gamma)} = \frac{d_c^*}{d_b^*}$ $\Leftrightarrow 2 \cdot P \cdot \frac{L_b}{d_b^*} \cdot \cos \gamma_1 - R \cdot \cos \gamma_1 + N_c \cdot \sin \gamma_1 = -P \cdot \frac{d_c^*}{d_b^*} \cdot \cos \gamma_2 + R \cdot \frac{L_c - d_b^*}{d_b^*} \cdot \cos \gamma_2 + N_c \cdot \frac{L_c - d_b^*}{d_b^*} \cdot \sin \gamma_2$ $\Leftrightarrow P \cdot [2 \cdot L_b \cdot \cos \gamma_1 + d_c^* \cdot \cos \gamma_2] - R \cdot [d_b^* \cdot \cos \gamma_1 + (L_c - d_b^*) \cdot \cos \gamma_2] + N_c \cdot [d_b^* \cdot \sin \gamma_1 - (L_c - d_b^*) \cdot \sin \gamma_2] = 0$ $\text{inject } R$ $\Leftrightarrow P \cdot [2 \cdot L_b \cdot \cos \gamma_1 + d_c^* \cdot \cos \gamma_2] - P \cdot [2 \cdot L_b \cdot \cos \gamma_1 + d_c^* \cdot \cos \gamma_2] + N_c \cdot [d_b^* \cdot \sin \gamma_1 - (L_c - d_b^*) \cdot \sin \gamma_2] - N_c \cdot [d_b^* \cdot \sin \gamma_1 - (L_c - d_b^*) \cdot \sin \gamma_2] = 0$ OK! $\Leftrightarrow 0 \hat{=} 0$
Node X		
\hat{X} :	$-N_1 - \frac{V_{CT}}{2} - N_{5,x} \cdot \cos \alpha + \left(\frac{M_{BR}}{d_b^*} - \frac{N_{BR}}{2} \right) = 0$ $\Leftrightarrow N_{5,x} = \sec \alpha \cdot \left[-V_{CT} + \left(\frac{M_{BR}}{d_b^*} - \frac{N_{BR}}{2} \right) + \left(\frac{M_{BL}}{d_b^*} + \frac{N_{BL}}{2} \right) \right]$ $\Leftrightarrow N_{5,x} = \sec \alpha \cdot \left[2 \cdot P \cdot \frac{L_b}{d_b^*} - R \right]$	$-N_1 \cdot \cos \gamma - \frac{V_{CT}}{2} \cdot \cos \gamma - N_{5,x} \cdot \cos(\alpha + \gamma) - \left(\frac{M_{CT}}{d_c^*} - \frac{N_{CT}}{2} \right) \cdot \sin \gamma + \left(\frac{M_{BR}}{d_b^*} - \frac{N_{BR}}{2} \right) = 0$ $\Leftrightarrow N_{5,x} = \sec(\alpha + \gamma) \cdot \left[-V_{CT} \cdot \cos \gamma + N_{CT} \cdot \sin \gamma + \left(\frac{M_{BR}}{d_b^*} - \frac{N_{BR}}{2} \right) + \left(\frac{M_{BL}}{d_b^*} + \frac{N_{BL}}{2} \right) \right]$ $\Leftrightarrow N_{5,x} = \sec(\alpha + \gamma) \cdot \left[2 \cdot P \cdot \frac{L_b}{d_b^*} \cdot \cos \gamma_1 - R \cdot \cos \gamma_1 + N_c \cdot \sin \gamma_1 \right]$

\hat{Y} :	$-N_2 - \frac{V_{BR}}{2} - N_{5,y} \cdot \sin \alpha + \left(\frac{M_{CT}}{d_c^*} - \frac{N_{CT}}{2} \right) = 0$ $\Leftrightarrow N_{5,y} = \csc \alpha \cdot \left[-V_{BR} + \left(\frac{M_{CB}}{d_c^*} + \frac{N_{CB}}{2} \right) + \left(\frac{M_{CT}}{d_c^*} - \frac{N_{CT}}{2} \right) \right]$ $\Leftrightarrow N_{5,y} = \csc \alpha \cdot \left[-P + R \cdot \frac{L_c - d_b^*}{d_c^*} \right]$	$-N_2 \cdot \cos \gamma - \frac{V_{BR}}{2} \cdot \cos \gamma - N_{5,y} \cdot \sin \alpha - \left(\frac{M_{BR}}{d_b^*} - \frac{N_{BR}}{2} \right) \cdot \sin \gamma + \left(\frac{M_{CT}}{d_c^*} - \frac{N_{CT}}{2} \right) = 0$ $\Leftrightarrow N_{5,y} = \csc \alpha \cdot \left[-V_{BR} \cdot \cos \gamma + N_{BR} \cdot \sin \gamma + \left(\frac{M_{CB}}{d_c^*} + \frac{N_{CB}}{2} \right) + \left(\frac{M_{CT}}{d_c^*} - \frac{N_{CT}}{2} \right) \right]$ $\Leftrightarrow N_{5,y} = \csc \alpha \cdot \left[-P \cdot \cos \gamma_2 + R \cdot \frac{L_c - d_b^*}{d_c^*} \cdot \cos \gamma_2 + N_c \cdot \frac{L_c - d_b^*}{d_c^*} \cdot \sin \gamma_2 \right]$
Check:	Similar to node Z	Similar to node Z
Axial forces in the truss model: summary		
N_1	$-P \cdot \frac{L_b}{d_b^*} + \frac{R}{2}$	$\frac{P}{2} \cdot \sin \gamma_1 \cdot \sec \gamma \cdot \left[1 - 2 \cdot \frac{L_b}{d_b^*} \cdot \cot \gamma_1 \right]$ $+ \frac{R}{2} \cdot \cos \gamma_2 \cdot \left[1 - \frac{L_c - d_b^*}{d_c^*} \cdot \tan \gamma + \tan \gamma_2 \cdot \tan \gamma \right]$ $+ \frac{N_c}{2} \cdot \sin \gamma_2 \cdot \left[1 - \frac{L_c - d_b^*}{d_c^*} \cdot \tan \gamma - \cot \gamma_2 \cdot \tan \gamma \right]$
N_2	$\frac{P}{2} - \frac{R}{2} \cdot \frac{L_c - d_b^*}{d_c^*} - \frac{N_c}{2}$	$\frac{P}{2} \cdot \cos \gamma_1 \cdot \left[1 - 2 \cdot \frac{L_b}{d_b^*} \cdot \tan \gamma + \tan \gamma_1 \cdot \tan \gamma \right]$ $+ \frac{R}{2} \cdot \sin \gamma_2 \cdot \sec \gamma \cdot \left[1 - \frac{L_c - d_b^*}{d_c^*} \cdot \cot \gamma_2 \right]$ $- \frac{N_c}{2} \cdot \cos \gamma_2 \cdot \sec \gamma \cdot \left[1 + \frac{L_c - d_b^*}{d_c^*} \cdot \tan \gamma_2 \right]$
N_3	$-P \cdot \frac{L_b}{d_b^*} + \frac{R}{2}$	$\frac{P}{2} \cdot \sin \gamma_1 \cdot \sec \gamma \cdot \left[1 - 2 \cdot \frac{L_b}{d_b^*} \cdot \cot \gamma_1 \right]$ $+ \frac{R}{2} \cdot \cos \gamma_2 \cdot \left[1 - \frac{L_c - d_b^*}{d_c^*} \cdot \tan \gamma + \tan \gamma_2 \cdot \tan \gamma \right]$ $+ \frac{N_c}{2} \cdot \sin \gamma_2 \cdot \left[1 - \frac{L_c - d_b^*}{d_c^*} \cdot \tan \gamma - \cot \gamma_2 \cdot \tan \gamma \right]$
N_4	$\frac{P}{2} - \frac{R}{2} \cdot \frac{L_c - d_b^*}{d_c^*} - \frac{N_c}{2}$	$\frac{P}{2} \cdot \cos \gamma_1 \cdot \left[1 - 2 \cdot \frac{L_b}{d_b^*} \cdot \tan \gamma + \tan \gamma_1 \cdot \tan \gamma \right]$ $+ \frac{R}{2} \cdot \sin \gamma_2 \cdot \sec \gamma \cdot \left[1 - \frac{L_c - d_b^*}{d_c^*} \cdot \cot \gamma_2 \right]$ $- \frac{N_c}{2} \cdot \cos \gamma_2 \cdot \sec \gamma \cdot \left[1 + \frac{L_c - d_b^*}{d_c^*} \cdot \tan \gamma_2 \right]$
N_5	$\begin{cases} \sec \alpha \cdot \left[2 \cdot P \cdot \frac{L_b}{d_b^*} - R \right] \\ \csc \alpha \cdot \left[-P + R \cdot \frac{L_c - d_b^*}{d_c^*} \right] \end{cases}$	$\begin{cases} \sec(\alpha + \gamma) \cdot \left[2 \cdot P \cdot \frac{L_b}{d_b^*} \cdot \cos \gamma_1 - R \cdot \cos \gamma_1 + N_c \cdot \sin \gamma_1 \right] \\ \csc \alpha \cdot \left[-P \cdot \cos \gamma_2 + R \cdot \frac{L_c - d_b^*}{d_c^*} \cdot \cos \gamma_2 + N_c \cdot \frac{L_c - d_b^*}{d_c^*} \cdot \sin \gamma_2 \right] \end{cases}$

Table B-6. Determination of the equivalent shear force $V_{Ek,num}^{PZ}$ acting on the PZ of an interior joint.

		Equivalent truss model	
		Undeformed configuration (1 st order)	Deformed configuration (2 nd order)
		<p>Fig. B-12. Geometric relationship between N_5 and $V_{Ek,num}^{PZ, }$ (resp. $V_{Ek,num}^{PZ,⊥}$) for the interior joint in undeformed shape.</p>	<p>Fig. B-13. Geometric relationship between N_5 and $V_{Ek,num}^{PZ, }$ (resp. $V_{Ek,num}^{PZ,⊥}$) for the interior joint in undeformed shape.</p>
$V_{Ek,num}^{PZ, }$	$= \cos \alpha \cdot N_5$ $= \left[P \cdot \frac{L_b}{d_b^*} - R \right]$ $= \frac{P \cdot \frac{1}{d_b^*} \cdot \frac{2 \cdot L_b \cdot L_c - 2 \cdot L_b \cdot d_b^* - d_c^* \cdot d_b^*}{L_c}}{\quad} \quad (B-9)$	$= \frac{\cos(\alpha + \gamma)}{\cos \gamma} \cdot N_5$ $= \frac{1}{\cos \gamma} \cdot \left[2 \cdot P \cdot \frac{L_b}{d_b^*} \cdot \cos \gamma_1 - R \cdot \cos \gamma_1 + N_c \cdot \sin \gamma_1 \right]$ $= \frac{P \cdot \frac{\cos \gamma_1 \cdot \cos \gamma_2}{\cos \gamma} \cdot \frac{1}{d_b^*} \cdot \frac{2 \cdot L_b \cdot L_c - 2 \cdot L_b \cdot d_b^* - d_c^* \cdot d_b^*}{(L_c - d_b^*) \cdot \cos \gamma_2 + d_b^* \cdot \cos \gamma_1} + N_c \cdot \tan \gamma \cdot \frac{L_c - d_b^*}{(L_c - d_b^*) \cdot \cos \gamma_2 + d_b^* \cdot \cos \gamma_1}}{\quad} \quad (B-10)$	
$V_{Ek,num}^{PZ,⊥}$	$= \sin \alpha \cdot N_5$ $= \left[-\frac{P}{2} + R \cdot \frac{L_c - d_b^*}{d_c^*} \right]$ $= \frac{P \cdot \frac{1}{2} \cdot \frac{2 \cdot L_b \cdot L_c - 2 \cdot L_b \cdot d_b^* - d_c^* \cdot d_b^*}{L_c}}{\quad} \quad (B-11)$ $= V_{Ek,num}^{PZ, } \cdot \frac{d_b^*}{d_c^*}$	$= \frac{\sin \alpha}{\cos \gamma} \cdot N_5$ $= \frac{1}{\cos \gamma} \cdot \left[-P \cdot \cos \gamma_2 + R \cdot \frac{L_c - d_b^*}{d_c^*} \cdot \cos \gamma_2 + N_c \cdot \frac{L_c - d_b^*}{d_c^*} \cdot \sin \gamma_2 \right]$ $= \frac{P \cdot \frac{\cos \gamma_1 \cdot \cos \gamma_2}{\cos \gamma} \cdot \frac{1}{d_c^*} \cdot \frac{2 \cdot L_b \cdot L_c - 2 \cdot L_b \cdot d_b^* - d_c^* \cdot d_b^*}{(L_c - d_b^*) \cdot \cos \gamma_2 + d_b^* \cdot \cos \gamma_1} + N_c \cdot \frac{d_b^*}{d_c^*} \cdot \tan \gamma \cdot \frac{L_c - d_b^*}{(L_c - d_b^*) \cdot \cos \gamma_2 + d_b^* \cdot \cos \gamma_1}}{\quad} \quad (B-12)$ $= V_{Ek,num}^{PZ, } \cdot \frac{d_b^*}{d_c^*}$	

B.1.3 Equivalent shear force $V_{Ek,num}^{CWP}$ acting on the CWP

The procedure of extraction of the equivalent shear force $V_{Ek,num}^{CWP}$ acting on the CWP from the FE results is a three-step procedure and is described as follows:

- The first step consists in isolating the PZ from the numerical model, as depicted in Fig. B-14(a) and (b). The PZ is assumed to be constituted of n rows of FE over its depth d_b^* .
- The second step consists in isolating the i^{th} row of FE, as depicted in Fig. B-14(b) and (c). For this i^{th} row of FE, shear stresses were integrated over the numerical effective shear area $A_{VC,i}^t$, highlighted in black in Fig. B-14(c), thus providing one numerical value $V_{Ek,row,i}^{CWP,t}$. This value characterizes the shear force applied to the i^{th} row of FE at time step t , as expressed through Eq. (B-13). Given the discrete FE mesh, the surface integral in Eq. (B-13) has been replaced by the summation of the shear level of each of the N elements placed over $A_{VC,i}^t$, where the parameters a_{ij}^t and τ_{ij}^t in Eq. (B-13) represent the shear stress and the area of the j^{th} element in the i^{th} row of FE at time step t , respectively.

N.B.: Eq. (B-13) applied to the central section of the CWP was used by several researchers (see [1]–[4]) as a good approximation of $V_{Ek,num}^{CWP}$. However, this approach does not capture the local effect of the $\tau - \sigma_i$ stress interaction on the plastic shear resistance of the CWP.

- Eq. (B-13) was thus applied to each of the n rows of FE constituting the PZ. The average of these n values is assumed to provide a rather reliable numerical estimation $V_{Ek,num}^{CWP,t}$ of the shear force acting on the CWP at time step t , as expressed through Eq. (B-14).

$$V_{Ek,row,i}^{CWP,t} = \int_{A_{VC,i}^t} \tau dA_{VC,i}^t = \sum_{j=1}^N a_{ij}^t \cdot \tau_{ij}^t \quad (\text{B-13})$$

$$V_{Ek,num}^{CWP,t} = \frac{1}{n} \sum_{i=1}^n \sum_{j=1}^N a_{ij}^t \cdot \tau_{ij}^t \quad (\text{B-14})$$

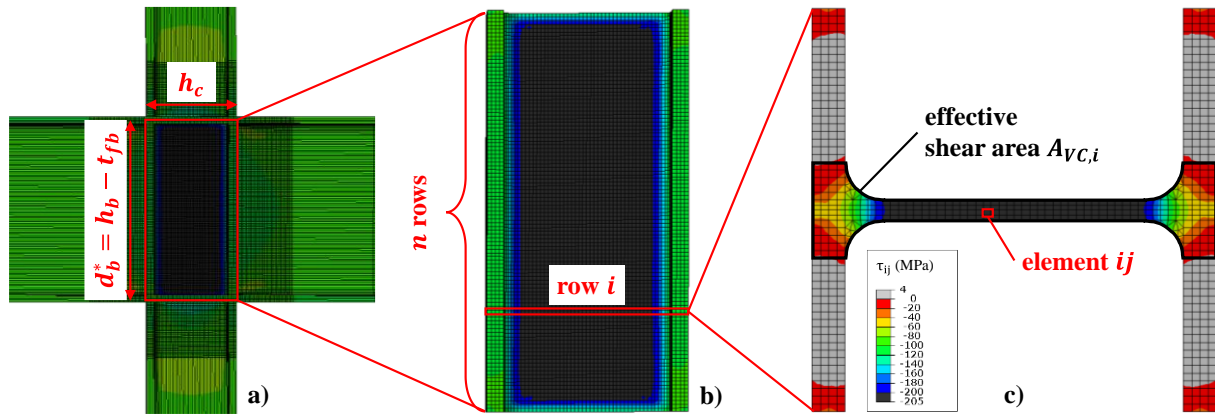


Fig. B-14. Description of the numerical integration procedure for the extraction of $V_{Ek,num}^{CWP}$: (a) numerical model (NR4-1-d-), (b) isolation of the PZ, (c) isolation of the i^{th} row of FE

Based on Eq. (B-14), it was possible to derive the shear force applied to the CWP at each time step t of the numerical simulations. Knowing the shear deformation γ^t at each time step t (see Section B.1.1) allowed to derive the CWP deformation curve $(V^{CWP} - \gamma)_{num}$ for each of the 32 numerical simulations. The results obtained with the fictitious elastic, perfectly-plastic material law are presented in APPENDIX A for each numerical simulation (see the orange solid curves in Fig. C-1(c) to Fig. C-32(c)). The results obtained with the full-range material law are presented in APPENDIX A for each numerical simulation (see the orange solid curves in Fig. C-1(d) to Fig. C-32(d)).

B.1.4 Equivalent shear force $\Delta V_{Ek,num}^{SE}$ acting on the SE

The expression of the equivalent shear force $\Delta V_{Ek,num}^{SE,t}$ acting on the SE at each time step t of the numerical simulations can be easily expressed through Eq. (B-15). It is obtained by subtracting the equivalent shear force $V_{Ek,num}^{CWP,t}$ acting on the CWP at each time step from the equivalent shear force $V_{Ek,num}^{PZ,t}$ acting on the PZ at each time step of the numerical simulations. The former can be derived following the procedure presented in Section B.1.3, while the latter can be derived following the procedure described in Section B.1.2.

$$\Delta V_{Ek,num}^{SE,t} = V_{Ek,num}^{PZ,t} - V_{Ek,num}^{CWP,t} \quad (\text{B-15})$$

Based on Eq. (B-15), it was possible to derive the shear force applied to the SE at each time step t of the numerical simulations. Knowing the shear deformation γ^t at each time step t (see Section B.1.1) allowed to derive the SE deformation curve $(\Delta V^{SE} - \gamma)_{num}$ for each of the 32 numerical simulations. The results obtained with the fictitious elastic, perfectly-plastic material law are presented in APPENDIX A for each numerical simulation (see the green solid curves in Fig. C-1(c) to Fig. C-32(c)). The results obtained with the full-range material law are presented in APPENDIX A for each numerical simulation (see the green solid curves in Fig. C-1(d) to Fig. C-32(d)).

B.2 Extraction of the $(M_B - \Phi)_{num}$ deformation curve of the joint

B.2.1 Rotation Φ of the joint

The total rotation Φ^t of the joint at time step t of the numerical simulations can be defined as the relative rotation between the beam and column axes. It can be expressed through Eq. (B-16) as the sum of two contributions, namely the shear deformation γ^t of the PZ and the rotation ϕ^t of the connection.

$$\Phi^t = \phi^t + \gamma^t \quad (\text{B-16})$$

The shear deformation γ^t of the PZ can be extracted at each time step t of the numerical simulations, using the procedure described in Section B.1.1. By contrast, the rotation ϕ^t of the connection is not easy to extract from the numerical simulations.

Therefore, the total rotation Φ^t of the joint was extracted from the gross rotation Φ_G^t of the beam end. This latter can be computed through Eq. (B-17), where v^t is the vertical displacement at time step t of the beam tip and L_b is the beam length, see Fig. B-15(a).

$$\Phi_G^t = \sin^{-1}(v^t/L_b) \quad (\text{B-17})$$

At each time step t , this global rotation Φ_G^t can be assumed to arise from four main contributions, namely:

- γ^t : the shear deformation of the PZ, see Fig. B-15(b);
- ϕ^t : the rotation of the connection, see Fig. B-15(c);
- $\theta_c^t = \frac{P^t \cdot L_b \cdot L_c}{12 \cdot E \cdot I_c}$: the rotation coming from the elastic deformation of the column, see Fig. B-15(d);
- $\theta_b^t = \frac{P^t \cdot L_b^2}{3 \cdot E \cdot I_b}$: the rotation coming from the elastic deformation of the beam, see Fig. B-15(e).

This is expressed through Eq. (B-18). Based on Eq. (B-17) and Eq. (B-18), an estimation of the total rotation Φ^t of the joint at each time step t can be obtained, see Eq. (B-19), as the difference between the gross rotation Φ_G^t of the beam end and the elastic rotation θ^t of the system.

$$\Phi_G^t = \underbrace{\gamma^t + \phi^t}_{\Phi^t} + \underbrace{\theta_c^t + \theta_b^t}_{\theta^t} \quad (\text{B-18})$$

$$\Phi^t = \Phi_G^t - \theta^t = \sin^{-1}\left(\frac{v^t}{L_b}\right) - \frac{P^t \cdot L_b \cdot L_c}{12 \cdot E \cdot I_c} - \frac{P^t \cdot L_b^2}{3 \cdot E \cdot I_b} \quad (\text{B-19})$$

B.2.2 Bending moment M_B of the joint

Knowing the total rotation Φ^t of the joint, the bending moment M_B^t of the joint can be computed at the beam-column interface for each time step t of the numerical simulations, using Eq. (B-20):

$$M_B^t = P^t \cdot L_b \cdot \cos \Phi^t \quad (\text{B-20})$$

Based on the values of Φ^t (see Eq. (B-19)) and M_B^t (see Eq. (B-20)) at each time step t , it was possible to derive the deformation curve $(M_B - \Phi)_{num}$ of the joint for each of the 32 numerical simulations. The results obtained with the fictitious elastic, perfectly-plastic material law are presented in APPENDIX A for each numerical simulation (see the black solid curves in Fig. C-1(e) to Fig. C-32(e)). The results obtained with the full-range material law are presented in APPENDIX A for each numerical simulation (see the black solid curves in Fig. C-1(f) to Fig. C-32(f)).

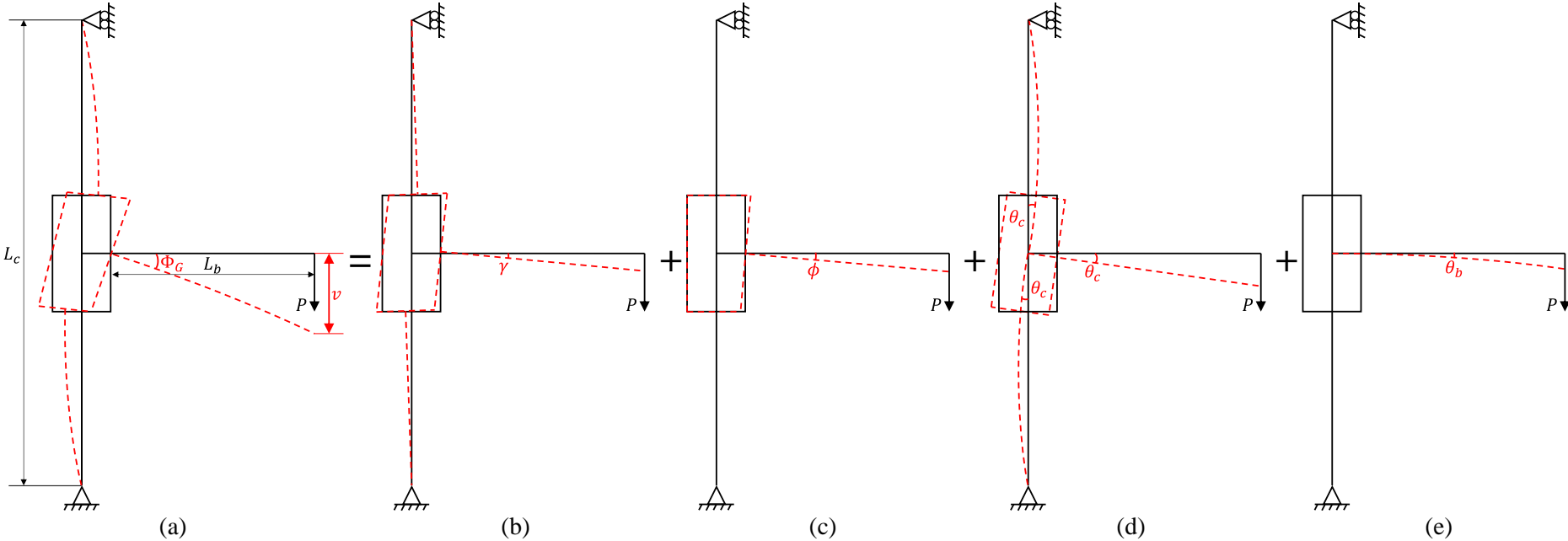


Fig. B-15. Sources of deformability of the system: (a) total gross rotation Φ_G of the beam, (b) shear deformation γ of the PZ, (c) rotation ϕ of the connection, (d) elastic rotation θ_c of the column and (e) elastic rotation θ_b of the beam.

C. NUMERICAL RESULTS

C.1 Model NR4

C.1.1 Simulation NR4-0-s-/

Table C-1. Component characterization for the prediction of the NR4-0-s-/ simulation full-range ($M_B - \Phi$)_{num} curve.

Jaspart (1991)	PZ	CWC*	CWT	CFB	BFC	Corman (2022)		CWP	SE
k_{ini}^c (mm)	2.32	8.16	8.16	-	-	K_y^{CWP} (kN)	K_y^{SE} (kN)	88,589.78	3,574.96
$F_{y,Rk}^c$ (kN)	354.15	353.74	353.74	526.64	896.51	$V_{y,mod}^{CWP}$ (kN)	$\Delta V_{y,mod}^{SE}$ (kN)	227.70	35.52
k_{pp}^c (mm)	0.046	0.287	0.163	-	-	$\Delta K_{y,mod}^{CWP}$ (kN)	-	1,955.57	-
$F_{u,Rk}^c$ (kN)	508.78	421.88	508.19	756.59	1,287.94	$V_{pp,mod}^{CWP}$ (kN)	-	283.00	-
S_{ini}^c (kNm/rad)	49,422.66	173,831.44	173,831.44	-	-	K_{pp}^{CWP} (kN)	K_{pp}^{SE} (kN)	2,112.00	252.80
$M_{y,Rk}^c$ (kNm)	112.80	112.67	112.67	167.73	285.54	V_u^{CWP} (kN)	-	382.71	-
S_{pp}^c (kNm/rad)	979.93	6,113.92	3,472.37	-	-	ΔK_{pp}^{CWP} (kN)	-	242.77	-
$M_{u,Rk}^c$ (kNm)	162.05	134.37	161.86	240.97	410.21	V_n^{CWP} (kN)	ΔV_n^{SE} (kN)	412.55	67.56
ϕ_u^c (rad)	0.0503	0.0035	0.0142	-	-	$\gamma_{f,mod}^{CWP}$ (rad)	$\gamma_{f,mod}^{SE}$ (rad)	0.2010	0.1367

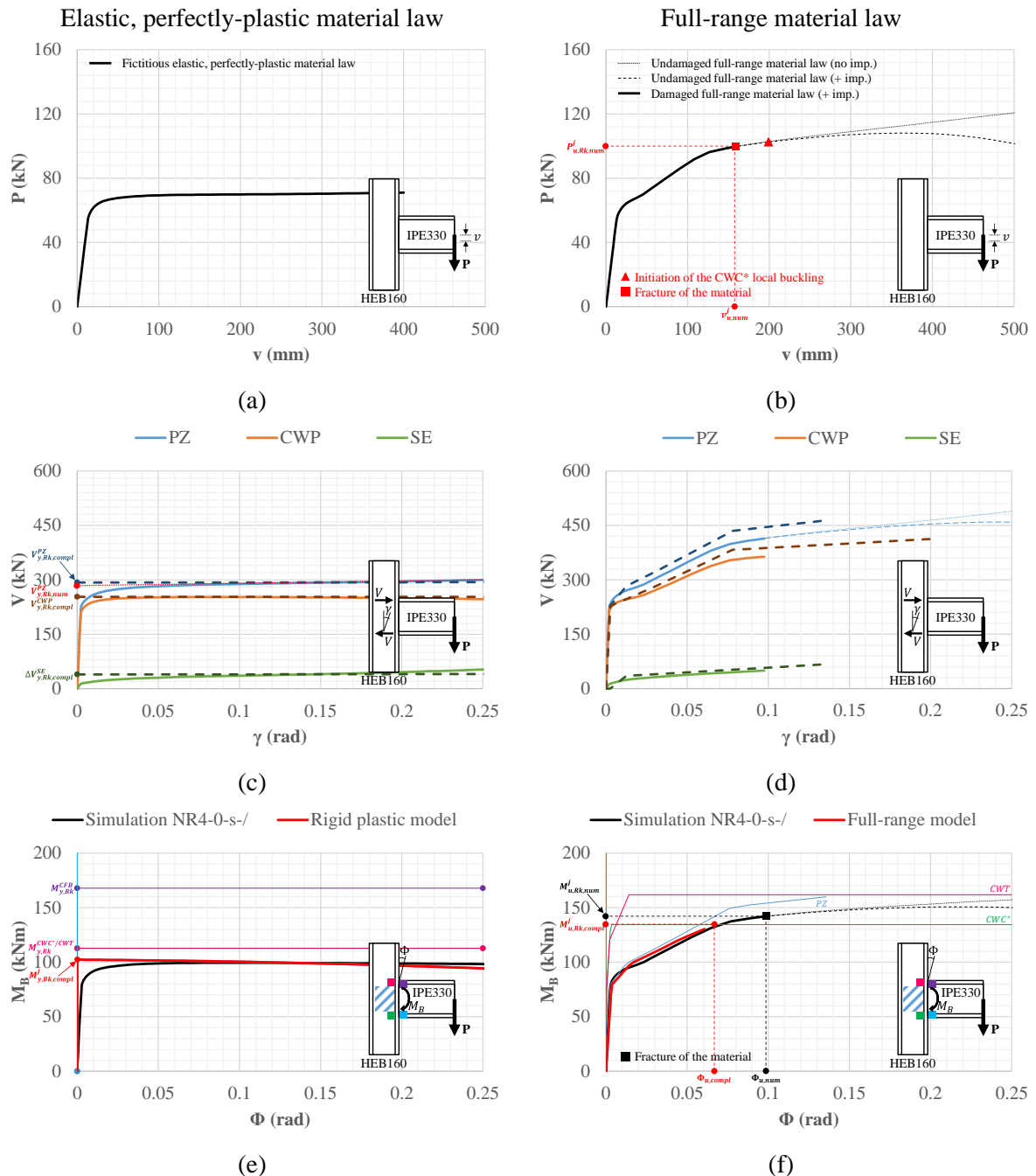


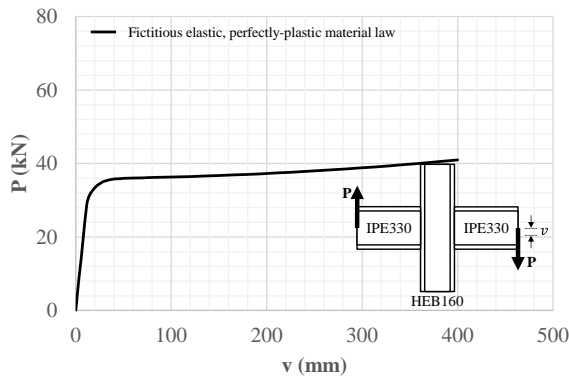
Fig. C-1. Numerical results for the NR4-0-s-/ simulation: (a)-(b) ($P - v$)_{num}, (c)-(d) ($V - \gamma$)_{num}, (e)-(f) ($M_B - \Phi$)_{num} curves.

C.1.2 Simulation NR4-0-d-/

Table C-2. Component characterization for the prediction of the NR4-0-d-/ simulation full-range $(M_B - \Phi)_{num}$ curve.

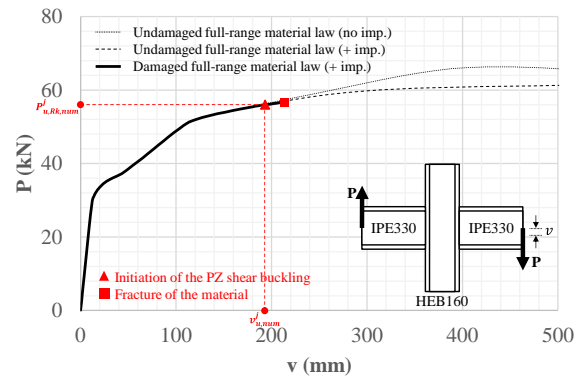
Jaspart (1991)	PZ	CWC*	CWT	CFB	BFC	Corman (2022)		CWP	SE
k_{ini}^c (mm)	1.16	8.16	8.16	-	-	K_y^{CWP} (kN)	K_y^{SE} (kN)	88,589.78	3,574.96
$F_{y,Rk}^c$ (kN)	177.08	249.00	249.00	526.64	896.51	$V_{y,mod}^{CWP}$ (kN)	$\Delta V_{y,mod}^{SE}$ (kN)	239.69	35.52
k_{pp}^c (mm)	0.023	0.287	0.163	-	-	$\Delta K_{y,mod}^{CWP}$ (kN)	-	1,955.57	-
$F_{u,Rk}^c$ (kN)	254.39	336.11	357.72	756.59	1,287.94	$V_{pp,mod}^{CWP}$ (kN)	-	297.90	-
S_{ini}^c (kNm/rad)	24,711.33	173,831.44	173,831.44	-	-	K_{pp}^{CWP} (kN)	K_{pp}^{SE} (kN)	2,112.00	252.80
$M_{y,Rk}^c$ (kNm)	56.40	79.31	79.31	167.73	285.54	V_u^{CWP} (kN)	-	402.85	-
S_{pp}^c (kNm/rad)	489.97	6,113.92	3,472.37	-	-	ΔK_n^{CWP} (kN)	-	242.77	-
$M_{u,Rk}^c$ (kNm)	81.02	107.05	113.93	240.97	410.21	V_n^{CWP} (kN)	ΔV_n^{SE} (kN)	434.27	67.56
ϕ_u^c (rad)	0.0502	0.0045	0.0100	-	-	$\gamma_{f,mod}^{CWP}$ (rad)	$\gamma_{f,mod}^{SE}$ (rad)	0.2116	0.1369

Elastic, perfectly-plastic material law

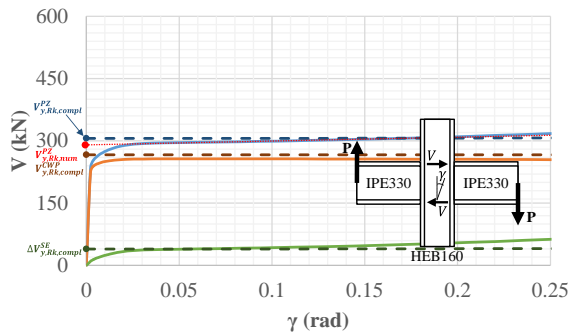


(a)

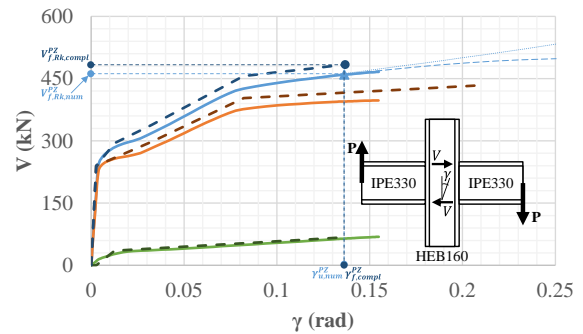
Full-range material law



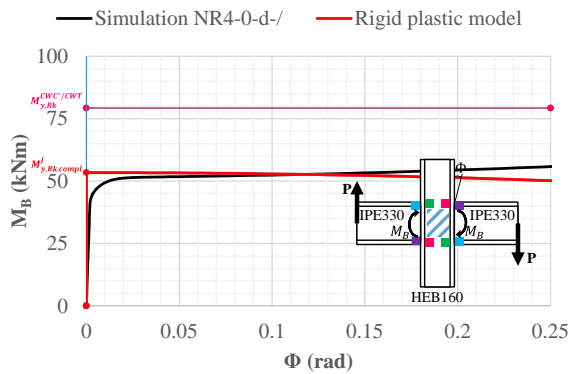
(b)



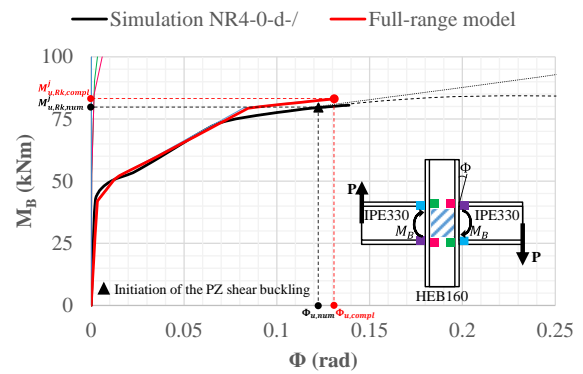
(c)



(d)



(e)



(f)

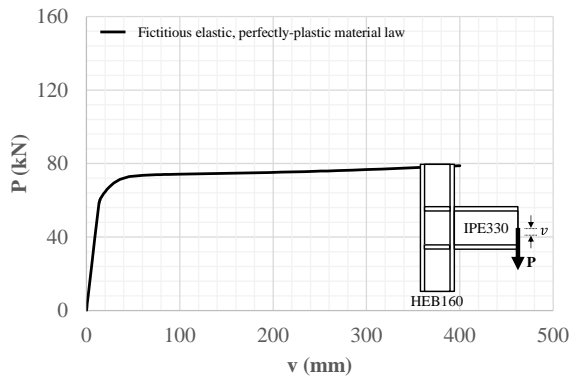
Fig. C-2. Numerical results for the NR4-0-d-/ simulation: (a)-(b) $(P - v)_{num}$ curves, (c)-(d) $(V - \gamma)_{num}$ curves and (e)-(f) $(M_B - \Phi)_{num}$ curves.

C.1.3 Simulation NR4-1-s-/

Table C-3. Component characterization for the prediction of the NR4-1-s-/
 simulation full-range ($M_B - \Phi$)_{num} curve.

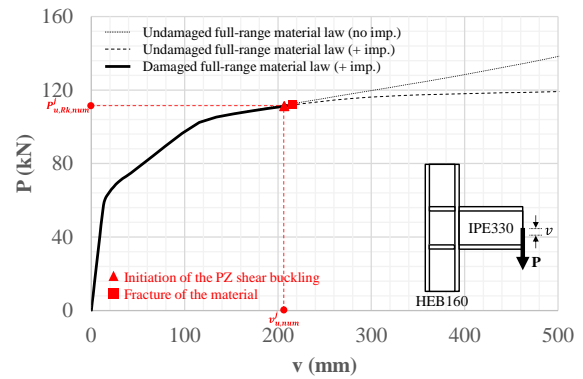
Jaspart (1991)	PZ	CWC*	CWT	CFB	BFC	Corman (2022)		CWP	SE
k_{ini}^c (mm)	2.32	-	-	-	-	$K_{y,mod}^{CWP}$ (kN)	$K_{y,mod}^{SE}$ (kN)	88,589.78	5,458.11
$F_{y,Rk}^c$ (kN)	384.61	-	-	526.64	896.51	$V_{y,mod}^{CWP}$ (kN)	$\Delta V_{y,mod}^{SE}$ (kN)	227.70	51.76
k_{pp}^c (mm)	0.046	-	-	-	-	$\Delta K_{y,mod}^{CWP}$ (kN)	-	1,955.57	-
$F_{u,Rk}^c$ (kN)	552.54	-	-	756.59	1,287.94	$V_{pp,mod}^{CWP}$ (kN)	-	283.00	-
S_{ini}^c (kNm/rad)	49,422.66	-	-	-	-	K_{pp}^{CWP} (kN)	K_{pp}^{SE} (kN)	2,112.00	385.97
$M_{y,Rk}^c$ (kNm)	122.50	-	-	167.73	285.54	V_u^{CWP} (kN)	-	382.71	-
S_{pp}^c (kNm/rad)	979.93	-	-	-	-	ΔK_n^{CWP} (kN)	-	242.77	-
$M_{u,Rk}^c$ (kNm)	175.98	-	-	240.97	410.23	V_n^{CWP} (kN)	ΔV_n^{SE} (kN)	414.97	98.37
ϕ_u^c (rad)	0.0546	-	-	-	-	$\gamma_{f,mod}^{CWP}$ (rad)	$\gamma_{f,mod}^{SE}$ (rad)	0.2110	0.1306

Elastic, perfectly-plastic material law

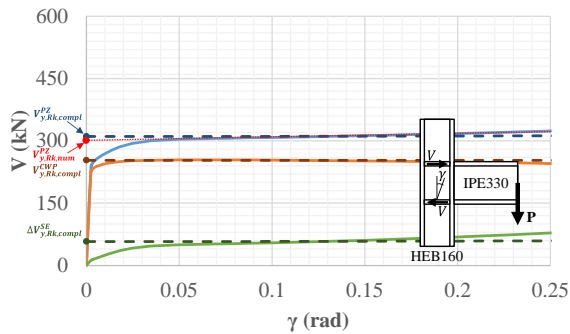


(a)

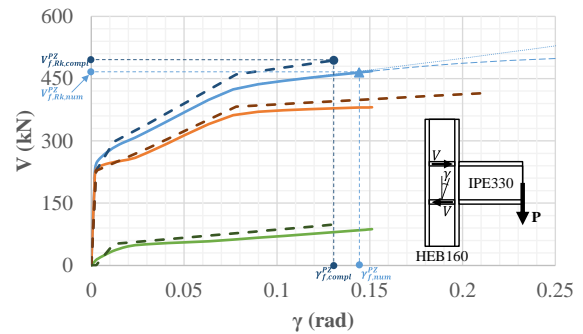
Full-range material law



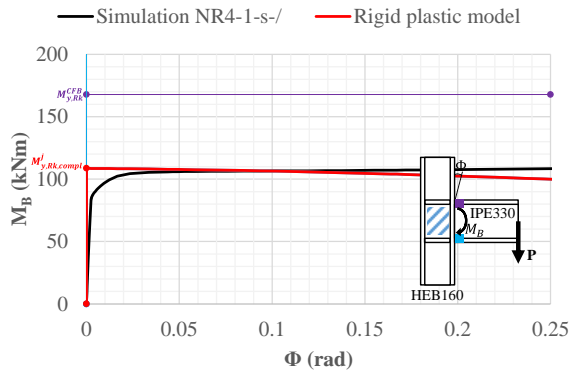
(b)



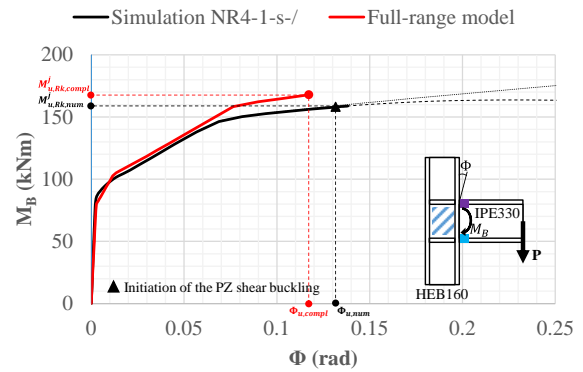
(c)



(d)



(e)



(f)

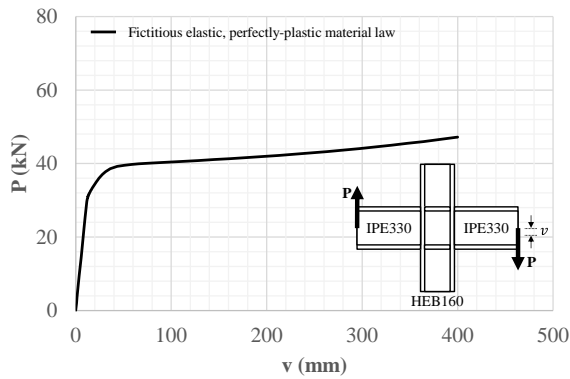
Fig. C-3. Numerical results for the NR4-1-s-/
 simulation: (a)-(b) ($P - v$)_{num} curves, (c)-(d) ($V - \gamma$)_{num} curves and (e)-(f) ($M_B - \Phi$)_{num} curves.

C.1.4 Simulation NR4-1-d-/

Table C-4. Component characterization for the prediction of the NR4-1-d-/ simulation full-range $(M_B - \Phi)_{num}$ curve.

Jaspart (1991)	PZ	CWC*	CWT	CFB	BFC	Corman (2022)		CWP	SE
k_{ini}^c (mm)	1.16	-	-	-	-	K_y^{CWP} (kN)	K_y^{SE} (kN)	88,589.78	7,341.27
$F_{y,Rk}^c$ (kN)	192.31	-	-	526.64	896.51	$V_{y,mod}^{CWP}$ (kN)	$\Delta V_{y,mod}^{SE}$ (kN)	239.69	57.48
k_{pp}^c (mm)	0.023	-	-	-	-	$\Delta K_{y,mod}^{CWP}$ (kN)	-	1,955.57	-
$F_{u,Rk}^c$ (kN)	276.27	-	-	756.59	1,287.94	$V_{pp,mod}^{CWP}$ (kN)	-	297.90	-
$S_{y,Rk}^c$ (kNm/rad)	24,711.33	-	-	-	-	K_{pp}^{CWP} (kN)	K_{pp}^{SE} (kN)	2,112.00	519.13
$M_{y,Rk}^c$ (kNm)	61.25	-	-	167.73	285.54	V_u^{CWP} (kN)	-	402.85	-
S_{pp}^c (kNm/rad)	489.97	-	-	-	-	ΔK_n^{CWP} (kN)	-	242.77	-
$M_{u,Rk}^c$ (kNm)	88.00	-	-	240.97	410.21	V_n^{CWP} (kN)	ΔV_n^{SE} (kN)	436.81	108.94
ϕ_u^c (rad)	0.0546	-	-	-	-	$\gamma_{f,mod}^{CWP}$ (rad)	$\gamma_{f,mod}^{SE}$ (rad)	0.2221	0.1084

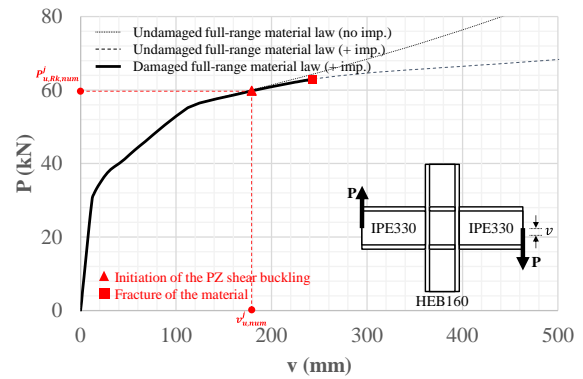
Elastic, perfectly-plastic material law



(a)

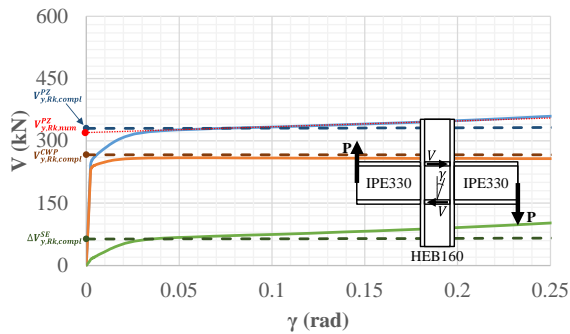
— PZ — CWP — SE

Full-range material law

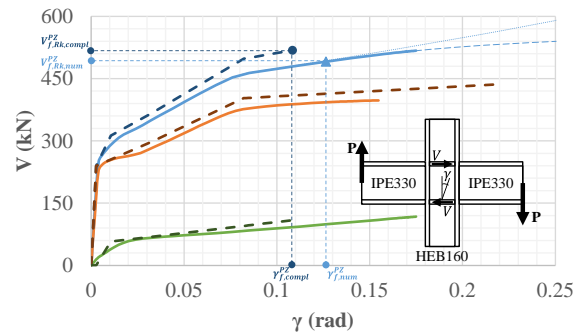


(b)

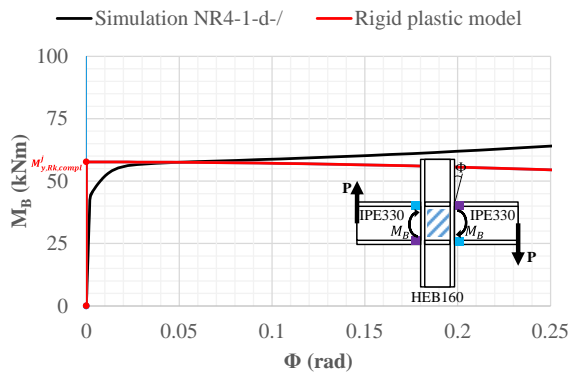
— PZ — CWP — SE



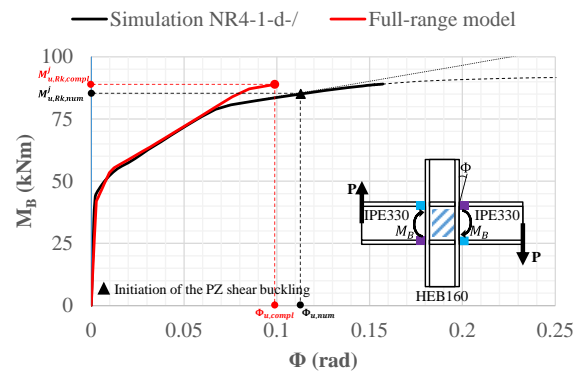
(c)



(d)



(e)



(f)

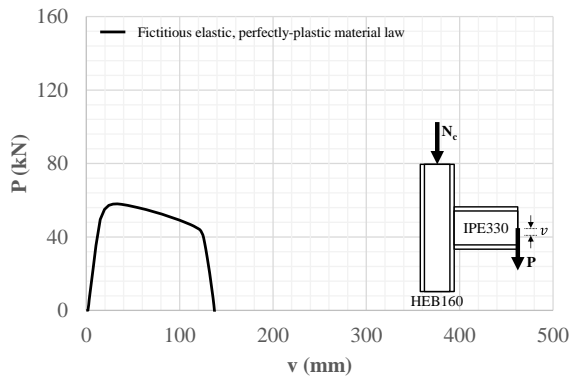
Fig. C-4. Numerical results for the NR4-1-d-/ simulation: (a)-(b) $(P - v)_{num}$ curves, (c)-(d) $(V - \gamma)_{num}$ curves and (e)-(f) $(M_B - \Phi)_{num}$ curves.

C.1.5 Simulation NR4-0-s-0.5N_{pl}

Table C-5. Component characterization for the prediction of the NR4-0-s-0.5N_{pl} simulation full-range ($M_B - \Phi$)_{num} curve.

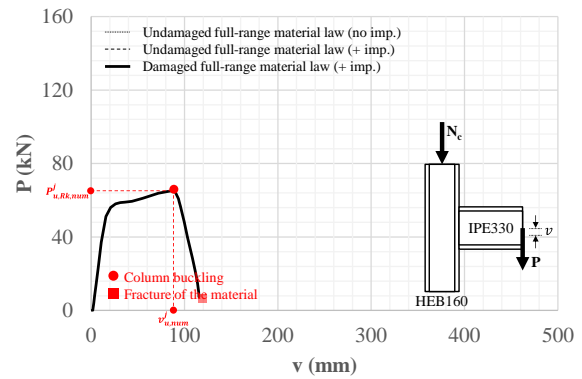
Jaspart (1991)	PZ	CWC*	CWT	CFB	BFC	Corman (2022)		CWP	SE
k_{ini}^c (mm)	2.32	8.16	8.16	-	-	$K_{y,mod}^{CWP}$ (kN)	K_y^{SE} (kN)	88,589.78	3,574.96
$F_{y,Rk}^c$ (kN)	354.15	353.74	353.74	526.64	896.51	$V_{y,mod}^{CWP}$ (kN)	$\Delta V_{y,mod}^{SE}$ (kN)	210.49	22.16
k_{pp}^c (mm)	0.046	0.287	0.163	-	-	$\Delta K_{y,mod}^{CWP}$ (kN)	-	1,955.57	-
$F_{u,Rk}^c$ (kN)	508.78	421.88	508.19	756.59	1,287.94	$V_{pp,mod}^{CWP}$ (kN)	-	262.41	-
S_{mi}^c (kNm/rad)	49,422.66	173,831.44	173,831.44	-	-	K_{pp}^{CWP} (kN)	K_{pp}^{SE} (kN)	2,112.00	252.80
$M_{y,Rk}^c$ (kNm)	112.80	112.67	112.67	167.73	285.54	V_u^{CWP} (kN)	-	370.89	-
S_{pp}^c (kNm/rad)	979.93	6,113.92	3,472.37	-	-	ΔK_n^{CWP} (kN)	-	242.77	-
$M_{u,Rk}^c$ (kNm)	162.05	134.37	161.86	240.97	410.21	V_n^{CWP} (kN)	ΔV_n^{SE} (kN)	402.51	58.84
ϕ_u^c (rad)	0.0503	0.0035	0.0142	-	-	$\gamma_{f,mod}^{CWP}$ (rad)	$\gamma_{f,mod}^{SE}$ (rad)	0.2149	0.1510

Elastic, perfectly-plastic material law

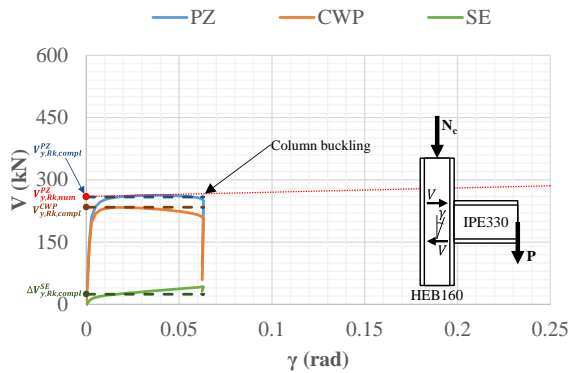


(a)

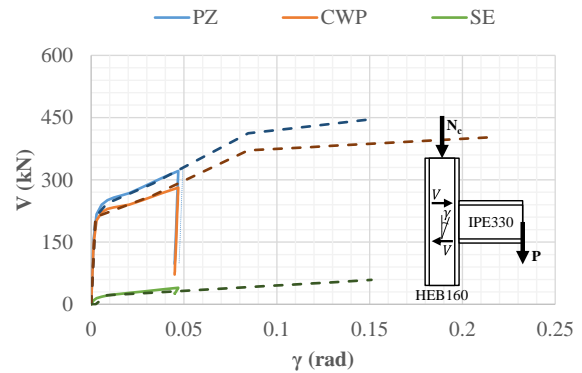
Full-range material law



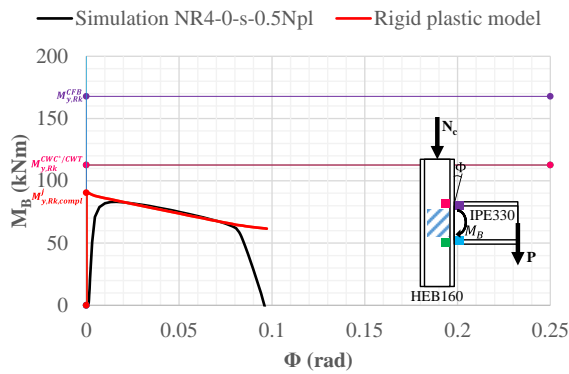
(b)



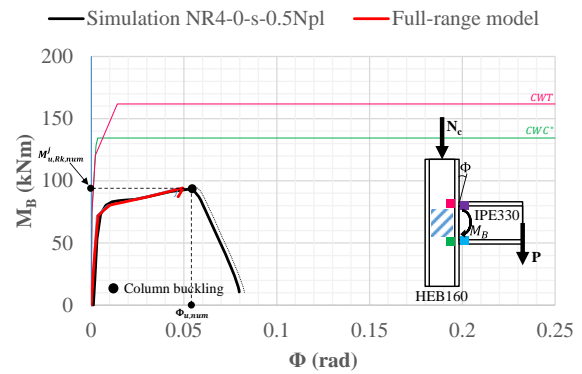
(c)



(d)



(e)



(f)

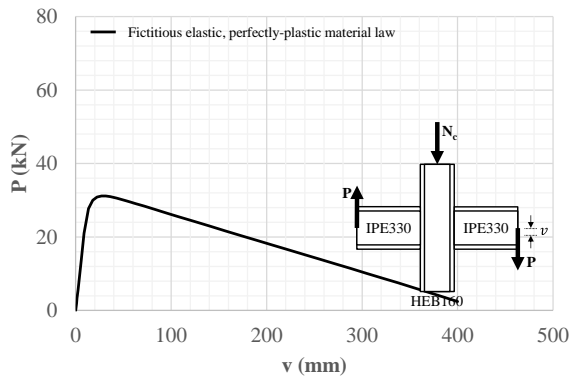
Fig. C-5. Numerical results for the NR4-0-s-0.5N_{pl} simulation: (a)-(b) ($P - v$)_{num} curves, (c)-(d) ($V - \gamma$)_{num} curves and (e)-(f) ($M_B - \Phi$)_{num} curves.

C.1.6 Simulation NR4-0-d-0.5N_{pl}

Table C-6. Component characterization for the prediction of the NR4-0-d-0.5N_{pl} simulation full-range ($M_B - \Phi$)_{num} curve.

Jaspart (1991)	PZ	CWC*	CWT	CFB	BFC	Corman (2022)		CWP	SE
k_{ini}^c (mm)	1.16	8.16	8.16	-	-	K_{y}^{CWP} (kN)	K_{y}^{SE} (kN)	88,589.78	3,574.96
$F_{y,Rk}^c$ (kN)	177.08	249.00	249.00	526.64	896.51	$V_{y,mod}^{CWP}$ (kN)	$\Delta V_{y,mod}^{SE}$ (kN)	221.57	22.16
k_{pp}^c (mm)	0.023	8.16	0.163	-	-	$\Delta K_{y,mod}^{CWP}$ (kN)	-	1,955.57	-
$F_{u,Rk}^c$ (kN)	254.39	336.11	357.72	756.59	1,287.94	$V_{pp,mod}^{CWP}$ (kN)	-	276.22	-
S_{ini}^c (kNm/rad)	24,711.33	173,831.44	173,831.44	-	-	K_{pp}^{CWP} (kN)	K_{pp}^{SE} (kN)	2,112.00	252.80
$M_{y,Rk}^c$ (kNm)	56.40	79.31	79.31	167.73	285.54	V_u^{CWP} (kN)	-	390.41	-
S_{pp}^c (kNm/rad)	489.97	6,113.92	3,472.37	-	-	ΔK_{n}^{CWP} (kN)	-	242.77	-
$M_{u,Rk}^c$ (kNm)	81.02	107.05	113.93	240.97	410.21	V_n^{CWP} (kN)	ΔV_n^{SE} (kN)	423.69	58.84
ϕ_u^c (rad)	0.0502	0.0045	0.0100	-	-	$\gamma_{f,mod}^{CWP}$ (rad)	$\gamma_{f,mod}^{SE}$ (rad)	0.2262	0.1512

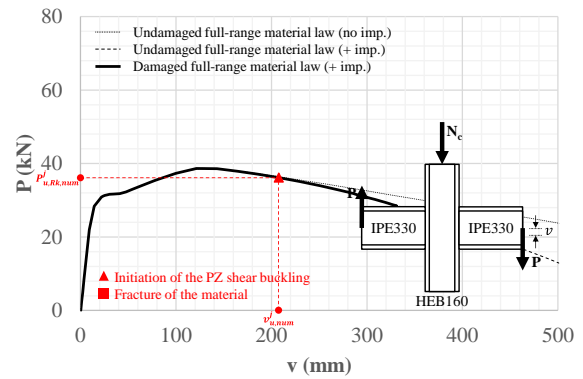
Elastic, perfectly-plastic material law



(a)

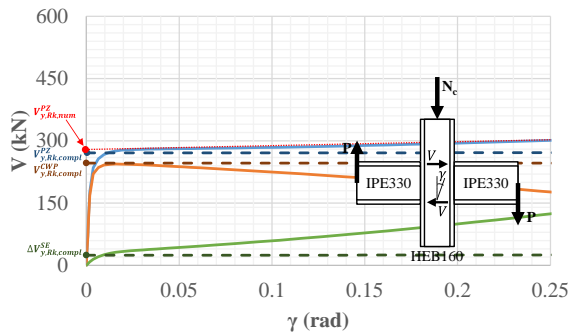
— PZ — CWP — SE

Full-range material law

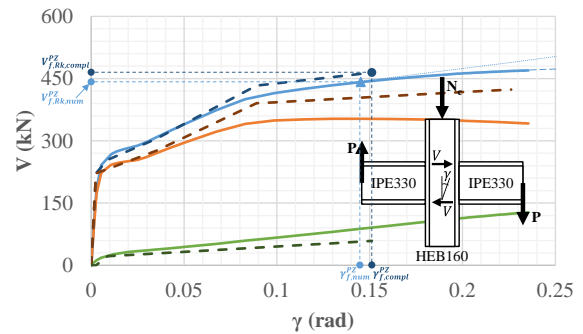


(b)

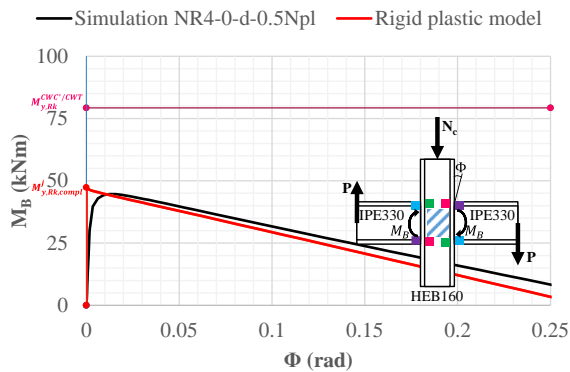
— PZ — CWP — SE



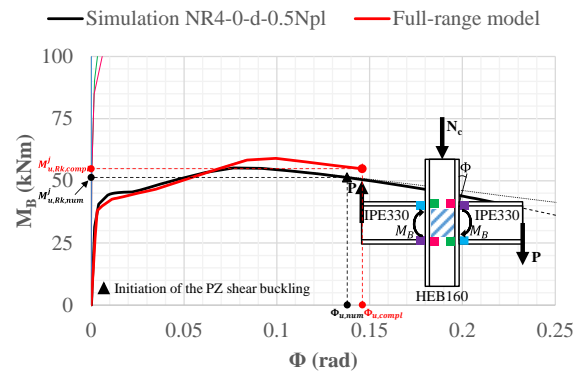
(c)



(d)



(e)



(f)

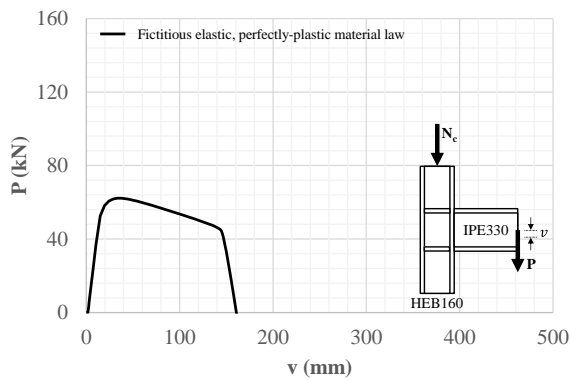
Fig. C-6. Numerical results for the NR4-0-d-0.5N_{pl} simulation: (a)-(b) ($P - v$)_{num} curves, (c)-(d) ($V - \gamma$)_{num} curves and (e)-(f) ($M_B - \Phi$)_{num} curves.

C.1.7 Simulation NR4-1-s-0.5N_{pl}

Table C-7. Component characterization for the prediction of the NR4-1-s-0.5N_{pl} simulation full-range ($M_B - \Phi$)_{num} curve.

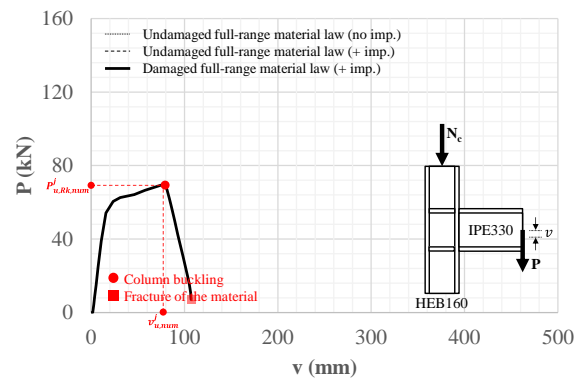
Jaspart (1991)	PZ	CWC*	CWT	CFB	BFC	Corman (2022)		CWP	SE
k_{ini}^c (mm)	2.32	-	-	-	-	K_{y}^{CWP} (kN)	K_{y}^{SE} (kN)	88,589.78	5,458.11
$F_{y,Rk}^c$ (kN)	384.61	-	-	526.64	896.51	$V_{y,mod}^{CWP}$ (kN)	$\Delta V_{y,mod}^{SE}$ (kN)	210.49	38.40
k_{pp}^c (mm)	0.046	-	-	-	-	$\Delta K_{y,mod}^{CWP}$ (kN)	-	1,955.57	-
$F_{u,Rk}^c$ (kN)	552.54	-	-	756.59	1,287.94	$V_{pp,mod}^{CWP}$ (kN)	-	262.41	-
S_{mi}^c (kNm/rad)	49,422.66	-	-	-	-	K_{pp}^{CWP} (kN)	K_{pp}^{SE} (kN)	2,112.00	385.97
$M_{y,Rk}^c$ (kNm)	122.50	-	-	167.73	285.54	V_u^{CWP} (kN)	-	370.89	-
S_{pp}^c (kNm/rad)	979.93	-	-	-	-	ΔK_{pp}^{CWP} (kN)	-	242.77	-
$M_{u,Rk}^c$ (kNm)	175.98	-	-	240.97	410.23	V_n^{CWP} (kN)	ΔV_n^{SE} (kN)	404.87	89.65
ϕ_u^c (rad)	0.0546	-	-	-	-	$\gamma_{f,mod}^{CWP}$ (rad)	$\gamma_{f,mod}^{SE}$ (rad)	0.2246	0.1399

Elastic, perfectly-plastic material law

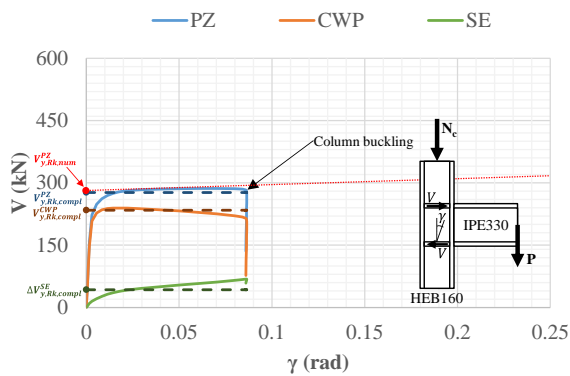


(a)

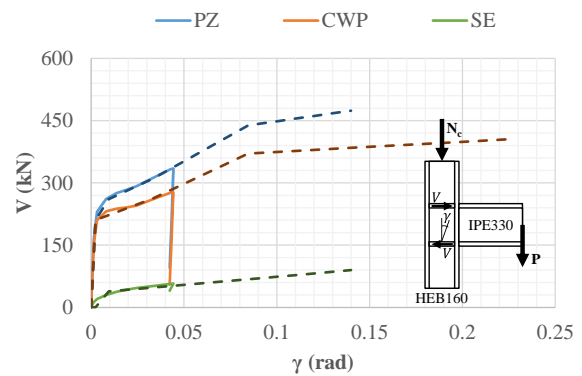
Full-range material law



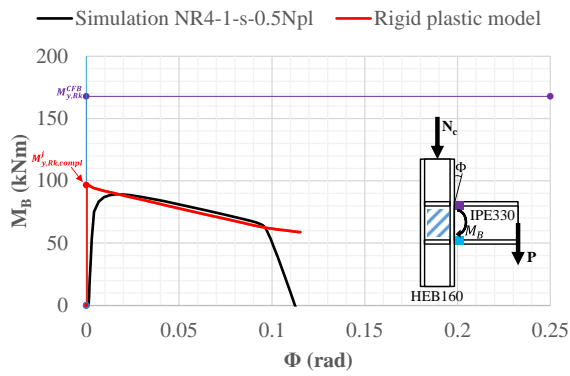
(b)



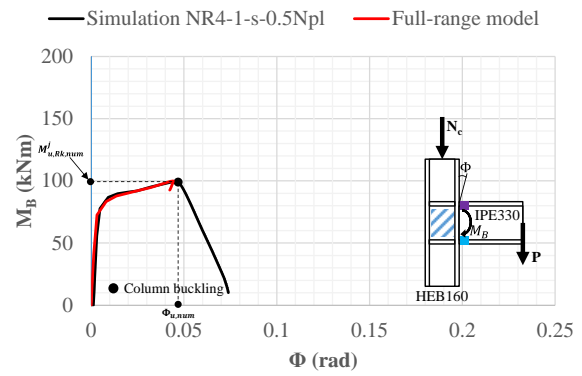
(c)



(d)



(e)



(f)

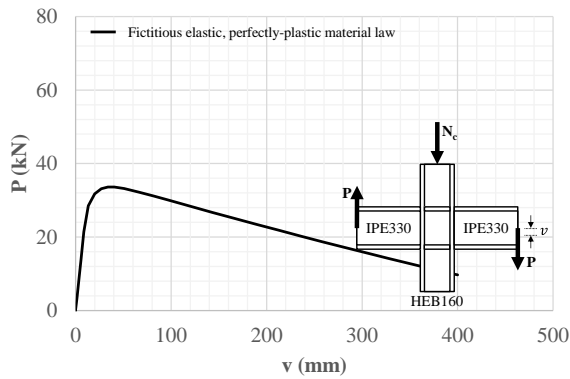
Fig. C-7. Numerical results for the NR4-1-s-0.5N_{pl} simulation: (a)-(b) ($P - v$)_{num} curves, (c)-(d) ($V - \gamma$)_{num} curves and (e)-(f) ($M_B - \Phi$)_{num} curves.

C.1.8 Simulation NR4-1-d-0.5N_{pl}

Table C-8. Component characterization for the prediction of the NR4-1-d-0.5N_{pl} simulation full-range ($M_B - \Phi$)_{num} curve.

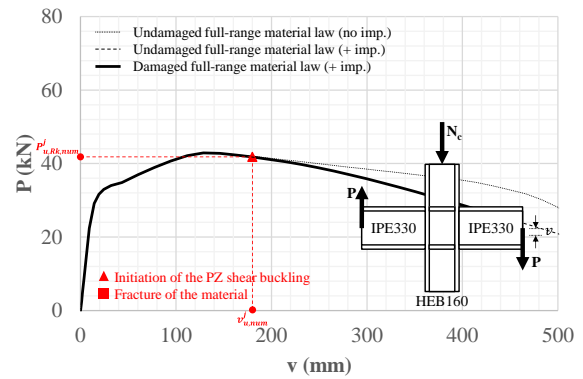
Jaspart (1991)	PZ	CWC*	CWT	CFB	BFC	Corman (2022)		CWP	SE
k_{ini}^c (mm)	1.16	-	-	-	-	K_{y}^{CWP} (kN)	K_{y}^{SE} (kN)	88,589.78	7,341.27
$F_{y,Rk}^c$ (kN)	192.31	-	-	526.64	896.51	$V_{y,mod}^{CWP}$ (kN)	$\Delta V_{y,mod}^{SE}$ (kN)	221.57	44.12
k_{pp}^c (mm)	0.023	-	-	-	-	$\Delta K_{y,mod}^{CWP}$ (kN)	-	1,955.57	-
$F_{u,Rk}^c$ (kN)	276.27	-	-	756.59	1,287.94	$V_{pp,mod}^{CWP}$ (kN)	-	276.22	-
S_{mi}^c (kNm/rad)	24,711.33	-	-	-	-	K_{pp}^{CWP} (kN)	K_{pp}^{SE} (kN)	2,112.00	519.13
$M_{y,Rk}^c$ (kNm)	61.25	-	-	167.73	285.54	V_u^{CWP} (kN)	-	390.41	-
S_{pp}^c (kNm/rad)	489.97	-	-	-	-	ΔK_n^{CWP} (kN)	-	242.77	-
$M_{u,Rk}^c$ (kNm)	88.00	-	-	240.97	410.21	V_n^{CWP} (kN)	ΔV_n^{SE} (kN)	426.18	100.21
ϕ_u^c (rad)	0.0546	-	-	-	-	$\gamma_{f,mod}^{CWP}$ (rad)	$\gamma_{f,mod}^{SE}$ (rad)	0.2364	0.1153

Elastic, perfectly-plastic material law

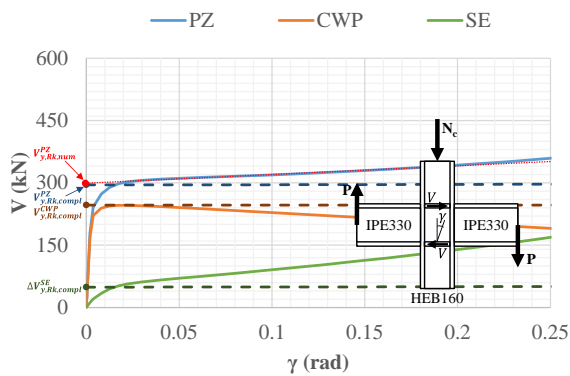


(a)

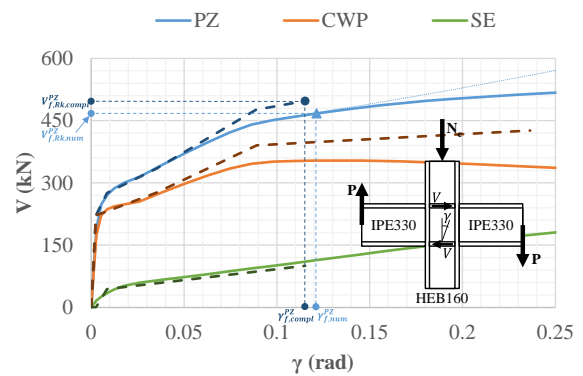
Full-range material law



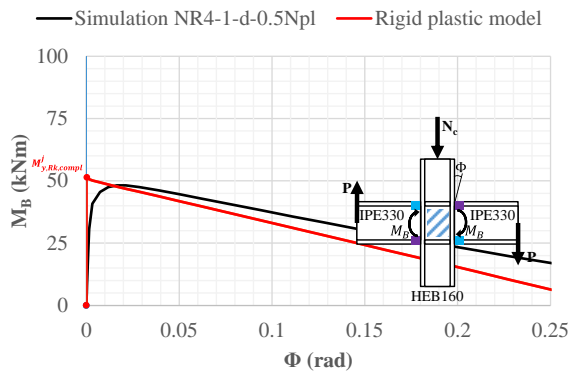
(b)



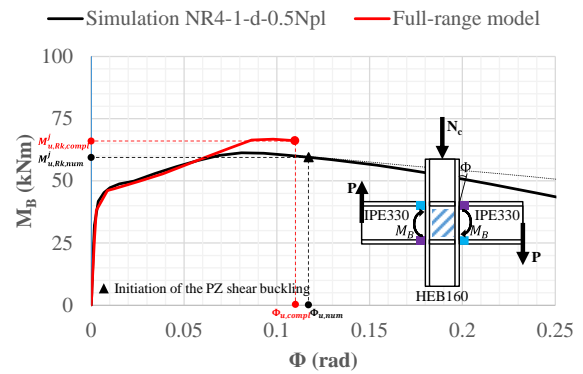
(c)



(d)



(e)



(f)

Fig. C-8. Numerical results for the NR4-1-d-0.5N_{pl} simulation: (a)-(b) ($P - v$)_{num} curves, (c)-(d) ($V - \gamma$)_{num} curves and (e)-(f) ($M_B - \Phi$)_{num} curves.

C.2 Model NR16

C.2.1 Simulation NR16-0-s-/

Table C-9. Component characterization for the prediction of the NR16-0-s-/ simulation full-range $(M_B - \Phi)_{num}$ curve.

Jaspart (1991)	PZ	CWC*	CWT	CFB	BFC	Corman (2022)		CWP	SE
k_{ini}^c (mm)	4.44	9.55	9.55	-	-	K_y^{CWP} (kN)	K_y^{SE} (kN)	243,718.08	10,671.83
$F_{y,Rk}^c$ (kN)	1,005.82	877.88	877.88	1,543.19	3,621.13	$V_{y,mod}^{CWP}$ (kN)	$\Delta V_{y,mod}^{SE}$ (kN)	601.85	98.92
k_{pp}^c (mm)	0.089	0.382	0.191	-	-	$\Delta K_{y,mod}^{CWP}$ (kN)	-	5,044.92	-
$F_{u,Rk}^c$ (kN)	1,444.98	877.88	1,261.17	2,216.97	5,202.18	$V_{pp,mod}^{CWP}$ (kN)	-	748.03	-
S_{ini}^c (kNm/rad)	207,723.80	446,793.31	446,793.31	-	-	K_{pp}^{CWP} (kN)	K_{pp}^{SE} (kN)	5,445.00	754.65
$M_{y,Rk}^c$ (kNm)	474.75	414.36	414.36	728.39	1,709.17	V_u^{CWP} (kN)	-	928.33	-
S_{pp}^c (kNm/rad)	4,163.83	17,871.73	8,935.87	-	-	ΔK_{pp}^{CWP} (kN)	-	-	-
$M_{u,Rk}^c$ (kNm)	682.03	414.36	595.27	728.39	1,709.17	V_n^{CWP} (kN)	ΔV_n^{SE} (kN)	-	187.91
ϕ_u^c (rad)	0.0498	0.0028	0.0202	-	-	$\gamma_{f,mod}^{CWP}$ (rad)	$\gamma_{f,mod}^{SE}$ (rad)	0.0646	0.1276

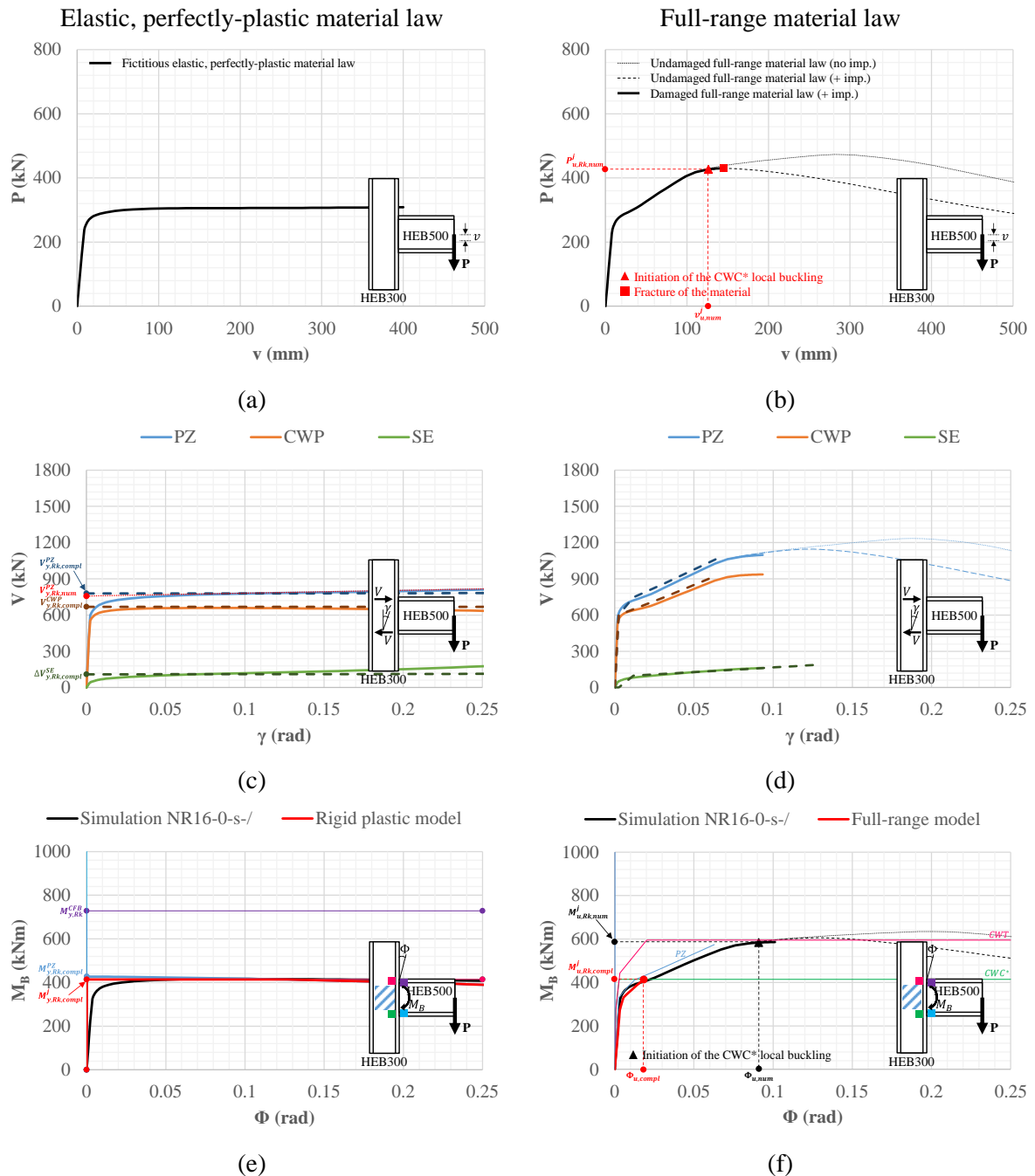


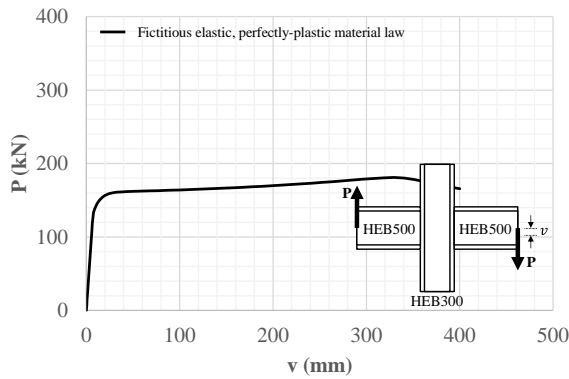
Fig. C-9. Numerical results for the NR16-0-s-/ simulation: (a)-(b) $(P - v)_{num}$, (c)-(d) $(V - \gamma)_{num}$ and (e)-(f) $(M_B - \Phi)_{num}$.

C.2.2 Simulation NR16-0-d-/

Table C-10. Component characterization for the prediction of the NR16-0-d-/ simulation full-range ($M_B - \Phi$)_{num} curve.

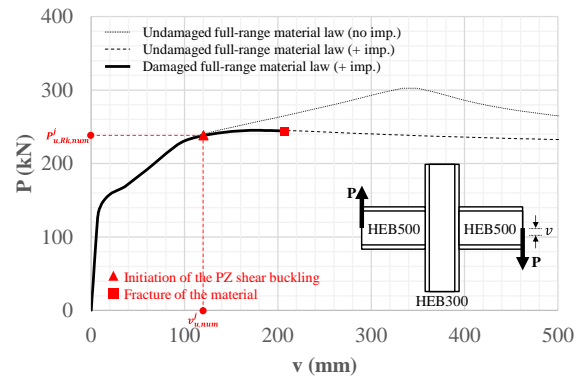
Jaspart (1991)	PZ	CWC*	CWT	CFB	BFC	Corman (2022)		CWP	SE
k_{ini}^c (mm)	2.22	9.55	9.55	-	-	$K_{y,mod}^{CWP}$ (kN)	K_y^{SE} (kN)	243,718.08	10,671.83
$F_{y,Rk}^c$ (kN)	502.91	657.18	657.18	1,543.19	3,621.13	$V_{y,mod}^{CWP}$ (kN)	$\Delta V_{y,mod}^{SE}$ (kN)	633.53	98.92
k_{pp}^c (mm)	0.044	0.382	0.191	-	-	$\Delta K_{y,mod}^{CWP}$ (kN)	-	5,044.92	-
$F_{u,Rk}^c$ (kN)	722.49	686.66	944.11	2,216.97	5,202.18	$V_{pp,mod}^{CWP}$ (kN)	-	787.40	-
S_{ini}^c (kNm/rad)	103,861.90	446,793.31	446,793.31	-	-	K_{pp}^{CWP} (kN)	K_{pp}^{SE} (kN)	5,445.00	754.65
$M_{y,Rk}^c$ (kNm)	237.37	310.19	310.19	728.39	1,709.17	V_u^{CWP} (kN)	-	977.18	-
S_{pp}^c (kNm/rad)	2,058.52	17,871.73	8,935.87	-	-	ΔK_n^{CWP} (kN)	-	-	-
$M_{u,Rk}^c$ (kNm)	341.02	324.10	445.62	1,046.41	2,455.43	V_n^{CWP} (kN)	ΔV_n^{SE} (kN)	-	187.91
ϕ_u^c (rad)	0.0504	0.0023	0.0152	-	-	$\gamma_{f,mod}^{CWP}$ (rad)	$\gamma_{f,mod}^{SE}$ (rad)	0.0680	0.1278

Elastic, perfectly-plastic material law



(a)

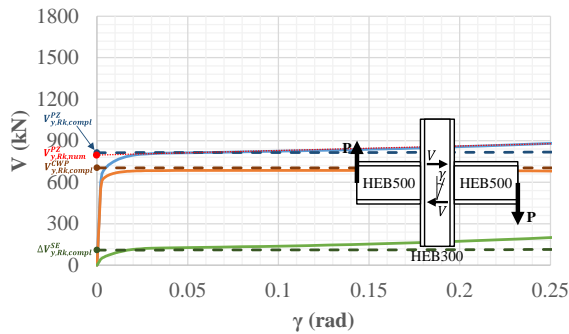
Full-range material law



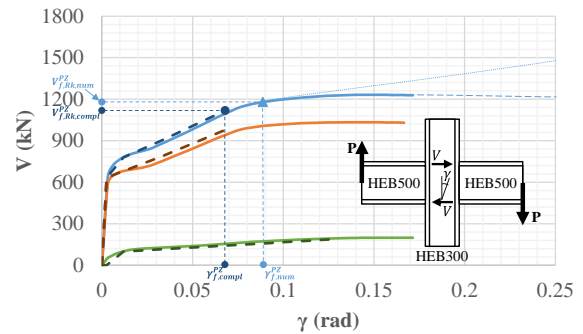
(b)

— PZ — CWP — SE

— PZ — CWP — SE

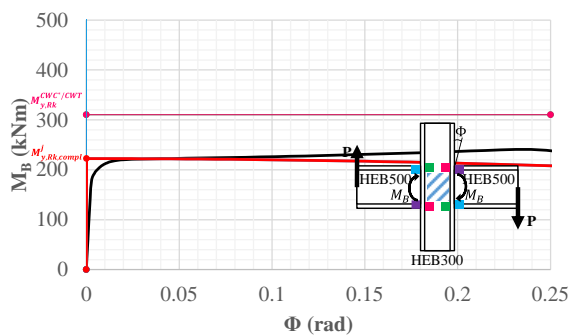


(c)



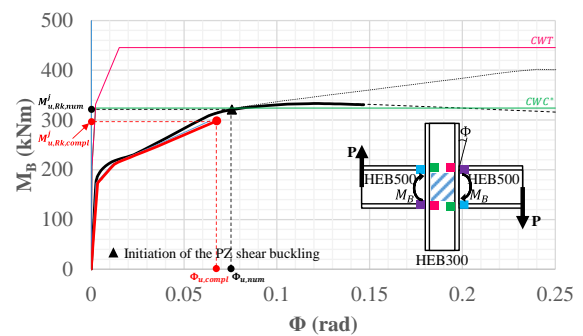
(d)

— Simulation NR16-0-d-/ — Rigid plastic model



(e)

— Simulation NR16-0-d-/ — Full-range model



(f)

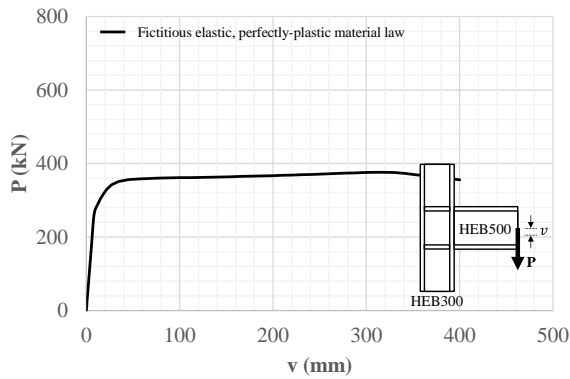
Fig. C-10. Numerical results for the NR16-0-d-/ simulation: (a)-(b) ($P - v$)_{num} curves, (c)-(d) ($V - \gamma$)_{num} curves and (e)-(f) ($M_B - \Phi$)_{num} curves.

C.2.3 Simulation NR16-1-s-/

Table C-11. Component characterization for the prediction of the NR16-1-s-/

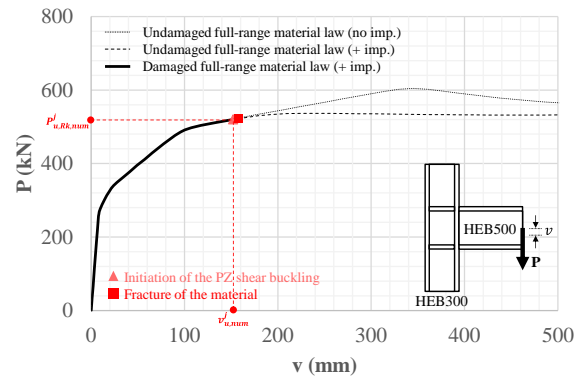
Jaspart (1991)	PZ	CWC*	CWT	CFB	BFC	Corman (2022)		CWP	SE
k_{ini}^c (mm)	4.44	-	-	-	-	K_{y}^{CWP} (kN)	K_{y}^{SE} (kN)	243,718.08	19,739.21
$F_{y,Rk}^c$ (kN)	1,099.47	-	-	1,543.19	3,621.13	$V_{y,mod}^{CWP}$ (kN)	$\Delta V_{y,mod}^{SE}$ (kN)	601.85	195.92
k_{pp}^c (mm)	0.089	-	-	-	-	$\Delta K_{y,mod}^{CWP}$ (kN)	-	5,044.92	-
$F_{u,Rk}^c$ (kN)	1,579.52	-	-	2,216.97	5,202.18	$V_{pp,mod}^{CWP}$ (kN)	-	748.03	-
S_{ini}^c (kNm/rad)	207,723.80	-	-	-	-	K_{pp}^{CWP} (kN)	K_{pp}^{SE} (kN)	5,445.00	1,395.84
$M_{y,Rk}^c$ (kNm)	518.95	-	-	728.39	1,709.17	V_u^{CWP} (kN)	-	971.90	-
S_{pp}^c (kNm/rad)	4,163.83	-	-	-	-	ΔK_{pp}^{CWP} (kN)	-	-	-
$M_{u,Rk}^c$ (kNm)	745.53	-	-	1,046.71	2,455.43	V_n^{CWP} (kN)	ΔV_n^{SE} (kN)	-	372.61
ϕ_u^c (rad)	0.0544	-	-	-	-	$\gamma_{f,mod}^{CWP}$ (rad)	$\gamma_{f,mod}^{SE}$ (rad)	0.0726	0.1365

Elastic, perfectly-plastic material law



(a)

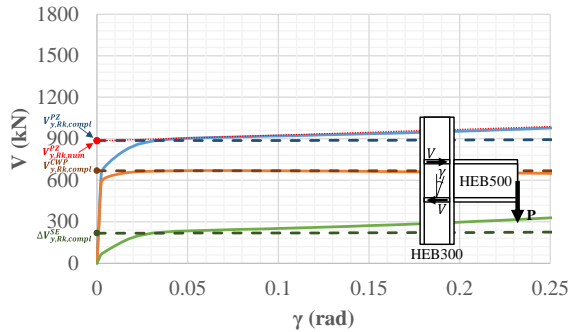
Full-range material law



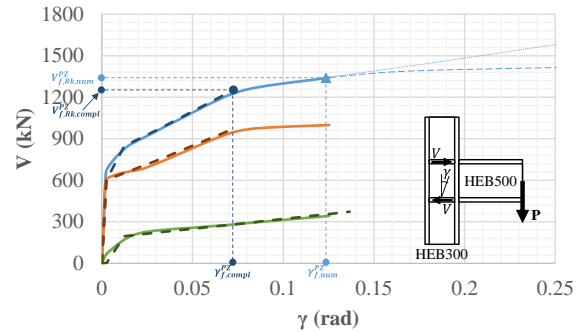
(b)

— PZ — CWP — SE

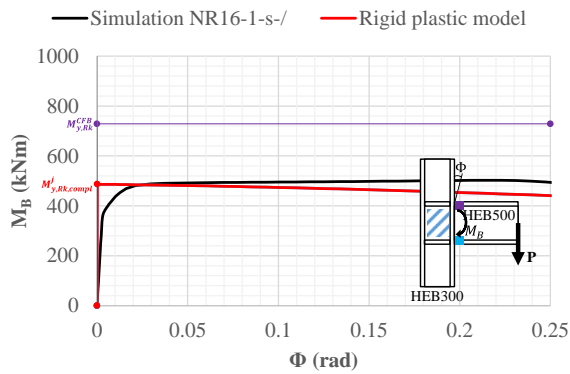
— PZ — CWP — SE



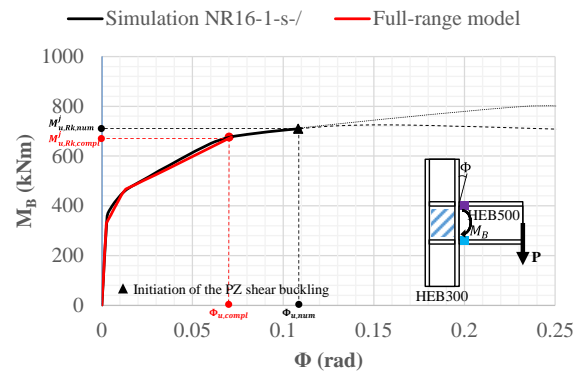
(c)



(d)



(e)



(f)

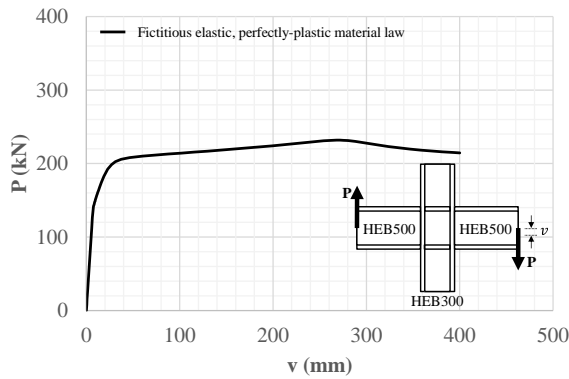
Fig. C-11. Numerical results for the NR16-1-s-/

C.2.4 Simulation NR16-1-d-/

Table C-12. Component characterization for the prediction of the NR16-1-d-/ simulation full-range ($M_B - \Phi$)_{num} curve.

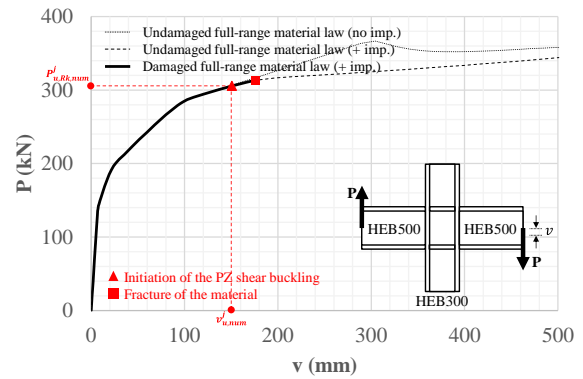
Jaspart (1991)	PZ	CWC*	CWT	CFB	BFC	Corman (2022)		CWP	SE
k_{ini}^c (mm)	2.22	-	-	-	-	K_y^{CWP} (kN)	K_y^{SE} (kN)	243,718.08	24,019.29
$F_{y,Rk}^c$ (kN)	549.73	-	-	1,543.19	3,621.13	$V_{y,mod}^{CWP}$ (kN)	$\Delta V_{y,mod}^{SE}$ (kN)	633.53	272.54
k_{pp}^c (mm)	0.044	-	-	-	-	$\Delta K_{y,mod}^{CWP}$ (kN)	-	5,044.92	-
$F_{u,Rk}^c$ (kN)	789.76	-	-	2,216.97	5,202.18	$V_{pp,mod}^{CWP}$ (kN)	-	787.40	-
S_{ini}^c (kNm/rad)	103,861.90	-	-	-	-	K_{pp}^{CWP} (kN)	K_{pp}^{SE} (kN)	5,445.00	1,698.51
$M_{y,Rk}^c$ (kNm)	259.47	-	-	728.39	1,709.17	V_u^{CWP} (kN)	-	1,023.05	-
S_{pp}^c (kNm/rad)	2,058.52	-	-	-	-	ΔK_{pp}^{CWP} (kN)	-	-	-
$M_{u,Rk}^c$ (kNm)	372.77	-	-	1046.41	2,455.43	V_n^{CWP} (kN)	ΔV_n^{SE} (kN)	-	519.82
ϕ_u^c (rad)	0.0550	-	-	-	-	$\gamma_{f,mod}^{CWP}$ (rad)	$\gamma_{f,mod}^{SE}$ (rad)	0.0764	0.1558

Elastic, perfectly-plastic material law

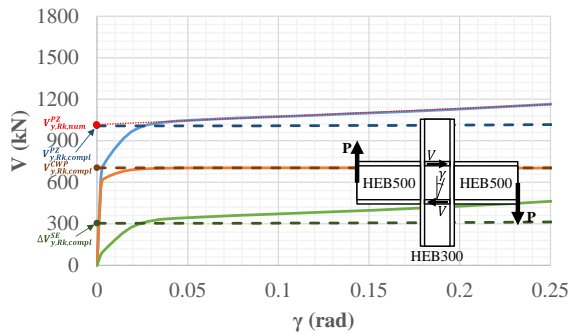


(a)

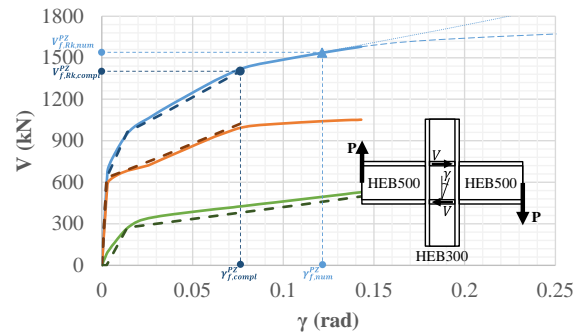
Full-range material law



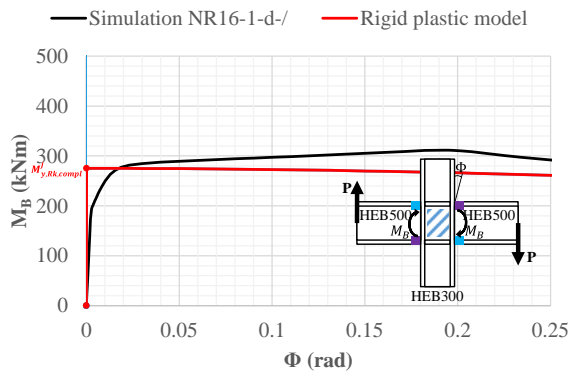
(b)



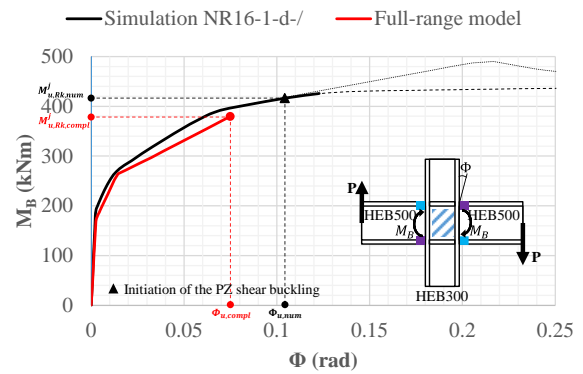
(c)



(d)



(e)



(f)

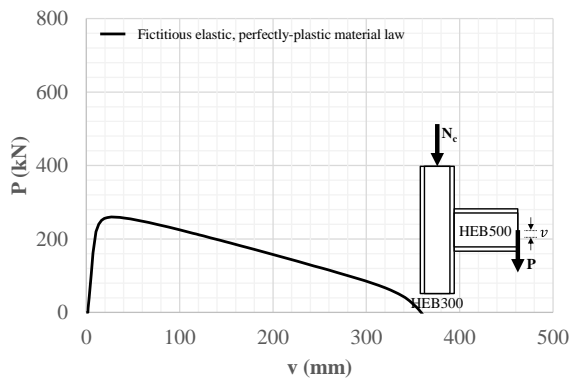
Fig. C-12. Numerical results for the NR16-1-d-/ simulation: (a)-(b) ($P - v$)_{num} curves, (c)-(d) ($V - \gamma$)_{num} curves and (e)-(f) ($M_B - \Phi$)_{num} curves.

C.2.5 Simulation NR16-0-s-0.5N_{pl}

Table C-13. Component characterization for the prediction of the NR16-0-s-0.5N_{pl} simulation full-range ($M_B - \Phi$)_{num} curve.

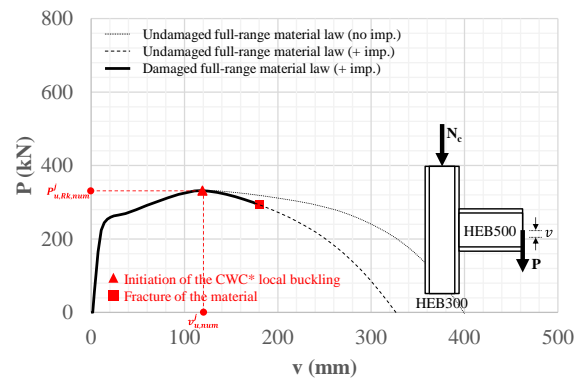
Jaspart (1991)	PZ	CWC*	CWT	CFB	BFC	Corman (2022)		CWP	SE
k_{ini}^c (mm)	4.44	9.55	9.55	-	-	$K_{y,mod}^{CWP}$ (kN)	K_y^{SE} (kN)	243,718.08	10,671.83
$F_{y,Rk}^c$ (kN)	1,005.82	877.88	877.88	1,543.19	3,621.13	$V_{y,mod}^{CWP}$ (kN)	$\Delta V_{y,mod}^{SE}$ (kN)	567.66	68.11
k_{pp}^c (mm)	0.089	0.382	0.191	-	-	$\Delta K_{y,mod}^{CWP}$ (kN)	-	5,044.92	-
$F_{u,Rk}^c$ (kN)	1,444.98	877.88	1,261.17	2,216.97	5,202.18	$V_{pp,mod}^{CWP}$ (kN)	-	707.08	-
S_{ini}^c (kNm/rad)	207,723.80	446,793.31	446,793.31	-	-	K_{pp}^{CWP} (kN)	K_{pp}^{SE} (kN)	5,445.00	754.65
$M_{y,Rk}^c$ (kNm)	474.75	414.36	414.36	728.39	1,709.17	V_u^{CWP} (kN)	-	906.47	-
S_{pp}^c (kNm/rad)	4,163.83	17,871.73	8,935.87	-	-	ΔK_{pp}^{CWP} (kN)	-	-	-
$M_{u,Rk}^c$ (kNm)	682.03	414.36	595.27	728.39	1,709.17	V_n^{CWP} (kN)	ΔV_n^{SE} (kN)	-	167.81
ϕ_u^c (rad)	0.0498	0.0028	0.0202	-	-	$\gamma_{f,mod}^{CWP}$ (rad)	$\gamma_{f,mod}^{SE}$ (rad)	0.0698	0.1387

Elastic, perfectly-plastic material law

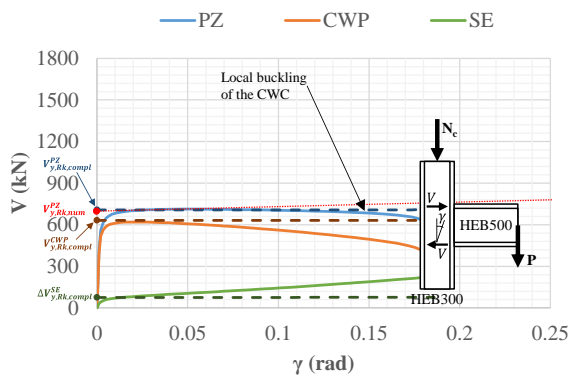


(a)

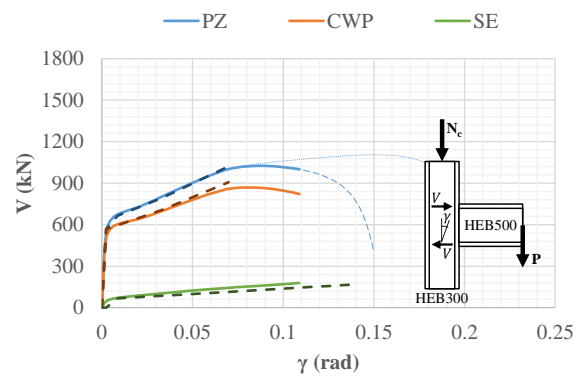
Full-range material law



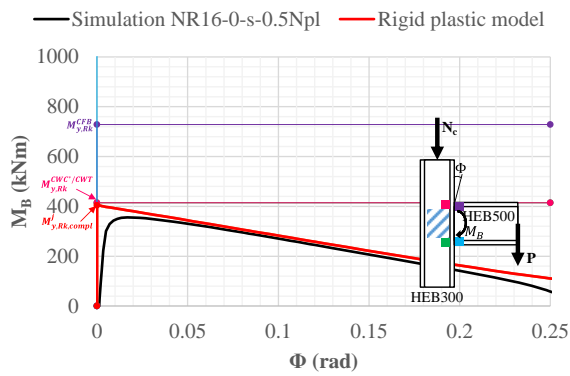
(b)



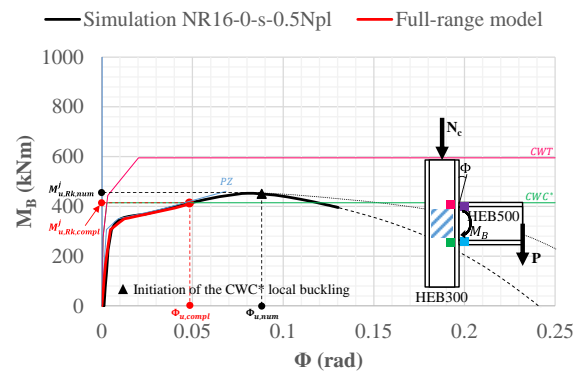
(c)



(d)



(e)



(f)

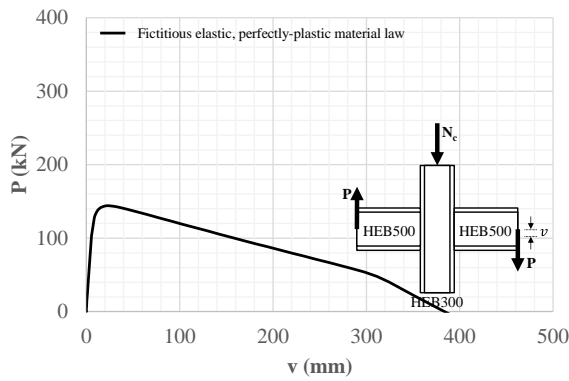
Fig. C-13. Numerical results for the NR16-0-s-0.5N_{pl} simulation: (a)-(b) ($P - v$)_{num} curves, (c)-(d) ($V - \gamma$)_{num} curves and (e)-(f) ($M_B - \Phi$)_{num} curves.

C.2.6 Simulation NR16-0-d-0.5N_{pl}

Table C-14. Component characterization for the prediction of the NR16-0-d-0.5N_{pl} simulation full-range ($M_B - \Phi$)_{num} curve.

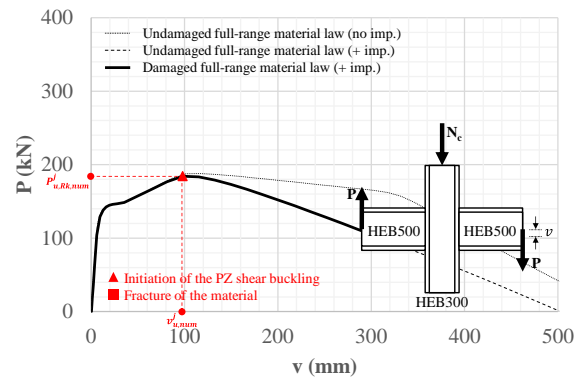
k_{ini}^c (mm)	PZ	CWC*	CWT	CFB	BFC	Corman (2022)		CWP	SE
$F_{y,Rk}^c$ (kN)	2.22	9.55	9.55	-	-	K_{y}^{CWP} (kN)	K_{y}^{SE} (kN)	243,718.08	10,671.83
k_{pp}^c (mm)	502.91	657.18	657.18	1,543.19	3,621.13	$V_{y,mod}^{CWP}$ (kN)	$\Delta V_{y,mod}^{SE}$ (kN)	597.54	68.11
$F_{u,Rk}^c$ (kN)	0.044	0.382	0.191	-	-	$\Delta K_{y,mod}^{CWP}$ (kN)	-	5,044.92	-
S_{ini}^c (kNm/rad)	722.49	686.66	944.11	2,216.97	5,202.18	$V_{pp,mod}^{CWP}$ (kN)	-	744.29	-
$M_{y,Rk}^c$ (kNm)	103,861.90	446,793.31	446,793.31	-	-	K_{pp}^{CWP} (kN)	K_{pp}^{SE} (kN)	5,445.00	754.65
S_{pp}^c (kNm/rad)	237.37	310.19	310.19	728.39	1,709.17	V_u^{CWP} (kN)	-	954.18	-
$M_{u,Rk}^c$ (kNm)	2,058.52	17,871.73	8,935.87	-	-	ΔK_{u}^{CWP} (kN)	-	-	-
Φ_u^c (rad)	341.02	324.10	445.62	1,046.41	2,455.43	V_n^{CWP} (kN)	ΔV_n^{SE} (kN)	-	167.81
k_{ini}^c (mm)	0.0504	0.0023	0.0152	-	-	$\gamma_{f,mod}^{CWP}$ (rad)	$\gamma_{f,mod}^{SE}$ (rad)	0.0735	0.1388

Elastic, perfectly-plastic material law

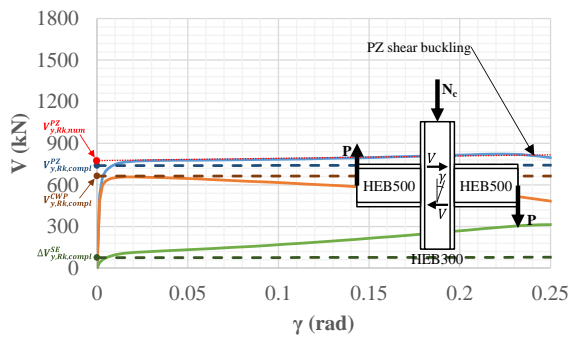


(a)

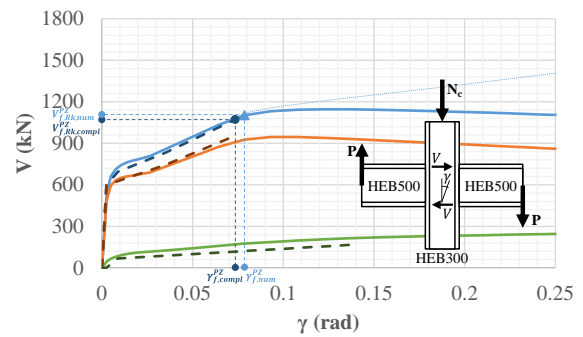
Full-range material law



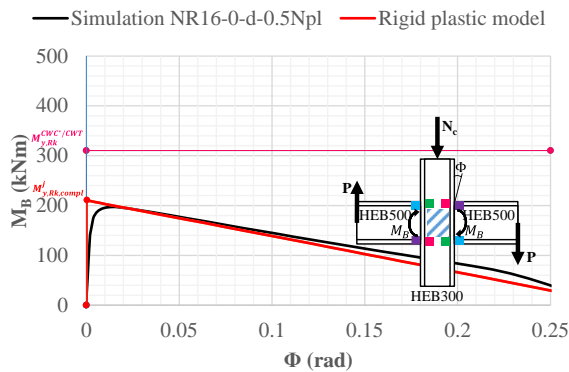
(b)



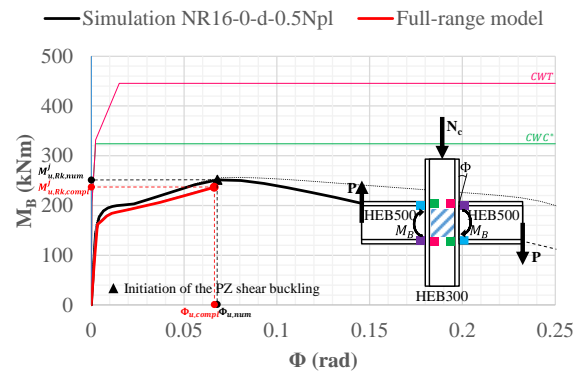
(c)



(d)



(e)



(f)

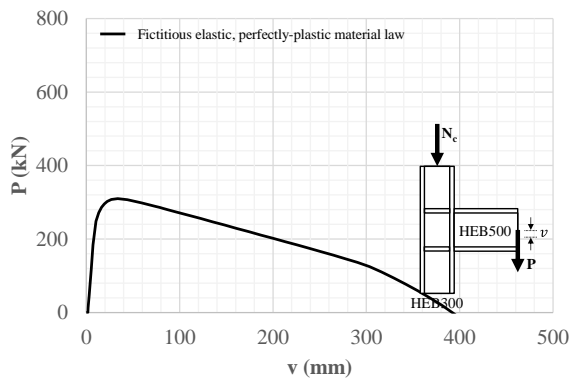
Fig. C-14. Numerical results for the NR16-0-d-0.5N_{pl} simulation: (a)-(b) ($P - v$)_{num} curves, (c)-(d) ($V - \gamma$)_{num} curves and (e)-(f) ($M_B - \Phi$)_{num} curves.

C.2.7 Simulation NR16-1-s-0.5N_{pl}

Table C-15. Component characterization for the prediction of the NR16-1-s-0.5N_{pl} simulation full-range ($M_B - \Phi$)_{num} curve.

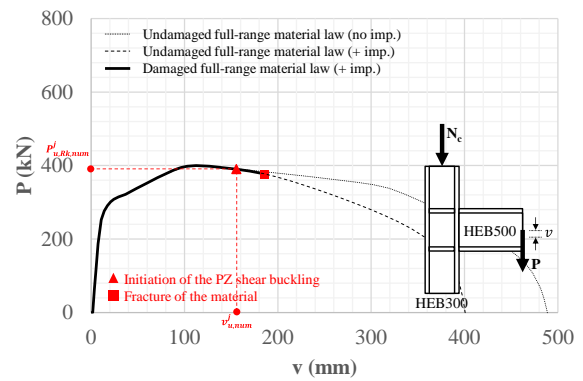
Jaspart (1991)	PZ	CWC*	CWT	CFB	BFC	Corman (2022)		CWP	SE
k_{ini}^c (mm)	4.44	-	-	-	-	$K_{y,mod}^{CWP}$ (kN)	K_y^{SE} (kN)	243,718.08	19,739.21
$F_{y,Rk}^c$ (kN)	1,099.47	-	-	1,543.19	3,621.13	$V_{y,mod}^{CWP}$ (kN)	$\Delta V_{y,mod}^{SE}$ (kN)	567.66	165.11
k_{pp}^c (mm)	0.089	-	-	-	-	$\Delta K_{y,mod}^{CWP}$ (kN)	-	5,044.92	-
$F_{u,Rk}^c$ (kN)	1,579.52	-	-	2,216.97	5,202.18	$V_{pp,mod}^{CWP}$ (kN)	-	707.08	-
S_{ini}^c (kNm/rad)	207,723.80	-	-	-	-	K_{pp}^{CWP} (kN)	K_{pp}^{SE} (kN)	5,445.00	1,395.84
$M_{y,Rk}^c$ (kNm)	518.95	-	-	728.39	1,709.17	V_u^{CWP} (kN)	-	949.01	-
S_{pp}^c (kNm/rad)	4,163.83	-	-	-	-	ΔK_{pp}^{CWP} (kN)	-	-	-
$M_{u,Rk}^c$ (kNm)	745.53	-	-	1,046.71	2,455.43	V_n^{CWP} (kN)	ΔV_n^{SE} (kN)	-	352.53
ϕ_u^c (rad)	0.0544	-	-	-	-	$\gamma_{f,mod}^{CWP}$ (rad)	$\gamma_{f,mod}^{SE}$ (rad)	0.0776	0.1424

Elastic, perfectly-plastic material law

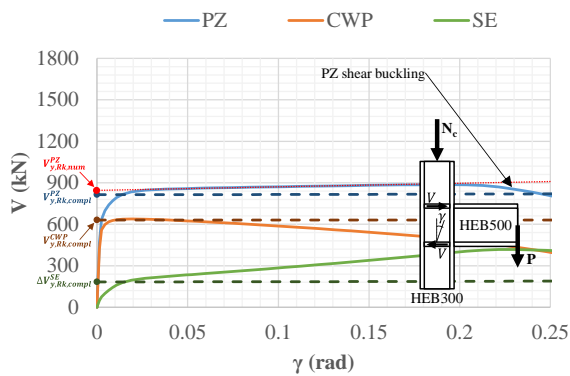


(a)

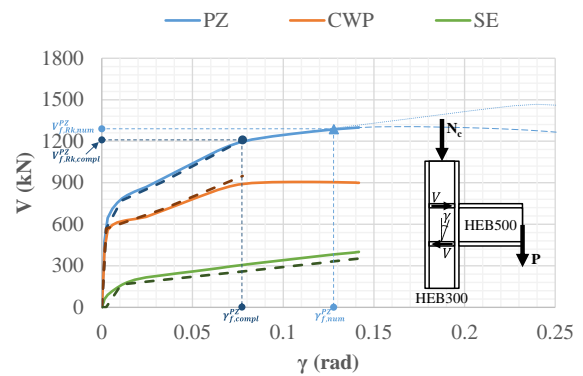
Full-range material law



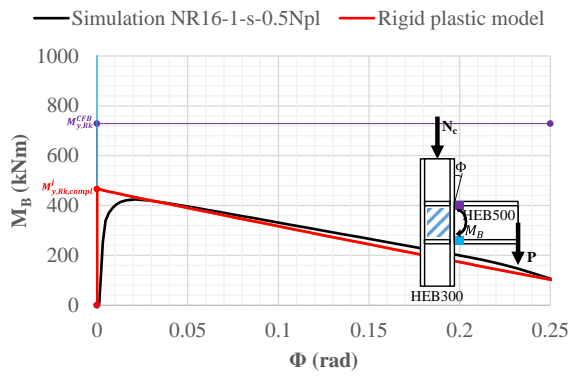
(b)



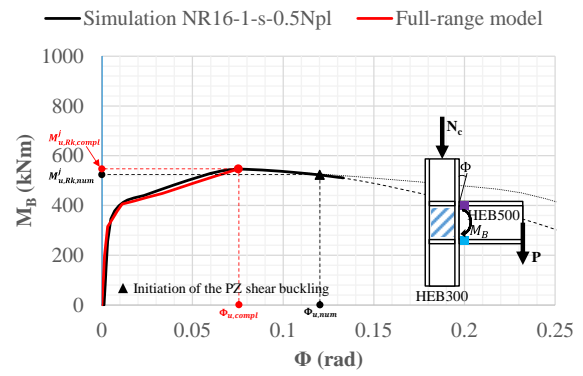
(c)



(d)



(e)



(f)

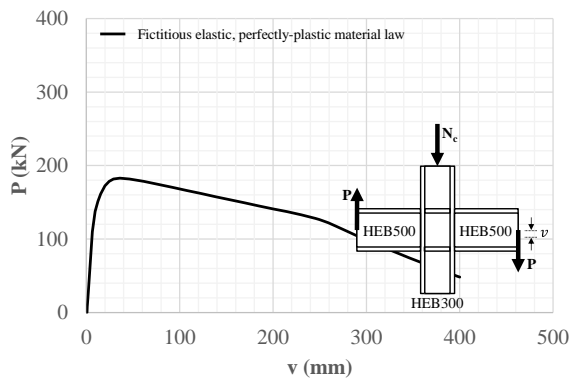
Fig. C-15. Numerical results for the NR16-1-s-0.5N_{pl} simulation: (a)-(b) ($P - v$)_{num} curves, (c)-(d) ($V - \gamma$)_{num} curves and (e)-(f) ($M_B - \Phi$)_{num} curves.

C.2.8 Simulation NR16-1-d-0.5N_{pl}

Table C-16. Component characterization for the prediction of the NR16-1-d-0.5N_{pl} simulation full-range ($M_B - \Phi$)_{num} curve.

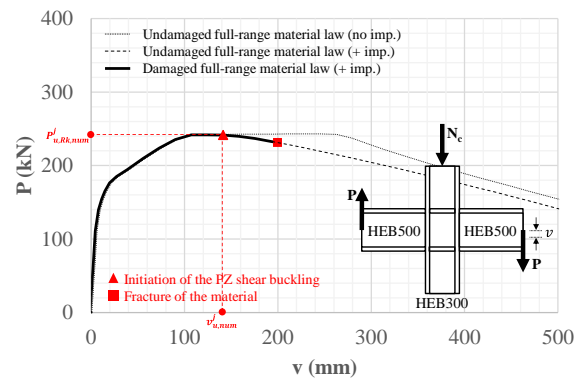
Jaspart (1991)	PZ	CWC*	CWT	CFB	BFC	Corman (2022)		CWP	SE
k_{ini}^c (mm)	2.22	-	-	-	-	K_y^{CWP} (kN)	K_y^{SE} (kN)	243,718.08	28,806.59
$F_{y,Rk}^c$ (kN)	549.73	-	-	1,543.19	3,621.13	$V_{y,mod}^{CWP}$ (kN)	$\Delta V_{y,mod}^{SE}$ (kN)	597.54	241.74
k_{pp}^c (mm)	0.044	-	-	-	-	$\Delta K_{y,mod}^{CWP}$ (kN)	-	5,044.92	-
$F_{u,Rk}^c$ (kN)	789.76	-	-	2,216.97	5,202.18	$V_{pp,mod}^{CWP}$ (kN)	-	744.29	-
S_{ini}^c (kNm/rad)	103,861.90	-	-	-	-	K_{pp}^{CWP} (kN)	K_{pp}^{SE} (kN)	5,445.00	2,037.04
$M_{y,Rk}^c$ (kNm)	259.47	-	-	728.39	1,709.17	V_u^{CWP} (kN)	-	998.96	-
S_{pp}^c (kNm/rad)	2,058.52	-	-	-	-	ΔK_{pp}^{CWP} (kN)	-	-	-
$M_{u,Rk}^c$ (kNm)	372.77	-	-	1046.41	2,455.43	V_n^{CWP} (kN)	ΔV_n^{SE} (kN)	-	497.60
ϕ_u^c (rad)	0.0550	-	-	-	-	$\gamma_{f,mod}^{CWP}$ (rad)	$\gamma_{f,mod}^{SE}$ (rad)	0.0817	0.1344

Elastic, perfectly-plastic material law

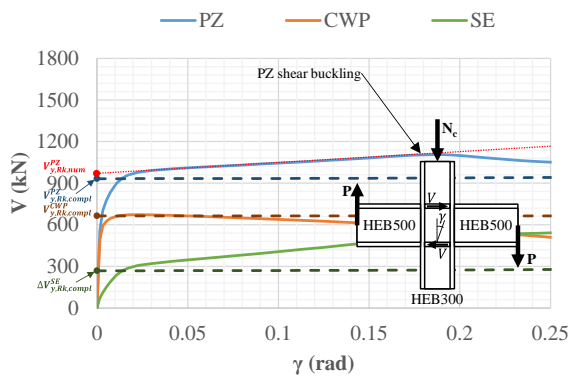


(a)

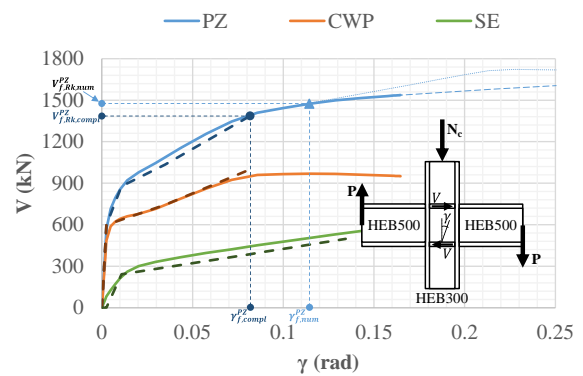
Full-range material law



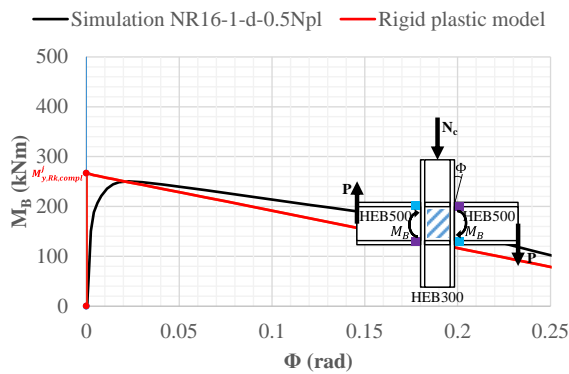
(b)



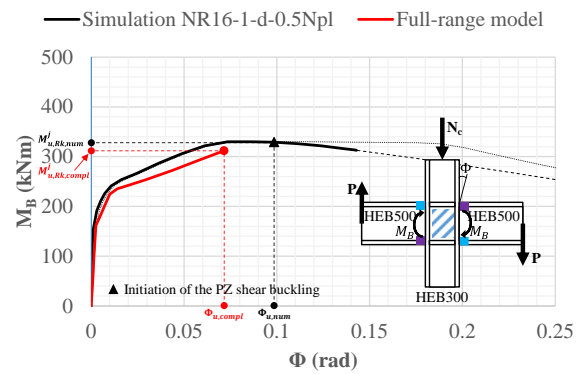
(c)



(d)



(e)



(f)

Fig. C-16. Numerical results for the NR16-1-d-0.5N_{pl} simulation: (a)-(b) ($P - v$)_{num} curves, (c)-(d) ($V - \gamma$)_{num} curves and (e)-(f) ($M_B - \Phi$)_{num} curves.

C.3 Model A

C.3.1 Simulation A-0-s-/

Table C-17. Component characterization for the prediction of the A-0-s-/ simulation full-range $(M_B - \Phi)_{num}$ curve.

Jaspart (1991)	PZ	CWC*	CWT	CFB	BFC	Corman (2022)		CWP	SE
k_{ini}^c (mm)	3.72	8.00	8.00	-	-	K_y^{CWP} (kN)	K_y^{SE} (kN)	97,498.32	5,945.82
$F_{y,Rk}^c$ (kN)	341.70	342.98	342.98	301.75	409.02	$V_{y,mod}^{CWP}$ (kN)	$\Delta V_{y,mod}^{SE}$ (kN)	227.70	59.08
k_{pp}^c (mm)	0.074	0.286	0.160	-	-	$\Delta K_{y,mod}^{CWP}$ (kN)	-	1,957.38	-
$F_{u,Rk}^c$ (kN)	490.89	413.63	492.73	433.50	587.60	$V_{pp,mod}^{CWP}$ (kN)	-	283.00	-
S_{ini}^c (kNm/rad)	28,648.36	61,609.38	61,609.38	-	-	K_{pp}^{CWP} (kN)	K_{pp}^{SE} (kN)	2,112.00	420.45
$M_{y,Rk}^c$ (kNm)	65.44	65.68	65.68	57.79	78.33	V_u^{CWP} (kN)	-	382.71	-
S_{pp}^c (kNm/rad)	569.89	2,202.54	1,232.19	-	-	ΔK_{pp}^{CWP} (kN)	-	242.77	-
$M_{u,Rk}^c$ (kNm)	94.01	79.21	94.36	83.02	112.53	V_n^{CWP} (kN)	ΔV_n^{SE} (kN)	413.77	112.35
ϕ_u^c (rad)	0.0501	0.0061	0.0233	-	-	$\gamma_{f,mod}^{CWP}$ (rad)	$\gamma_{f,mod}^{SE}$ (rad)	0.2057	0.1365

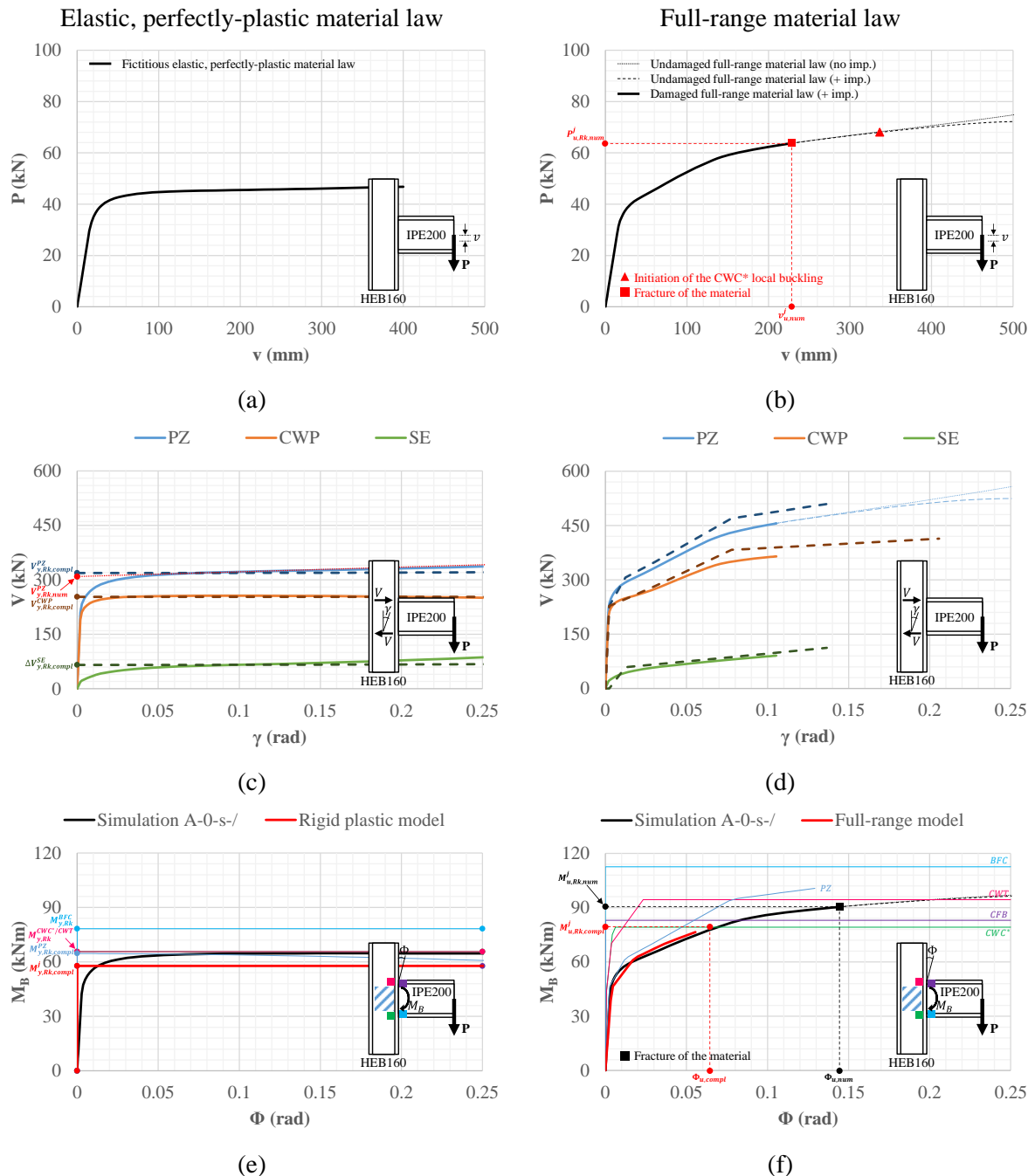


Fig. C-17. Numerical results for the A-0-s-/ simulation: (a)-(b) $(P - v)_{num}$, (c)-(d) $(V - \gamma)_{num}$, (e)-(f) $(M_B - \Phi)_{num}$ curves.

C.3.2 Simulation A-0-d-/

Table C-18. Component characterization for the prediction of the A-0-d-/ simulation full-range $(M_B - \Phi)_{num}$ curve.

Jaspart (1991)	PZ	CWC*	CWT	CFB	BFC	Corman (2022)		CWP	SE
k_{ini}^c (mm)	1.86	8.00	8.00	-	-	K_{y}^{CWP} (kN)	K_y^{SE} (kN)	97,498.32	5,945.82
$F_{y,Rk}^c$ (kN)	170.85	240.20	240.20	301.75	409.02	$V_{y,mod}^{CWP}$ (kN)	$\Delta V_{y,mod}^{SE}$ (kN)	239.69	59.08
k_{pp}^c (mm)	0.037	0.286	0.160	-	-	$\Delta K_{y,mod}^{CWP}$ (kN)	-	1,957.38	-
$F_{u,Rk}^c$ (kN)	245.45	328.25	345.08	433.50	587.60	$V_{pp,mod}^{CWP}$ (kN)	-	297.90	-
S_{ini}^c (kNm/rad)	14,324.18	61,609.38	61,609.38	-	-	K_{pp}^{CWP} (kN)	K_{pp}^{SE} (kN)	2,112.00	420.45
$M_{y,Rk}^c$ (kNm)	32.72	46.00	46.00	57.79	78.33	V_u^{CWP} (kN)	-	402.85	-
S_{pp}^c (kNm/rad)	284.94	2,202.54	1,232.19	-	-	ΔK_{pp}^{CWP} (kN)	-	242.77	-
$M_{u,Rk}^c$ (kNm)	47.00	62.86	66.08	83.02	112.53	V_n^{CWP} (kN)	ΔV_n^{SE} (kN)	435.55	112.36
ϕ_u^c (rad)	0.0501	0.0077	0.0163	-	-	$V_{f,mod}^{CWP}$ (rad)	$\gamma_{f,mod}^{SE}$ (rad)	0.2166	0.1366

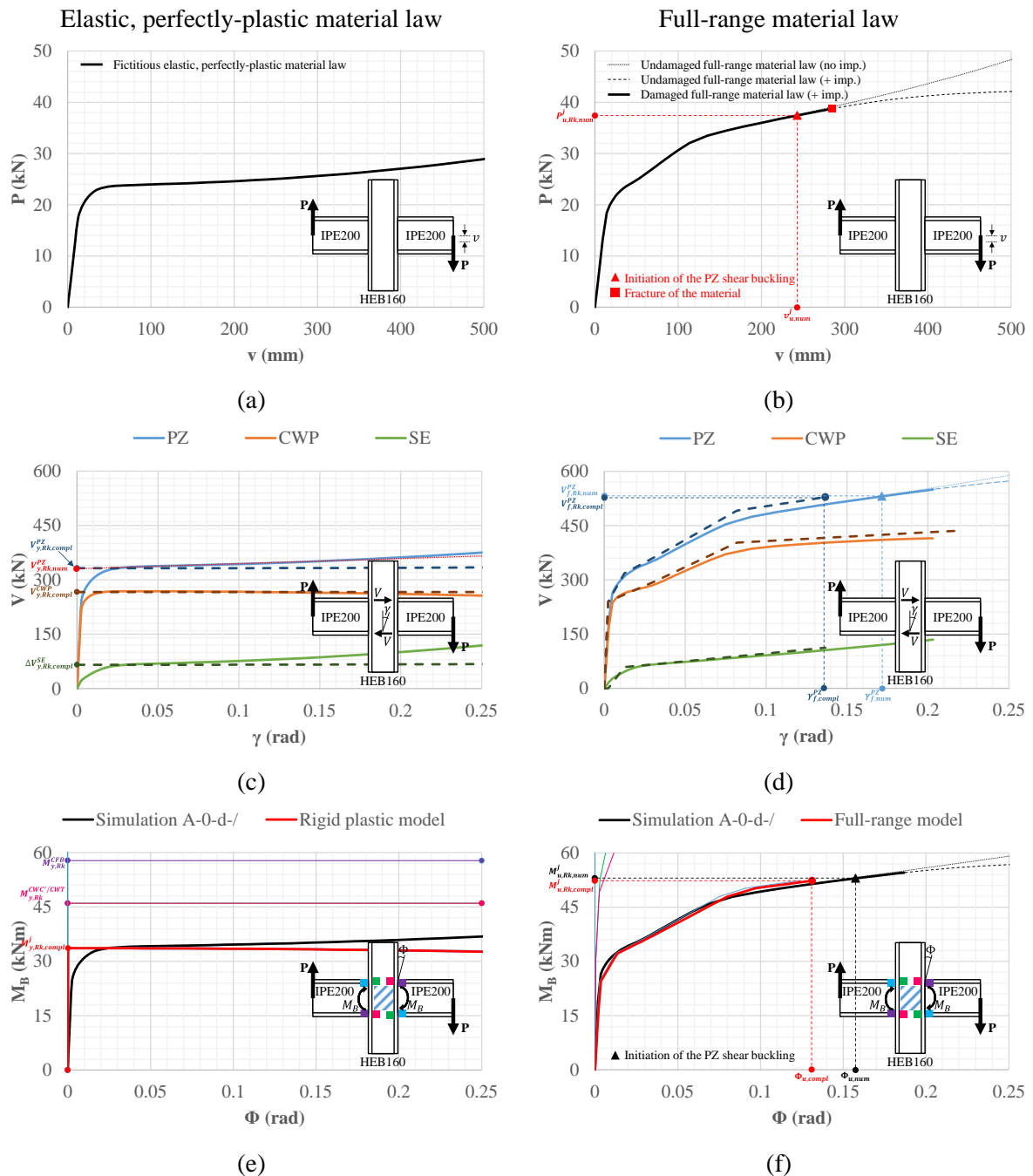


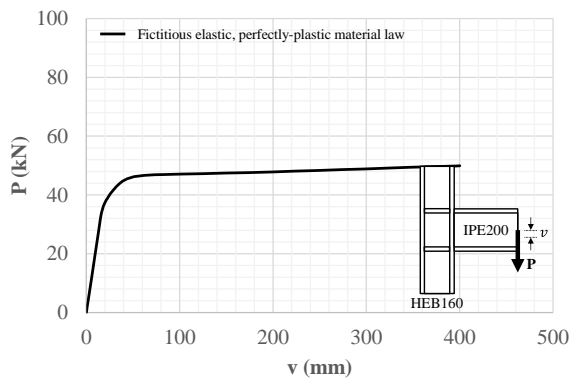
Fig. C-18. Numerical results for the A-0-d-/ simulation: (a)-(b) $(P - v)_{num}$ curves, (c)-(d) $(V - \gamma)_{num}$ curves and (e)-(f) $(M_B - \Phi)_{num}$ curves.

C.3.3 Simulation A-1-s-/

Table C-19. Component characterization for the prediction of the A-1-s-/ simulation full-range $(M_B - \Phi)_{num}$ curve.

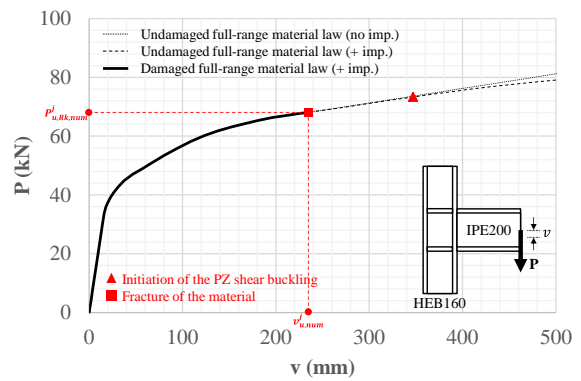
Jaspart (1991)	PZ	CWC*	CWT	CFB	BFC	Corman (2022)		CWP	SE
k_{ini}^c (mm)	3.720	-	-	-	-	$K_{y,CWP}^{CWP}$ (kN)	K_y^{SE} (kN)	97,498.32	6,962.26
$F_{y,Rk}^c$ (kN)	383.71	-	-	301.75	409.02	$V_{y,mod}^{CWP}$ (kN)	$\Delta V_{y,mod}^{SE}$ (kN)	227.70	69.21
k_{pp}^c (mm)	0.074	-	-	-	-	$\Delta K_{y,mod}^{CWP}$ (kN)	-	1,957.38	-
$F_{u,Rk}^c$ (kN)	551.24	-	-	433.50	587.60	$V_{pp,mod}^{CWP}$ (kN)	-	283.00	-
S_{ini}^c (kNm/rad)	28,648.36	-	-	-	-	K_{pp}^{CWP} (kN)	K_{pp}^{SE} (kN)	2,112.00	492.33
$M_{y,Rk}^c$ (kNm)	73.48	-	-	57.79	78.33	V_u^{CWP} (kN)	-	382.71	-
S_{pp}^c (kNm/rad)	569.89	-	-	-	-	ΔK_{pp}^{CWP} (kN)	-	242.77	-
$M_{u,Rk}^c$ (kNm)	105.56	-	-	83.02	112.53	V_n^{CWP} (kN)	ΔV_n^{SE} (kN)	417.10	129.70
ϕ_u^c (rad)	0.0563	-	-	-	-	$V_{f,mod}^{CWP}$ (rad)	$\gamma_{f,mod}^{SE}$ (rad)	0.2195	0.1346

Elastic, perfectly-plastic material law

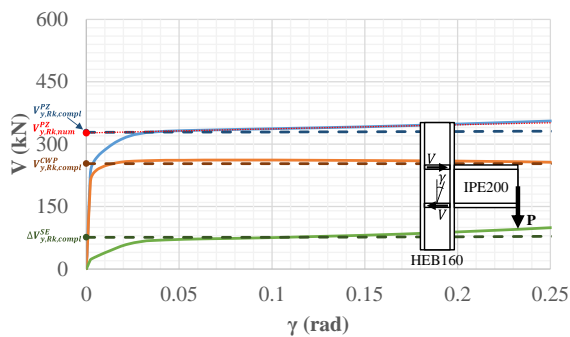


(a)

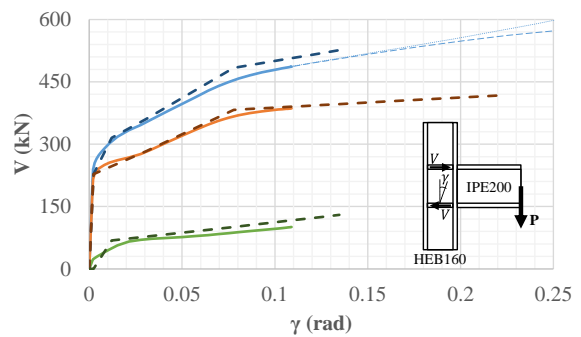
Full-range material law



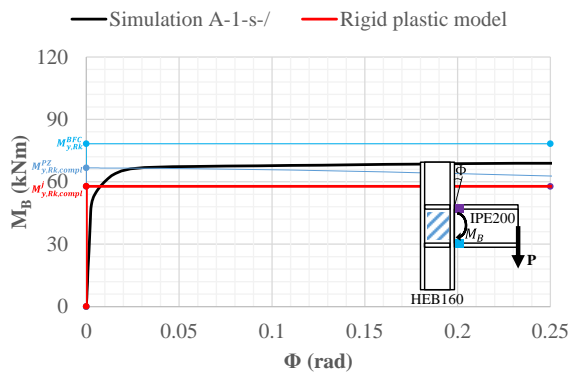
(b)



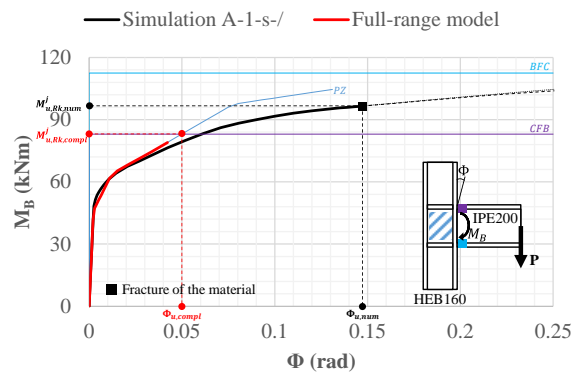
(c)



(d)



(e)



(f)

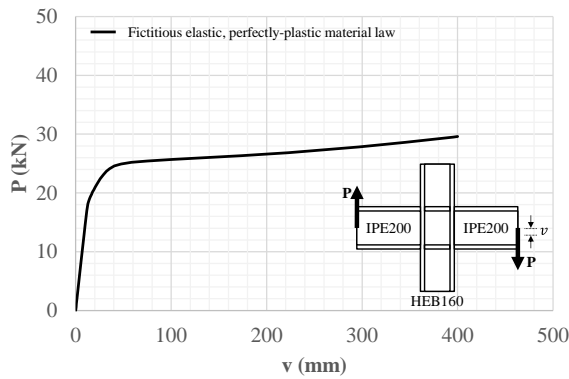
Fig. C-19. Numerical results for the A-1-s-/ simulation: (a)-(b) $(P - v)_{num}$ curves, (c)-(d) $(V - \gamma)_{num}$ curves and (e)-(f) $(M_B - \Phi)_{num}$ curves.

C.3.4 Simulation A-1-d-/

Table C-20. Component characterization for the prediction of the A-1-d-/ simulation full-range $(M_B - \Phi)_{num}$ curve.

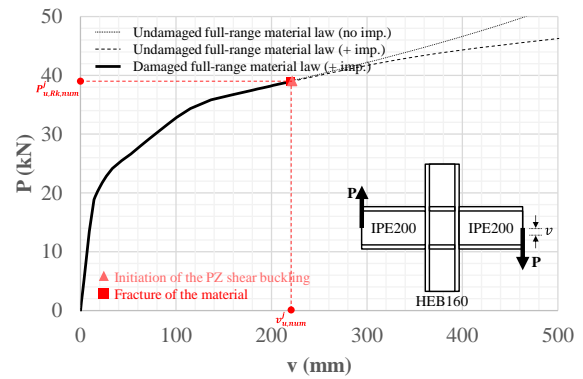
Jaspart (1991)	PZ	CWC*	CWT	CFB	BFC	Corman (2022)		CWP	SE
k_{ini}^c (mm)	1.86	-	-	-	-	K_{y}^{CWP} (kN)	K_y^{SE} (kN)	97,498.32	7,978.71
$F_{y,Rk}^c$ (kN)	191.85	-	-	301.75	409.02	$V_{y,mod}^{CWP}$ (kN)	$\Delta V_{y,mod}^{SE}$ (kN)	239.69	77.35
k_{pp}^c (mm)	0.037	-	-	-	-	$\Delta K_{y,mod}^{CWP}$ (kN)	-	1,957.38	-
$F_{u,Rk}^c$ (kN)	275.62	-	-	433.50	587.60	$V_{pp,mod}^{CWP}$ (kN)	-	297.90	-
S_{ini}^c (kNm/rad)	14,324.18	-	-	-	-	K_{pp}^{CWP} (kN)	K_{pp}^{SE} (kN)	2,112.00	564.21
$M_{y,Rk}^c$ (kNm)	36.74	-	-	57.79	78.33	V_u^{CWP} (kN)	-	402.85	-
S_{pp}^c (kNm/rad)	284.94	-	-	-	-	ΔK_{pp}^{CWP} (kN)	-	242.77	-
$M_{u,Rk}^c$ (kNm)	52.78	-	-	83.02	112.53	V_n^{CWP} (kN)	ΔV_n^{SE} (kN)	439.05	147.04
ϕ_u^c (rad)	0.0563	-	-	-	-	$\gamma_{f,mod}^{CWP}$ (rad)	$\gamma_{f,mod}^{SE}$ (rad)	0.2310	0.1334

Elastic, perfectly-plastic material law

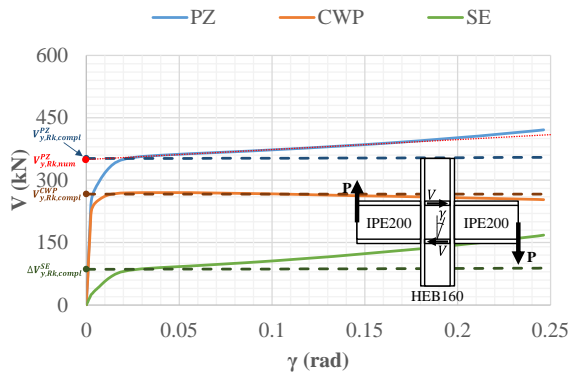


(a)

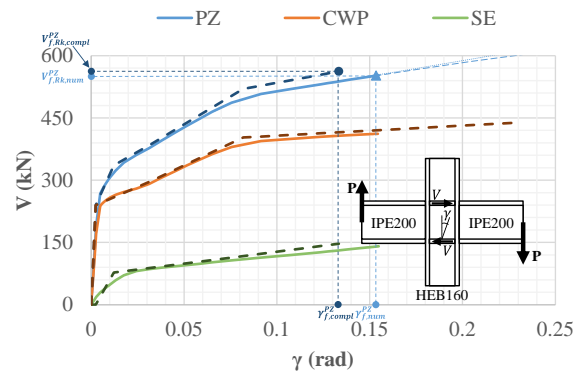
Full-range material law



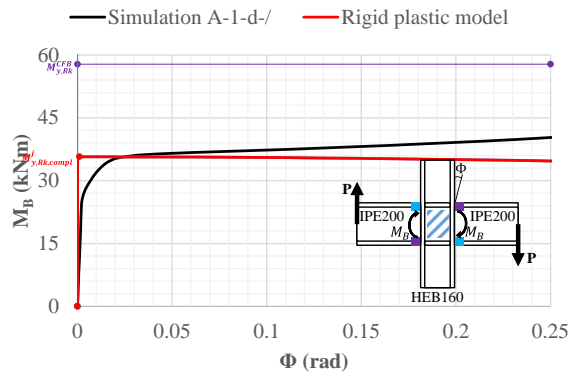
(b)



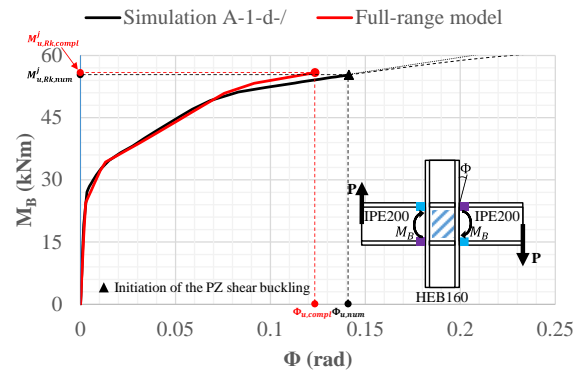
(c)



(d)



(e)



(f)

Fig. C-20. Numerical results for the A-1-d-/ simulation: (a)-(b) $(P - v)_{num}$ curves, (c)-(d) $(V - \gamma)_{num}$ curves and (e)-(f) $(M_B - \Phi)_{num}$ curves.

C.3.5 Simulation A-0-s-0.5N_{pl}

Table C-21. Component characterization for the prediction of the A-0-s-0.5N_{pl} simulation full-range ($M_B - \Phi$)_{num} curve.

Jaspart (1991)	PZ	CWC*	CWT	CFB	BFC	Corman (2022)		CWP	SE
k_{ini}^c (mm)	3.72	8.00	8.00	-	-	K_y^{CWP} (kN)	K_y^{SE} (kN)	97,498.32	5,945.82
$F_{y,Rk}^c$ (kN)	341.70	342.98	342.98	301.75	409.02	$V_{y,mod}^{CWP}$ (kN)	$\Delta V_{y,mod}^{SE}$ (kN)	210.49	36.86
k_{pp}^c (mm)	0.074	0.286	0.160	-	-	$\Delta K_{y,mod}^{CWP}$ (kN)	-	1,957.38	-
$F_{u,Rk}^c$ (kN)	490.89	413.63	492.73	433.50	587.60	$V_{pp,mod}^{CWP}$ (kN)	-	262.41	-
S_{ini}^c (kNm/rad)	28,648.36	61,609.38	61,609.38	-	-	K_{pp}^{CWP} (kN)	K_{pp}^{SE} (kN)	2,112.00	420.45
$M_{y,Rk}^c$ (kNm)	65.44	65.68	65.68	57.79	78.33	V_u^{CWP} (kN)	-	370.89	-
S_{pp}^c (kNm/rad)	569.89	2,202.54	1,232.19	-	-	ΔK_{pp}^{CWP} (kN)	-	242.77	-
$M_{u,Rk}^c$ (kNm)	94.01	79.21	94.36	83.02	112.53	V_n^{CWP} (kN)	ΔV_n^{SE} (kN)	403.70	97.86
ϕ_u^c (rad)	0.0501	0.0061	0.0233	-	-	$V_{f,mod}^{CWP}$ (rad)	$\gamma_{f,mod}^{SE}$ (rad)	0.2195	0.1508

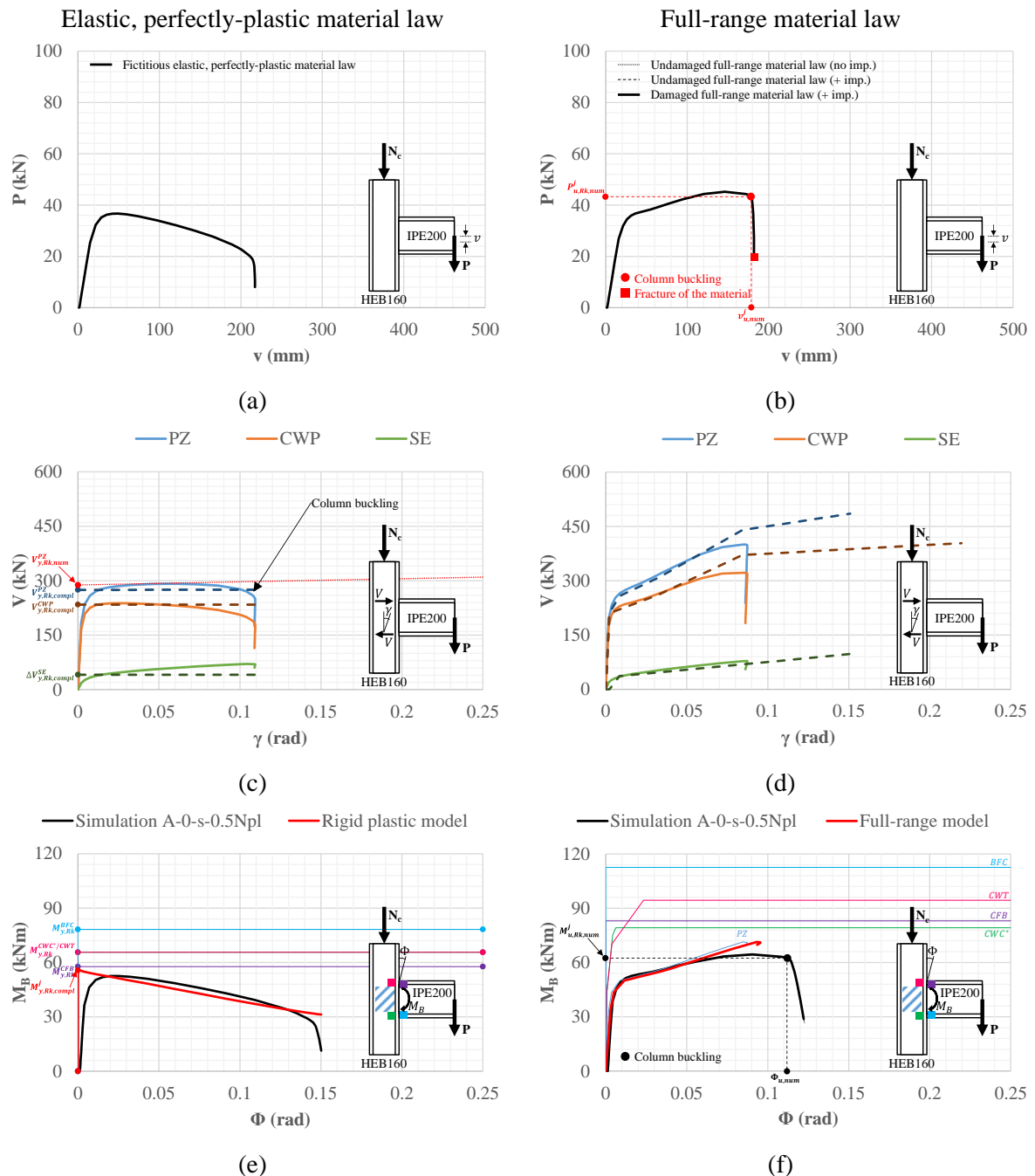


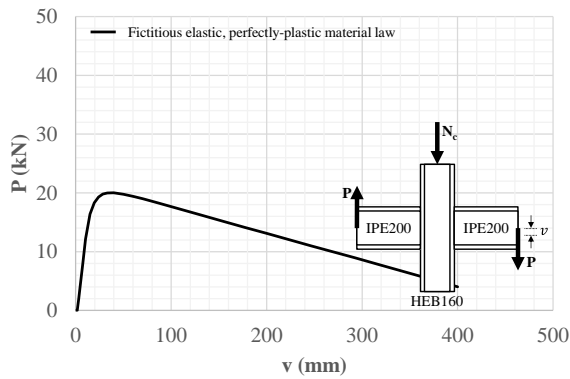
Fig. C-21. Numerical results for the A-0-s-0.5N_{pl} simulation: (a)-(b) ($P - v$)_{num} curves, (c)-(d) ($V - \gamma$)_{num} curves and (e)-(f) ($M_B - \Phi$)_{num} curves.

C.3.6 Simulation A-0-d-0.5N_{pl}

Table C-22. Component characterization for the prediction of the A-0-d-0.5N_{pl} simulation full-range ($M_B - \Phi$)_{num} curve.

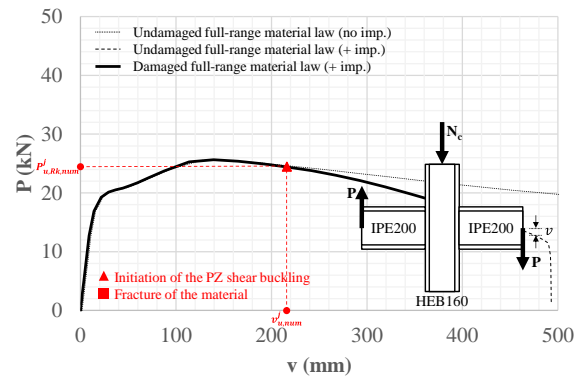
Jaspart (1991)	PZ	CWC*	CWT	CFB	BFC	Corman (2022)		CWP	SE
k_{ini}^c (mm)	1.86	8.00	8.00	-	-	$K_{y,mod}^{CWP}$ (kN)	K_y^{SE} (kN)	97,498.32	5,945.82
$F_{y,Rk}^c$ (kN)	170.85	240.20	240.20	301.75	409.02	$V_{y,mod}^{CWP}$ (kN)	$\Delta V_{y,mod}^{SE}$ (kN)	221.57	36.86
k_{pp}^c (mm)	0.037	0.286	0.160	-	-	$\Delta K_{y,mod}^{CWP}$ (kN)	-	1,957.38	-
$F_{u,Rk}^c$ (kN)	245.45	328.25	345.08	433.50	587.60	$V_{pp,mod}^{CWP}$ (kN)	-	276.22	-
S_{ini}^c (kNm/rad)	14,324.18	61,609.38	61,609.38	-	-	K_{pp}^{CWP} (kN)	K_{pp}^{SE} (kN)	2,112.00	420.45
$M_{y,Rk}^c$ (kNm)	32.72	46.00	46.00	57.79	78.33	V_u^{CWP} (kN)	-	390.41	-
S_{pp}^c (kNm/rad)	284.94	2,202.54	1,232.19	-	-	ΔK_{pp}^{CWP} (kN)	-	242.77	-
$M_{u,Rk}^c$ (kNm)	47.00	62.86	66.08	83.02	112.53	V_n^{CWP} (kN)	ΔV_n^{SE} (kN)	424.94	97.86
ϕ_u^c (rad)	0.0501	0.0077	0.0163	-	-	$\gamma_{f,mod}^{CWP}$ (rad)	$\gamma_{f,mod}^{SE}$ (rad)	0.2311	0.1509

Elastic, perfectly-plastic material law

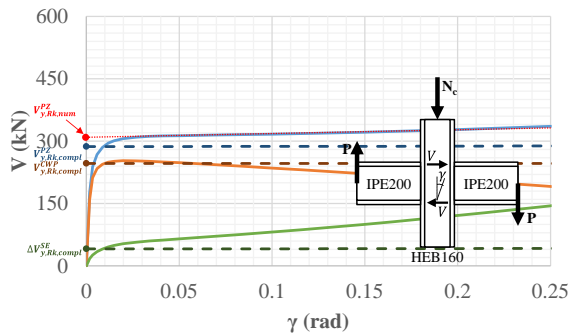


(a)

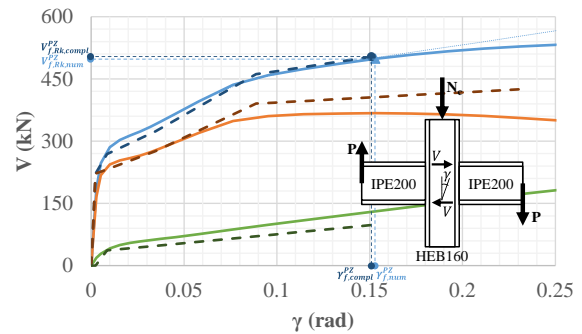
Full-range material law



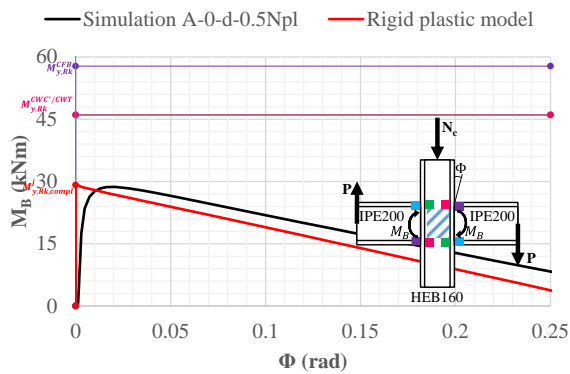
(b)



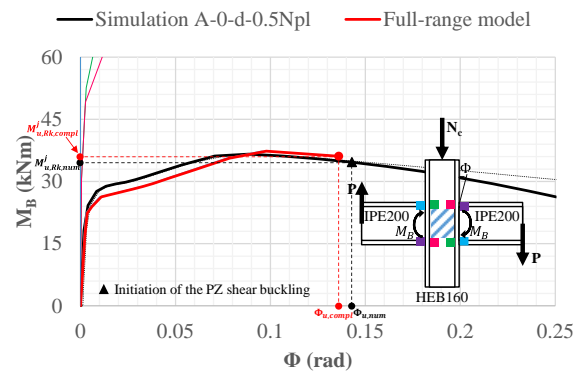
(c)



(d)



(e)



(f)

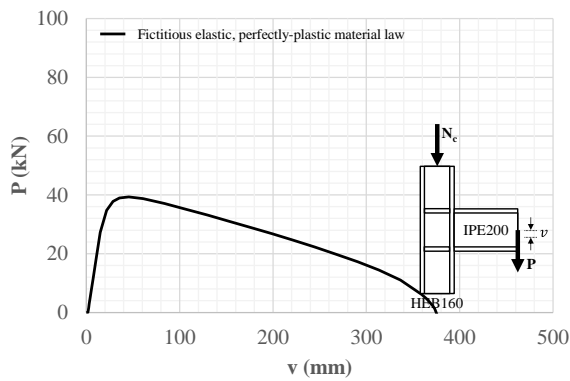
Fig. C-22. Numerical results for the A-0-d-0.5N_{pl} simulation: (a)-(b) ($P - v$)_{num} curves, (c)-(d) ($V - \gamma$)_{num} curves and (e)-(f) ($M_B - \Phi$)_{num} curves.

C.3.7 Simulation A-1-s-0.5N_{pl}

Table C-23. Component characterization for the prediction of the A-1-s-0.5N_{pl} simulation full-range ($M_B - \Phi$)_{num} curve.

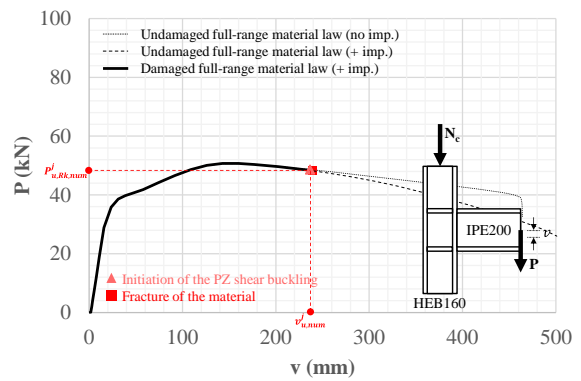
Jaspart (1991)	PZ	CWC*	CWT	CFB	BFC	Corman (2022)		CWP	SE
k_{ini}^c (mm)	3.72	-	-	-	-	$K_{y,CWP}^{CWP}$ (kN)	K_y^{SE} (kN)	97,498.32	6,962.26
$F_{y,Rk}^c$ (kN)	383.71	-	-	301.75	409.02	$V_{y,mod}^{CWP}$ (kN)	$\Delta V_{y,mod}^{SE}$ (kN)	210.49	45.99
k_{pp}^c (mm)	0.074	-	-	-	-	$\Delta K_{y,mod}^{CWP}$ (kN)	-	1,957.38	-
$F_{u,Rk}^c$ (kN)	551.24	-	-	433.50	587.60	$V_{pp,mod}^{CWP}$ (kN)	-	262.41	-
S_{ini}^c (kNm/rad)	28,648.36	-	-	-	-	K_{pp}^{CWP} (kN)	K_{pp}^{SE} (kN)	2,112.00	492.33
$M_{y,Rk}^c$ (kNm)	73.48	-	-	57.79	78.33	V_u^{CWP} (kN)	-	370.89	-
S_{pp}^c (kNm/rad)	569.89	-	-	-	-	ΔK_{pp}^{CWP} (kN)	-	242.77	-
$M_{u,Rk}^c$ (kNm)	105.56	-	-	83.02	112.53	V_n^{CWP} (kN)	ΔV_n^{SE} (kN)	406.95	115.20
ϕ_u^c (rad)	0.0563	-	-	-	-	$V_{f,mod}^{CWP}$ (rad)	$\gamma_{f,mod}^{SE}$ (rad)	0.2329	0.1468

Elastic, perfectly-plastic material law

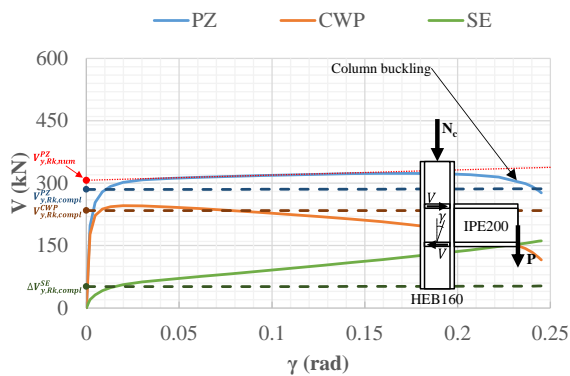


(a)

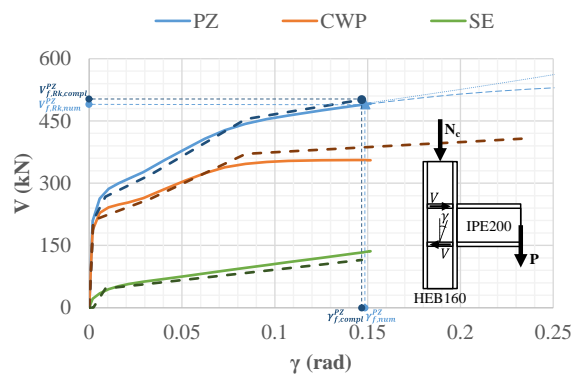
Full-range material law



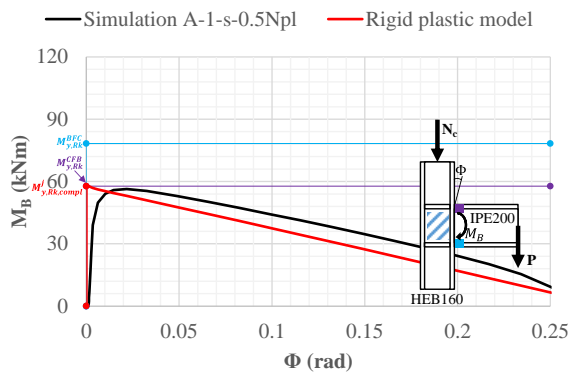
(b)



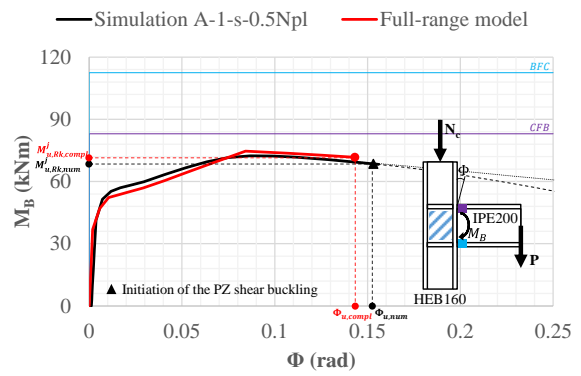
(c)



(d)



(e)



(f)

Fig. C-23. Numerical results for the A-1-s-0.5N_{pl} simulation: (a)-(b) ($P - v$)_{num} curves, (c)-(d) ($V - \gamma$)_{num} curves and (e)-(f) ($M_B - \Phi$)_{num} curves.

C.3.8 Simulation A-1-d-0.5N_{pl}

Table C-24. Component characterization for the prediction of the A-1-d-0.5N_{pl} simulation full-range ($M_B - \Phi$)_{num} curve.

Jaspart (1991)	PZ	CWC*	CWT	CFB	BFC	Corman (2022)		CWP	SE
k_{ini}^c (mm)	1.86	-	-	-	-	$K_{y,mod}^{CWP}$ (kN)	K_y^{SE} (kN)	97,498.32	7,978.71
$F_{y,Rk}^c$ (kN)	191.85	-	-	301.75	409.02	$V_{y,mod}^{CWP}$ (kN)	$\Delta V_{y,mod}^{SE}$ (kN)	221.57	55.13
k_{pp}^c (mm)	0.037	-	-	-	-	$\Delta K_{y,mod}^{CWP}$ (kN)	-	1,957.38	-
$F_{u,Rk}^c$ (kN)	275.62	-	-	433.50	587.60	$V_{pp,mod}^{CWP}$ (kN)	-	276.22	-
S_{mi}^c (kNm/rad)	14,324.18	-	-	-	-	K_{pp}^{CWP} (kN)	K_{pp}^{SE} (kN)	2,112.00	564.21
$M_{y,Rk}^c$ (kNm)	36.74	-	-	57.79	78.33	V_u^{CWP} (kN)	-	390.41	-
S_{pp}^c (kNm/rad)	284.94	-	-	-	-	ΔK_{pp}^{CWP} (kN)	-	242.77	-
$M_{u,Rk}^c$ (kNm)	52.78	-	-	83.02	112.53	V_n^{CWP} (kN)	ΔV_n^{SE} (kN)	428.37	132.55
ϕ_u^c (rad)	0.0563	-	-	-	-	$V_{f,mod}^{CWP}$ (rad)	$\gamma_{f,mod}^{SE}$ (rad)	0.2452	0.1440

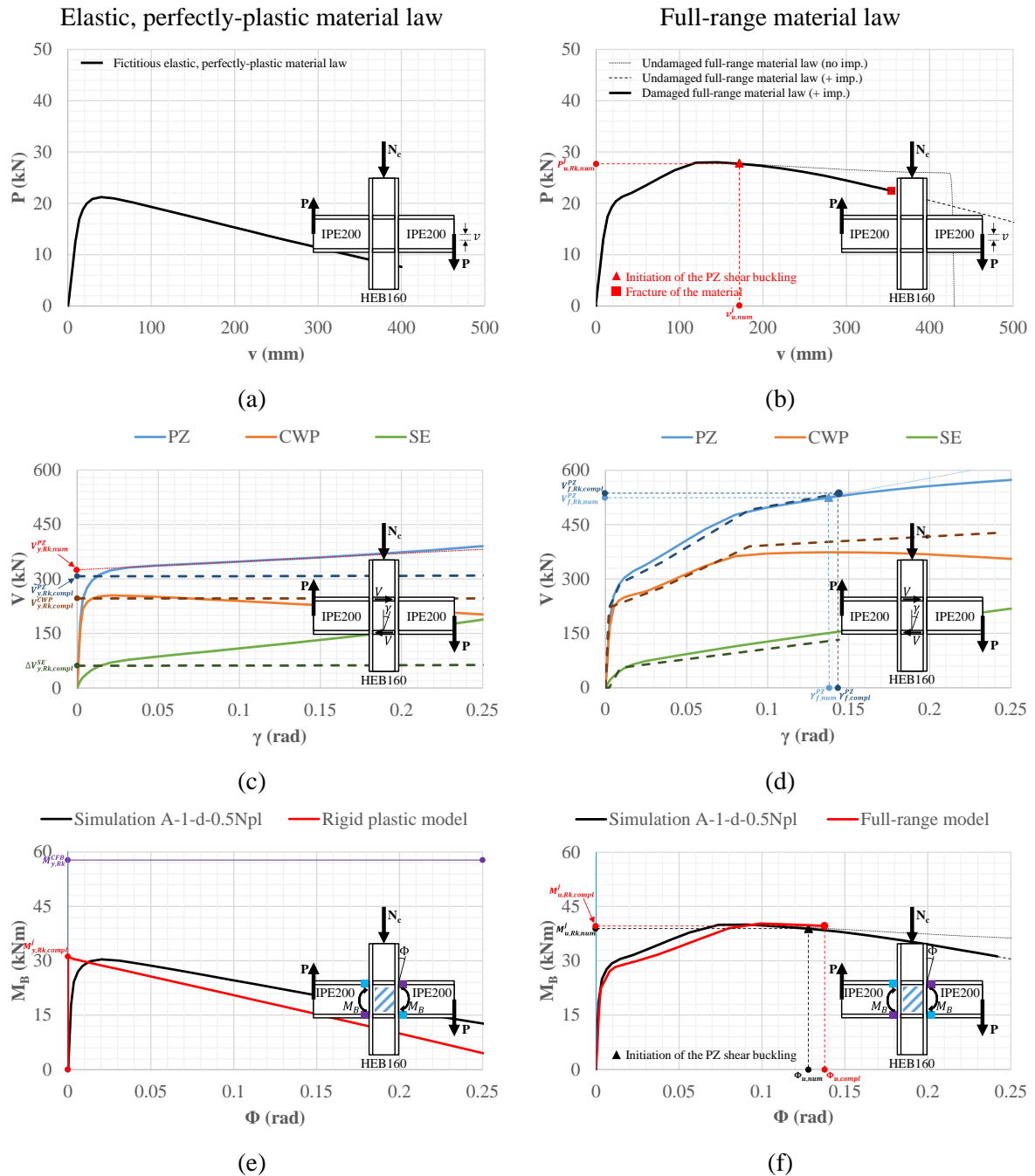


Fig. C-24. Numerical results for the A-1-d-0.5N_{pl} simulation: (a)-(b) ($P - v$)_{num} curves, (c)-(d) ($V - \gamma$)_{num} curves and (e)-(f) ($M_B - \Phi$)_{num} curves.

C.4 Model B

C.4.1 Simulation B-0-s-/

Table C-25. Component characterization for the prediction of the B-0-s-/ simulation full-range $(M_B - \Phi)_{num}$ curve.

Jaspart (1991)	PZ	CWC ^c	CWT	CFB	BFC	Corman (2022)		CWP	SE
k_{ini}^c (mm)	8.11	8.75	8.75	-	-	K_y^{CWP} (kN)	K_y^{SE} (kN)	319,984.53	20,377.90
$F_{y,Rk}^c$ (kN)	1,125.70	943.74	943.74	569.78	771.06	$V_{y,mod}^{CWP}$ (kN)	$\Delta V_{y,mod}^{SE}$ (kN)	740.62	199.08
k_{pp}^c (mm)	0.162	0.400	0.175	-	-	$\Delta K_{y,mod}^{CWP}$ (kN)	-	6,240.80	-
$F_{u,Rk}^c$ (kN)	1,617.20	943.74	1,355.79	818.55	1,107.71	$V_{pp,mod}^{CWP}$ (kN)	-	920.51	-
S_{ini}^c (kNm/rad)	142,540.09	153,788.63	153,788.63	-	-	K_{pp}^{CWP} (kN)	K_{pp}^{SE} (kN)	6,732.00	1,441.00
$M_{y,Rk}^c$ (kNm)	325.67	273.02	273.02	164.84	223.07	V_u^{CWP} (kN)	-	1,159.90	-
S_{pp}^c (kNm/rad)	2,847.29	7,030.34	3,075.77	-	-	ΔK_{pp}^{CWP} (kN)	-	-	-
$M_{u,Rk}^c$ (kNm)	467.86	273.02	392.23	236.81	320.46	V_n^{CWP} (kN)	ΔV_n^{SE} (kN)	-	378.52
ϕ_u^c (rad)	0.0499	0.0018	0.0388	-	-	$\gamma_{f,mod}^{CWP}$ (rad)	$\gamma_{f,mod}^{SE}$ (rad)	0.0667	0.1342

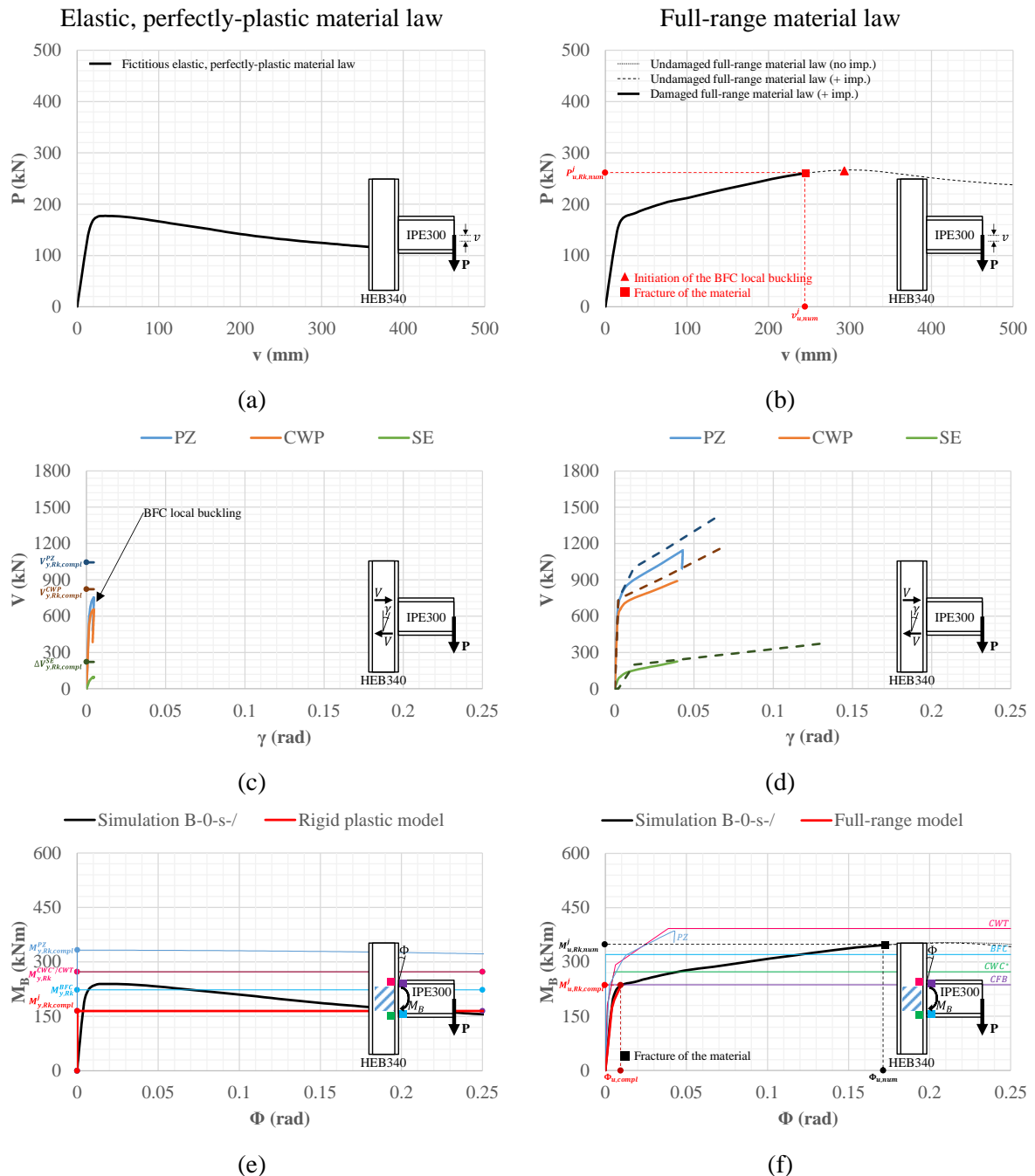


Fig. C-25. Numerical results for the B-0-s-/ simulation: (a)-(b) $(P - v)_{num}$, (c)-(d) $(V - \gamma)_{num}$, (e)-(f) $(M_B - \Phi)_{num}$ curves.

C.4.2 Simulation B-0-d-/

Table C-26. Component characterization for the prediction of the B-0-d-/ simulation full-range $(M_B - \Phi)_{num}$ curve.

Jaspart (1991)	PZ	CWC*	CWT	CFB	BFC	Corman (2022)		CWP	SE
k_{ini}^c (mm)	4.06	8.75	8.75	-	-	K_y^{CWP} (kN)	K_y^{SE} (kN)	319,984.53	20,377.90
$F_{y,Rk}^c$ (kN)	562.85	717.35	717.35	569.78	771.06	$V_{y,mod}^{CWP}$ (kN)	$\Delta V_{y,mod}^{SE}$ (kN)	779.60	199.08
k_{pp}^c (mm)	0.081	0.400	0.175	-	-	$\Delta K_{y,mod}^{CWP}$ (kN)	-	6,240.80	-
$F_{u,Rk}^c$ (kN)	808.60	754.63	1,030.56	818.55	1,107.71	$V_{pp,mod}^{CWP}$ (kN)	-	968.95	-
S_{ini}^c (kNm/rad)	71,357.92	153,788.63	153,788.63	-	-	K_{pp}^{CWP} (kN)	K_{pp}^{SE} (kN)	6,732.00	1,441.01
$M_{y,Rk}^c$ (kNm)	162.83	207.53	207.53	164.84	223.07	V_u^{CWP} (kN)	-	1,220.95	-
S_{pp}^c (kNm/rad)	1,423.64	7,030.34	3,075.77	-	-	ΔK_{pp}^{CWP} (kN)	-	-	-
$M_{u,Rk}^c$ (kNm)	233.93	218.31	298.14	236.81	320.46	V_n^{CWP} (kN)	ΔV_n^{SE} (kN)	-	378.36
ϕ_u^c (rad)	0.0499	0.0045	0.0295	-	-	$\gamma_{f,mod}^{CWP}$ (rad)	$\gamma_{f,mod}^{SE}$ (rad)	0.0702	0.1344

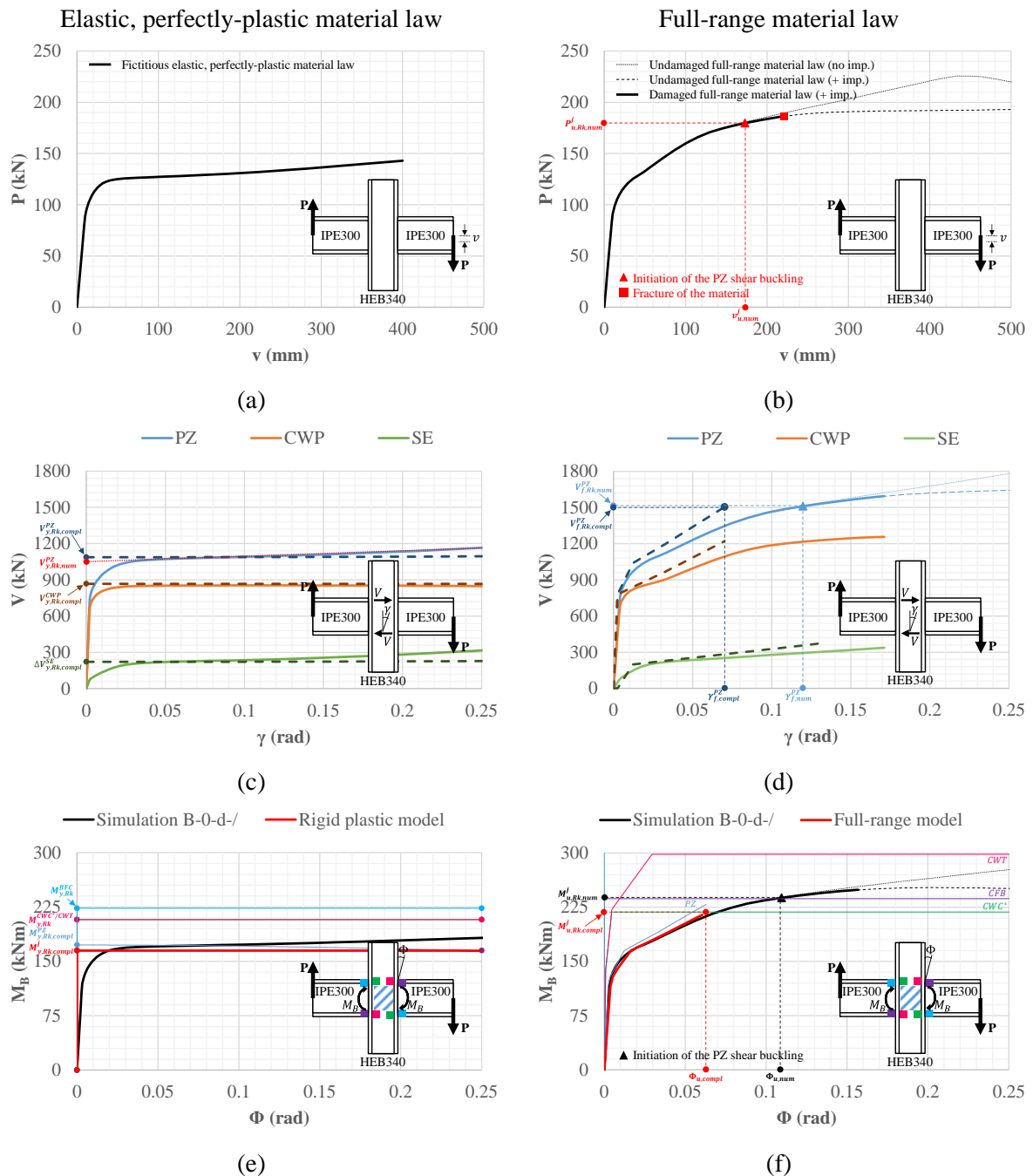


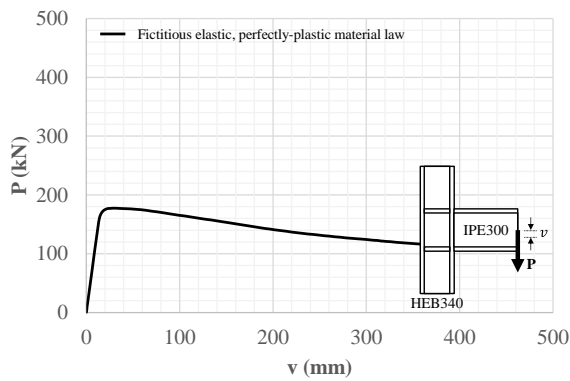
Fig. C-26. Numerical results for the B-0-d-/ simulation: (a)-(b) $(P - v)_{num}$ curves, (c)-(d) $(V - \gamma)_{num}$ curves and (e)-(f) $(M_B - \Phi)_{num}$ curves.

C.4.3 Simulation B-1-s-/

Table C-27. Component characterization for the prediction of the B-1-s-/ simulation full-range $(M_B - \Phi)_{num}$ curve.

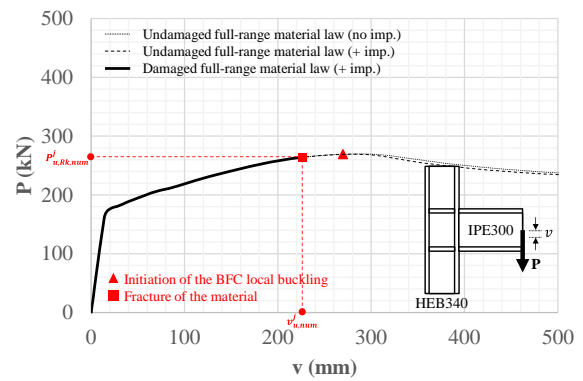
Jaspart (1991)	PZ	CWC*	CWT	CFB	BFC	Corman (2022)		CWP	SE
k_{ini}^c (mm)	8.11	-	-	-	-	K_y^{CWP} (kN)	K_y^{SE} (kN)	319,984.53	21,860.68
$F_{y,Rk}^c$ (kN)	1,247.12	-	-	569.78	771.06	$V_{y,mod}^{CWP}$ (kN)	$\Delta V_{y,mod}^{SE}$ (kN)	740.62	212.58
k_{pp}^c (mm)	0.162	-	-	-	-	$\Delta K_{y,mod}^{CWP}$ (kN)	-	6,240.80	-
$F_{u,Rk}^c$ (kN)	1,791.63	-	-	818.55	1,107.71	$V_{pp,mod}^{CWP}$ (kN)	-	920.51	-
$S_{y,Rk}^c$ (kNm/rad)	142,540.09	-	-	-	-	K_{pp}^{CWP} (kN)	K_{pp}^{SE} (kN)	6,732.00	1,545.86
$M_{y,Rk}^c$ (kNm)	360.79	-	-	164.84	223.07	V_u^{CWP} (kN)	-	1,179.46	-
S_{pp}^c (kNm/rad)	2,847.29	-	-	-	-	ΔK_{pp}^{CWP} (kN)	-	-	-
$M_{u,Rk}^c$ (kNm)	518.32	-	-	236.81	320.46	V_n^{CWP} (kN)	ΔV_n^{SE} (kN)	-	403.98
ϕ_u^c (rad)	0.0553	-	-	-	-	$\gamma_{f,mod}^{CWP}$ (rad)	$\gamma_{f,mod}^{SE}$ (rad)	0.0696	0.1336

Elastic, perfectly-plastic material law

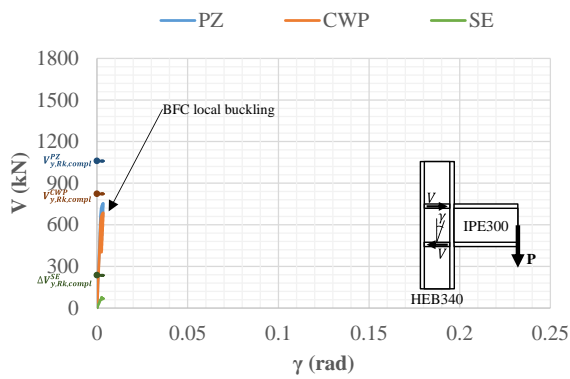


(a)

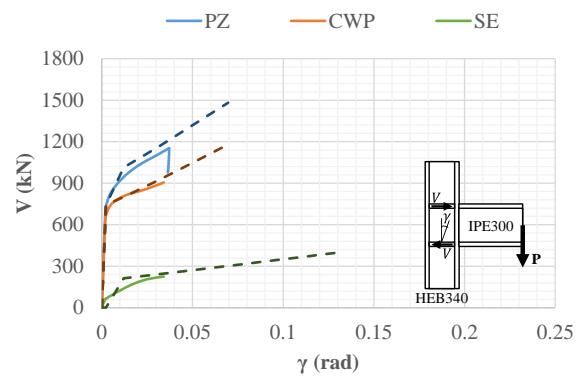
Full-range material law



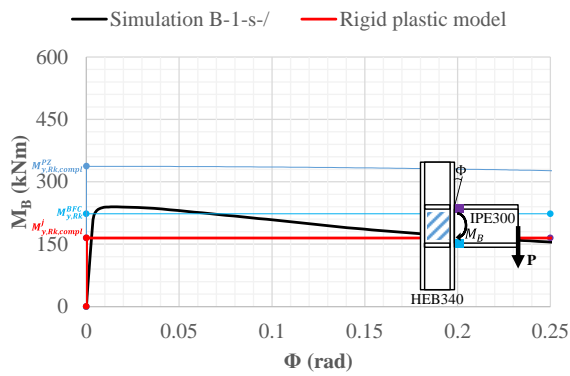
(b)



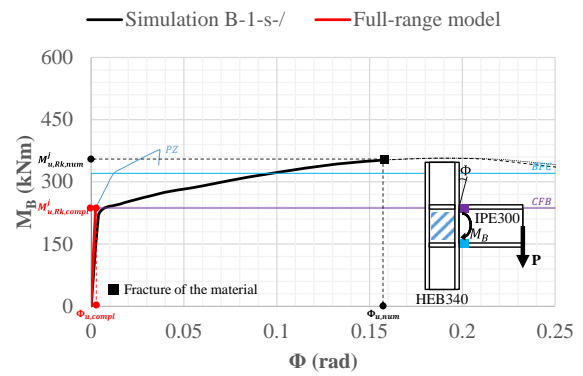
(c)



(d)



(e)



(f)

Fig. C-27. Numerical results for the B-1-s-/ simulation: (a)-(b) $(P - v)_{num}$ curves, (c)-(d) $(V - \gamma)_{num}$ curves and (e)-(f) $(M_B - \Phi)_{num}$ curves.

C.4.4 Simulation B-1-d-/

Table C-28. Component characterization for the prediction of the B-1-d-/ simulation full-range $(M_B - \Phi)_{num}$ curve.

Jaspart (1991)	PZ	CWC*	CWT	CFB	BFC	Corman (2022)		CWP	SE
k_{ini}^c (mm)	4.06	-	-	-	-	$K_{y,mod}^{CWP}$ (kN)	$K_{y,mod}^{SE}$ (kN)	319,984.53	23,343.46
$F_{y,Rk}^c$ (kN)	623.56	-	-	569.78	771.06	$V_{y,mod}^{CWP}$ (kN)	$\Delta V_{y,mod}^{SE}$ (kN)	779.60	226.08
k_{pp}^c (mm)	0.081	-	-	-	-	$\Delta K_{y,mod}^{CWP}$ (kN)	-	6,240.80	-
$F_{u,Rk}^c$ (kN)	895.82	-	-	818.55	1,107.71	$V_{pp,mod}^{CWP}$ (kN)	-	968.95	-
S_{ini}^c (kNm/rad)	71,357.92	-	-	-	-	K_{pp}^{CWP} (kN)	K_{pp}^{SE} (kN)	6,732.00	1,650.72
$M_{y,Rk}^c$ (kNm)	180.40	-	-	164.84	223.07	V_u^{CWP} (kN)	-	1,241.54	-
S_{pp}^c (kNm/rad)	1,423.64	-	-	-	-	ΔK_{pp}^{CWP} (kN)	-	-	-
$M_{u,Rk}^c$ (kNm)	259.16	-	-	236.81	320.46	V_n^{CWP} (kN)	ΔV_n^{SE} (kN)	-	429.58
ϕ_u^c (rad)	0.0553	-	-	-	-	$V_{f,mod}^{CWP}$ (rad)	$\gamma_{f,mod}^{SE}$ (rad)	0.0733	0.1332

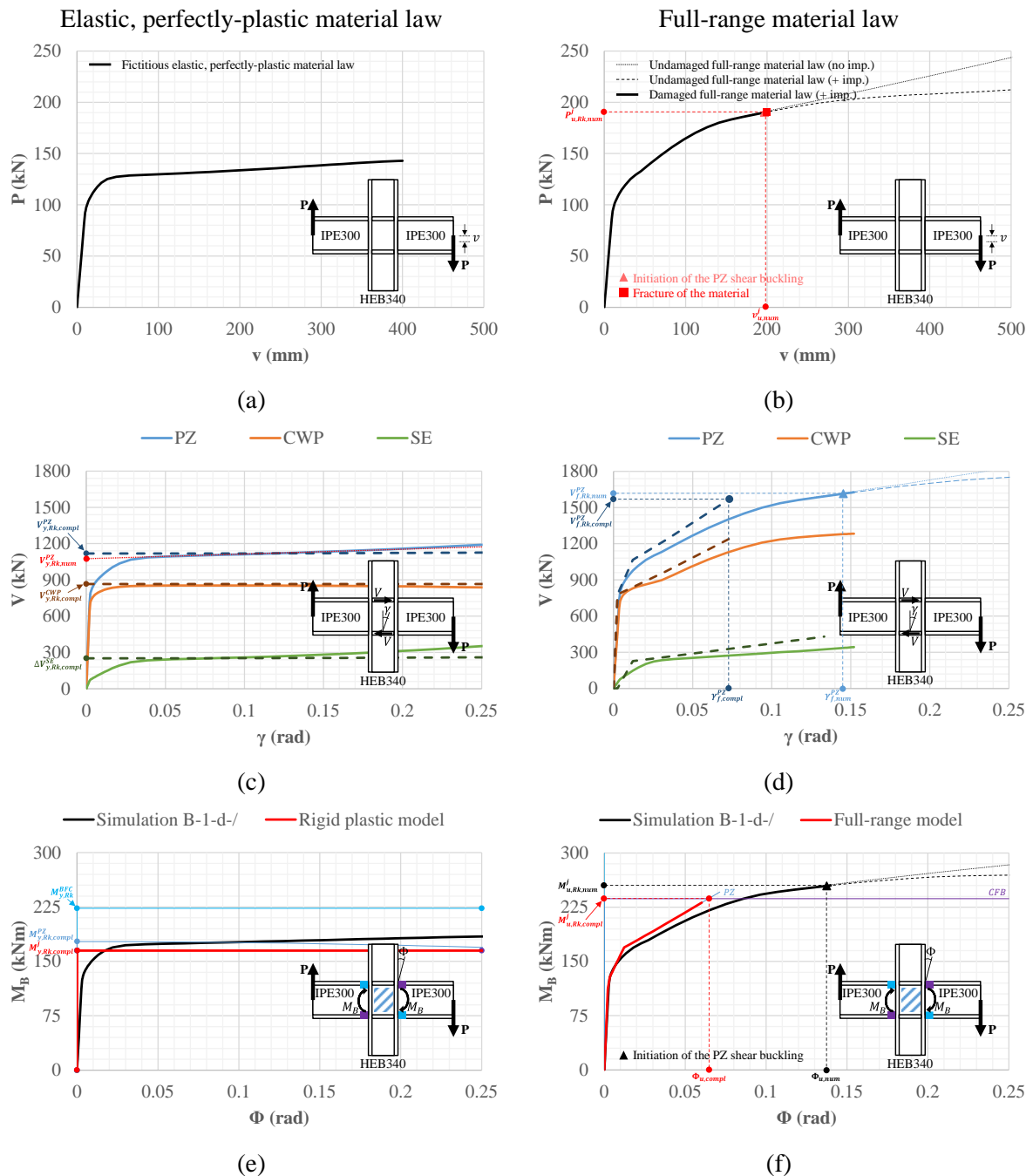


Fig. C-28. Numerical results for the B-1-d-/ simulation: (a)-(b) $(P - v)_{num}$ curves, (c)-(d) $(V - \gamma)_{num}$ curves and (e)-(f) $(M_B - \Phi)_{num}$ curves.

C.4.5 Simulation B-0-s-0.5N_{pl}

Table C-29. Component characterization for the prediction of the B-0-s-0.5N_{pl} simulation full-range ($M_B - \Phi$)_{num} curve.

Jaspart (1991)	PZ	CWC*	CWT	CFB	BFC	Corman (2022)		CWP	SE
k_{ini}^c (mm)	8.11	8.75	8.75	-	-	$K_{y,mod}^{CWP}$ (kN)	K_y^{SE} (kN)	319,984.53	20,377.90
$F_{y,Rk}^c$ (kN)	1,125.70	943.74	943.74	569.78	771.06	$V_{y,mod}^{CWP}$ (kN)	$\Delta V_{y,mod}^{SE}$ (kN)	695.35	128.31
k_{pp}^c (mm)	0.162	0.400	0.175	-	-	$\Delta K_{y,mod}^{CWP}$ (kN)	-	6,240.80	-
$F_{u,Rk}^c$ (kN)	1,617.21	943.74	1,355.79	818.55	1,107.71	$V_{pp,mod}^{CWP}$ (kN)	-	866.31	-
S_{ini}^c (kNm/rad)	142,540.09	153,788.63	153,788.63	-	-	K_{pp}^{CWP} (kN)	K_{pp}^{SE} (kN)	6,732.00	1,441.01
$M_{y,Rk}^c$ (kNm)	325.67	273.02	273.02	164.84	223.07	V_u^{CWP} (kN)	-	1,130.79	-
S_{pp}^c (kNm/rad)	2,847.29	7,030.34	3,075.77	-	-	ΔK_{pp}^{CWP} (kN)	-	-	-
$M_{u,Rk}^c$ (kNm)	467.86	273.02	392.23	236.81	320.46	V_n^{CWP} (kN)	ΔV_n^{SE} (kN)	-	332.35
ϕ_u^c (rad)	0.0499	0.0018	0.0388	-	-	$\gamma_{f,mod}^{CWP}$ (rad)	$\gamma_{f,mod}^{SE}$ (rad)	0.0724	0.1476

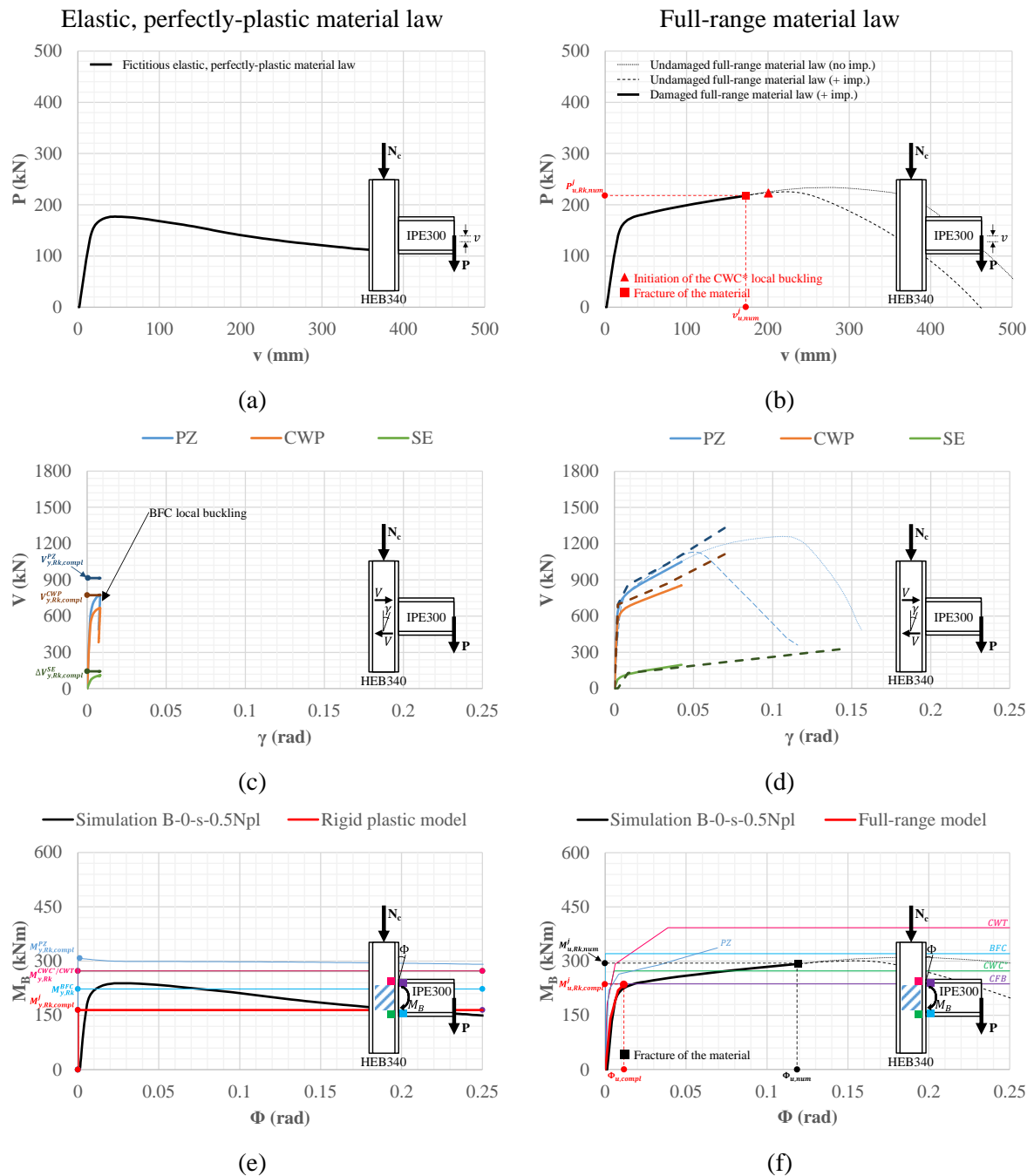


Fig. C-29. Numerical results for the B-0-s-0.5N_{pl} simulation: (a)-(b) ($P - v$)_{num} curves, (c)-(d) ($V - \gamma$)_{num} curves and (e)-(f) ($M_B - \Phi$)_{num} curves.

C.4.6 Simulation B-0-d-0.5N_{pl}

Table C-30. Component characterization for the prediction of the B-0-d-0.5N_{pl} simulation full-range ($M_B - \Phi$)_{num} curve.

Jaspart (1991)	PZ	CWC*	CWT	CFB	BFC	Corman (2022)		CWP	SE
k_{ini}^c (mm)	4.06	8.75	8.75	-	-	$K_{y,mod}^{CWP}$ (kN)	K_y^{SE} (kN)	319,984.53	20,377.90
$F_{y,Rk}^c$ (kN)	562.85	717.35	717.35	569.78	771.06	$V_{y,mod}^{CWP}$ (kN)	$\Delta V_{y,mod}^{SE}$ (kN)	731.94	128.31
k_{pp}^c (mm)	0.081	0.400	0.175	-	-	$\Delta K_{y,mod}^{CWP}$ (kN)	-	6,240.80	-
$F_{u,Rk}^c$ (kN)	808.60	754.63	1,030.56	818.55	1,107.71	$V_{pp,mod}^{CWP}$ (kN)	-	911.90	-
S_{ini}^c (kNm/rad)	71,357.92	153,788.63	153,788.63	-	-	K_{pp}^{CWP} (kN)	K_{pp}^{SE} (kN)	6,732.00	1,441.01
$M_{y,Rk}^c$ (kNm)	162.83	207.53	207.53	164.84	223.07	V_u^{CWP} (kN)	-	1,190.31	-
S_{pp}^c (kNm/rad)	1,423.64	7,030.34	3,075.77	-	-	ΔK_{pp}^{CWP} (kN)	-	-	-
$M_{u,Rk}^c$ (kNm)	233.93	218.31	298.14	236.81	320.46	V_n^{CWP} (kN)	ΔV_n^{SE} (kN)	-	332.36
ϕ_u^c (rad)	0.0499	0.0045	0.0295	-	-	$\gamma_{f,mod}^{CWP}$ (rad)	$\gamma_{f,mod}^{SE}$ (rad)	0.0762	0.1477

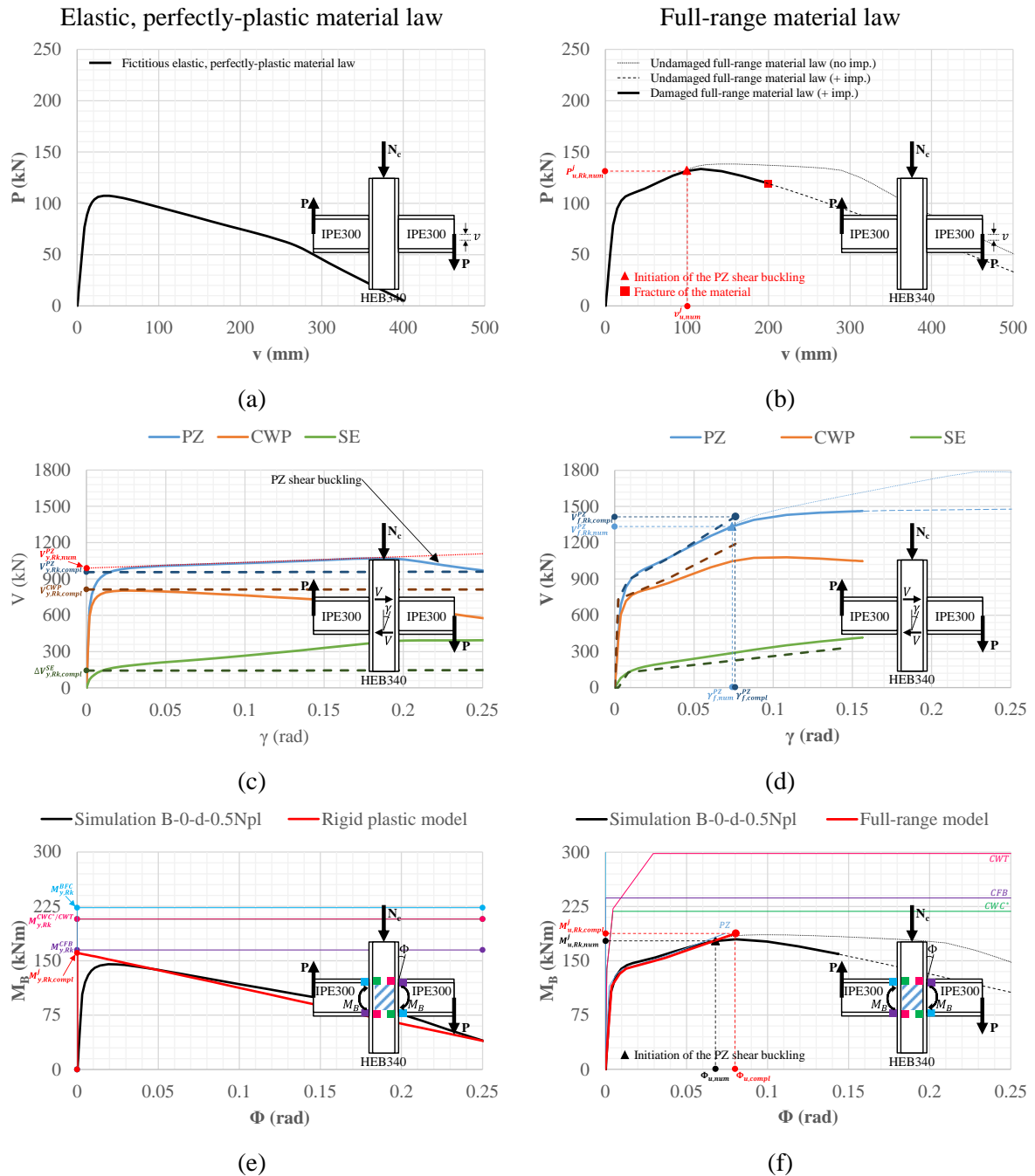


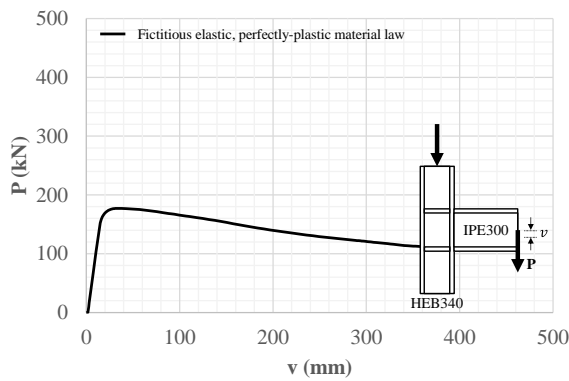
Fig. C-30. Numerical results for the B-0-d-0.5N_{pl} simulation: (a)-(b) ($P - v$)_{num} curves, (c)-(d) ($V - \gamma$)_{num} curves and (e)-(f) ($M_B - \Phi$)_{num} curves.

C.4.7 Simulation B-1-s-0.5N_{pl}

Table C-31. Component characterization for the prediction of the B-1-s-0.5N_{pl} simulation full-range ($M_B - \Phi$)_{num} curve.

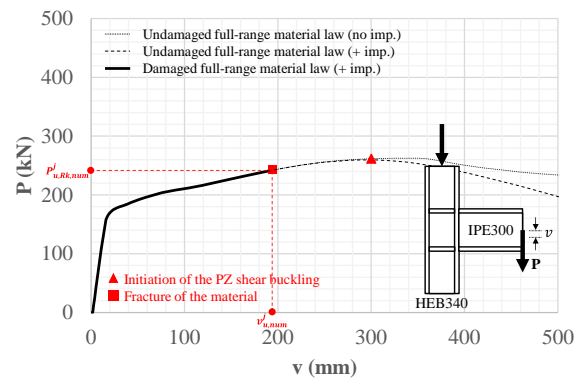
Jaspart (1991)	PZ	CWC*	CWT	CFB	BFC	Corman (2022)		CWP	SE
k_{ini}^c (mm)	8.11	-	-	-	-	$K_{y,mod}^{CWP}$ (kN)	K_y^{SE} (kN)	319,984.53	21,860.68
$F_{y,Rk}^c$ (kN)	1,247.12	-	-	569.78	771.06	$V_{y,mod}^{CWP}$ (kN)	$\Delta V_{y,mod}^{SE}$ (kN)	695.35	141.81
k_{pp}^c (mm)	0.162	-	-	-	-	$\Delta K_{y,mod}^{CWP}$ (kN)	-	6,240.80	-
$F_{u,Rk}^c$ (kN)	1,791.63	-	-	818.55	1,107.71	$V_{pp,mod}^{CWP}$ (kN)	-	866.31	-
$S_{y,Rk}^c$ (kNm/rad)	142,540.09	-	-	-	-	K_{pp}^{CWP} (kN)	K_{pp}^{SE} (kN)	6,732.00	1,545.86
$M_{y,Rk}^c$ (kNm)	360.79	-	-	164.84	223.07	V_u^{CWP} (kN)	-	1,149.86	-
S_{pp}^c (kNm/rad)	2,847.29	-	-	-	-	ΔK_{pp}^{CWP} (kN)	-	-	-
$M_{u,Rk}^c$ (kNm)	518.32	-	-	236.81	320.46	V_n^{CWP} (kN)	ΔV_n^{SE} (kN)	-	341.07
ϕ_u^c (rad)	0.0553	-	-	-	-	$V_{f,mod}^{CWP}$ (rad)	$\gamma_{f,mod}^{SE}$ (rad)	0.0752	0.1460

Elastic, perfectly-plastic material law



(a)

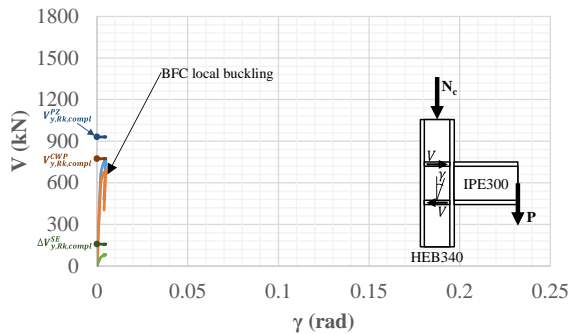
Full-range material law



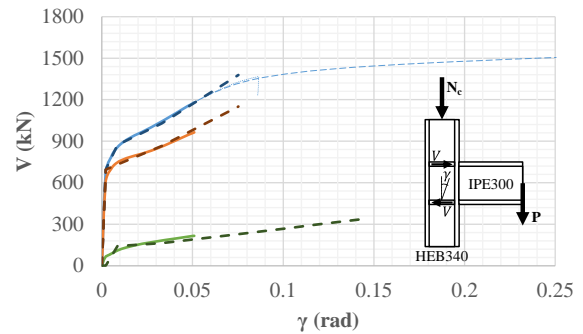
(b)

— PZ — CWP — SE

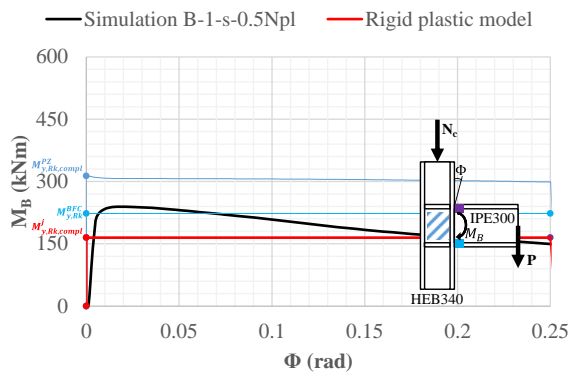
— PZ — CWP — SE



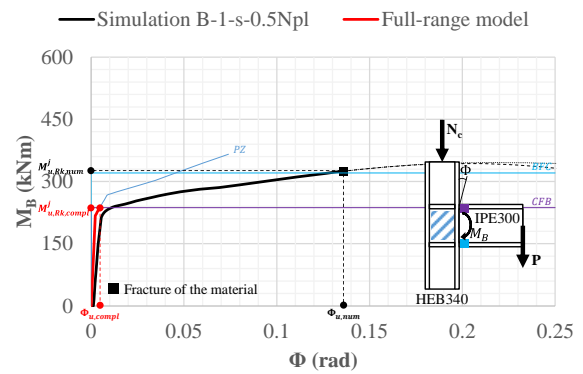
(c)



(d)



(e)



(f)

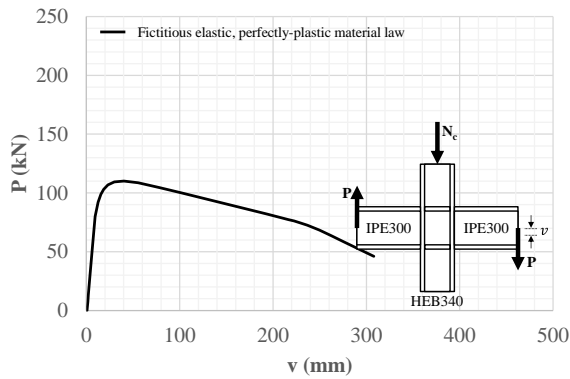
Fig. C-31. Numerical results for the B-1-s-0.5N_{pl} simulation: (a)-(b) ($P - v$)_{num} curves, (c)-(d) ($V - \gamma$)_{num} curves and (e)-(f) ($M_B - \Phi$)_{num} curves.

C.4.8 Simulation B-1-d-0.5N_{pl}

Table C-32. Component characterization for the prediction of the B-1-d-0.5N_{pl} simulation full-range ($M_B - \Phi$)_{num} curve.

Jaspart (1991)	PZ	CWC*	CWT	CFB	BFC	Corman (2022)		CWP	SE
k_{ini}^c (mm)	4.06	-	-	-	-	K_{y}^{CWP} (kN)	K_y^{SE} (kN)	319,984.53	23,343.46
$F_{y,Rk}^c$ (kN)	623.56	-	-	569.78	771.06	$V_{y,mod}^{CWP}$ (kN)	$\Delta V_{y,mod}^{SE}$ (kN)	731.94	155.31
k_{pp}^c (mm)	0.081	-	-	-	-	$\Delta K_{y,mod}^{CWP}$ (kN)	-	6,240.80	-
$F_{u,Rk}^c$ (kN)	895.82	-	-	818.55	1,107.71	$V_{pp,mod}^{CWP}$ (kN)	-	911.90	-
S_{ini}^c (kNm/rad)	71,357.92	-	-	-	-	K_{pp}^{CWP} (kN)	K_{pp}^{SE} (kN)	6,732.00	1,650.72
$M_{y,Rk}^c$ (kNm)	180.40	-	-	164.84	223.07	V_u^{CWP} (kN)	-	1,210.38	-
S_{pp}^c (kNm/rad)	1,423.64	-	-	-	-	ΔK_{pp}^{CWP} (kN)	-	-	-
$M_{u,Rk}^c$ (kNm)	259.16	-	-	236.81	320.46	V_n^{CWP} (kN)	ΔV_n^{SE} (kN)	-	383.63
ϕ_u^c (rad)	0.0553	-	-	-	-	$V_{f,mod}^{CWP}$ (rad)	$\gamma_{f,mod}^{SE}$ (rad)	0.0792	0.1448

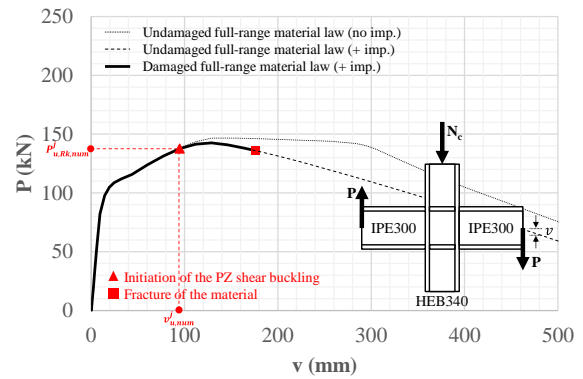
Elastic, perfectly-plastic material law



(a)

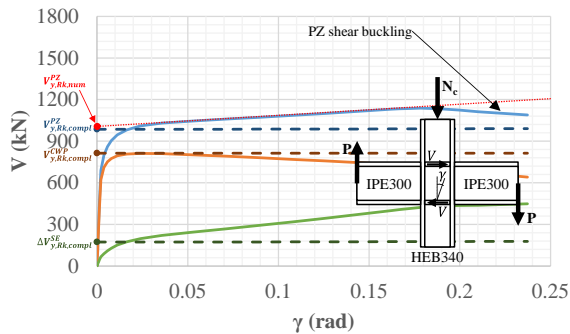
— PZ — CWP — SE

Full-range material law

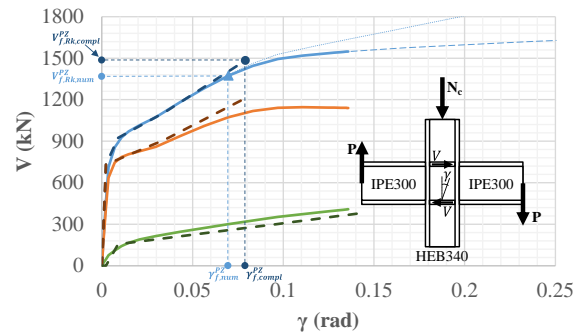


(b)

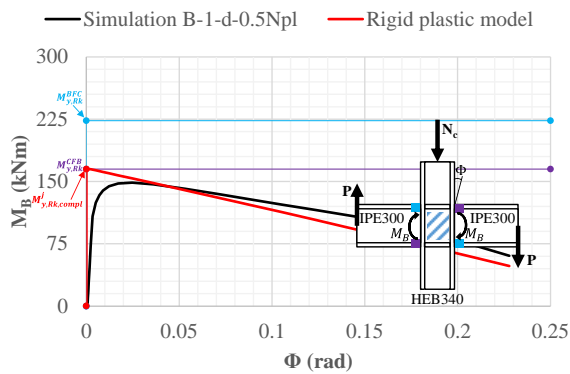
— PZ — CWP — SE



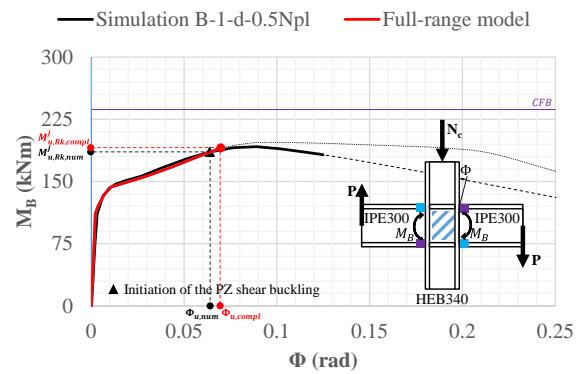
(c)



(d)



(e)



(f)

Fig. C-32. Numerical results for the B-1-d-0.5N_{pl} simulation: (a)-(b) ($P - v$)_{num} curves, (c)-(d) ($V - \gamma$)_{num} curves and (e)-(f) ($M_B - \Phi$)_{num} curves.

D. PLASTIC HINGE CHARACTERIZATION

D.1 Geometric properties

A T-shaped flange consists of two main parts, namely a rectangular flange and a root fillets region. This is depicted in Fig. D-1. To compute the geometric properties of these latter, the T-shaped flange was divided into a series of i sub-parts which are easier to characterize. The geometric properties of the latter are given in Table D-1. They consist of the cross-sectional area A_i , the centre of gravity $y_{CG,i}$, the first moment of area S_i and the second moment of area I_i .

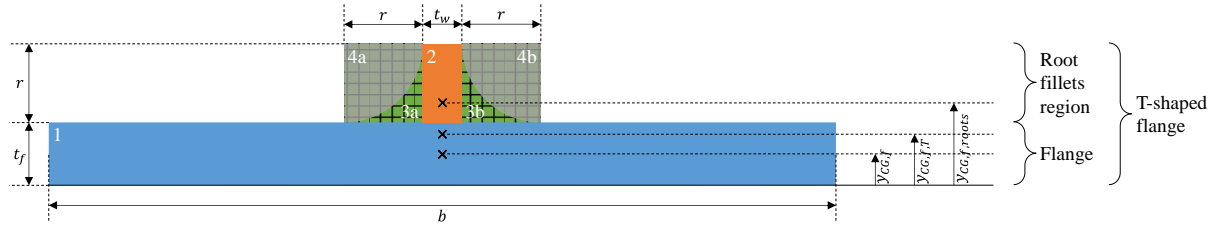


Fig. D-1. Description of a T-shaped flange.

Table D-1. Characterization of the i sub-parts of a T-shaped flange.

i	A_i (mm^2)	$y_{CG,i}$ (mm)	$S_i = A_i \cdot y_{CG,i}$ (mm^3)	I_i (mm^4)
1	$b \cdot t_f$	$\frac{t_f}{2}$	$b \cdot \frac{t_f^2}{2}$	$\frac{b \cdot t_f^3}{12}$
2	$t_w \cdot r$	$t_f + \frac{r}{2}$	$t_w \cdot r \cdot \left(t_f + \frac{r}{2}\right)$	$\frac{t_w \cdot r^3}{12}$
3a	r^2	$t_f + \frac{r}{2}$	$r^2 \cdot \left(t_f + \frac{r}{2}\right)$	$\frac{r^4}{12}$
3b	r^2	$t_f + \frac{r}{2}$	$r^2 \cdot \left(t_f + \frac{r}{2}\right)$	$\frac{r^4}{12}$
4a	$-\frac{\pi \cdot r^2}{4}$	$t_f + r \cdot \frac{3 \cdot \pi - 4}{3 \cdot \pi}$	$-\frac{\pi \cdot r^2}{4} \cdot \left(t_f + r \cdot \frac{3 \cdot \pi - 4}{3 \cdot \pi}\right)$	$-\frac{r^4}{12} \cdot \left(\frac{3 \cdot \pi}{4} - \frac{16}{3 \cdot \pi}\right)$
4b	$-\frac{\pi \cdot r^2}{4}$	$t_f + r \cdot \frac{3 \cdot \pi - 4}{3 \cdot \pi}$	$-\frac{\pi \cdot r^2}{4} \cdot \left(t_f + r \cdot \frac{3 \cdot \pi - 4}{3 \cdot \pi}\right)$	$-\frac{r^4}{12} \cdot \left(\frac{3 \cdot \pi}{4} - \frac{16}{3 \cdot \pi}\right)$

Based on Table D-1, it was possible to derive the main geometric properties (i.e. the cross-sectional area, the centre of gravity and the second moment of area) of a T-shaped flange, a rectangular flange and a root fillets region, see Eq. (D-1) to Eq. (D-9). In addition, the characteristic length of a T-shaped and rectangular flange is given by Eq. (D-10) and Eq. (D-11), respectively.

Cross-sectional area:

$$A_{f,T} = \sum_{i=1}^{4b} A_i = b \cdot t_f + t_w \cdot r + 2 \cdot r^2 - 2 \cdot \frac{\pi \cdot r^2}{4} = b \cdot t_f + t_w \cdot r + 2 \cdot r^2 \cdot \left(1 - \frac{\pi}{4}\right) \quad (D-1)$$

$$A_f = \sum_{i=1}^1 A_i = b \cdot t_f \quad (D-2)$$

$$A_{f,roots} = \sum_{i=2}^{4b} A_i = A_{f,T} - A_f = t_w \cdot r + 2 \cdot r^2 \cdot \left(1 - \frac{\pi}{4}\right) \quad (D-3)$$

Centre of gravity:

$$y_{CG,f,T} = \frac{\sum_{i=1}^{4b} S_i}{\sum_{i=1}^{4b} A_i} = \frac{1}{A_{f,T}} \cdot \left[b \cdot \frac{t_f^2}{2} + t_w \cdot r \cdot \left(t_f + \frac{r}{2} \right) + \left(1 - \frac{\pi}{2} \right) \cdot r^2 \cdot \left(t_f + \frac{r}{3} \cdot \frac{10 - 3 \cdot \pi}{4 - \pi} \right) \right] \quad (D-4)$$

$$y_{CG,f} = \frac{\sum_{i=1}^1 S_i}{\sum_{i=1}^1 A_i} = \frac{1}{A_f} \cdot \left[b \cdot \frac{t_f^2}{2} \right] = \frac{t_f}{2} \quad (D-5)$$

$$y_{CG,f,roots} = \frac{\sum_{i=2}^{4b} S_i}{\sum_{i=2}^{4b} A_i} = \frac{1}{A_{f,roots}} \cdot \left[t_w \cdot r \cdot \left(t_f + \frac{r}{2} \right) + \left(1 - \frac{\pi}{2} \right) \cdot r^2 \cdot \left(t_f + \frac{r}{3} \cdot \frac{10 - 3 \cdot \pi}{4 - \pi} \right) \right] \quad (D-6)$$

Second moment of area:

$$\begin{aligned} I_{f,T} &= \sum_{i=1}^{4b} I_i + \sum_{i=1}^{4b} A_i \cdot \left(y_{CG,i} - y_{CG,f,T} \right)^2 \\ &= \left[\frac{b \cdot t_f^3}{12} + b \cdot t_f \cdot \left(\frac{t_f}{2} - y_{CG,f,T} \right)^2 \right] + \left[\frac{t_w \cdot r^3}{12} + t_w \cdot r \cdot \left(t_f + \frac{r}{2} - y_{CG,f,T} \right)^2 \right] \\ &\quad + \left[\frac{r^4}{12} \cdot \left(1 - \frac{3 \cdot \pi}{4} - \frac{16}{3 \cdot \pi} \right) + 2 \cdot r^2 \cdot \left(t_f + \frac{r}{2} - y_{CG,f,T} \right)^2 - \frac{\pi}{2} \cdot r^2 \right. \\ &\quad \left. \cdot \left(t_f + r \cdot \frac{3 \cdot \pi - 4}{3 \cdot \pi} - y_{CG,f,T} \right)^2 \right] \end{aligned} \quad (D-7)$$

$$I_f = \sum_{i=1}^1 I_i + \sum_{i=1}^1 A_i \cdot \left(y_{CG,i} - y_{CG,f} \right)^2 = \left[\frac{b \cdot t_f^3}{12} + b \cdot t_f \cdot \left(\frac{t_f}{2} - y_{CG,f} \right)^2 \right] = \frac{b \cdot t_f^3}{12} \quad (D-8)$$

$$\begin{aligned} I_{f,roots} &= \sum_{i=2}^{4b} I_i + \sum_{i=2}^{4b} A_i \cdot \left(y_{CG,i} - y_{CG,f,roots} \right)^2 \\ &= \left[\frac{t_w \cdot r^3}{12} + t_w \cdot r \cdot \left(t_f + \frac{r}{2} - y_{CG,f,roots} \right)^2 \right] \\ &\quad + \left[\frac{r^4}{12} \cdot \left(1 - \frac{3 \cdot \pi}{4} - \frac{16}{3 \cdot \pi} \right) + 2 \cdot r^2 \cdot \left(t_f + \frac{r}{2} - y_{CG,f,roots} \right)^2 - \frac{\pi}{2} \cdot r^2 \right. \\ &\quad \left. \cdot \left(t_f + r \cdot \frac{3 \cdot \pi - 4}{3 \cdot \pi} - y_{CG,f,roots} \right)^2 \right] \end{aligned} \quad (D-9)$$

Characteristic length:

$$L_{f,T} = 2 \cdot y_{CG,f,T} \quad (D-10)$$

$$L_f = 2 \cdot y_{CG,f} = t_f \quad (D-11)$$

D.2 Mechanical properties

Based on the geometric properties derived in Section D.1, one can derive the mechanical properties (i.e. the plastic strength, the plastic moment resistance and the M-N interaction curve) of a T-shaped flange, of a rectangular flange and of a root fillets region.

Plastic strength:

$$N_{pl,f,T} = A_{f,T} \cdot f_y \quad (D-12)$$

$$N_{pl,f} = A_f \cdot f_y \quad (D-13)$$

$$N_{pl,f,roots} = A_{f,roots} \cdot f_y \quad (D-14)$$

Plastic moment resistance:

$$M_{pl,f,T} = -\frac{N_{pl,f,T}^2}{4 \cdot b \cdot f_y} + N_{pl,f,T} \cdot y_{CG,f,T} + N_{pl,f} \cdot (y_{CG,f} - y_{CG,f,T}) + N_{pl,f,roots} \cdot (y_{CG,f,roots} - y_{CG,f,T}) \quad (D-15)$$

$$M_{pl,f} = \frac{b \cdot t_f^2}{4} \cdot f_y \quad (D-16)$$

M-N interaction curve:

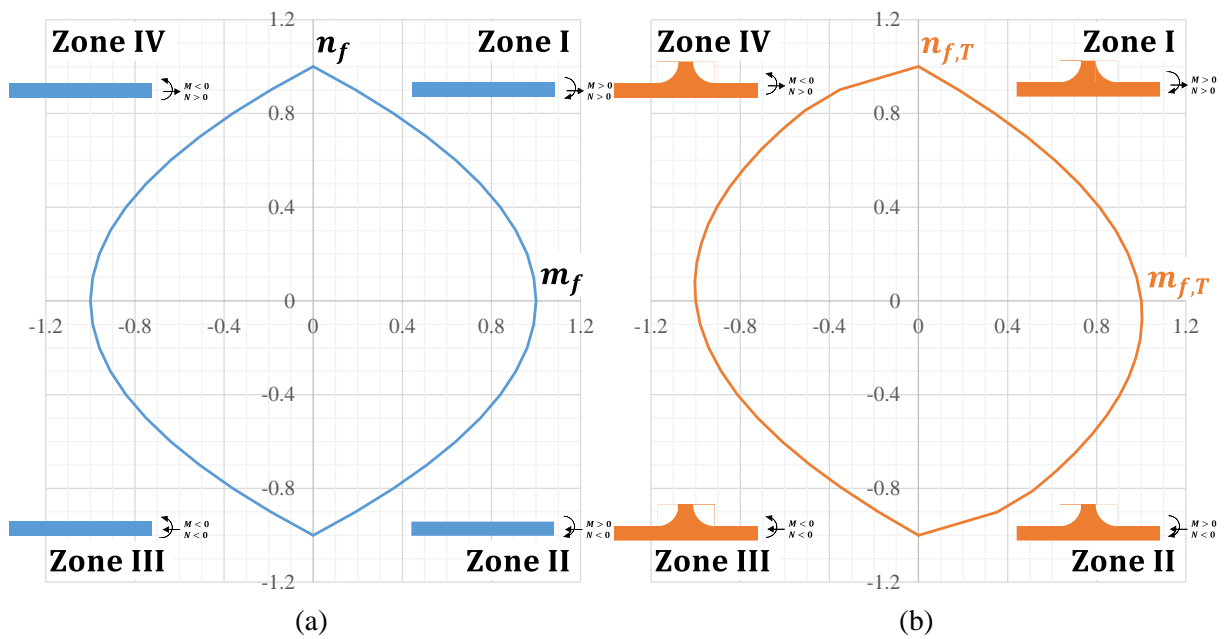


Fig. D-2. M-N interaction curve: (a) rectangular flange and (b) T-shaped flange.

Table D-2. Description of the M-N interaction curves.

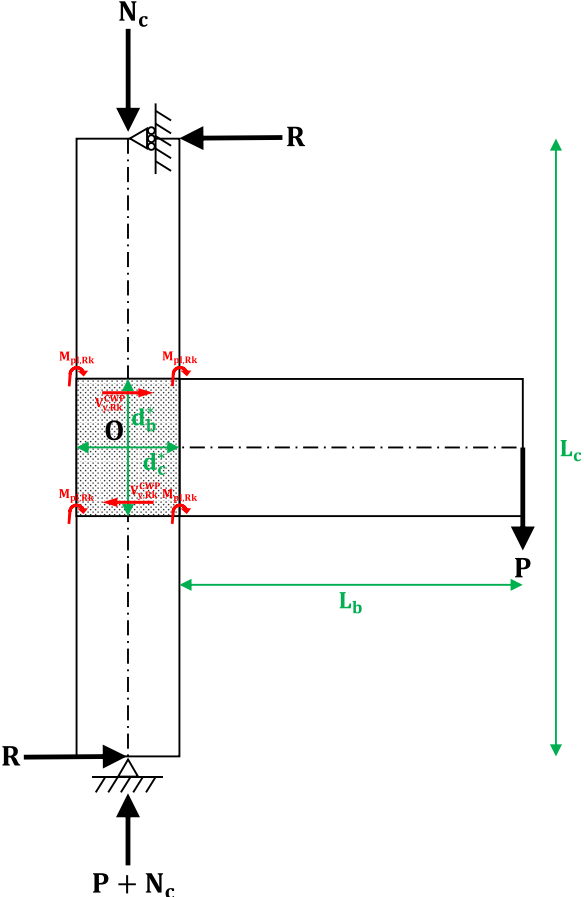
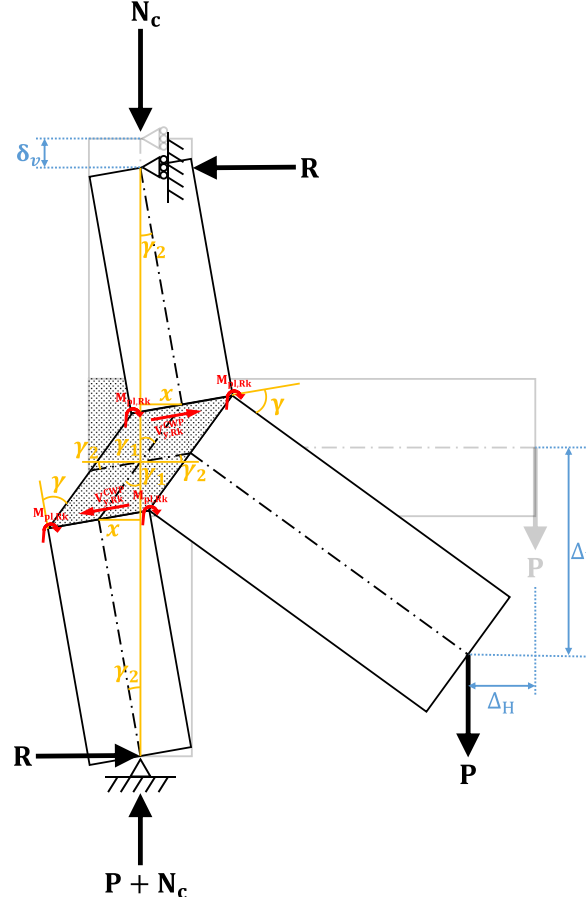
Zone I
$M = -N_{pl,f}^2 \cdot \frac{(1-n_f)^2}{4 \cdot b \cdot f_y} + N_{pl,f} \cdot y_{CG} \cdot (1-n_f) \quad \text{with} \quad \begin{cases} n_f = N/N_{pl,f} \\ m_f = M/M_{pl,f} \end{cases}$
$M = -N_{pl,f,T}^2 \cdot \frac{(1-n_{f,T})^2}{4 \cdot b \cdot f_y} + N_{pl,f,T} \cdot y_{CG,T} \cdot (1-n_{f,T}) + N_{pl,f} \cdot (y_{CG,f} - y_{CG,T}) + N_{pl,f,roots} \cdot (y_{CG,roots} - y_{CG,T}) \quad \text{with} \quad \begin{cases} n_{f,T} = N/N_{pl,f,T} \\ m_{f,T} = M/M_{pl,f,T} \end{cases}$

Zone II
$M = -N_{pl,f}^2 \cdot \frac{(1+n_f)^2}{4 \cdot b \cdot f_y} + N_{pl,f} \cdot y_{CG} \cdot (1 - n_f) \quad \text{with} \begin{cases} n_f = N/N_{pl,f} \\ m_f = M/M_{pl,f} \end{cases}$ $M = -N_{pl,f,T}^2 \cdot \frac{(1+n_{f,T})^2}{4 \cdot b \cdot f_y} + N_{pl,f,T} \cdot y_{CG,T} \cdot (1 + n_{f,T}) + N_{pl,f} \cdot (y_{CG,f} - y_{CG,T}) + N_{pl,f,roots} \cdot (y_{CG,roots} - y_{CG,T}) \quad \text{with} \begin{cases} n_{f,T} = N/N_{pl,f,T} \\ m_{f,T} = M/M_{pl,f,T} \end{cases}$
Zone III
$M = -N_{pl,f}^2 \cdot \frac{(1-n_f)^2}{4 \cdot b \cdot f_y} + N_{pl,f} \cdot y_{CG} \cdot (1 - n_f) \quad \text{with} \begin{cases} n_f = N/N_{pl,f} \\ m_f = M/M_{pl,f} \end{cases}$ $M = -N_{pl,f,T}^2 \cdot \frac{(1-n_{f,T})^2}{4 \cdot b \cdot f_y} + N_{pl,f,T} \cdot y_{CG,T} \cdot (1 - n_{f,T}) + N_{pl,f} \cdot (y_{CG,f} - y_{CG,T}) + N_{pl,f,roots} \cdot (y_{CG,roots} - y_{CG,T}) \quad \text{with} \begin{cases} n_{f,T} = N/N_{pl,f,T} \\ m_{f,T} = M/M_{pl,f,T} \end{cases}$
Zone IV
$M = -N_{pl,f}^2 \cdot \frac{(1+n_f)^2}{4 \cdot b \cdot f_y} + N_{pl,f} \cdot y_{CG} \cdot (1 - n_f) \quad \text{with} \begin{cases} n_f = N/N_{pl,f} \\ m_f = M/M_{pl,f} \end{cases}$ $M = -N_{pl,f,T}^2 \cdot \frac{(1+n_{f,T})^2}{4 \cdot b \cdot f_y} + N_{pl,f,T} \cdot y_{CG,T} \cdot (1 + n_{f,T}) + N_{pl,f} \cdot (y_{CG,f} - y_{CG,T}) + N_{pl,f,roots} \cdot (y_{CG,roots} - y_{CG,T}) \quad \text{with} \begin{cases} n_{f,T} = N/N_{pl,f,T} \\ m_{f,T} = M/M_{pl,f,T} \end{cases}$

E. GEOMETRIC 2ND ORDER EFFECTS

E.1 Exterior joints

Table E-1. Determination of the geometrical 2nd order effects in an exterior joint.

Geometry	
Undeformed configuration (1 st order)	Deformed configuration (2 nd order)
 <p>Fig. E-1. Exterior joint in undeformed shape.</p>	 <p>Fig. E-2. Exterior joint in deformed shape.</p>

Angles					
$\sin \gamma_1$	$= \frac{x}{d_b^*}$ $= 2 \cdot \frac{x}{d_b^*}$	(E-1)	$\frac{d}{dy}(\sin \gamma_1)$	$= \dots$ $= \cos \gamma_1 \cdot \frac{d}{dy}(\gamma_1)$	(E-2)
$\sin \gamma_2$	$= \frac{x}{L_c - d_b^*}$ $= 2 \cdot \frac{x}{L_c - d_b^*}$	(E-3)	$\frac{d}{dy}(\sin \gamma_2)$	$= \dots$ $= \cos \gamma_2 \cdot \frac{d}{dy}(\gamma_2)$	(E-4)
$\stackrel{\text{Eq. (E-1)}}{\Leftrightarrow}$	$\sin \gamma_2 = 2 \cdot \frac{1}{L_c - d_b^*} \cdot \frac{d_b^*}{2} \cdot \sin \gamma_1$ $\Leftrightarrow \dots$ $\Leftrightarrow \sin \gamma_2 = \frac{d_b^*}{L_c - d_b^*} \cdot \sin \gamma_1$	(E-5)	$\stackrel{\text{Eq. (E-5)}}{\Leftrightarrow}$	$\frac{d}{dy}(\sin \gamma_2) = \frac{d_b^*}{L_c - d_b^*} \cdot \frac{d}{dy}(\sin \gamma_1)$ $\Leftrightarrow \cos \gamma_2 \cdot \frac{d}{dy}(\gamma_2) = \frac{d_b^*}{L_c - d_b^*} \cdot \cos \gamma_1 \cdot \frac{d}{dy}(\gamma_1)$ $\Leftrightarrow \frac{d}{dy}(\gamma_2) = \frac{d_b^*}{L_c - d_b^*} \cdot \frac{\cos \gamma_1}{\cos \gamma_2} \cdot \frac{d}{dy}(\gamma_1)$	(E-6)
$\cos \gamma_1$	$= \sqrt{1 - \sin^2(\gamma_1)}$ $= \sqrt{1 - \left(2 \cdot \frac{x}{d_b^*}\right)^2}$	(E-7)	$\frac{d}{dy}(\cos \gamma_1)$	$= \dots$ $= -\sin \gamma_1 \cdot \frac{d}{dy}(\gamma_1)$	(E-8)
$\cos \gamma_2$	$= \sqrt{1 - \sin^2 \gamma_2}$ $= \sqrt{1 - \left(2 \cdot \frac{x}{L_c - d_b^*}\right)^2}$	(E-9)	$\frac{d}{dy}(\cos \gamma_2)$	$= \dots$ $= -\sin \gamma_2 \cdot \frac{d}{dy}(\gamma_2)$	(E-10)
$\stackrel{\text{Eq. (E-1)}}{\Leftrightarrow}$	$\cos \gamma_2 = \sqrt{1 - \left(2 \cdot \frac{1}{L_c - d_b^*} \cdot \frac{d_b^*}{2} \cdot \sin \gamma_1\right)^2}$ $\Leftrightarrow \cos \gamma_2 = \sqrt{1 - \left(\frac{d_b^*}{L_c - d_b^*}\right)^2 \cdot (1 - \cos^2 \gamma_1)}$ $\Leftrightarrow \cos \gamma_2 = \frac{1}{L_c - d_b^*} \cdot \sqrt{L_c^2 - 2 \cdot L_c \cdot d_b^* + (d_b^* \cdot \cos \gamma_1)^2}$	(E-11)	$\stackrel{\text{Eqs. (E-3), (E-6)}}{\Leftrightarrow}$	$\frac{d}{dy}(\cos \gamma_2) = -\frac{d_b^*}{L_c - d_b^*} \cdot \sin \gamma_1 \cdot \frac{d_b^*}{L_c - d_b^*} \cdot \frac{\cos \gamma_1}{\cos \gamma_2} \cdot \frac{d}{dy}(\gamma_1)$ $\Leftrightarrow \frac{d}{dy}(\cos \gamma_2) = \dots$ $\Leftrightarrow \frac{d}{dy}(\cos \gamma_2) = -\left(\frac{d_b^*}{L_c - d_b^*}\right)^2 \cdot \frac{\cos \gamma_1 \cdot \sin \gamma_1}{\cos \gamma_2} \cdot \frac{d}{dy}(\gamma_1)$	(E-12)
γ	$= \gamma_1 + \gamma_2$ $\stackrel{\text{Eq. (E-5)}}{\approx} \gamma_1 + \frac{d_b^*}{L_c - d_b^*} \cdot \gamma_1$ $\approx \gamma_1 \cdot \left(1 + \frac{d_b^*}{L_c - d_b^*}\right)$	(E-13)	$\frac{d}{dy}(\gamma)$	$= \frac{d}{dy}(\gamma_1 + \gamma_2)$ $= \frac{d}{dy}(\gamma_1) + \frac{d_b^*}{L_c - d_b^*} \cdot \frac{\cos \gamma_1}{\cos \gamma_2} \cdot \frac{d}{dy}(\gamma_1)$ $= \left(1 + \frac{d_b^*}{L_c - d_b^*} \cdot \frac{\cos \gamma_1}{\cos \gamma_2}\right) \cdot \frac{d}{dy}(\gamma_1)$	(E-14)

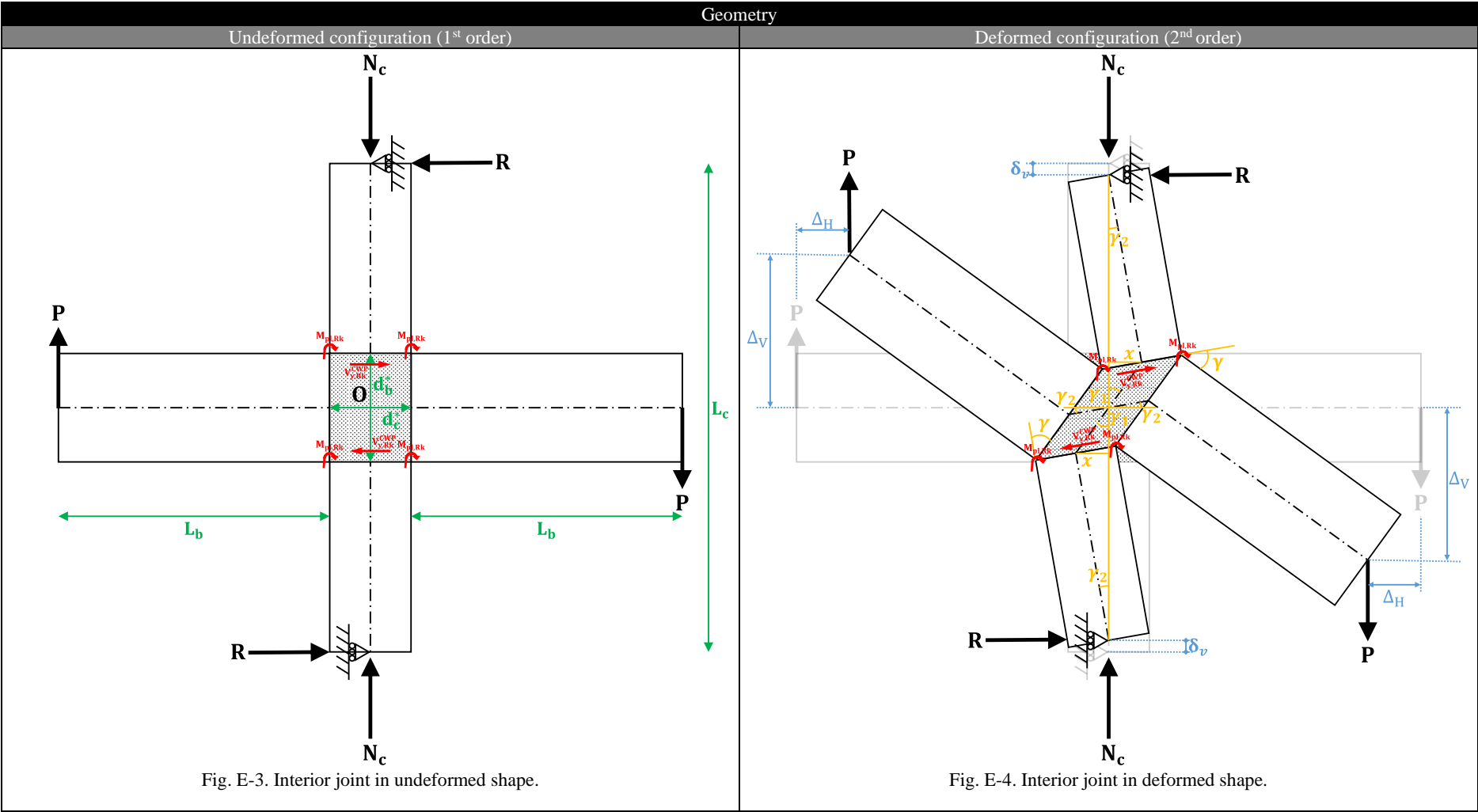
Displacements					
δ_v	$= L_c - \left(2 \cdot \frac{L_c - d_b^*}{2} \cdot \cos \gamma_2 + d_b^* \cdot \cos \gamma_1 \right)$ $= \dots$ $= \dots$ $= L_c \cdot (1 - \cos \gamma_2) + d_b^* \cdot (\cos \gamma_2 - \cos \gamma_1)$	(E-15)	$\frac{d}{d\gamma}(\delta_v)$	$= -L_c \cdot \frac{d}{d\gamma}(\cos \gamma_2) + d_b^* \cdot \left(\frac{d}{d\gamma}(\cos \gamma_2) + \sin \gamma_1 \cdot \frac{d}{d\gamma}(\gamma_1) \right)$ $= (-L_c + d_b^*) \cdot \frac{d}{d\gamma}(\cos \gamma_2) + d_b^* \cdot \sin \gamma_1 \cdot \frac{d}{d\gamma}(\gamma_1)$ $= (L_c - d_b^*) \cdot \left(\frac{d_b^*}{L_c - d_b^*} \right)^2 \cdot \frac{\cos \gamma_1 \cdot \sin \gamma_1}{\cos \gamma_2} \cdot \frac{d}{d\gamma}(\gamma_1) + d_b^* \cdot \sin \gamma_1 \cdot \frac{d}{d\gamma}(\gamma_1)$ $= d_b^* \cdot \sin \gamma_1 \cdot \left(1 + \frac{d_b^*}{L_c - d_b^*} \cdot \frac{\cos \gamma_1}{\cos \gamma_2} \right) \cdot \frac{d}{d\gamma}(\gamma_1)$	(E-16)
Δ_V	$= \frac{L_c}{2} - \left(\frac{L_c - d_b^*}{2} \cdot \cos \gamma_2 + d_b^* \cdot \cos \gamma_1 + \frac{d_c^*}{2} \cdot \sin \gamma_2 - L_b \cdot \sin \gamma_1 \right)$ $= \frac{L_c}{2} \cdot (1 - \cos \gamma_2) + \frac{d_b^*}{2} \cdot (\cos \gamma_2 - \cos \gamma_1) - \frac{d_c^*}{2} \cdot \sin \gamma_2 + L_b \cdot \sin \gamma_1$ $= \frac{\delta_v}{2} + \sin \gamma_1 \cdot \left(L_b - \frac{d_c^*}{2} \cdot \frac{d_b^*}{L_c - d_b^*} \right)$	(E-17)	$\frac{d}{d\gamma}(\Delta_V)$	$= \frac{d}{d\gamma} \left[\frac{\delta_v}{2} + \sin \gamma_1 \cdot \left(L_b - \frac{d_c^*}{2} \cdot \frac{d_b^*}{L_c - d_b^*} \right) \right]$ $= \frac{1}{2} \cdot \frac{d}{d\gamma}(\delta_v) + \frac{d}{d\gamma}(\sin \gamma_1) \cdot \left(L_b - \frac{d_c^*}{2} \cdot \frac{d_b^*}{L_c - d_b^*} \right)$ $= \frac{d_b^*}{2} \cdot \sin \gamma_1 \cdot \left(1 + \frac{d_b^*}{L_c - d_b^*} \cdot \frac{\cos \gamma_1}{\cos \gamma_2} \right) \cdot \frac{d}{d\gamma}(\gamma_1) + \cos \gamma_1 \cdot \left(L_b - \frac{d_c^*}{2} \cdot \frac{d_b^*}{L_c - d_b^*} \right) \cdot \frac{d}{d\gamma}(\gamma_1)$	(E-18)
Δ_H	$= L_b + \frac{d_c^*}{2} - \left(\frac{d_c^*}{2} \cdot \cos \gamma_2 + L_b \cdot \cos \gamma_1 + \frac{d_b^*}{2} \cdot \sin \gamma_1 - \frac{L_c - d_b^*}{2} \cdot \sin \gamma_2 \right)$ $= \dots$ $= \dots$ $= \dots$ $= L_b \cdot (1 - \cos \gamma_1) + \frac{d_c^*}{2} \cdot (1 - \cos \gamma_2) - \frac{d_b^*}{2} \cdot (\sin \gamma_1 + \sin \gamma_2) + \frac{L_c}{2} \cdot \sin \gamma_2$	(E-19)	$\frac{d}{d\gamma}(\Delta_H)$	$= -L_b \cdot \frac{d}{d\gamma}(\cos \gamma_1) - \frac{d_c^*}{2} \cdot \frac{d}{d\gamma}(\cos \gamma_2) - \frac{d_b^*}{2} \cdot \left(\frac{d}{d\gamma}(\sin \gamma_1) + \frac{d}{d\gamma}(\sin \gamma_2) \right) + \frac{L_c}{2} \cdot \frac{d}{d\gamma}(\sin \gamma_2)$ $= L_b \cdot \sin \gamma_1 \cdot \frac{d}{d\gamma}(\gamma_1) + \frac{d_c^*}{2} \cdot \left(\frac{d_b^*}{L_c - d_b^*} \right)^2 \cdot \frac{\cos \gamma_1 \cdot \sin \gamma_1}{\cos \gamma_2} \cdot \frac{d}{d\gamma}(\gamma_1) - \frac{d_b^*}{2} \cdot \cos \gamma_1 \cdot \frac{d}{d\gamma}(\gamma_1) - \frac{d_b^*}{2} \cdot \frac{d_b^*}{L_c - d_b^*} \cdot \cos \gamma_1 \cdot \frac{d}{d\gamma}(\gamma_1) + \frac{L_c}{2} \cdot \frac{d_b^*}{L_c - d_b^*} \cdot \cos \gamma_1 \cdot \frac{d}{d\gamma}(\gamma_1)$ $= \cos \gamma_1 \cdot \left[L_b \cdot \tan \gamma_1 + \frac{d_c^*}{2} \cdot \left(\frac{d_b^*}{L_c - d_b^*} \right)^2 \cdot \frac{\sin \gamma_1}{\cos \gamma_2} - \frac{d_b^*}{2} - \frac{d_b^*}{2} \cdot \frac{d_b^*}{L_c - d_b^*} + \frac{L_c}{2} \cdot \frac{d_b^*}{L_c - d_b^*} \right] \cdot \frac{d}{d\gamma}(\gamma_1)$ $= \cos \gamma_1 \cdot \left[L_b \cdot \tan \gamma_1 + \frac{d_c^*}{2} \cdot \left(\frac{d_b^*}{L_c - d_b^*} \right)^2 \cdot \frac{\sin \gamma_1}{\cos \gamma_2} \right] \cdot \frac{d}{d\gamma}(\gamma_1)$ $= \sin \gamma_1 \cdot \left[L_b + \frac{d_c^*}{2} \cdot \left(\frac{d_b^*}{L_c - d_b^*} \right)^2 \cdot \frac{\cos \gamma_1}{\cos \gamma_2} \right] \cdot \frac{d}{d\gamma}(\gamma_1)$	(E-20)

Determinatation of the 2 nd order effects					
Virtual work principle					
W_{EXT}	$= P \cdot \Delta_V + N_c \cdot \delta_v$ $= P \cdot \left[\frac{\delta_v}{2} + \sin \gamma_1 \cdot \left(L_b - \frac{d_c^*}{2} \cdot \frac{d_b^*}{L_c - d_b^*} \right) \right] + N_c \cdot \delta_v$ $= \left(\frac{P}{2} + N_c \right) \cdot \delta_v + P \cdot \sin \gamma_1 \cdot \left(L_b - \frac{d_c^*}{2} \cdot \frac{d_b^*}{L_c - d_b^*} \right)$	(E-21)	$\frac{d}{d\gamma}(W_{EXT})$	$= P \cdot \frac{d}{d\gamma}(\Delta_V) + N_c \cdot \frac{d}{d\gamma}(\delta_v)$ $= \left(\frac{P}{2} + N_c \right) \cdot \frac{d}{d\gamma}(\delta_v) + P \cdot \frac{d}{d\gamma}(\sin \gamma_1) \cdot \left(L_b - \frac{d_c^*}{2} \cdot \frac{d_b^*}{L_c - d_b^*} \right)$ $= \left(\frac{P}{2} + N_c \right) \cdot d_b^* \cdot \sin \gamma_1 \cdot \left(1 + \frac{d_b^*}{L_c - d_b^*} \cdot \frac{\cos \gamma_1}{\cos \gamma_2} \right) \cdot \frac{d}{d\gamma}(\gamma_1) + P \cdot \cos \gamma_1 \cdot \left(L_b - \frac{d_c^*}{2} \cdot \frac{d_b^*}{L_c - d_b^*} \right) \cdot \frac{d}{d\gamma}(\gamma_1)$	(E-22)
W_{INT}	$= \dots$ $= V_{y,Rk}^{CWP} \cdot d_b^* \cdot \sin \gamma + \Delta V_{y,Rk}^{SE} \cdot d_b^* \cdot \gamma$	(E-23)	$\frac{d}{d\gamma}(W_{INT})$	$= V_{y,Rk}^{CWP} \cdot d_b^* \cdot \frac{d}{d\gamma}(\sin \gamma) + \Delta V_{y,Rk}^{SE} \cdot d_b^* \cdot \frac{d}{d\gamma}(\gamma)$ $= V_{y,Rk}^{CWP} \cdot d_b^* \cdot \cos \gamma + \Delta V_{y,Rk}^{SE} \cdot d_b^*$	(E-24)
$W_{EXT} = W_{INT}$	$\left(\frac{P}{2} + N_c \right) \cdot [L_c \cdot (1 - \cos \gamma_2) + d_b^* \cdot (\cos \gamma_2 - \cos \gamma_1)] + P \cdot \sin \gamma_1 \cdot \left(L_b - \frac{d_c^*}{2} \cdot \frac{d_b^*}{L_c - d_b^*} \right) = V_{y,Rk}^{CWP} \cdot d_b^* \cdot \sin \gamma + \Delta V_{y,Rk}^{SE} \cdot d_b^* \cdot \gamma$ $\Leftrightarrow \frac{P}{2} \cdot \gamma_1 \cdot \frac{2 \cdot L_b \cdot L_c - 2 \cdot L_b \cdot d_b^* + d_c^* \cdot d_b^*}{L_c - d_b^*} = V_{y,Rk}^{CWP} \cdot d_b^* \cdot \gamma + \Delta V_{y,Rk}^{SE} \cdot d_b^* \cdot \gamma$ $\Leftrightarrow \frac{P}{2} \cdot \frac{L_c - d_b^*}{L_c} \cdot \gamma \cdot \frac{2 \cdot L_b \cdot L_c - 2 \cdot L_b \cdot d_b^* + d_c^* \cdot d_b^*}{L_c - d_b^*} = V_{y,Rk}^{CWP} \cdot d_b^* \cdot \gamma + \Delta V_{y,Rk}^{SE} \cdot d_b^* \cdot \gamma$ $\Leftrightarrow \frac{P}{2} \cdot \frac{2 \cdot L_b \cdot L_c - 2 \cdot L_b \cdot d_b^* + d_c^* \cdot d_b^*}{L_c} = V_{y,Rk}^{CWP} \cdot d_b^* + \Delta V_{y,Rk}^{SE} \cdot d_b^*$ $\Leftrightarrow P = \dots$ $\Leftrightarrow P = \dots$ $\Leftrightarrow P = \dots$ $\Leftrightarrow P = 2 \cdot (V_{y,Rk}^{CWP} + \Delta V_{y,Rk}^{SE}) \cdot \frac{L_c \cdot d_b^*}{2 \cdot L_b \cdot L_c - 2 \cdot L_b \cdot d_b^* + d_c^* \cdot d_b^*}$	(E-25)	$\frac{d}{d\gamma}(W_{EXT})$ $= \frac{d}{d\gamma}(W_{INT})$	$\left(\frac{P}{2} + N_c \right) \cdot d_b^* \cdot \sin \gamma_1 \cdot \left(1 + \frac{d_b^*}{L_c - d_b^*} \cdot \frac{\cos \gamma_1}{\cos \gamma_2} \right) \cdot \frac{d}{d\gamma}(\gamma_1) + P \cdot \cos \gamma_1 \cdot \left(L_b - \frac{d_c^*}{2} \cdot \frac{d_b^*}{L_c - d_b^*} \right) \cdot \frac{d}{d\gamma}(\gamma_1) = V_{y,Rk}^{CWP} \cdot d_b^* \cdot \cos \gamma + \Delta V_{y,Rk}^{SE} \cdot d_b^*$ $\Leftrightarrow \left(\frac{P}{2} + N_c \right) \cdot d_b^* \cdot \sin \gamma_1 + \frac{P}{2} \cdot \cos \gamma_1 \cdot \frac{2 \cdot L_b \cdot L_c - 2 \cdot L_b \cdot d_b^* + d_c^* \cdot d_b^*}{L_c - d_b^*} \cdot \frac{(L_c - d_b^*) \cdot \cos \gamma_2}{(L_c - d_b^*) \cdot \cos \gamma_2 + d_b^* \cdot \cos \gamma_1} = V_{y,Rk}^{CWP} \cdot d_b^* \cdot \cos \gamma + \Delta V_{y,Rk}^{SE} \cdot d_b^*$ $\Leftrightarrow \left(\frac{P}{2} + N_c \right) \cdot d_b^* \cdot \sin \gamma_1 + \frac{P}{2} \cdot \cos \gamma_1 \cdot \cos \gamma_2 \cdot \frac{2 \cdot L_b \cdot L_c - 2 \cdot L_b \cdot d_b^* + d_c^* \cdot d_b^*}{(L_c - d_b^*) \cdot \cos \gamma_2 + d_b^* \cdot \cos \gamma_1} = V_{y,Rk}^{CWP} \cdot d_b^* \cdot \cos(\gamma) + \Delta V_{y,Rk}^{SE} \cdot d_b^*$ $\Leftrightarrow \frac{P}{2} \cdot d_b^* \cdot \sin \gamma_1 + \frac{P}{2} \cdot \cos \gamma_1 \cdot \cos \gamma_2 \cdot \frac{2 \cdot L_b \cdot L_c - 2 \cdot L_b \cdot d_b^* + d_c^* \cdot d_b^*}{(L_c - d_b^*) \cdot \cos \gamma_2 + d_b^* \cdot \cos \gamma_1} = V_{y,Rk}^{CWP} \cdot d_b^* \cdot \cos \gamma + \Delta V_{y,Rk}^{SE} \cdot d_b^* - N_c \cdot d_b^* \cdot \sin \gamma_1$ $\Leftrightarrow \frac{P}{2} \cdot d_b^* \cdot \sin \gamma_1 \cdot [(L_c - d_b^*) \cdot \cos \gamma_2 + d_b^* \cdot \cos \gamma_1] + \frac{P}{2} \cdot \cos \gamma_1 \cdot \cos \gamma_2 \cdot (2 \cdot L_b \cdot L_c - 2 \cdot L_b \cdot d_b^* + d_c^* \cdot d_b^*) = (V_{y,Rk}^{CWP} \cdot \cos \gamma + \Delta V_{y,Rk}^{SE} - N_c \cdot \sin \gamma_1) \cdot d_b^* \cdot [(L_c - d_b^*) \cdot \cos \gamma_2 + d_b^* \cdot \cos \gamma_1]$ $\Leftrightarrow \frac{P}{2} \cdot \cos \gamma_1 \cdot \cos \gamma_2 \cdot [d_b^* \cdot (L_c - d_b^*) \cdot \tan \gamma_1 + d_b^{*2} \cdot \frac{\sin \gamma_1}{\cos \gamma_2} + 2 \cdot L_b \cdot L_c - 2 \cdot L_b \cdot d_b^* + d_c^* \cdot d_b^*] = (V_{y,Rk}^{CWP} \cdot \cos \gamma + \Delta V_{y,Rk}^{SE} - N_c \cdot \sin \gamma_1) \cdot d_b^* \cdot [(L_c - d_b^*) \cdot \cos \gamma_2 + d_b^* \cdot \cos \gamma_1]$ $\Leftrightarrow \frac{P}{2} \cdot \cos \gamma_1 \cdot \cos \gamma_2 \cdot [d_b^* \cdot (L_c - d_b^*) \cdot \tan \gamma_1 + d_b^* \cdot (L_c - d_b^*) \cdot \tan \gamma_2 + 2 \cdot L_b \cdot L_c - 2 \cdot L_b \cdot d_b^* + d_c^* \cdot d_b^*] = (V_{y,Rk}^{CWP} \cdot \cos \gamma + \Delta V_{y,Rk}^{SE} - N_c \cdot \sin \gamma_1) \cdot d_b^* \cdot [(L_c - d_b^*) \cdot \cos \gamma_2 + d_b^* \cdot \cos \gamma_1]$ $\Leftrightarrow P = 2 \cdot (V_{y,Rk}^{CWP} \cdot \cos \gamma + \Delta V_{y,Rk}^{SE} - N_c \cdot \sin \gamma_1) \cdot \frac{d_b^*}{\cos \gamma_1 \cdot \cos \gamma_2} \cdot \frac{(L_c - d_b^*) \cdot \cos \gamma_2 + d_b^* \cdot \cos \gamma_1}{d_b^* \cdot (L_c - d_b^*) \cdot (\tan \gamma_1 + \tan \gamma_2) + 2 \cdot L_b \cdot L_c - 2 \cdot L_b \cdot d_b^* + d_c^* \cdot d_b^*}$	(E-26)

Conclusion					
<p>Eq. (E-25) ⇒ Eq. (B-5)</p>	$V_{y,Rk}^{PZ} = \frac{P}{2} \cdot \frac{1}{d_b^*} \cdot \frac{2 \cdot L_b \cdot L_c - 2 \cdot L_b \cdot d_b^* - d_c^* \cdot d_b^*}{L_c}$ $\Leftrightarrow V_{y,Rk}^{PZ} = \dots$ $\Leftrightarrow V_{y,Rk}^{PZ} = \dots$ $\Leftrightarrow V_{y,Rk}^{PZ} = \dots$ $\Leftrightarrow V_{y,Rk}^{PZ} = \dots$ $\Leftrightarrow V_{y,Rk}^{PZ} = \dots$ $\Leftrightarrow V_{y,Rk}^{PZ} = \dots$ $\Leftrightarrow V_{y,Rk}^{PZ} = \dots$ $\Leftrightarrow V_{y,Rk}^{PZ} = V_{y,Rk}^{CWP} + \Delta V_{y,Rk}^{SE}$	<p>Eq. (E-26) ⇒ Eq. (B-6)</p>	$V_{y,Rk}^{PZ} = \frac{P}{2} \cdot \frac{\cos \gamma_1 \cdot \cos \gamma_2 \cdot \frac{1}{d_b^*}}{\cos \gamma} \cdot \frac{1}{d_b^*} \cdot \frac{2 \cdot L_b \cdot L_c - 2 \cdot L_b \cdot d_b^* - d_c^* \cdot d_b^* + d_b^* \cdot (L_c - d_b^*) \cdot (\tan \gamma_2 + \tan \gamma_1)}{(L_c - d_b^*) \cdot \cos \gamma_2 + d_b^* \cdot \cos \gamma_1} + N_c \cdot \tan \gamma \cdot \frac{1}{L_c - d_b^*} \cdot \frac{1}{(L_c - d_b^*) \cdot \cos \gamma_2 + d_b^* \cdot \cos \gamma_1}$ $\Leftrightarrow V_{y,Rk}^{PZ} = \left(V_{y,Rk}^{CWP} \cdot \cos \gamma + \Delta V_{y,Rk}^{SE} - N_c \cdot \sin \gamma_1 \right) \cdot \frac{1}{\cos \gamma} + N_c \cdot \tan \gamma \cdot \frac{L_c - d_b^*}{(L_c - d_b^*) \cdot \cos \gamma_2 + d_b^* \cdot \cos \gamma_1}$ $\Leftrightarrow V_{y,Rk}^{PZ} = \left(V_{y,Rk}^{CWP} \cdot \cos \gamma + \Delta V_{y,Rk}^{SE} \right) \cdot \frac{1}{\cos \gamma} + N_c \cdot \left(-\frac{\sin \gamma_1}{\cos \gamma} + \tan \gamma \cdot \frac{L_c - d_b^*}{(L_c - d_b^*) \cdot \cos \gamma_2 + d_b^* \cdot \cos \gamma_1} \right)$ $\Leftrightarrow V_{y,Rk}^{PZ} = \left(V_{y,Rk}^{CWP} + \Delta V_{y,Rk}^{SE} \cdot \frac{1}{\cos \gamma} \right) + N_c \cdot \left(-\tan \gamma \cdot \frac{\sin \gamma_1}{\sin \gamma} + \tan \gamma \cdot \frac{L_c - d_b^*}{(L_c - d_b^*) \cdot \cos \gamma_2 + d_b^* \cdot \cos \gamma_1} \right)$ $\Leftrightarrow V_{y,Rk}^{PZ} = \left(V_{y,Rk}^{CWP} + \Delta V_{y,Rk}^{SE} \cdot \frac{1}{\cos \gamma} \right) + N_c \cdot \tan \gamma \cdot \left(-\frac{\sin \gamma_1}{\sin \gamma} + \frac{L_c - d_b^*}{(L_c - d_b^*) \cdot \cos \gamma_2 + d_b^* \cdot \cos \gamma_1} \right)$ $\Leftrightarrow V_{y,Rk}^{PZ} = \left(V_{y,Rk}^{CWP} + \Delta V_{y,Rk}^{SE} \cdot \frac{1}{\cos \gamma} \right) + N_c \cdot \tan \gamma \cdot \left(-\frac{1}{\frac{\sin \gamma_1 \cdot \cos \gamma_2 + \cos \gamma_1 \cdot \sin \gamma_2}{\sin \gamma_1} + \frac{L_c - d_b^*}{(L_c - d_b^*) \cdot \cos \gamma_2 + d_b^* \cdot \cos \gamma_1}} \right)$ $\Leftrightarrow V_{y,Rk}^{PZ} = \left(V_{y,Rk}^{CWP} + \Delta V_{y,Rk}^{SE} \cdot \frac{1}{\cos \gamma} \right) + N_c \cdot \tan \gamma \cdot \left(-\frac{1}{\cos \gamma_2 + \frac{d_b^*}{L_c - d_b^*} \cdot \cos \gamma_1} + \frac{L_c - d_b^*}{(L_c - d_b^*) \cdot \cos \gamma_2 + d_b^* \cdot \cos \gamma_1} \right)$ $\Leftrightarrow V_{y,Rk}^{PZ} = \left(V_{y,Rk}^{CWP} + \Delta V_{y,Rk}^{SE} \cdot \frac{1}{\cos \gamma} \right) + N_c \cdot \tan \gamma \cdot \left(-\frac{L_c - d_b^*}{(L_c - d_b^*) \cdot \cos \gamma_2 + d_b^* \cdot \cos \gamma_1} + \frac{L_c - d_b^*}{(L_c - d_b^*) \cdot \cos \gamma_2 + d_b^* \cdot \cos \gamma_1} \right)$ $\Leftrightarrow V_{y,Rk}^{PZ} = V_{y,Rk}^{CWP} + \Delta V_{y,Rk}^{SE} \cdot \frac{1}{\cos \gamma}$	<p>(E-27)</p>	<p>(E-28)</p>

E.2 Interior joints

Table E-2. Determination of the geometrical 2nd order effects in an interior joint.



Angles					
$\sin \gamma_1$	$= \frac{x}{d_b^*}$ $= 2 \cdot \frac{x}{d_b^*}$	(E-29)	$\frac{d}{dy}(\sin \gamma_1)$	$= \dots$ $= \cos \gamma_1 \cdot \frac{d}{dy}(\gamma_1)$	(E-30)
$\sin \gamma_2$	$= \frac{x}{L_c - d_b^*}$ $= 2 \cdot \frac{x}{L_c - d_b^*}$	(E-31)	$\frac{d}{dy}(\sin \gamma_2)$	$= \dots$ $= \cos \gamma_2 \cdot \frac{d}{dy}(\gamma_2)$	(E-32)
Eq. (E-1) \Leftrightarrow	$\sin \gamma_2 = 2 \cdot \frac{1}{L_c - d_b^*} \cdot \frac{d_b^*}{2} \cdot \sin \gamma_1$ $\Leftrightarrow \dots$ $\Leftrightarrow \sin \gamma_2 = \frac{d_b^*}{L_c - d_b^*} \cdot \sin \gamma_1$	(E-33)	Eq.(E-5) \Leftrightarrow	$\frac{d}{dy}(\sin \gamma_2) = \frac{d_b^*}{L_c - d_b^*} \cdot \frac{d}{dy}(\sin \gamma_1)$ $\Leftrightarrow \cos \gamma_2 \cdot \frac{d}{dy}(\gamma_2) = \frac{d_b^*}{L_c - d_b^*} \cdot \cos \gamma_1 \cdot \frac{d}{dy}(\gamma_1)$ $\Leftrightarrow \frac{d}{dy}(\gamma_2) = \frac{d_b^*}{L_c - d_b^*} \cdot \frac{\cos \gamma_1}{\cos \gamma_2} \cdot \frac{d}{dy}(\gamma_1)$	(E-34)
$\cos \gamma_1$	$= \sqrt{1 - \sin^2(\gamma_1)}$ $= \sqrt{1 - \left(2 \cdot \frac{x}{d_b^*}\right)^2}$	(E-35)	$\frac{d}{dy}(\cos \gamma_1)$	$= \dots$ $= -\sin \gamma_1 \cdot \frac{d}{dy}(\gamma_1)$	(E-36)
$\cos \gamma_2$	$= \sqrt{1 - \sin^2 \gamma_2}$ $= \sqrt{1 - \left(2 \cdot \frac{x}{L_c - d_b^*}\right)^2}$	(E-37)	$\frac{d}{dy}(\cos \gamma_2)$	$= \dots$ $= -\sin \gamma_2 \cdot \frac{d}{dy}(\gamma_2)$	(E-38)
Eq. (E-1) \Leftrightarrow	$\cos \gamma_2 = \sqrt{1 - \left(2 \cdot \frac{1}{L_c - d_b^*} \cdot \frac{d_b^*}{2} \cdot \sin \gamma_1\right)^2}$ $\Leftrightarrow \cos \gamma_2 = \sqrt{1 - \left(\frac{d_b^*}{L_c - d_b^*}\right)^2 \cdot (1 - \cos^2 \gamma_1)}$ $\Leftrightarrow \cos \gamma_2 = \frac{1}{L_c - d_b^*} \cdot \sqrt{L_c^2 - 2 \cdot L_c \cdot d_b^* + (d_b^* \cdot \cos \gamma_1)^2}$	(E-39)	Eqs.(E-3),(E-6) \Leftrightarrow	$\frac{d}{dy}(\cos \gamma_2) = -\frac{d_b^*}{L_c - d_b^*} \cdot \sin \gamma_1 \cdot \frac{d_b^*}{L_c - d_b^*} \cdot \frac{\cos \gamma_1}{\cos \gamma_2} \cdot \frac{d}{dy}(\gamma_1)$ $\Leftrightarrow \frac{d}{dy}(\cos \gamma_2) = \dots$ $\Leftrightarrow \frac{d}{dy}(\cos \gamma_2) = -\left(\frac{d_b^*}{L_c - d_b^*}\right)^2 \cdot \frac{\cos \gamma_1 \cdot \sin \gamma_1}{\cos \gamma_2} \cdot \frac{d}{dy}(\gamma_1)$	(E-40)
γ	$= \gamma_1 + \gamma_2$ $\stackrel{\text{Eq.(E-5)}}{\approx} \gamma_1 + \frac{d_b^*}{L_c - d_b^*} \cdot \gamma_1$ $\approx \gamma_1 \cdot \left(1 + \frac{d_b^*}{L_c - d_b^*}\right)$	(E-41)	$\frac{d}{dy}(\gamma)$	$= \frac{d}{dy}(\gamma_1 + \gamma_2)$ $= \frac{d}{dy}(\gamma_1) + \frac{d_b^*}{L_c - d_b^*} \cdot \frac{\cos \gamma_1}{\cos \gamma_2} \cdot \frac{d}{dy}(\gamma_1)$ $= \left(1 + \frac{d_b^*}{L_c - d_b^*} \cdot \frac{\cos \gamma_1}{\cos \gamma_2}\right) \cdot \frac{d}{dy}(\gamma_1)$	(E-42)

Displacements					
δ_v	$= \frac{L_c}{2} - \left(\frac{L_c - d_b^*}{2} \cdot \cos \gamma_2 + \frac{d_b^*}{2} \cdot \cos \gamma_1 \right)$ $= \dots$ $= \dots$ $= \frac{L_c}{2} \cdot (1 - \cos \gamma_2) + \frac{d_b^*}{2} \cdot (\cos \gamma_2 - \cos \gamma_1)$	(E-43)	$\frac{d}{d\gamma}(\delta_v)$	$= -\frac{L_c}{2} \cdot \frac{d}{d\gamma}(\cos \gamma_2) + \frac{d_b^*}{2} \cdot \left(\frac{d}{d\gamma}(\cos \gamma_2) + \sin \gamma_1 \cdot \frac{d}{d\gamma}(\gamma_1) \right)$ $= \left(\frac{-L_c + d_b^*}{2} \right) \cdot \frac{d}{d\gamma}(\cos \gamma_2) + \frac{d_b^*}{2} \cdot \sin \gamma_1 \cdot \frac{d}{d\gamma}(\gamma_1)$ $= -\left(\frac{-L_c + d_b^*}{2} \right) \cdot \left(\frac{d_b^*}{L_c - d_b^*} \right)^2 \cdot \frac{\cos \gamma_1 \cdot \sin \gamma_1}{\cos \gamma_2} \cdot \frac{d}{d\gamma}(\gamma_1) + \frac{d_b^*}{2} \cdot \sin \gamma_1 \cdot \frac{d}{d\gamma}(\gamma_1)$ $= \frac{d_b^*}{2} \cdot \sin \gamma_1 \cdot \left(1 + \frac{d_b^*}{L_c - d_b^*} \cdot \frac{\cos \gamma_1}{\cos \gamma_2} \right) \cdot \frac{d}{d\gamma}(\gamma_1)$	(E-44)
Δ_V	$= L_b \cdot \sin \gamma_1 - \frac{d_c^*}{2} \cdot \sin \gamma_2$ $= L_b \cdot \sin \gamma_1 - \frac{d_c^*}{2} \cdot \sin \gamma_2$ $= \sin \gamma_1 \cdot \left(L_b - \frac{d_c^*}{2} \cdot \frac{d_b^*}{L_c - d_b^*} \right)$	(E-45)	$\frac{d}{d\gamma}(\Delta_V)$	$= \frac{d}{d\gamma} \left[\sin \gamma_1 \cdot \left(L_b - \frac{d_c^*}{2} \cdot \frac{d_b^*}{L_c - d_b^*} \right) \right]$ $= \frac{d}{d\gamma}(\sin \gamma_1) \cdot \left(L_b - \frac{d_c^*}{2} \cdot \frac{d_b^*}{L_c - d_b^*} \right)$ $= \cos \gamma_1 \cdot \left(L_b - \frac{d_c^*}{2} \cdot \frac{d_b^*}{L_c - d_b^*} \right) \cdot \frac{d}{d\gamma}(\gamma_1)$	(E-46)
Δ_H	$= L_b + \frac{d_c^*}{2} - \left(\frac{d_c^*}{2} \cdot \cos \gamma_2 + L_b \cdot \cos \gamma_1 \right)$ $= \dots$ $= L_b \cdot (1 - \cos \gamma_1) + \frac{d_c^*}{2} \cdot (1 - \cos \gamma_2)$	(E-47)	$\frac{d}{d\gamma}(\Delta_H)$	$= -L_b \cdot \frac{d}{d\gamma}(\cos \gamma_1) - \frac{d_c^*}{2} \cdot \frac{d}{d\gamma}(\cos \gamma_2)$ $= L_b \cdot \sin \gamma_1 \cdot \frac{d}{d\gamma}(\gamma_1) + \frac{d_c^*}{2} \cdot \left(\frac{d_b^*}{L_c - d_b^*} \right)^2 \cdot \frac{\cos \gamma_1 \cdot \sin \gamma_1}{\cos \gamma_2} \cdot \frac{d}{d\gamma}(\gamma_1)$ $= \sin \gamma_1 \cdot \left[L_b + \frac{d_c^*}{2} \cdot \left(\frac{d_b^*}{L_c - d_b^*} \right)^2 \cdot \frac{\cos \gamma_1}{\cos \gamma_2} \right] \cdot \frac{d}{d\gamma}(\gamma_1)$	(E-48)

Determinatation of the 2 nd order effects					
Virtual work principle					
W_{EXT}	$= 2 \cdot P \cdot \Delta_V + 2 \cdot N_c \cdot \delta_v$ $= 2 \cdot P \cdot \sin \gamma_1 \cdot \left(L_b - \frac{d_c^*}{2} \cdot \frac{d_b^*}{L_c - d_b^*} \right) + 2 \cdot N_c$ $\cdot \left[\frac{L_c}{2} \cdot (1 - \cos \gamma_2) + \frac{d_b^*}{2} \cdot (\cos \gamma_2 - \cos \gamma_1) \right]$ $= P \cdot \sin \gamma_1 \cdot \frac{2 \cdot L_c \cdot L_b - 2 \cdot L_b \cdot d_b^* - d_c^* \cdot d_b^*}{L_c - d_b^*} + N_c$ $\cdot [L_c \cdot (1 - \cos \gamma_2) + d_b^* \cdot (\cos \gamma_2 - \cos \gamma_1)]$	(E-49)	$\frac{d}{dy}(W_{EXT})$	$= 2 \cdot P \cdot \frac{d}{dy}(\Delta_V) + 2 \cdot N_c \cdot \frac{d}{dy}(\delta_v)$ $= 2 \cdot P \cdot \cos \gamma_1 \cdot \left(L_b - \frac{d_c^*}{2} \cdot \frac{d_b^*}{L_c - d_b^*} \right) \cdot \frac{d}{dy}(\gamma_1) + 2 \cdot N_c \cdot \frac{d_b^*}{2} \cdot \sin \gamma_1$ $\cdot \left(1 + \frac{d_b^*}{L_c - d_b^*} \cdot \frac{\cos \gamma_1}{\cos \gamma_2} \right) \cdot \frac{d}{dy}(\gamma_1)$ $= P \cdot \cos \gamma_1 \cdot \frac{2 \cdot L_c \cdot L_b - 2 \cdot L_b \cdot d_b^* - d_c^* \cdot d_b^*}{L_c - d_b^*} \cdot \frac{d}{dy}(\gamma_1) + N_c \cdot d_b^* \cdot \sin \gamma_1 \cdot$ $\left(1 + \frac{d_b^*}{L_c - d_b^*} \cdot \frac{\cos \gamma_1}{\cos \gamma_2} \right) \cdot \frac{d}{dy}(\gamma_1)$	(E-50)
W_{INT}	$= \dots$ $= V_{y,Rk}^{CWP} \cdot d_b^* \cdot \sin \gamma + \Delta V_{y,Rk}^{SE} \cdot d_b^* \cdot \gamma$	(E-51)	$\frac{d}{dy}(W_{INT})$	$= V_{y,Rk}^{CWP} \cdot d_b^* \cdot \frac{d}{dy}(\sin \gamma) + \Delta V_{y,Rk}^{SE} \cdot d_b^* \cdot \frac{d}{dy}(\gamma)$ $= V_{y,Rk}^{CWP} \cdot d_b^* \cdot \cos \gamma + \Delta V_{y,Rk}^{SE} \cdot d_b^*$	(E-52)
$W_{EXT} = W_{INT}$	$P \cdot \sin \gamma_1 \cdot \frac{2 \cdot L_c \cdot L_b - 2 \cdot L_b \cdot d_b^* - d_c^* \cdot d_b^*}{L_c - d_b^*} + N_c \cdot [L_c \cdot (1 - \cos \gamma_2) + d_b^* \cdot$ $(\cos \gamma_2 - \cos \gamma_1)] = V_{y,Rk}^{CWP} \cdot d_b^* \cdot \sin \gamma + \Delta V_{y,Rk}^{SE} \cdot d_b^* \cdot \gamma$ $\Leftrightarrow P \cdot \gamma_1 \cdot \frac{2 \cdot L_b \cdot L_c - 2 \cdot L_b \cdot d_b^* + d_c^* \cdot d_b^*}{L_c - d_b^*} = V_{y,Rk}^{CWP} \cdot d_b^* \cdot \gamma + \Delta V_{y,Rk}^{SE} \cdot d_b^* \cdot \gamma$ $\Leftrightarrow P \cdot \frac{L_c - d_b^*}{L_c} \cdot \gamma \cdot \frac{2 \cdot L_b \cdot L_c - 2 \cdot L_b \cdot d_b^* + d_c^* \cdot d_b^*}{L_c - d_b^*} = V_{y,Rk}^{CWP} \cdot d_b^* \cdot \gamma + \Delta V_{y,Rk}^{SE} \cdot d_b^* \cdot$ γ $\Leftrightarrow P \cdot \frac{2 \cdot L_b \cdot L_c - 2 \cdot L_b \cdot d_b^* + d_c^* \cdot d_b^*}{L_c} = V_{y,Rk}^{CWP} \cdot d_b^* + \Delta V_{y,Rk}^{SE} \cdot d_b^*$ $\Leftrightarrow P = (V_{y,Rk}^{CWP} + \Delta V_{y,Rk}^{SE}) \cdot \frac{L_c \cdot d_b^*}{2 \cdot L_b \cdot L_c - 2 \cdot L_b \cdot d_b^* + d_c^* \cdot d_b^*}$	(E-53)	$\frac{d}{dy}(W_{EXT})$ $= \frac{d}{dy}(W_{INT})$	$P \cdot \cos \gamma_1 \cdot \frac{2 \cdot L_c \cdot L_b - 2 \cdot L_b \cdot d_b^* - d_c^* \cdot d_b^*}{L_c - d_b^*} \cdot \frac{d}{dy}(\gamma_1) + N_c \cdot d_b^* \cdot \sin \gamma_1 \cdot$ $\left(1 + \frac{d_b^*}{L_c - d_b^*} \cdot \frac{\cos \gamma_1}{\cos \gamma_2} \right) \cdot \frac{d}{dy}(\gamma_1) = V_{y,Rk}^{CWP} \cdot d_b^* \cdot \cos \gamma + \Delta V_{y,Rk}^{SE} \cdot d_b^*$ $\Leftrightarrow P \cdot \cos \gamma_1 \cdot \frac{2 \cdot L_c \cdot L_b - 2 \cdot L_b \cdot d_b^* - d_c^* \cdot d_b^*}{L_c - d_b^*} \cdot \frac{(L_c - d_b^*) \cdot \cos \gamma_2}{(L_c - d_b^*) \cdot \cos \gamma_2 + d_b^* \cdot \cos \gamma_1} + N_c \cdot d_b^* \cdot$ $\sin \gamma_1 \cdot \frac{(L_c - d_b^*) \cdot \cos \gamma_2 + d_b^* \cdot \cos \gamma_1}{(L_c - d_b^*) \cdot \cos \gamma_2} \cdot \frac{(L_c - d_b^*) \cdot \cos \gamma_2}{(L_c - d_b^*) \cdot \cos \gamma_2 + d_b^* \cdot \cos \gamma_1} = V_{y,Rk}^{CWP} \cdot d_b^* \cdot$ $\cos \gamma + \Delta V_{y,Rk}^{SE} \cdot d_b^*$ $\Leftrightarrow P \cdot \cos \gamma_1 \cdot \cos \gamma_2 \cdot \frac{2 \cdot L_c \cdot L_b - 2 \cdot L_b \cdot d_b^* - d_c^* \cdot d_b^*}{(L_c - d_b^*) \cdot \cos \gamma_2 + d_b^* \cdot \cos \gamma_1} + N_c \cdot d_b^* \cdot \sin \gamma_1 =$ $V_{y,Rk}^{CWP} \cdot d_b^* \cdot \cos \gamma + \Delta V_{y,Rk}^{SE} \cdot d_b^*$ $\Leftrightarrow P \cdot \cos \gamma_1 \cdot \cos \gamma_2 \cdot \frac{2 \cdot L_c \cdot L_b - 2 \cdot L_b \cdot d_b^* - d_c^* \cdot d_b^*}{(L_c - d_b^*) \cdot \cos \gamma_2 + d_b^* \cdot \cos \gamma_1} = (V_{y,Rk}^{CWP} \cdot \cos \gamma +$ $\Delta V_{y,Rk}^{SE} - N_c \cdot \sin \gamma_1) \cdot d_b^*$ $\Leftrightarrow P = (V_{y,Rk}^{CWP} \cdot \cos \gamma + \Delta V_{y,Rk}^{SE} - N_c \cdot \sin \gamma_1) \cdot \frac{d_b^*}{\cos \gamma_1 \cdot \cos \gamma_2} \cdot$ $\frac{(L_c - d_b^*) \cdot \cos \gamma_2 + d_b^* \cdot \cos \gamma_1}{2 \cdot L_b \cdot L_c - 2 \cdot L_b \cdot d_b^* + d_c^* \cdot d_b^*}$	(E-54)

Conclusion					
<p>Eq. (E-53) ⇒ Eq. (B-9)</p>	$V_{y,Rk}^{PZ} = P \cdot \frac{1}{d_b^*} \cdot \frac{2 \cdot L_b \cdot L_c - 2 \cdot L_b \cdot d_b^* - d_c^* \cdot d_b^*}{L_c}$ $\Leftrightarrow V_{y,Rk}^{PZ} = \dots$ $\Leftrightarrow V_{y,Rk}^{PZ} = \dots$ $\Leftrightarrow V_{y,Rk}^{PZ} = \dots$ $\Leftrightarrow V_{y,Rk}^{PZ} = \dots$ $\Leftrightarrow V_{y,Rk}^{PZ} = \dots$ $\Leftrightarrow V_{y,Rk}^{PZ} = \dots$ $\Leftrightarrow V_{y,Rk}^{PZ} = \dots$ $\Leftrightarrow V_{y,Rk}^{PZ} = V_{y,Rk}^{CWP} + \Delta V_{y,Rk}^{SE}$	<p>Eq. (E-54) ⇒ Eq. (B-10)</p>	$V_{y,Rk}^{PZ} = P \cdot \frac{\cos \gamma_1 \cdot \cos \gamma_2}{\cos \gamma} \cdot \frac{1}{d_b^*} \cdot \frac{2 \cdot L_b \cdot L_c - 2 \cdot L_b \cdot d_b^* - d_c^* \cdot d_b^*}{(L_c - d_b^*) \cdot \cos \gamma_2 + d_b^* \cdot \cos \gamma_1} + N_c \cdot \tan \gamma \cdot$ $\Leftrightarrow V_{y,Rk}^{PZ} = \left(V_{y,Rk}^{CWP} \cdot \cos \gamma + \Delta V_{y,Rk}^{SE} - N_c \cdot \sin \gamma_1 \right) \cdot \frac{1}{\cos \gamma} + N_c \cdot \tan \gamma \cdot \frac{L_c - d_b^*}{(L_c - d_b^*) \cdot \cos \gamma_2 + d_b^* \cdot \cos \gamma_1}$ $\Leftrightarrow V_{y,Rk}^{PZ} = \left(V_{y,Rk}^{CWP} \cdot \cos \gamma + \Delta V_{y,Rk}^{SE} \right) \cdot \frac{1}{\cos \gamma} + N_c \cdot \left(-\frac{\sin \gamma_1}{\cos \gamma} + \tan \gamma \cdot \frac{L_c - d_b^*}{(L_c - d_b^*) \cdot \cos \gamma_2 + d_b^* \cdot \cos \gamma_1} \right)$ $\Leftrightarrow V_{y,Rk}^{PZ} = \left(V_{y,Rk}^{CWP} + \Delta V_{y,Rk}^{SE} \cdot \frac{1}{\cos \gamma} \right) + N_c \cdot \left(-\tan \gamma \cdot \frac{\sin \gamma_1}{\sin \gamma} + \tan \gamma \cdot \frac{L_c - d_b^*}{(L_c - d_b^*) \cdot \cos \gamma_2 + d_b^* \cdot \cos \gamma_1} \right)$ $\Leftrightarrow V_{y,Rk}^{PZ} = \left(V_{y,Rk}^{CWP} + \Delta V_{y,Rk}^{SE} \cdot \frac{1}{\cos \gamma} \right) + N_c \cdot \tan \gamma \cdot \left(-\frac{\sin \gamma_1}{\sin \gamma} + \frac{L_c - d_b^*}{(L_c - d_b^*) \cdot \cos \gamma_2 + d_b^* \cdot \cos \gamma_1} \right)$ $\Leftrightarrow V_{y,Rk}^{PZ} = \left(V_{y,Rk}^{CWP} + \Delta V_{y,Rk}^{SE} \cdot \frac{1}{\cos \gamma} \right) + N_c \cdot \tan \gamma \cdot \left(-\frac{1}{\frac{\sin \gamma_1 \cdot \cos \gamma_2 + \cos \gamma_1 \cdot \sin \gamma_2}{\sin \gamma_1}} + \frac{L_c - d_b^*}{(L_c - d_b^*) \cdot \cos \gamma_2 + d_b^* \cdot \cos \gamma_1} \right)$ $\Leftrightarrow V_{y,Rk}^{PZ} = \left(V_{y,Rk}^{CWP} + \Delta V_{y,Rk}^{SE} \cdot \frac{1}{\cos \gamma} \right) + N_c \cdot \tan \gamma \cdot \left(-\frac{1}{\cos \gamma_2 + \frac{d_b^*}{L_c - d_b^*} \cdot \cos \gamma_1} + \frac{L_c - d_b^*}{(L_c - d_b^*) \cdot \cos \gamma_2 + d_b^* \cdot \cos \gamma_1} \right)$ $\Leftrightarrow V_{y,Rk}^{PZ} = \left(V_{y,Rk}^{CWP} + \Delta V_{y,Rk}^{SE} \cdot \frac{1}{\cos \gamma} \right) + N_c \cdot \tan \gamma \cdot \left(-\frac{L_c - d_b^*}{(L_c - d_b^*) \cdot \cos \gamma_2 + d_b^* \cdot \cos \gamma_1} + \frac{L_c - d_b^*}{(L_c - d_b^*) \cdot \cos \gamma_2 + d_b^* \cdot \cos \gamma_1} \right)$ $\Leftrightarrow V_{y,Rk}^{PZ} = V_{y,Rk}^{CWP} + \Delta V_{y,Rk}^{SE} \cdot \frac{1}{\cos \gamma}$	<p>(E-55)</p>	<p>(E-56)</p>

**F. prEN 1993-1-8: PROPOSALS
FOR IMPROVEMENT OF THE PZ
CONSTITUTIVE MODEL**

F.1 Stiffness coefficient $k_{ini,EU}^{PZ}$ *

For single-sided joint configurations, or for double-sided joint configurations in which the beam depths are similar, the stiffness coefficient k_{ini}^{PZ} associated to the PZ component should be determined as follows, regardless the presence or otherwise of transverse column web stiffeners:

$$k_{ini,EU}^{PZ} = \frac{0.38 \cdot A_{VC}^{simpl}}{\beta \cdot z_{eq}} \quad (F-1)$$

where

A_{VC}^{simpl} : area of the CWP, taken as:

- for hot-rolled sections: $A_{VC}^{simpl} = h_c \cdot t_{wc}$
- for built-up H or I sections: $A_{VC}^{simpl} = h_w \cdot t_{wc}$

with

h_c : column depth

h_w : depth of the web measured between the flanges

t_{wc} : column web thickness

β : transformation parameter, see Eq. (3-3) of the main manuscript.

z_{eq} : equivalent lever arm, see Eq. (2-5) of the main manuscript.

F.2 Design resistance $V_{y,Rd,EU}^{PZ}$

F.2.1 Unstiffened joints

For single-sided joint configurations or for double-sided joint configurations in which the beam depths are similar, the design shear resistance $V_{y,Rd,EU}^{PZ}$ of an unstiffened PZ, subject to a design shear force V_{Ed}^{PZ} (see Eq. (2-1)), should be determined as follows:

$$V_{y,Rd,EU}^{PZ} = V_{y,Rd,EU}^{CWP} + \Delta V_{y,Rd,EU}^{SE} \quad (\text{F-2})$$

where

$V_{y,Rd,EU}^{CWP}$: contribution to the resistance of the CWP, which should be obtained from Eq. (F-3)

$\Delta V_{y,Rd,EU}^{SE}$: contribution to the resistance of the SE, which should be obtained from Eq. (F-4)

For the derivation of the $V_{y,Rd,EU}^{CWP}$ contribution of the CWP to the PZ resistance:

$$V_{y,Rd,EU}^{CWP} = \frac{0.9 \cdot f_{y,wc} \cdot A_{VC}^{simpl}}{\sqrt{3} \cdot \gamma_{M0}} \quad (\text{F-3})$$

where

$f_{y,wc}$: column web yield strength

γ_{M0} : partial safety factor, see EN 1993-1-1

A_{VC}^{simpl} : area of the CWP, taken as:

- for hot-rolled sections: $A_{VC}^{simpl} = h_c \cdot t_{wc}$
- for built-up H or I sections: $A_{VC}^{simpl} = h_w \cdot t_{wc}$

with

h_c : column depth

h_w : depth of the web measured between the flanges

t_{wc} : column web thickness

For the derivation of the $\Delta V_{y,Rd,EU}^{SE}$ contribution of the SE to the PZ resistance:

$$\Delta V_{y,Rd,EU}^{SE} = \frac{4 \cdot M_{pl,fc,Rd}}{z_{wp}} \quad (\text{F-4})$$

where

$M_{pl,fc,Rd}$: design plastic moment resistance of a column flange, obtained from:

$$M_{pl,fc,Rd} = \frac{b_{fc} \cdot t_{fc}^2 \cdot f_{y,fc}}{4 \cdot \gamma_{M0}} \quad (\text{F-5})$$

with

b_{fc} : column flange width

t_{fc} : column flange thickness

$f_{y,fc}$: column flange yield strength

z_{wp} : lever arm corresponding to the height of the activated CWP, taken as:

- for a welded connection: $z_{wp} = h_b - t_{fb}$
- for a bolted connection: $z_{wp} = h_r$

with

h_b : beam depth

t_{fb} : beam flange thickness

h_r : distance between the centre of compression of the connection, which is supposed to be located at the compressed beam flange centreline, and the bolt-row r in the tension zone of the connection, for which the total design resistance $\sum_r F_{y,Rd,r}$ of all bolt-rows up to and including the bolt-row r is equal to the design resistance of the sheared PZ divided by the transformation parameter β , i.e. $V_{y,Rd,EU}^{PZ}/\beta$. In the case where $\sum_r F_{y,Rd,r}$ is not greater than $V_{y,Rd,EU}^{PZ}/\beta$, r should be selected as the bolt-row closest to the centre of compression.

F.2.2 Stiffened joints

If transverse column web stiffeners are used in the compression and/or tension zones of joints with welded connections, the design shear resistance $V_{y,Rd,EU}^{PZ}$ of the stiffened PZ should be obtained from Eq. (F-2), where $\Delta V_{y,Rd,EU}^{SE}$ should be obtained from:

- stiffeners in both tension and compression zones:

$$\Delta V_{y,Rd,EU}^{SE} = \begin{cases} 4 \cdot \frac{M_{pl,fc,Rd}}{z_{wp}} + \min \left(4 \cdot \frac{M_{pl,st,Rd}}{z_{wp}} ; 2 \cdot \frac{M_{pl,fb,Rd}}{z_{wp}} \right) & \text{single – sided joints} \\ 4 \cdot \frac{M_{pl,fc,Rd}}{z_{wp}} + \min \left(4 \cdot \frac{M_{pl,st,Rd}}{z_{wp}} ; 4 \cdot \frac{M_{pl,fb,Rd}}{z_{wp}} \right) & \text{double – sided joints} \end{cases} \quad (\text{F-6})$$

- stiffeners in the tension or compression zone only:

$$\Delta V_{y,Rd,EU}^{SE} = \begin{cases} 4 \cdot \frac{M_{pl,fc,Rd}}{z_{wp}} + \min \left(2 \cdot \frac{M_{pl,st,Rd}}{z_{wp}} ; 1 \cdot \frac{M_{pl,fb,Rd}}{z_{wp}} \right) & \text{single – sided joints} \\ 4 \cdot \frac{M_{pl,fc,Rd}}{z_{wp}} + \min \left(2 \cdot \frac{M_{pl,st,Rd}}{z_{wp}} ; 2 \cdot \frac{M_{pl,fb,Rd}}{z_{wp}} \right) & \text{double – sided joints} \end{cases} \quad (\text{F-7})$$

where

$M_{pl,fb,Rd}$: design plastic moment resistance of a beam flange, obtained from:

$$M_{pl,fb,Rd} = \frac{b_{fb} \cdot t_{fb}^2 \cdot f_{y,fb}}{4 \cdot \gamma_{M0}} \quad (\text{F-8})$$

with

b_{fb} : beam flange width

t_{fb} : beam flange thickness

$f_{y,fb}$: beam flange yield strength

$M_{pl,st,Rd}$: design plastic moment resistance of a stiffener, obtained from:

$$M_{pl,st,Rd} = \frac{b_{st} \cdot t_{st}^2}{4} \cdot \frac{f_{y,st}}{\gamma_{M0}} \quad (F-9)$$

with

b_{st} : width of both stiffeners, including column web thickness

t_{st} : stiffener thickness

$f_{y,st}$: stiffener yield strength

If transverse column web stiffeners are used in the compression and/or tension zones of joints with bolted connections, the design shear resistance $V_{y,Rd,EU}^{PZ}$ of the stiffened PZ should be obtained from Eq. (F-2), where $\Delta V_{y,Rd,EU}^{SE}$ should be obtained from:

- stiffeners in both tension and compression zones:

$$\Delta V_{y,Rd,EU}^{SE} = \begin{cases} 4 \cdot \frac{M_{pl,fc,Rd}}{z_{wp}} + 4 \cdot \frac{M_{pl,st,Rd}}{z_{wp}} & \text{if } z_{wp} \geq d_s \\ 4 \cdot \frac{M_{pl,fc,Rd}}{z_{wp}} + 2 \cdot \frac{M_{pl,st,Rd}}{z_{wp}} & \text{if } z_{wp} < d_s \end{cases} \quad (F-10)$$

- stiffeners in the tension zone only:

$$\Delta V_{y,Rd,EU}^{SE} = \begin{cases} 4 \cdot \frac{M_{pl,fc,Rd}}{z_{wp}} + 2 \cdot \frac{M_{pl,st,Rd}}{z_{wp}} & \text{if } z_{wp} \geq d_s \\ 4 \cdot \frac{M_{pl,fc,Rd}}{z_{wp}} & \text{if } z_{wp} < d_s \end{cases} \quad (F-11)$$

- stiffeners in the compression zone only:

$$\Delta V_{y,Rd,EU}^{SE} = 4 \cdot \frac{M_{pl,fc,Rd}}{z_{wp}} + 2 \cdot \frac{M_{pl,st,Rd}}{z_{wp}} \quad (F-12)$$

where

$M_{pl,fc,Rd}$: design plastic moment resistance of a column flange, obtained from Eq. (F-5)

$M_{pl,st,Rd}$: design plastic moment resistance of a stiffener, obtained from Eq. (F-9)

d_s : distance between the centrelines of the stiffeners

F.3 Ultimate deformation capacity $\gamma_{u,EU}^{PZ}$

For single-sided joint configurations, or for double-sided joint configurations in which the beam depths are similar, the ultimate deformation capacity $\gamma_{u,EU}^{PZ}$ associated to the PZ component should be determined as follows, regardless the presence or otherwise of transverse column web stiffeners:

$$\gamma_{u,EU}^{PZ} = \gamma_y^{PZ} \cdot \left[-0.15 - 0.225 \cdot \frac{G}{f_{u,wc}} \cdot \left(1 - 1.45 \cdot \frac{f_{u,wc}}{f_{y,wc}} \right) \right] \quad (\text{F-13})$$

where

$f_{y,wc}$: column web yield strength

$f_{u,wc}$: column web ultimate strength

G : shear modulus of steel, given by:

$$G = \frac{E}{2 \cdot (1 + \nu)} \quad (\text{F-14})$$

with

E : Young's modulus of steel

ν : Poisson's ratio

γ_y^{PZ} : yield shear deformation of the PZ, obtained from:

$$\gamma_y^{PZ} = \frac{f_{y,wc}}{\sqrt{3} \cdot G} \quad (\text{F-15})$$

BIBLIOGRAPHY

- [1] S. Jordão, “Behaviour of internal welded joints with beams of different depths and high strength steel (PhD thesis, in Portuguese),” University of Coimbra, Coimbra (Portugal), 2008.
- [2] S. Jordão, L. Simões Da Silva, and R. Simões, “Behaviour of welded beam-to-column joints with beams of unequal depth,” *J. Constr. Steel Res.*, vol. 91, pp. 42–59, 2013, doi: 10.1016/j.jcsr.2013.07.023.
- [3] H. Augusto, J. M. Castro, C. Rebelo, and L. S. Da Silva, “Characterization of the Cyclic Behavior of the Web Components in End-plate Beam-to-column Joints,” *Procedia Eng.*, vol. 160, no. Icmfm Xviii, pp. 101–108, 2016, doi: 10.1016/j.proeng.2016.08.868.
- [4] H. Augusto, “Characterization of the behaviour of partial-strength joints under cyclic and seismic loading conditions (PhD thesis),” University of Coimbra, Coimbra (Portugal), 2017.